`

The University Of Sheffield.

A MECHANOBIOLOGY STUDY ON THE RESPONSE TO MECHANICAL COMPRESSION OF MESENCHYMAL PROGENITOR CELLS CULTURED IN A COMPOSITE SCAFFOLD MADE OF 3D INSERT® PCL AND COLLAGEN GEL

A THESIS SUBMITTED IN PARTIAL FULFILMENT OF THE REQUIREMENTS FOR THE DEGREE OF

DOCTOR OF PHILOSOPHY

Marzia Brunelli, M.Sc.

SUPERVISOR:

Prof. Damien Lacroix

CO-SUPERVISOR:

Dr. Cécile M. Perrault

Department of Mechanical Engineering

INSIGNEO Institute for in silico Medicine

The University of Sheffield

Faculty of Engineering

December 2015

INTERNAL EXAMINER:

Dr. Gwendolein Reilly

EXTERNAL EXAMINER:

Prof. Daniel Kelly

Success is not final, failure is not fatal: it is the courage to continue that counts.

- Winston Churchill -

ACKNOWLEDGEMENTS

I would like to thank my supervisors to have believed in me and have significantly contributed to the achievement of this doctoral degree. First Damien, my supervisor, for the constant guidance, and for the help provided facing new challenges. I would like to thank also for the opportunity to attend a wide number of conferences which have deeply enriched my competence in the field and my professional experience. Last but not least, thanks for your understanding, and your professionally as well as personally inspirational advices. Second, I would like to thank Cecile, my co-supervisor, for her guidance, and to contribute with her background experience. Often, it helped looking at the problem from another perspective.

Then, I would like to thank co-workers whose contribute was decisive for the realization of this work: Enrico, for sharing his knowledge of mechanics, and for the prompt and friendly support; Jafar, for the time spent together in front of the despicable Simpleware; Stefania and Sofia, for the amazing support out of hours; Claudi for the help freezing, feeding and killing cells on my behalf; and Silvia for the quick and essential corrections.

Eventually, I would like to thank all friends and my family for the amazing support during these three years. In particular, thank you Ana, my dear friend, for the smiles among tears, for the hugs when mattered the most, and for the help drawing points. Thanks to my soulmate for the smart ideas, the close support, and to keep my dreaming side alive. Thanks to Papa` and la So to be there: you are my shields in the battle, my light in the dark, my shelter in rainy days.

I wish to dedicate the entire work to my beloved mum: thank you, Mamma, I bet you have been watching over me lately.

CONTENTS

ABBREVIATIONS

2D	two-dimensional
3D	three-dimensional
3D PCL	3D Insert ® PCL
ADSCs	adipose derived stem cells
ALP	alkaline phosphatase
ANOVA	analysis of variances
BMP	bone morphogenic protein
BMSCSs	bone marrow stem cells
BXR	biaxial rotating
CO	carbon dioxide
cPCL	3D Insert ® PCL embedding collagen gel
d	diameter
dH_2O	distilled water
DMA	dynamic mechanical analysis
DNA	deoxyribonucleic acid
ε	strain
E_a	apparent elastic modulus
ECM	extracellular matrix
EMF	electromagnetic field
ESCs	embryonic stem cells
FGF	fibroblasts growth factor

GAG	glycosaminoglycan
GV	grey values
HD	high density collagen
ICM	inner cell mass
hES-MPs	human bone marrow progenitor stem cells
LD	low density collagen
LDM	low temperature deposition modelling
L1	single series of compression cycles (5 days)
L2	double series of compression cycles (5+5 days)
µ	kinematic viscosity
MG63	human bone marrow osteosarcoma cells
MSC	mesenchymal stem cells
hES-MPs	human bone marrow progenitor stem cells
microCT	micro computed tomography
n	number of repeated samples
N	number of repeated experiments
OCN	osteocalcin
OPN	ostepontin
P	porosity
PAM	pressure applied micro syringe process
PBS	phosphate buffered saline solution
PDMS	polydimethylsiloxane

PDMS2	PDMS 2 mm height
PDMS10	PDMS 10 mm height
PEM	pulsatile electromagnetic field
PGA	poly glycolic acid
PLA	poly lactic acid
PLGA	poly glycolic lactic acid
PCL	polycaprolactone
PBS	phosphate-buffered saline
ROI	region of interest
RT-PCR	reverse transcriptase polymerase chain reaction
RWV	rotator well vessel
σ	stress
SEM	scanning electron microscopy
SF	spinner flask
SLA	stereolithography
T-Test	student T test
TE	tissue engineering
TGF	transforming growth factor
U	non-loaded condition
UV	ultra violet
v	velocity of particles
v_{inlet}	inlet flow rate
V_c	volume of collagen

V_{mat}	volume of material
V_{media}	volume of culture media
V_{NaOH}	volume of sodium hydroxide
V_{PBS}	volume of PBS
V_{ROI}	volume of ROI
V_{tot}	total volume

LIST OF FIGURES

LIST OF TABLES

ABSTRACT

The increased awareness of the ability of cells in detecting mechanical cues from the external environment [1] led to consider the possibility of triggering a cellular response by applying external mechanical forces [2]. In order to drive the commitment of differentiated cells and obtain in vitro engineered implants as replacement for bone fracture sites, a scaffold closely mimicking the 3D distribution of forces acting on bone cells in vivo is required and is still ongoing research. On this purpose, a composite scaffold embedded with collagen (cPCL) is proposed in this study as structure to transmit externally applied mechanical forces to embryonic human mesenchymal stem cells (hES-MPs) through a gelatinous matrix of collagen. A collagen concentration of 2 mg/ml and plasma treatment of scaffolds were selected as optimal conditions for survival and uniform seeding distribution of cells. Then, the second part of the study allowed to fully characterize, by mechanical testing and x-ray imaging, a novel hybrid scaffold able to provide an optimal environment for controlled-bone progenitor cells growth. The objective of the last part of the study focused on the evaluation of how short bursts of compressive strain, applied as series of cycles at early stages (L1) and late stages (L2) of culture, affects cellular proliferation, bone tissue formation and the osteogenic response of hES-MPs. Short bursts of compression were found to strongly affect hES-MPs proliferation, suggesting cyclic compressive loading to delay the proliferation of samples compressed once. On the other side, L2 prevented proliferation to occur over 28 days, although greatly enhancing the production of mineral which, instead, was null for samples undergoing L1. This study underlined the existence of a strong link between proliferation and mineralization potential of cells and confirms the possibility to vary their response by short bursts of compression applied on hES-MPs seeded in 3D hybrid scaffolds.

INTRODUCTION

1.1 The clinical problem

Bone tissue fracture is a worldwide issue caused by tissue deterioration as a consequence of ageing, bone related diseases, and severe traumas. When bone fracture occurs, surgical intervention is often required to stabilize the bone and restore functionality of the damaged tissue [3]. In the past, implants made by metals and ceramics based material were the most common solution to restore the functionality of injured sites located in the musculoskeletal apparatus. Metals were employed to restore joints or load bearing sites due to their remarkable ability to support mechanical load [4]. The use of metals, often, led to failure and/or malfunctioning of the implant caused either by an inflammatory response [5] or misplacement [6]. Indeed, the metallic prosthesis shields the bone from absorbing stresses due to its high stiffness, causing bone resorption at the implant-bone interface. In some cases, mismatches with the healing site occurred also as a consequence of forces acting at the contact surface [7], and inducing bone absorption and remodelling. In order to avoid release of ions, ceramics were considered as replacement of contact areas between articulations where friction forces elicit their action. [8]. Despite their good resistance to biological and rubbing corrosion, ceramics are highly brittle. Consequently, they are unsuitable for many applications as they tend to break or crack in locations governed by torsion and bending stresses [9].

The limitations encountered with the techniques mentioned above pushed toward the increasing demand for the use of implants reproducing the same characteristic as the tissue to replace in terms of geometrical architecture, chemical composition and mechanical behaviour. The ideal scenario involves embedding the implant with living cells to obtain a graft able to progressively adapt to the implantation site, to induce new tissue formation, and fully

integrate into the host-body. Nowadays, common grafting materials for bone regeneration purposes are composed of osteogenic cells interacting with bone tissue [10]. The ideal cell source would be tissue harvested from another site of the patient (generally the iliac crest) to develop cancellous, cortical and bone marrow autologous grafts. Bone ingrowth by autologous grafts occurs at first just by the activity of cells embedded in the implant, while the surrounding tissue is involved in the healing process after four weeks from the graft implantation. Autologous cancellous bone grafts vascularize easily, and present osteoconductive and osteoinductive properties. Indeed, the bone matrix supports bone ingrowth and the infiltration of osteoblasts and osteoblast precursors through the structure. At the same time, it releases proteins which promote cell proliferation. The main drawbacks of autologous cancellous bone grafts are that the lack of mechanical support prevents their use for load bearing sites regeneration. On the other hand, autologous cortical bone grafts provide mechanical support to mechanical load during the initial phase of bone formation and have good osteoinductive capabilities. However, these grafts lack of osteoconductivity as cortical bone presents a compact osteon-made structure rather than a porous net made of randomly aligned rods. Both cancellous and cortical grafts had high rates of success especially in the treatment of defects up to 5-6 cm [10]. A lack of immunogenic response is among the main advantages characterizing autologous grafts, and satisfactory results were also obtained by direct injection of bone marrow grafts in the healing site [11]. Despite this, the concentration and the quality of cells choosen for the development of in vitro engineered scaffolds affect the implant success in vivo and may vary depending on patient, target site and technique used [10]. Despite the autologous grafts rate of success, the method is limited by the amount of tissue available, especially treating patients with chronic diseases and when multiple surgical procedures are required causing donor site morbidity. The use of cells deriving from tissue harvested from other donors (allografts) or animals (xenografts) is the most common alternative but it can cause tissue rejection, immunogenicity effects, risk of infections and high costs [10]. Some good results were achieved in cartilage repair where the

immunogenic response is lessen by the absence of vascularized tissue [12]. Due to the limited evidences of success in the replacement of bone tissue, graft methods need improvement to obtain an implant able to fully integrate in the healing site and to actively work in synergy with the host body in the bone formation process.

1.2 Tissue engineering and the in vitro approach

Since the 1950s, understanding of bone regeneration processes increased enormously thanks to: 1) the development of new technologies, allowing studies to be performed at the microscopic level such as microcomputed tomography, finite-element modelling and nanotechnologies; 2) the advances made in cellular and molecular biology on the characterization of bone-forming cells in vitro and in vivo; and 3) the identification of proteins involved and genes expressed in the bone repair processes. A promising solution to the development of adequate grafts for bone-tissue replacement is known as Tissue Engineering (TE). TE aims to fully restore the functionality of a tissue and induce new functional tissue formation applying engineering and life science principles [13]. According to TE, the combination of cells, adequate extracellular matrix, growth factors, and mechanical stimuli allows to obtain in vitro tissue having the same biological and physical properties as the target material. The choice of the correct cell type, scaffold properties and mechanical/chemical stimulation depends on the characteristic of the tissue to regenerate. Scaffolds used for TE purposes must be: 1) biocompatible to avoid immuno-rejection; 2) shaped to match the healing site to avoid mismatches and misalignments of the implant; 3) able to bear mechanical stimuli providing support for cell activities. Moreover, biodegradable, porous, osteoinductive and osteoconductive scaffolds are preferred to guarantee harmless expulsion from the body, and satisfactory seeding efficiency and tissue formation rate [14]. As cells are required to produce matrix rapidly and

differentiated cells often have low availability due to the difficulties of harvesting tissue, stem cells are currently used as cell source. They present remarkable proliferation and differentiation capability but precise control over their commitment toward a well-defined lineage is still an open issue. It is clear that biochemical factors have a strong impact on cell commitment and that mechanical forces influence cells behaviour [15]. The behaviour of a population of cells was already widely examined on non-rigid 2D substrates, clarifying the role of substrate stiffness [16], surface functionalization [17], and response to various tensile and shear stress stimuli on stem cell commitment [18]. However, the current knowledge related to the effect of mechanical stimuli on human bone marrow progenitor stem cells (hMSCs) is mainly limited to 2D surfaces or 3D soft matrices. As the stimulus is not directly applied to cells but to the scaffold embedding cells, the actual load experienced may be different from the externally applied one depending on the material properties, geometry and architecture of the structure.

1.3 Aim of the thesis

This thesis aims to clarify the behaviour of human embryonic stem cell-derived mesodermal progenitors (hES-MPs) when global compression stimuli are applied externally on 3D polymeric scaffolds embedded with collagen gel and hES-MPs. In the literature, the effect of compression when cells are cultured on two dimensional (2D) or soft materials is becoming increasingly clear. However, both materials are not ideal for mimicking the tissue environment. Indeed, the former does not provide the three-dimensionality of tissue, while the latter, due to its low stiffness, prevents the application of high stresses representative of bone. As a consequence, the focus recently moved toward the use of 3D polymeric structures able to bear mechanical stimuli and whose chemical properties can be modified in order to match the mechanical stability

required for a particular application. 3D Insert® PCL is a good candidate to be used to mimic the environment found in bone in vivo due to the high reproducibility obtained by the fuse deposition modelling fabrication technique and its porosity matching the range for bone formation [19]. Despite this, the three dimensionality of the construct is not sensed at cellular level due to the small dimensions of the contact surface between cells and scaffolds so that the stresses sensed by cells are spread along 2 axes (Fig. 1.1.3A). In order to better mimic the mechanics of bone tissue, this study aims to develop a composite scaffold formed by an external solid structure responsible for bearing the mechanical load, and an internal soft collagenous matrix. Such a structure exploits the mechanical resistance of polymers and the deformability of collagen, allowing the transmission of stresses all around the surface of cells (Fig. 1.1.3B). This approach increases the three-dimensionality of the structure and, at the same time, provides a matrix of the most common protein making up bone tissue. hES-MPs were chosen as the cell source because of their reduced risk of tumour development due to the fact that their differentiation pathway is already partly defined and because they are expected to be more stable compared to embryonic stem cells enabling future therapeutic applications and advantages for bulk production of cells for therapy [20]. Moreover, hES-MPs led to an higher production of tissue formation compared to adult mesenchymal stem cells when culture in column bioreactors showing great potential for the development of bone substitutes [21].

This thesis is part of a European Research Council grant (FP7-258321) where in vitro experiments are developed in synergy with computational simulations, mutually exchanging information to provide a complete description of the phenomenon observed.

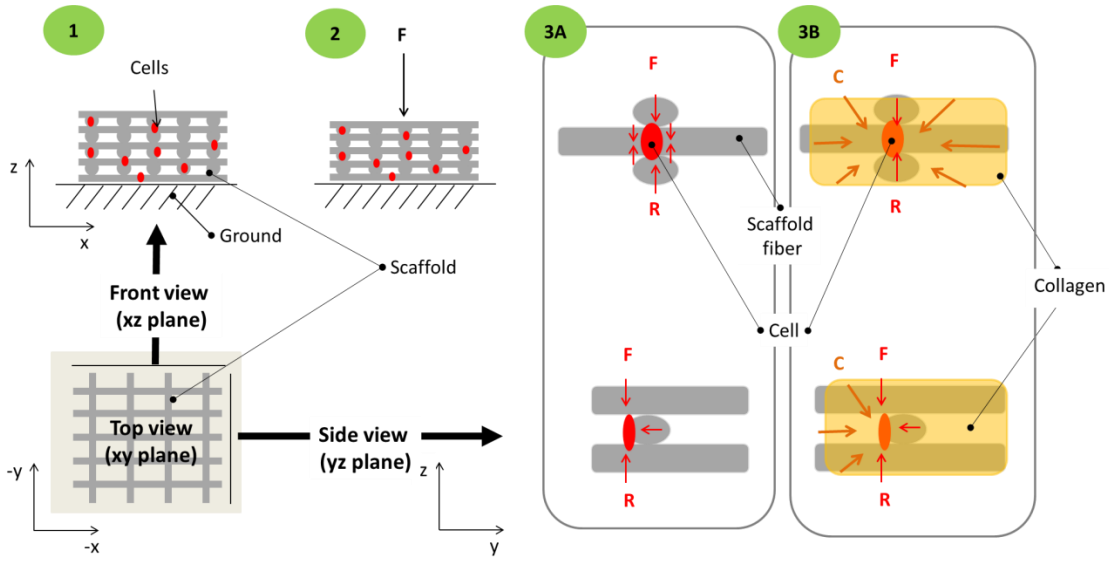

Fig. 1.1: Scheme representing (1) the scaffold with cells from a frontal plane. (2) Forces F were externally applied along the z-axes causing the deformation of the structure. (3) The structure transmitted stresses to cells which were further affected by the reaction force R with the ground. (A) Deformation of the scaffold structure alone caused stresses to act at the cell-scaffold contact surface, limiting the mechanical stimulation along 2 axes. (B) Including collagen in the structure provided further compressive forces C to act on cells because of the deformation of the collagenous matrix. The resulting stresses are expected to be uniformly spread around the space surrounding the cell, providing a 3D mechanical environment which better mimics the in vivo tissue matrix.

A review of the current state of the art, in accordance to the field of study, is depicted in Chapter 2. Chapter 3 gives an overview of the general methodologies and the materials employed through the whole study, aiming to provide a collection of common procedures for the analysis of cellular behaviour and scaffold analysis. Geometrical and mechanical properties of 3D Insert ® PCL (Biotek, USA), the 3D scaffolds, used as external structure for bearing the mechanical compression, are presented in Chapter 4. Here, a sensitivity analysis evaluating the contribution given by the geometrical architecture of scaffolds to the overall variability in the mechanical response is discussed. Chapter 5 focuses on the comparison between static and perfusion seeding techniques. For this purpose, an in-house, low cost and versatile microfluidic device was developed to test the effect of different velocities and system configurations on seeding efficiency. In Chapter 6, the scaffold embedded with collagen (cPCL) is characterized by Micro Computed Tomography. Then, the effect of collagen concentration and plasma treatment

on hES-MPs seeded scaffolds is further discussed. This part determines the optimal conditions enhancing cell activities and provides well-characterized controls for further studies embedding cells. Eventually, the effect of applying cyclic mechanical compression short periods of time on scaffolds embedded with collagen and hES-MPs, including resting periods among stimulation, is presented in Chapter 7. Chapter 8 is focused on the discussion of the overall results, and conclusions are presented in Chapter 9.

Chapter 2

LITERATURE REVIEW

2.1 BONE TISSUE

2.1.1 Anatomical structure of bone and cartilage

Tissues are assemblies of cells and proteins organised in 3D structures and giving structural support to the body. Metabolism, fate, shape and cellular commitment are influenced by composition and organization of the extracellular matrix (ECM) which varies depending on the function of the target tissue. The skeleton apparatus is composed of two main tissues, bone and cartilage, working together as a strong structure to provide the optimal resistance to solicitations due either to internal action of muscles and tendons or external forces.

The adult skeleton has a total of 206 bones which provide structural support during movements and locomotion, protect vital organs and guarantee mineral homeostasis. Bone is a biological tissue formed by living cells embedded in a rigid framework. Bones in the human body are divided in four main categories: long bones, short bones, irregular bones and flat bones. Long bones are divided in three main areas: diaphysis, metaphysis and epiphysis (Fig. 2.1a). Diaphysis is for a strong structure able to support the body weight in vertical direction and is mainly composed of compact cortical bone [22] (Fig. 2.1c). Cortical bone is dense, rigid and surrounds the bone marrow. It is organized in lamellae which overlap forming cylindrical structures giving shape to osteons (Fig. 2.1c). Osteons are wrapped together and form the so called Haversian system, hosting a blood vessel in the centre responsible providing nutriments through the structure. Osteons organize to form a hollow cylindrical structure

containing bone marrow confined in an inner canal made of endosteum, which is a thin interconnected layer of osteogenic cells lacking of fibrous tissue (Fig. 2.1c). The external surface is covered by the periosteum, an external vascularized double layer tissue strongly connected to the underlying cortical bone by collagenous fibers called Sharpeys' fibers and covered by a thicker outer layer formed by dense connective tissue.

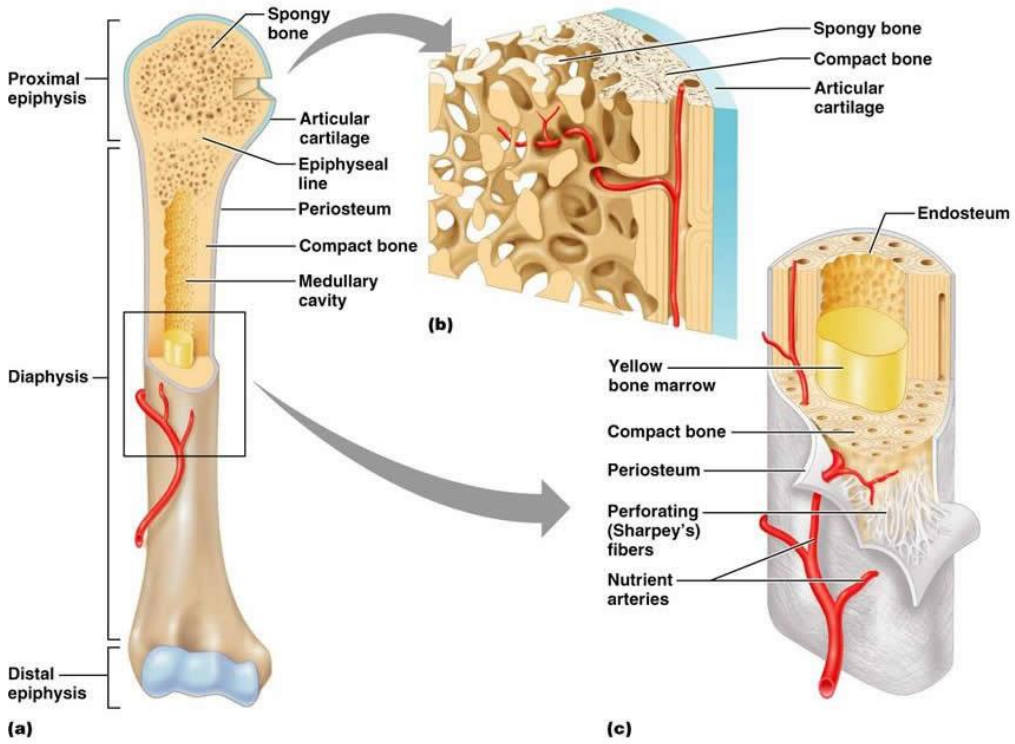

Fig. 2.1: a) long bone structure, b) trabecular and c) cortical bone architecture. Taken from http://classes.midlandstech.edu/carterp/Courses/bio210/chap06/Slide3.JPG

Trabecular bone is less dense and is characterized by a network of plates and rods randomly organized to form a sponge-like structure with anisotropic properties (Fig. 2.1b). Although presenting a different organization at the macroscopic level, cortical and trabecular bone are composed of the same extracellular matrix made of 50 to 70% mineral phase, 20 to 40% organic matrix, less than 3% lipids and 20% water. The mineral component is mainly formed by 200 Å crystals of hydroxyapatite and is responsible for conferring

the load-bearing strength to bone, while the organic matrix provides elasticity and flexibility. Collagenous proteins among which collagen type 1 are the most abundant, while non collagenous proteins make up the 10-15% of bone forming proteins and may be responsible for regulating mineralization and cells proliferation.

Cartilage is made of cells called chondrocytes embedded in connective tissue, and proteoglycans and collagen packed in a dense fibrous membrane called perichondrium. Cartilage in the human body can have three different compositions leading to hyaline cartilage, elastic cartilage or fibrous cartilage. Hyaline cartilage is formed by chondrocytes located in spaces called lacunae and a high concentration of collagen conferring flexibility, elasticity and strength to the resulting tissue. It can be found in trachea, nose and joints aiming to reduce friction effects, to promote movements and to enhance longitudinal growth. Elastic cartilage has a similar composition as hyaline cartilage but the former includes also elastic fibers spreading through the structure in all directions. Elastic cartilage is found in ears, epiglottis and larynx and works as support for maintaining the organs' shape. Fibrous cartilage is extremely tough and composed of bundles with different orientations depending on the acting stresses. It can be found in intervertebral disks and the glenoid cavity of the shoulder joint where it acts as shock absorbers and prevents dislocations.

2.1.2 Bone cells

Bone activities are regulated by the action of active cells embedded in the bone matrix: osteoprogenitor cells, osteoblasts, osteocytes and osteoclasts [23]. Progenitor cells initiate their differentiation process (Fig. 2.2) becoming osteoblasts precursors at first and mature osteoblasts later.

Osteoblasts are cubical in shape, and are metabolically active cells responsible for secreting matrix and increasing bone mass [24]. Mature osteoblasts have a large nucleus, an expanded Golgi apparatus and an

extensive endoplasmic reticulum secreting collagen type I and other matrix proteins. Terminally differentiated osteoblasts lead to osteocytes working as support for the bone structure and as metabolic regulators.

Osteocytes are fully differentiated osteoblasts trapped into the matrix with extended cytoplasmatic processes forming a connected network to promote cell-cell communication by secreting connexions [25]. They sense the shear stress due to fluid flow through the lacuno-canicula network caused by mechanical forces acting on the bone matrix and translate it in a biochemical signal through the production of signalling molecules modulating osteoblasts and osteoclasts activity [15].

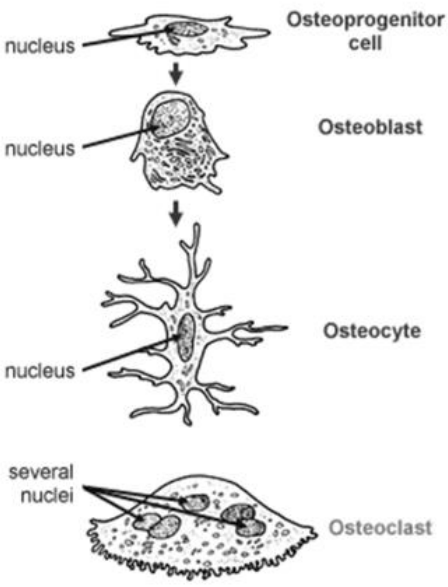

Fig. 2.2: Bone cells development. Mono-nucleated osteoprogenitor cells differentiate in osteoblasts and then extend protrusions fully differentiating in osteocytes. Osteoclasts, instead, are multi-nucleated and derive from the macrophage lineage. Taken from http://www.zoology.ubc.ca/~biomania/tutorial/bonets/anc01.htm

Activated multinucleated osteoclasts derive from mononuclear precursor cells of the monocyte-macrophage lineage [22] and are responsible for bone resorption. During the remodelling process, osteoclasts bind the bone matrix via integrins receptors and polarize, performing their resorbing action by

releasing hydrogens ions and hydrolytic enzymes to digest the mineral and protein matrix [26].

2.1.3 Bone growth, healing and remodelling

2.1.3.1 Bone growth

Bone grows progressively from childhood to adolescence in radial and longitudinal directions following two different mechanisms: intramembranous ossification [27] and endochondral ossification [28]. Intramembranous ossification is the mechanism followed by primary fractures healing and during development, and takes place in the epiphysis of bones where osteoprogenitor cells directly differentiate into osteoblasts.

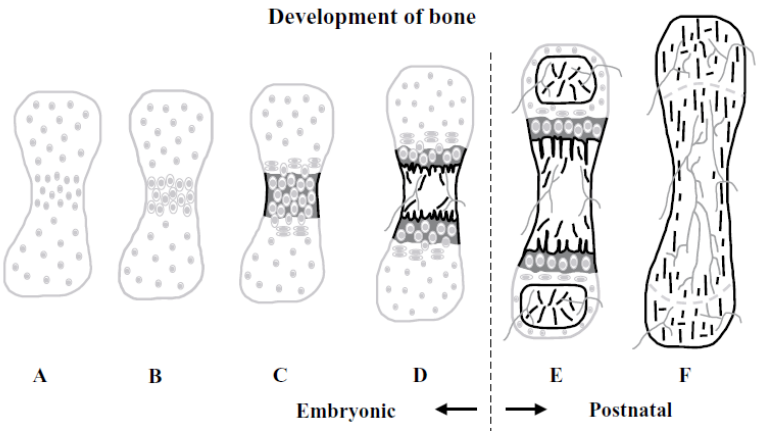

Fig. 2.3: From embryonic to postnatal development of bone: (A) cartilage portion with chondrocytes, (B) chondrocytes swelling, (C) mineralization of bone occurring around the hypertrophic chondrocytes, (D) formation of blood vessels and bone formation starts, (E) formation of secondary ossification centres, (F) fully developed bone. Taken from [29]**.**

Osteoprogenitor cells derive from (1) mesenchymal stem cells (MSCs) present in various tissues such as bone marrow, tooth pulp, fetal cord blood and liver,

and (2) flattened bone-lining cells forming the endosteum and periosteum. On the contrary, long bone growth occurs through endochondral ossification where MSCs differentiate first in proliferating chondrocytes which produce a large amount of cartilage, and then further differentiate in hypertrophic chondrocytes (Fig. 2.3 A, B). On the perichondrium, the external tissue of developing limbs, stem cells differentiate into osteoblasts surrounding the matrix of hypertrophic chondrocytes (Fig. 2.3 C). Eventually, the hypertrophic cartilage is invaded by blood vessels and replaced by bone and marrow (Fig. 2.3 D). At the distal ends other ossification centres are likely to appear, enhancing the progressive growth in longitudinal direction (Fig. 2.3E). The space of contact between ossification centres is called growth plate and it undergoes postnatal mineralization [29].

2.1.3.2 Bone healing and remodelling

During life, bone models its overall shape in response to physiological stimuli to maintain the mineral homeostasis and preserve its strength, constantly replacing packets of old bone with new ones through the dependent action of bone cells. The balance between production and absorption of extracellular matrix determines the ability of bones to satisfy the demand for mechanical support following the functional adaptation criteria consisting in maximal strength and minimal bone mass [30]. Bone remodelling is also observed in response to mechanical forces as bone change its load-bearing axes or its strength [31] depending on the external forces acting on the structure. The global load acting on bone during locomotion is non-uniform distributed ranging from 0 to 1800 microstrain in the cortical midshaft during locomotion [32] and maximum peaks of load of 2000 microstrain were measured in the tibia during vigorous activity [33]. Forces felt by cells depend on local stresses developing as consequence of fluid shear stress, hydrostatic pressure and mechanical loading due to the action of external reaction forces, muscles and tendons. To estimate the forces acting on cells different computational models were developed showing shear stresses up to 0.8-3 Pa, hydrostatic

compression up to 1-28 MPa at 1 Hz resulting from locomotion and physiological strains of bone in vivo typically in the range between 0.04- 0.3% [34].

Bone remodelling is involved also in the process of bone healing. It is commonly divided into three phases: 1) early inflammatory stage, 2) repair stage and 3) remodelling stage. The first inflammatory stage involves the formation of a hematoma recruiting cells such as macrophages, monocytes, lymphocytes and fibroblasts, responsible for the development of granulation tissue. Then, MSCs migrate to the healing site and vascularization of the new forming tissue begins by the action of fibroblasts laying on the stroma. During the repair stage, osteoblasts shape osteoids and secrete collagen, leading to the formation of a soft callus which eventually ossifies to bridge the woven bone in the facture. Eventually, the callus is further remodelled by the action of osteoblasts and osteoclasts, and the healing process is complete when the complete functionality is restored and the bone acquires again its optimal shape, structure and mechanical strength. The effect of forces on the healing process can be appreciated by observing the endochondral ossification in secondary fractures. Experiments have indeed demonstrated stiffer bone and larger callus formation when the healing site is subject to cyclic load rather than rigid fixation [29]. Animal studies have shown that strain rate is more important than strain amplitude in the bone formation process and low strain at high frequency stimulates bone growth as they are common stimuli associate with daily life [30].

2.2 BONE TISSUE ENGINEERING

2.2.1 Culturing cells from 2D to 3D

In the past, cells were mainly cultured in flasks or petri dishes due to the high viability of cells growing on two-dimensional (2D) surfaces. However, cellular

tissues consist of an extracellular matrix organized in a 3D highly interconnected network made by fibers and pores with an architecture much different from the 2D conditions. Indeed, 2D substrates require an adaptation by cells to the lack of the ECM environment, strongly affecting their differentiation process. The increasing demand for overcoming 2D limitation led to the development of 3D culture matrices, known as scaffolds, with different architecture, composition and surface properties.

For tissue engineering purposes, polymers have been intensively studied as raw material to be employed for scaffolds development as they allow control over mechanical properties, degradation kinesis, shape, architecture, pores morphologic features, and surface functionalization. Polymers can be generally divided into natural and synthetic, and can be processed through numerous techniques to manufacture scaffolds with various shape and properties depending on the application. 3D matrices can be used for clinical studies or in vitro 3D models. In the former case, scaffolds are required to provide initial support during the tissue formation and then degrade at rate of tissue formation [35]. In the latter, scaffolds are employed to facilitate analysis of tissue formation at cellular level to improve the understanding of the tissue formation process.

Scaffolds have three levels of structural control: macro-, micro- and nano-scale. The macroscale controls properties such as size, shape and overall architecture of the scaffold, allowing developing constructs which perfectly match the geometry of the implantation site. For tissue regeneration purposes, scaffolds are required to match shape and size of the defect to provide support for tissue integration. For biology characterization of cell behaviour, scaffolds need to be accessible to imaging tools and have highly controlled matrix properties. At the microscale, the scaffold architecture can be controlled in term of porosity, interconnectivity, pore geometry and distribution, and topography. Porosity and interconnectivity are among the most important parameters to take into account for cell attachment and survival [19], [36]. Indeed, small pores and low interconnectivity lead to non-uniformly seeded scaffolds, and difficulties in supplying nutrients and oxygen in the inner portion

of the structure. On the other side, large pores may prevent cell attachment due to the low rate of contact between cells and the walls of the scaffold. Pores between 200-400 μm are preferred for bone ingrowth, allowing good seeding efficiency and nutrients supply in the construct [19]. Moreover, features at the microscale define the bulk properties of the material, determining scaffold response to mechanical stimulation and degradation rate, but also factors influencing cells shape and consequently their differentiation [16]. Indeed, it has been shown on 2D surfaces that soft matrices (0.1-1 kPa) mimicking brain tissue are found to be neurogenic, stiffer matrices (8-17 kPa) mimicking muscles are myogenic, and rigid matrices (25-40 kPa) mimicking bone are osteogenic. hMSCs cultured in 3D polycaprolactone (PCL) scaffolds [37] showed increased proliferation and better distribution throughout the constructs when a bimodal porosity was present further underlying the importance of micro and nano features on hMSCs behaviour. Last but not least, microscale and nanoscale patterns can activate different genes modulating cellular behaviours such as neuronal cells polarization [38] and myoblast alignment [39].

2.2.2 Natural polymers and collagen

Natural polymers are derived from proteins or polysaccharides available in nature. Table 2.1 gives an overview of the most common natural polymers employed for biomedical applications regarding drug delivery or tissue engineering purposes [40]. Natural polymers have optimal biodegradability properties preventing inflammation and rejection while their chemical and structural properties can be easily varied to provide the optimal environment enhancing tissue growth. Chitosan, for example, is a cationic polymer obtained from chitin, a natural polysaccharide found in the shell of crustacean. It is biologically renewable, biodegradable, biocompatible, non-antigenic, non-toxic and biofunctional. Preparing chitosan is inexpensive, easy, and its mechanical properties are tuneable by varying the degree of crosslinking between molecules [41]. The same versatility can be found in alginates and in

hyaluronic composites. Moreover, the latter are pH-sensitive allowing a strict control over the release of biomolecules and implying their use for drug delivery applications and cell encapsulations.

Table 2.1: TE applications for natural polymers.

MATERIALS	POLYMER ARCHICTURE	TE APPLICATION	REFERENCE
COLLAGEN	SPONGE	BONE	[42]
	GEL	SKIN	[43]
GELATIN	HYDROGEL	BONE	[44]
		CARTILAGE	[45]
SILK-FIBROIN	HYDROGEL	BONE	[46]
FIBRIN	GEL	VASCULAR TISSUE	[47]
		BONE	[48], [49]
		DRUG DELIVERY	[50]
		SKIN	[51]
		VASCULAR	[52]
ALGINATE	HYDROGEL	VASCULAR	[53]
		CARTILAGE	[54], [55]
		SKIN	[56]
	BEADS	DRUG DELIVERY	[57]
HYALURONAN	GEL	DRUG DELIVERY	[58]
	MEMBRANE	SKIN	[59]

Among natural polymers, collagen is the most commonly used for TE applications as it is the major component of the ECM of mammalian tissues including bone, cartilage, tendon, skin. In the body 29 types of collagen differing in chemical composition can be found, and collagen I is the most abundant [60]. Collagen molecules are formed by three alpha chains (Fig. 2.4a) each composed of thousands of aminoacids based most commonly on the sequence Glycine-Proline-Hydroxyproline. The three α-chains assemble in tropocollagen molecules through covalent bonding of glycine. Tropocollagen assembles in collagen precursors molecules called pro-collagen. Once secreted in the ECM, they self-assemble forming 10-300 nm sized fibrils (Fig. 2.4.b) which agglomerate into 0.5 to 3 μm collagen fibers (Fig. 2.4 c).

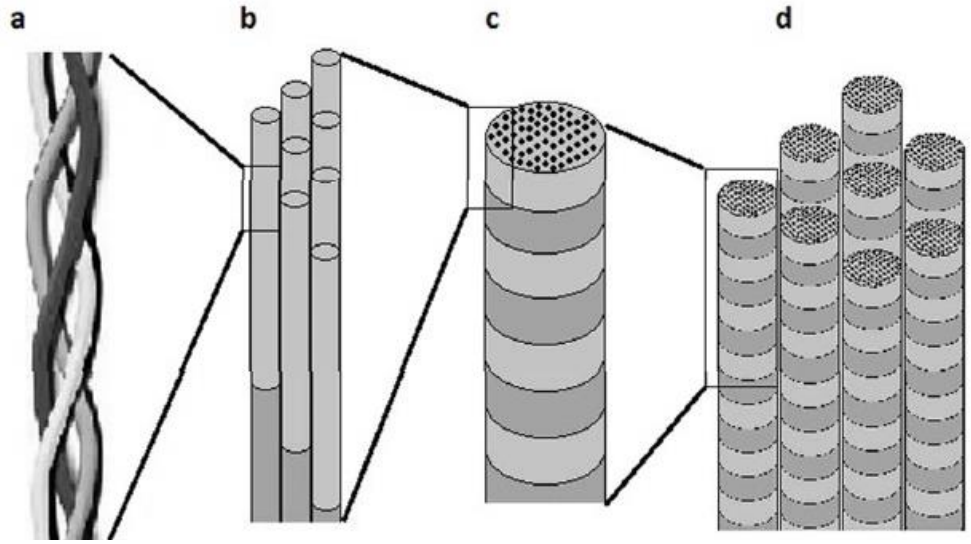

Fig. 2.4: collagen architecture composed of a) three alpha chains bonded together at atomic level and assembling (b) in fibrils and then in (c) fibers which can be wrapped together to organize in (d) fibrous structures. Taken from [60]**.**

Collagen presents high mechanical strength, good biocompatibility, and modifiable mechanical properties by playing with the crosslinking degree between fibers. Normally, collagen is harvested from animal tissues including bovine skin and tendons, porcine skin and rat tail. In order to enable the use of xenogenic collagen, complex enzymatic treatments and filtrations steps are

performed [61] to reduce its immunogenic response. In general, collagen is purified by treatments with pepsin, to eliminate the main antigenic determinants situated in the telopeptine regions, and by increasing the degree of crosslinking to hide the antigenic molecules placed in the alpha chains [62]. Collagen can be further processed by alkaline or acidic procedure developing gelatinous material.

Collagen gel

Collagen gel has been widely investigated as TE constructs [63] because among its advantages, it is easy injectable and has a biocompatible matrix. Collagen gel is generally characterized by a mesh of collagen fibers or molecules dissolved in a solvent and connected through hydrophobic and electrostatic bonds. Collagen gels exist in non-fibrillar or fibrillar form. Non-fibrillar gels are formed by entangled rod-like molecules developing a viscous solution when dissolved in aqueous media. Molecules are much thinner than fibers whose porosity is obviously reduced up to 4 to 30 nm depending on concentration and additives [63]. The resulting gel is highly viscous and its charge can be tuned by varying the preparation method. Methylation produces a net positive charge on the molecules at neutral pH, while succinylation provides a net negative charge. On the other side, fibrillary collagen gel is composed of fibrils organized in a chain-like architecture, developing fibers variable in length and thickness. The behaviour of the gel is temperature-dependent. The gel can be fluidized between 10-25°C, while incubation between 30-37°C confers a compact structure. Beyond temperature, collagen properties can be varied also by covalently modifying the level of crosslinking by exposure to physical or chemical treatments such as UV and gamma irradiation [60] or glutaraldehyde solutions [64]. Collagen gels have found applications in TE in the replacement of skin burns, myocardial tissue, vascular grafts [63]. Despite this, the lack of control over the final mechanical properties of the gel and the necessity to improve the gel strength for load bearing purposes in vivo led to the development of new collagenous solid forms such as sponges, sheets and preformed fibers. Among those, sponges are the most

interesting as they maintain the porous 3D structure typical of biological niches. Sponges are systems obtained from lyophilisation of collagen solutions whose porosity depends on temperature and speed of the freezing process before lyophilisation, and pH of the collagen solutions. Low temperature (-80°C) produces homogeneous small pores of about 15 μm, while higher freezing temperature (-20°C) provides larger and less homogeneous pores ranging between 25-110 μm. Moreover, it was found that the lower the pH is, the smaller the pores are [62].

2.2.3 Synthetic polymers and 3D scaffolds fabrication

2.2.3.1 Synthetic polymers

Synthetics polymers (Table 2.2) were employed in the TE field during the past years finding applications in bone, cartilage as well as skin repair [65]. Synthetic polymers are particularly appealing, not only because their biodegradability rate can be easily tuneable, but also because it leads to the production of waste molecules well-tolerated by the host body, preventing immunorejection. The degradation rate of a polymer can be easily tuned by varying configurational structure, copolymer ratio, crystallinity, molecular weight, morphology, amount of residual monomer, porosity and site of implantation. Good biocompatibility is observed in polyesters whose erosion products are glycolic or lactic acid, ultimately expelled as carbon dioxide and water by the respiratory system. However, polyglycolic acid (PGA) and poly-anhydride scaffolds have low molecular weight, resulting in a structure with poor mechanical properties and undergoing fast degradation [66]. Moreover, if the degradation rate of glycolic acid-based scaffolds is not optimized, a local increase in acids concentration occurs in the implant site, damaging the surrounding tissue. For this reason, polylactic acid (PLA) is preferred for biological applications. Not only it is highly hydrophobe and resistant to hydrolytic attack but it is also more easily metabolized by the body than the

other enantiomers of the same family. Copolymers of PGA and PLA show different properties depending on the ratio of each compound used in the fabrication process. The copolymers PLGA used in bone repair was shown to be biocompatible, non-toxic, and non-inflammatory, considered safe for use as replacement implants in musculoskeletal tissue [66].

Table 2.2: TE application for synthetic polymers

MATERIALS	TE APPLICATIONS	REFERENCE
PLA	BONE	[67]
	BONE	[68]
	CARTILAGE	[69]
	BONE	[70]
PGA	CARTILAGE	[71]
	BONE	[68]
	SKIN	[72]
	BONE	[73]
	CARTILAGE	[74]
PA	ORTHOPAEDIC	[65]
PCL	CARTILAGE	[74]
	BONE	[75]

Polycaprolactone (PCL) is a semicristalline polyester with glass transition temperature at -60°C and low melting point between 59°C and 64°C. It degrades at lower rate than PLA. It is prepared by a ring opening

polymerization of the cyclic monomer ε-caprolactone. Homopolymers present a high degradation varying with molecular weight and were shown to be non-toxic and biocompatible [76]. The degradation rate, porosity, interconnectivity and mechanical properties of polymeric scaffolds are strictly related to the processes employed for the fabrication.

2.2.3.2 Polymeric scaffolds and common manufacturing techniques

In order to achieve the desired characteristic at the macro-, micro- and nano-scale different techniques can be employed in the fabrication process [77]. For the creation of porous materials, the most common techniques involve solvent casting, particulate leaching and freeze-drying processes. Solvent casting followed by particulate leaching is the most common technique for its simplicity, and strong control over pore size and interconnectivity of the resulting structure. It consists in mixing a water-soluble salt with a biodegradable polymeric solution in a container of desired shape followed by solvent evaporation.

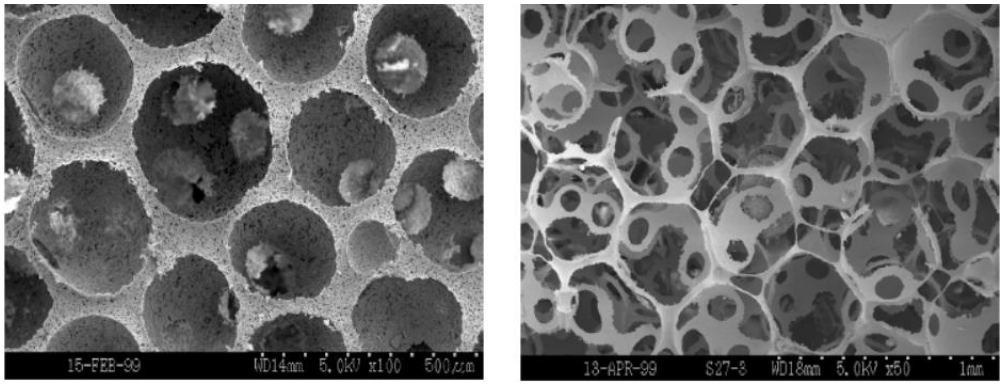

Fig. 2.5: PLLA scaffold prepared using different particles size. Taken from [77]**.**

Afterwards, the salt particles are leached by dissolving them in the appropriate solvent [77]. Pore size and interconnectivity can be adjusted by choosing

appropriate salt particles and varying the salt/polymer ratio to obtain constructs with different geometrical properties (Fig. 2.5). The dimensions of scaffolds created by this technique are restricted to a range of 0.5 to 2 mm because of the difficulties related to remove salt particles and enhancing nutrients diffusion in the inner of the scaffold [78]. The same drawback affects the production of freeze-dried gelatines. In this case, highly porous structures are formed by rapidly cooling the salt-polymer-solvent emulsion to lock the liquid state, and then the solvent and the water are removed by freeze drying. The resulting scaffolds were found to reach up to 90% porosity with closed pore size of 20-200 μm (Fig. 2.6a) [79].

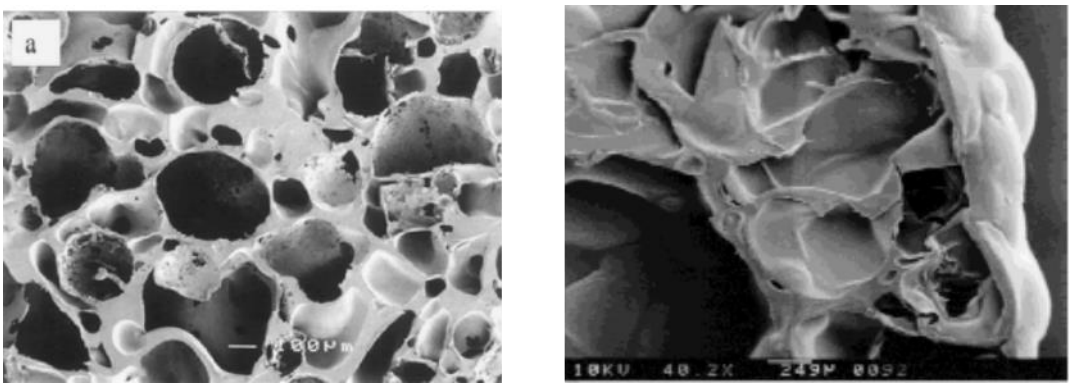

Fig. 2.6: (a) PLLA scaffolds prepared by freeze drying [79] **and (b) PLGA scaffolds prepared by gas foaming. Taken from** [80]**.**

The use of solvents can affect the biocompatibility of the scaffolds due to residual compound left in the structure. This problem can be overcome by the gas foaming approach allowing the fabrication of highly porous polymeric foams employing carbon dioxide as bubble forming agents. The procedure consists in saturating the solid polymer by high pressure CO_2 exposure and then in rapidly decreasing the pressure. This would lead to the nucleation and growth of CO_2 bubbles responsible for the formation of pores. This technique was made to develop, for example, polymeric sponges with porosity down to 100 μm size. The main drawback of this technique is related to the formation of closed pore structures with just 10-30% of interconnectivity (Fig. 2.6b) and

poor mechanical properties [70]. Improvement in the mechanical properties can be observed in other techniques involving phase preparation steps and allowing to tune pore morphology and mechanical properties by varying polymer, solvent, concentration of the polymer solution and phase separation temperature [77]. Although mainly limited to the development of 2D structures, an example of phase separation techniques is the electrospinning method, currently involved in the fabrication of fibrous polymeric scaffolds. Electrospinning consists in applying an electric field to control the formation and deposition of polymer fibers onto a target substrate. A polymer solution is injected with an electrical potential to create a charge imbalance. At a critical voltage, the charge imbalance begins to overcome the surface tension of the polymer solution to form an electrically charged jet directed toward the target. This electrospinning technique can fabricate fibrous polymer scaffolds in a sheet-like shape with fiber diameters ranging from several microns down to hundreds of nanometres [81].

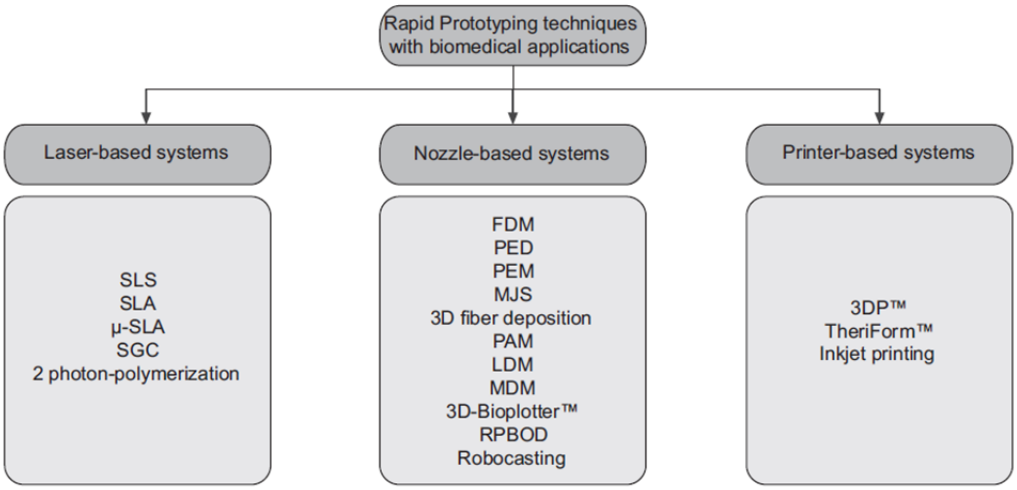

Fig. 2.7: Rapid prototyping techniques for biomedical applications. Taken from [82]**.**

Rapid prototyping emerged with the development of manufacturing industries. It enables the realization of highly interconnected structures and control over geometrical micrometric features. Rapid prototyping can be split in three main

branches called laser-based, nozzle-based or printer–based systems, depending on the working principle [82]. Laser based systems design predefined patterns on photolinkable prepolymers by applying high energy lasers. An example is the process of stereolithography (SLA) [39] consisting in (1) a reservoir containing the photocurable resin; (2) a laser source (normally UV) connected to a system controlling the movements on the beam in the XY plane; and (3) a platform moving on the Z axis (Fig. 2.8). This technique can follow either the bottom-up or the top-down approach and consists in depositing a layer of material on the top of the next by moving a platform toward the light source. The main difference between the two approaches consists in the position of the light source which is located respectively at the top or at the bottom of the reservoir containing the resin to cure. A further improvement of SLA was achieved by the introduction of μSLA [83] allowing the control of features at micro scale.

Nozzle-based systems are generally based on melting polymers at elevated temperatures, which is undesirable from the perspective of scaffold bioactivity [82]. However with the development of the new technologies, systems using micro-syringes or deposition modelling were developed to avoid drawbacks related to the use of high temperatures.

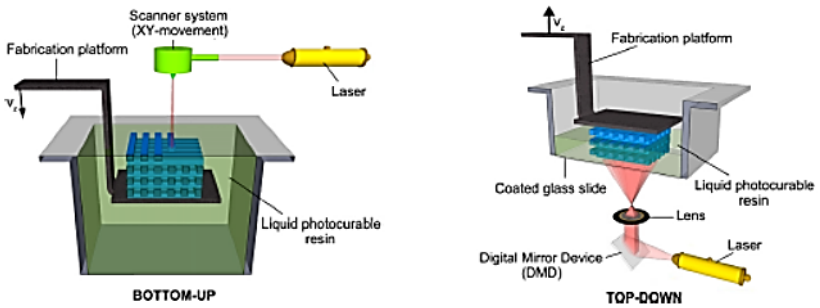

Fig. 2.8: Scheme representing the bottom-up and top-down approach followed by the SLA. Taken from [82]**.**

For example, the Pressure Applied Micro-syringe process (PAM) employs a glass capillary syringe moving on the vertical plane and depositing material on

a platform while the Low temperature Deposition Modelling (LDM) consists in a liquefying process of the materials by applying temperatures below 0°C. The LDM technique is particularly worth to mention as it finds application in the development of bioactive scaffolds by involving multiple nozzles dispensing different materials simultaneously [84]. A further improvement in the realization of scaffolds suitable for TE was made by the arrival of 3D-plotters fitted with a computer- controlled syringe moving in the three planar directions and releasing material on a stationary platform. The key features of this process are the ability to plot viscous materials into liquid (aqueous) solutions with the same density, and the possibility to process thermally sensible biomolecules and even cells [85]. Among the main advantages, this technique supports the continuous deposition of micro-strands or discontinuous dots, providing high degree of control over the entire fabrication process. Moreover, strand thickness can be modulated varying viscosity, deposition speed, tip diameter or pressure. Despite the versatility, 3D plotting of scaffolds leads to smooth surfaces, requiring further functionalization to enhance cellular attachment.

Printer-based systems can be used to fabricate parts in a wide variety of materials, including ceramic, metal, metal-ceramic composite and polymeric materials. The workflow is formed by three steps. In the first step, the powder is lifted while fabrication platform is moved toward the bottom where the powder lies (Fig. 2.9).

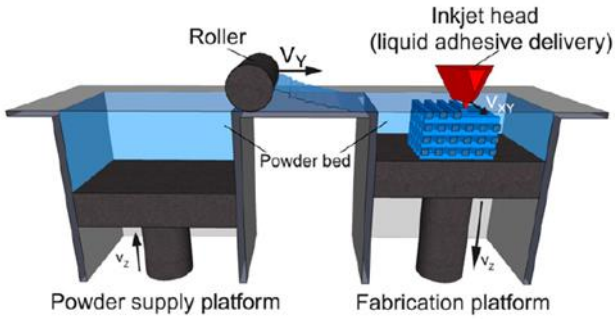

Fig. 2.9: 3D printing working principle. Taken from [82]**.**

During the second step, a roller spreads the powder in a thin layer and removes the excess of material. Eventually, an inkjet print head releases a liquid compound working as bonding agent between adjacent particles of powder. Once the process is finished, any excess of powder is further removed by washing with solvents. A key requirement for the employment of such system in the development of scaffolds for TE purposes is the availability of biocompatible powder-binder systems [86]. The powder can be pure or surface-coated and also the use of multiple powders in the same application is permitted. The inkjet printing uses the same principle and workflow presented for the 3D printing but the powder is substituted with a liquid.

2.2.4 Cell source

In order to obtain versatile scaffolds able to progressively modify their architecture and eventually perfectly integrate into the healing site, cells are employed as active compound. The ideal scenario would be having access to a source of mature cells coming from the target tissue and able to produce high quantities of extracellular matrix. For bone regeneration, osteoblasts are the most obvious choice as they can be directly harvested from the patient (autologous cells), thus avoiding the immunologic effects. As the number of cells harvested from the tissue and their expansion rate are relatively low [23], other cell sources are required, especially in event of multiple surgical intervention. A promising alternative employs stem cells as they present high proliferation capabilities, multi-lineage differentiation and self-renewal properties. Stem cells are able to express different phenotypes depending on their stage of differentiation. The most primitive cellular form derives from the zygote which divides in blastocyst developing the embryos, and the Inner Cell Mass (ICM). The latter is formed by embryonic stem cells (ESCs), pluripotent cells with unlimited self-renewal capabilities and able to differentiate towards every lineage.

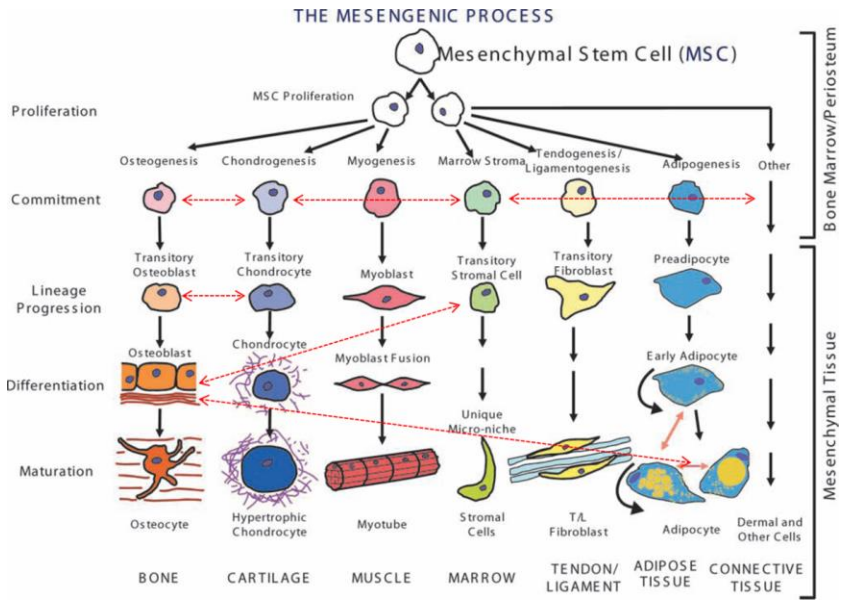

Fig. 2.10: differentiation pathways followed by cone marrow progenitor stem cells. Taken from [87]**.**

The development of a method able to directly differentiate ESCs toward a defined phenotype and obtain a fully functional and perfectly integrated tissue is still ongoing study [88]. ESCs may indeed be tumorigenic because of their unlimited proliferative capabilities, and immunological compatibility issues may also arise [89]. ESCs lead to the development of adult stem cells (ASCs) whose differentiation capabilities are narrowed to a limited amount of cell lineages depending on their embryonary origin (Fig. 2.10). So far, ASCs were found in bone marrow, fat, muscles, brain and skin [23]. Bone marrow stem cells (BMSCs) acquired increasing interest [23] as they can differentiate toward multiple lineages such as bone, cartilage, muscles, tendons or connective tissue (Fig. 2.10). BMSCs present also other important properties beside their regeneration potential such as high proliferation rates and reduced spontaneous differentiation with increased number of passages [23]. Moreover, they secrete a large number of immunosuppressive molecules promoting the use of allogenic cells. However, the low concentration of BMSCs makes the isolation process very elaborate and time consuming. Moreover, their differentiation potential was shown to vary depending on age of subjects [87]. Overall, BMSCs are considered more advantageous compared to ES for

bone tissue purposes and are already in clinical trials for clinical applications [90]. Eventually, other cell sources of mesenchymal origin for bone regeneration applications were found in fat tissue. Adipose derived stem cells (ADSCs), are under increasing consideration as they demonstrate to undergo osteogenesis in vitro and in vivo and can be easily isolated from visceral or subcutaneous fat in a relatively high amount [91]. On the other hand, mesenchymal stem cells lose their differentiation capability and show reduced proliferation after long term use demanding for a more stable cell source. Currently cells holding a great potential for tissue engineering purposes are the human embryonic stem cell-derived mesodermal progenitor (hES-MPs) which were demonstrated to induce higher tissue formation [21] compared to adult stem cells and to be more stable and less tumorogenic [20], [92] compared to ESC.

2.2.5 External factors influencing cell activities

Once expanded to the desired amount, cells are seeded on scaffolding material and undergo external stimulations to drive their differentiation toward a defined pathway. As a consequence of the sensed stimuli, cells activate biochemical pathways defining the functional properties of the resulting engineered tissue [93]. Among external stimuli having a high impact on cell commitment, chemical stimulation was found to be particularly promising. Fibroblasts growth factors (FGF) showed to increase self-renewal and to maintain cell multi-lineage differentiation potential. Transforming growth factors (TGF) and serum free medium induce chondrogenesis, while bone morphogenic proteins (BMP) and dexamethasone, the most relevant chemical factors inducing osteogenesis, are already employed for clinical treatments such as spinal fusion and long bone fractures [94].

In the last two decades, the use of external mechanical stimuli on cell differentiation has become more and more common as evidence has shown how mechanical stimulation can greatly influence the cell behaviour [95], [96].

Hydrostatic pressure, fluid shear stress, mechanical strain and electric fields generated by interstitial flow passing on charged bone crystals trigger variations in the cell behaviour [1]. Studies performed on differentiated bone cells showed that continuous hydrostatic pressure decreases collagen production by osteoblasts, while intermittent compressive force enhances osteoblasts activity and decreases osteoclasts resorption [1]. Also chondrocytes behaviour is modulated by the type of regime applied. Indeed, constant hydrostatic pressure induces chondrogenesis differentiation, while intermittent strain leads to hypertrophy [1]. When bone is loaded by tension, compression or torsion stimuli, the interstitial fluid is moved toward regions of low pressure to come back when the load is removed, inducing an oscillatory fluid flow of 0.8 Pa up to 3 Pa *in vivo*. This regime results in a dramatic amplification of local strains in proximity of the osteocyte processes [30], [97]. Osteocytes are able to sense these variations in the interstitial fluid as demonstrated by multiple studies where shear stress triggered mechano-activated biochemical pathways regulating nitric oxide production in osteocytes [1], [98]. Compared to other bone cells, osteocytes are more responsive also to mechanical stimuli and are believed to play a role in regulating the activity of osteoblasts and osteoclasts [99]. Mechanical stimuli were shown to regulate calcium deposition with osteoblast cells increasing mineralization as a result of cyclic loading [100], [101].

2.3 A REVIEW OF BIOREACTORS AND MECHANICAL STIMULI

2.3.1 Bioreactors for tissue engineering

In order to find a correlation between mechanical forces and differentiation, a controlled micro mechanical environment is provided by advanced scaffold

designs combined with complex bioreactors [102]–[104]. Bioreactors facilitate the monitoring and control of biological or biochemical processes undergoing within the scaffold during the bone forming process. Bioreactors are generally adapted to fit within an incubator which controls the external environment and maintains constant physiological conditions: 37°C temperature, 5% CO_2 concentration and 99% humidity. A bioreactor suitable for cell culture purposes must be inert to the harsh chemistry of the biological environment preventing corrosion and toxic reactions. Moreover, the diffusion limit and uniform distribution of cells in the scaffolds are key factors to consider in the development of functional tissue. With this purpose, bioreactors aim to maximize the supply of nutrients and oxygen to cells seeded in internal areas exceeding the diffusion limit distance of 100-200 µm [105] to maintain their viability. Systems able to provide exchange of substances within the scaffold can be also employed during the seeding phase to increase seeding efficiency and uniform distribution of cells [106]. Current techniques use convection of medium by perfusion, centrifugation and spinner flasks [102]. Moreover, bioreactors can be designed to apply shear strain forces, mechanical strain or pulsed electromagnetic fields with a high control over the stimuli to reproduce the biological environment, and clarify the relationship between mechanical stimulation and tissue formation.

2.3.2 Cell mechanotransduction

As a matter of fact, bone is constantly under loading conditions arising from the daily activities. Deformations which occur in bone are defined in strains, where 1000 microstrains equal to 0.01% change in length compared to the initial length. Vigorous exercise induces bone strains up to 1000 microstrains which was associated with bone mass increase in humans [97].

Recently, the impact of mechanical stimulation on bone cells is under investigation to define a relationship between applied mechanical strain and cellular differentiation. The key cues to consider to better understand the effect

of mechanical stimuli on cell commitment are (1) the mechanical properties of cells themselves, depending on the forces applied by the cytoskeleton and the contractile components on the surrounding environment; (2) how the stiffness of the surrounding environment is sensed by cells through durotaxis, affecting the lineage differentiation; and (3) how external mechanical stimuli generated by gravitational action, muscles and other cells are translated into biochemical processes driving cell differentiation. In skeletogenesis, the differentiation of stem cells toward the osteogenic or chondrogenic pathway is regulated by many external factors [96][96],[107] influencing cytoskeletal organization, shape, motility [108], [109] and consequently cellular functions. Depending on the surrounding mechanical environment, different signalling pathways are activated inside the cell controlling the expression of transcription factors [110]. For example, the Wnt/ß-catenin or Rho/ROCK signalling pathways are known to play a crucial role for the control of cell commitment towards the osteogenic or chondrogenic pathway through the expression of Sox9 and Runx2 at early stage of differentiation [96]. Sox9 is put alongside with expression of collagen II, TGF and glycosaminoglycan (GAG) genes and identify differentiation toward the chondrogenic lineage, while Runx2 identifies osteogenic differentiation and induces expression of collagen I and non-collagenous proteins such as alkaline phosphatase (ALP), osteocalcin (OCN) and osteopontin (OP). ALP is an early marker for osteogenesis, while OCN and OP are normally expressed at late stage of differentiation and help regulating the size of mineral crystals deposited by mature osteoblasts [22].

2.3.3 Bioreactors for fluid flow induced cell differentiation

The first step when developing an engineered bone tissue is to achieve a homogeneous cellular distribution and provide good exchange of nutrients and oxygen within the scaffolding material. Due to the three dimensional architecture of novel scaffolds, static seeding is no longer an optimal method as it leads to a low seeding efficiency, cellular inhomogeneous distribution and low diffusion of fluids or gases in the internal regions causing cell apoptosis. In

order to overcome these limitations, different systems were considered among which spinner flask (SF), rotating wall vessel (RWV), biaxial rotating (BXR) and perfusion bioreactors. Compared to the static methods where molecules exchange occurs by diffusion, these systems are more efficient by inducing a convective flow and thereby enhancing cell attachment, proliferation and differentiation.

2.3.3.1 Rotating bioreactors

SF bioreactors consist in a vessel provided with side arms for gas exchange and a stirring mechanism able to create a flow though the culture media (Fig. 2.11a). In order to avoid scaffold fluctuation, pins are connected to the top lid for allocating samples. SF bioreactors were shown to increase the seeding efficiency compared to static methods [111] and to induce osteogenic differentiation though the expression of ALP and OCN, and increased calcium deposition [112]. RWV bioreactors consist in a hollow cylinder provided with an external chamber for scaffolds allocation and working as medium reservoir, rotating along the radial axis (Fig. 2.11b). The laminar flow generated by the rotating motion induces shear stress on cells, preventing their detachment, and partially overcomes the diffusional limitations encountered with static and SF seeding method. However, the RWV approach leads to lower cell number and decreased matrix production than SF because scaffolds seeded by RWV are free to float inside the chamber hitting against the walls of the rotating vessel. Solutions include the use of (1) rotating bed bioreactors where scaffolds are fixed to the cylindrical structure and moved alternatively between gas and liquid phase [113]; (2) scaffolds with lower density than water [114]; or (3) a rotation rate able to prevent contact with the walls [102]. According to a recent study [102], the gold standard seeding performance is given by BXR consisting in a spherical chamber, pins for scaffold allocation, a medium reservoir and a perfusion system (Fig. 2.11c). The spherical chamber is able to rotate simultaneously in two perpendicular axes overcoming diffusion problems observed with SF. Furthermore, it has apposite spaces for scaffolds allocation

preventing cell detachment phenomena observed in RWV. Moreover, BXR show all the advantages of the perfusion systems while it overcomes, at the same time, the “cell washout” phenomena observed in perfusion bioreactors.

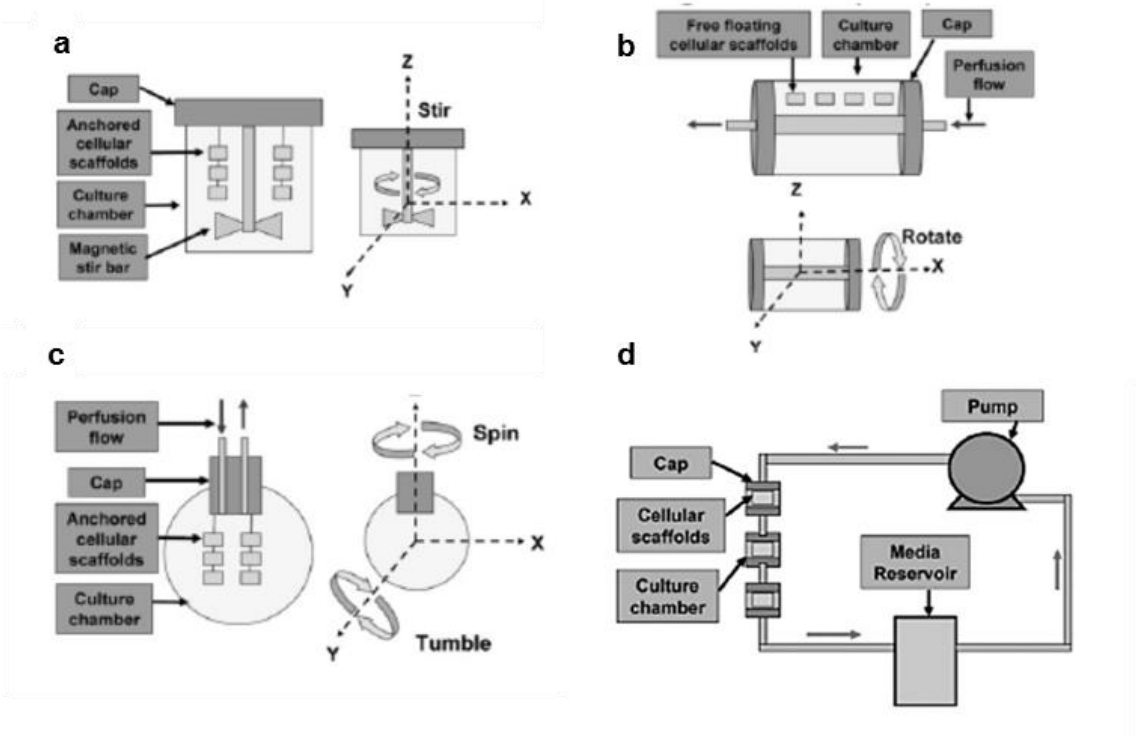

Fig. 2.11: Bioreactors for seeding and differentiation of MSCs due to effect of fluid flow. Spinner flask (a) and rotating wall vessel (b) bioreactors provide rotation toward an axis while the biaxial rotating wall vessel (c) systems allow rotation in two directions providing homogeneous shear stress distribution in the culture chamber. Closed loop perfusion bioreactor (d) scheme employing a serial multichamber configuration. Taken from [102]**.**

Indeed not allocating the scaffold directly in the flow stream prevented cell to detach from the side of the scaffold facing the oncoming flow, resulting in higher homogeneous distribution of cells. BXR increase considerably cell attachment, proliferation, molecule diffusion and osteogenic differentiation compared to SF, RWV and even perfusion bioreactors working in optimal conditions [102].

2.3.3.2 Perfusion bioreactors

In the last decade, the attention turned toward perfusion bioreactors (Fig. 2.11 d) composed of a chamber fitting the geometry of the scaffold, a medium reservoir for supply of nutrients and a waste reservoir. Some perfusion bioreactors are closed loop and do not use a waste reservoir but nutrients are continuously pumped into the system [115]. Perfusion bioreactors force the fluid through the entire scaffold allowing cells to reach the interior of the structure and enhancing homogeneous distribution and optimal supply of gases and nutrients. The two main challenges developing perfusion systems are related to prevent air bubbles formation and to guarantee a solid anchorage of the scaffold. Air bubbles are the main cause of local stress variation as air blocks the passage of fluid, causing an increase in the local flow rate. As a consequence, an inhomogeneous distribution of stresses arises inside the culture chamber, which might compromise the seeding process.

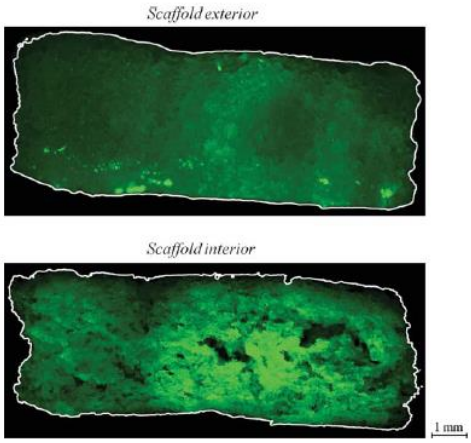

Fig. 2.12: Seeding of scaffolds by perfusion. Fluorescence staining showed uniform distribution of cell either in the exterior or in the interior of the structure. Taken from [116]**.**

A similar effect is observed when scaffolds are not completely anchored to the walls of the bioreactor chamber. In this case, void areas arise and become the preferred pathway for fluid to flow. The shear stresses generated by the fluid

flowing through the scaffold are not only dependent on the inlet flow rate but also on the scaffold pore size and interconnectivity [117]–[119]. Despite the difficulties in developing efficient perfusion systems, a number of studies have investigated the effect of perfusion flow on cell attachment, proliferation, matrix production and differentiation. While turbulent flow caused mainly cell detachment or programmed cell death due to the high shear stress [120], laminar regimes such as continuous, oscillating and pulsating flow led to satisfactory results and increased performances compared to static conditions (Fig. 2.13a). Koch et al. demonstrated the effect of velocity and number of cycles on cell attachment applying a perfusion flow oscillatory in nature. Velocities up to 5 mm/s were necessary to obtain uniform cell distribution in the interior of the scaffold (Fig. 2.13b) but the main effects on seeding efficiency were elicited by the number of cycles applied rather than the velocity used.

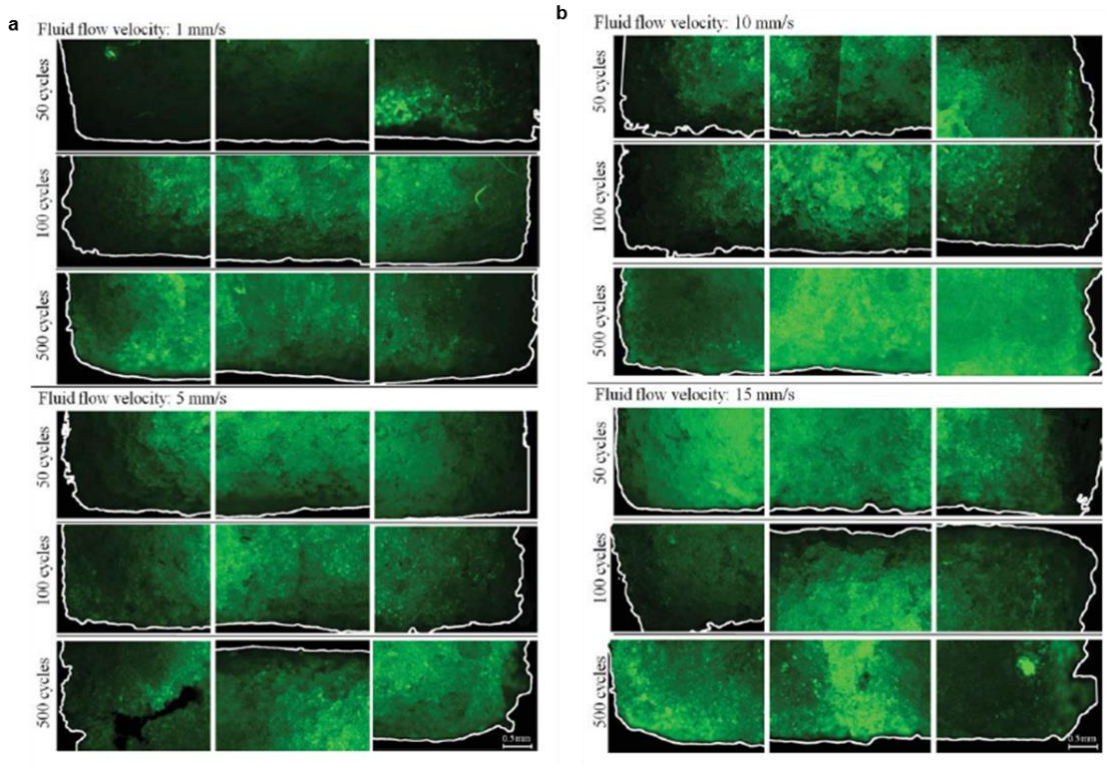

Fig. 2.13: Effect of velocity and number of cycles on cell attachment in the interior of the scaffold. Taken from [116]**.**

Surprisingly, a lower number of cycles led to higher seeding efficiency percentages up to 51%, suggesting the dual role of shear stress in promoting cell attachment just at the early stages of the seeding process and causing cell detachment if applied for longer periods of time. Although fluid velocity of fluid flow had no role on seeding efficiency, the viability of cells on the exterior of the scaffold was found to be affected by increased cell apoptosis with increasing shear stress (Fig. 2.14). These outcomes underline the need to define the optimal conditions enhancing uniform cell distribution, high seeding efficiency and cell viability

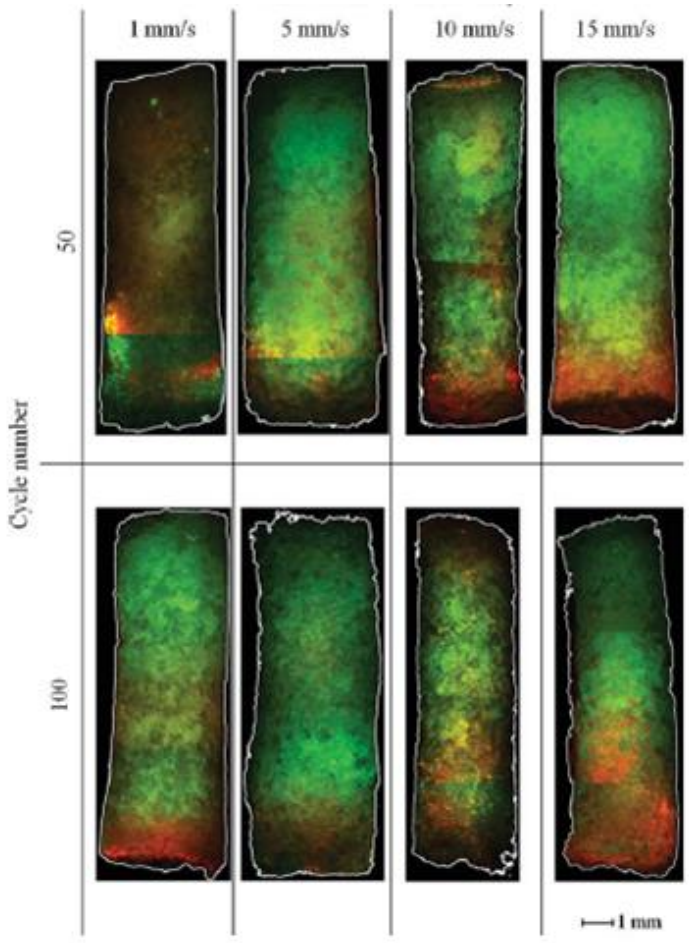

Fig. 2.14: Cells distribution on the exterior of the scaffold employing different velocities and number of cycles. Alive cells are shown in green while apoptotic/dead cells are shown in red. Taken from [116]**.**

. Compared to static seeding, continuous unidirectional flow of cell suspension was also demonstrated to increase cell attachment and distribution [121], [122], ECM production and osteogenic differentiation [116], [123]–[126]. Beyond guaranteeing a good distribution of cells, a laminar flow oscillating in nature mimics the in vivo conditions applied to bone cells, and stimulates calcium production in osteoblast-like cells [116] and human bone marrow stromal cells [127]. However, pulsating flow was found to be the most efficient in enhancing mineralization [128], [129], inhibiting cell apoptosis [130] and regulating matrix deposition [98], [131]. The main drawback of perfusion bioreactors is the high amount of reagents needed, which has led to the development of perfusion microfluidic systems.

Microfluidic systems are easy to develop, require a low amount of reagents and, above all, allow to perform many experiments in parallel [132]. The new generation of “lab on a chip” microfluidic devices allow to simultaneously apply identical and reproducible experimental conditions on multiple samples and it has already found application in the development of in vitro vascular implants [133]. Polydimethylsiloxane (PDMS) is the most commonly used material for microfluidic perfusion culture systems since it is non-cytotoxic, autoclavable, gas permeable, flexible, inexpensive and easy to mold. PDMS has low autofluorescence making it suitable for fluorescence imaging operation. Moreover, it is transparent to light finding application for optical imaging [134]. For cellular culture purposes, most common systems consist in a glass-PDMS configuration [135] as PDMS can be easily covalently bonded to glass substrates by surface activation through gas plasma treatments [136], [137]. Microfluidics systems made of glass-PDMS were applied as support for 2D and 3D culture studies in investigating the differentiation toward muscular tissue [138], the effect of different flow rates on cells morphology and proliferation [139], liver toxicology [140], cell seeding and monitoring [141], and comparison between cell lineages response to hydrostatic pressure [142]. The main challenges in creating a microfluidic system are the fabrication of a robustly sealed channel and the prevention of bubble nucleation [134]. In general, the fluid flow in a microfluidic perfusion system has multiple roles as it can be employed for cell seeding purposes, for nutrients and gases delivery,

or for the transport of molecules probing cells to perform cellular assays to test for cellular activities or viability [143]. Normally fluid perfusion is controlled by external pumps and valves and can employ multiple inputs. Cell seeding needs optimization as low flow rate leads to cells settling in reservoir, culture chamber and tubes while high shear stresses compromise cell viability and have detrimental effects. Cell settling is normally overcome by minimizing the distance between cell reservoir and culture chamber, employing a viscous carrier able to decrease the settling rate, or by rotating the reservoir [134].

2.3.4 Bioreactors for mechanically induced cell differentiation

2.3.4.1 Common bioreactor types

Common bioreactor systems for mechanically induced differentiation include a vessel containing the culture media, spaces to allocate scaffolds, and clamping parts aiming to apply tension or compression stimuli through an external computer control. In simple stretching devices, the extremities of the scaffold are anchored to grips connected to external automatic controls which moves on a plane transmitting the displacement to the structure (Fig. 2.15a). Four-point bending devices (Fig. 2.15b) are another widely used and fairly simple configuration. The working principle consists in placing the structure on two vertical pillars and applying a force perpendicular to the plane of the structure [111]. Both setups allow high control over the mechanical stimuli employing load and displacement sensors, actuators and an external control interface. Four-point bending systems equipped with micromanipulators and cameras were also used to transmit tension as well as compression stimuli though a piezoelectric actuator bending when voltage was applied [103]. Upon application of voltage, a piezoelectric layer shrunk while the other stretched, bending the actuator and transmitting the resulting displacement to the sample (Fig. 2.15c). When the polarity was inverted, the actuator bent on the other

direction, enabling the testing of cell behaviour under both stimuli on 2D collagen layers.

The addition of multiple chamber configurations allows high throughput studies and increases repeatability and reproducibility of the tested conditions [144]. Recently, novel bioreactors are developed to fit in incubators and maximize sterile conditions such as the BOSE Electroforce® systems (Fig. 2.15d) already employed in studies on scaffold mechanical characterization [145], hMSCs differentiation [104] and vascularization of bone grafts [146]. The biodynamic chamber works as a bioreactor providing (1) sterile and isolated environment; (2) samples immersed state preventing drying phenomena; (3) high controlled tension or compression stimuli and simultaneously fluid shear stress by an external pumping system; and (4) multiple motors configuration for parallel experiments.

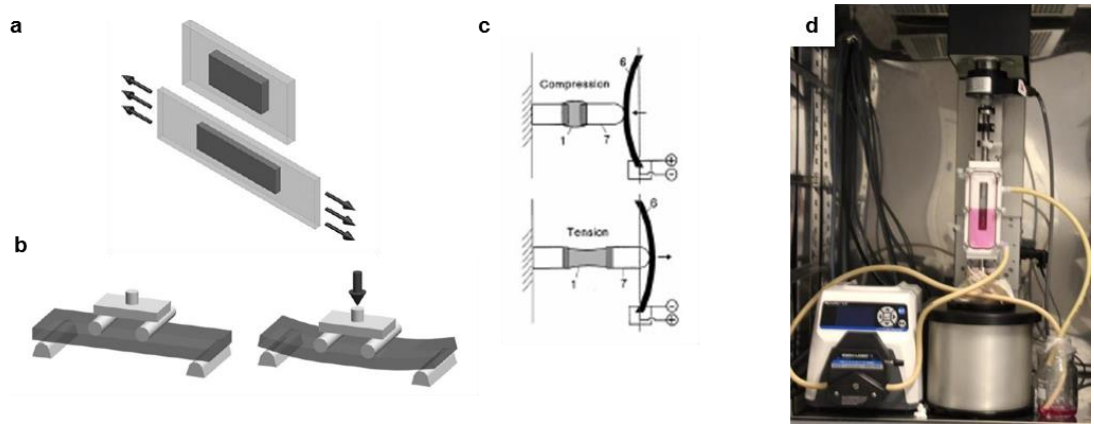

Fig. 2.15: Stretching principle to apply tension stimuli (A) and four-point bending system (B) while applying deformation on 2D seeded substrates (taken from [113]**). Four point bending system equipped with piezoelectric actuators (C) able to exploit tension and compression stimuli by varying the external voltage applied (taken from** [103]**) and BOSE Electroforce ® equipped with culture chamber form mechanicals stimulation and simultaneous perfusion of media.**

2.3.4.2 Mechanical load and cell commitment

The effect of tension on mesenchymal stem cell osteogenic commitment was studied on 2D surfaces or 3D structures by employing stretching devices or four-point bending systems (2.3). In 2D studies MSCs behaviour was investigated on silicone membranes coated with collagen, showing increased osteogenic differentiation through synthesis of BMP2 and collagen 1 in multiple studies [147]–[149]. Haudenshild et al. demonstrated the dual effect of applying tension and compression on 3D alginate phosphate scaffolds seeded with hMSCs [150]. Volume, surface area, skeletal length and diameter of cells were quantified by confocal images and revealed variation in cell morphology depending on the stimuli received. Compression stimuli led to round and shorter cells while tension led to more elongated and spread cells compared to controls. Moreover, gene microarray screening and RT-PCR analysis showed upregulation of a wide range of osteogenic genes and downregulation of chondrogenic genes in samples undergoing tension stimuli. The opposite expression profile was characteristic in samples undergoing compression. Compression stimuli were mainly investigated on hydrogels because of their remarkable properties such as biocompatibility, biomimetic, easy moulding and transmission of uniform distribution of stresses through the structure. Last but not least, accessibility through fluorescence and optical light allows not only the investigation of cell viability to the exterior of the scaffold but also to monitor cell conditions within the core [151]. For example, cell and collagen fibers alignment after static or cyclic compression of collagen gel scaffolds embedding hMSCs were monitored and characterized in multiple studies by real time acquisition. Both static or cyclic loading conditions were shown to affect cell alignment inducing cells to orient parallel to the direction of the applied stress [152]. However, collagen orientation, GAG and cellular metabolism were unaffected, suggesting that mechanical loading alone have no effect on the collagen remodelling action performed by hMSCs.

Table 2.3: Studies on differentiation of stem cells following mechanical stimulation on different scaffolds.

CELLS	SCAFFOLDS	MEDIA	PARAMETERS	DIFFERENTATION	REFERENCES
STRETCHING DEVICES					
MSCs	Silicon membrane	-	0.5 % strain 0.17 Hz 4 hours/day 3 days/week	Osteogenesis↑	[147]
			4 and 8% strain 0.5 Hz 4h/day	Osteogenesis ↑	[148]
		Osteogenic	0.3% strain 1 Hz 15 mins/day	Osteogenesis↑	[149]
			2 or 8% strain 1 Hz 2h/day 3days/week	Strain 8%: Osteogenesis↑	[153]
FOUR POINT BENDING					
BMSCSs	Partially demineralized bone	Osteogenic	0.2mm 0.2 Hz 250 cycles/24 hours	Depending on dexamethasone concentration: Osteogenesis↑	[111]
Osteoblasts	Collagen gels	-	0.3% strain Low VS broad frequencies	Low amplitude, high frequencies: Osteogenesis ↑	[154]
MSCs	Collagen gels	-	10% strain 1,0.5,0.1 Hz 1h/day 7days/week	Chondrogenesis↓ Osteogenesis↓	[152]
Porcine MSCs	Agarose hydrogels	Chondrogenic VS untreated	10% strain 1Hz 1h/day 5 days/week	Supplementing chondrogenic media: Chondrogenesis ↑	[155],[156]
OTHER SYSTEMS					
Porcine MSCs	Agarose hydrogels	Chondrogenic	10% strain 1 Hz 1h/day 5 days/week	Confined compression: Chondrogenesis ↑	[104]
MSCs	Poly ethylene hydrogels	Chondrogenic VS untreated	10% strain 1Hz 1,2,2.5,4 hours/day	Chondrogenesis ↑	[88]
	Fibrin Poly-urethane 3D scaffolds	Chondrogenic	15, 20, 30% strain 0.1, 1 Hz	High strain, high frequency: chondrogenesis ↑	[157]
	Poly ethylene hydrogels	-	15% strain 0.3 Hz 4 hours/day 14 days	Chondrogenesis↓ Osteogenesis↓	[158]
	Agarose hydrogels	-	9% strain 0.03, 0.15,0.33 Hz 12,54,120 mins/day 3days/week	54, 120 mins: chondrogenesis ↑	[159]

2.3.4.3 Loading parameters affecting cells response

The presence of chemical factors has a high effect in modulating the response of cells to mechanical forces. The osteogenic ability of BMSCSs cultured in demineralized bone scaffolds under cyclic tension was found to be strictly related to the concentration of dexamethasone, varying ALP and OP expression. Absence as well as high amounts of dexamethasone (100nM) led to suppression of osteogenic markers. Similar results were obtained investigating compression stimuli. When coupled with chondrogenic media, mechanical compression increased chondrogenesis gene expression [155]. However, compression forces alone were proved in multiple studies to induce no significant differences in cell phenotype compared to free swelling samples [88], [156].

Amplitude, frequency and duration of the stimuli can play a role in the activation of mechano-transduction pathways [160] and in modulating osteogenic or chondrogenic protein expression. Applying 2% and 8% cyclic tensile strain on MSCs, ALP activity and OCN expression were upregulated when 8% strain was applied regardless of the presence of dexamethasone [153]. Maintaining constant amplitude, frequency was varied and the effect of sinusoidal frequencies (S), broad frequencies (V) and a combination of both (S+V) stimuli was investigated on osteoblasts. OCN was 2.6 fold higher when S+V was applied, other osteogenic markers were upregulated after 4 days from V exposure but no significant differences were noticed by applying S alone [154]. Varying both the parameters Li et al. observed increased chondrogenic marker expression of the TGF family as a result of high strain and high frequency stimulations [157]. Low amplitude high frequency stimuli were shown to produce the same effect as high amplitude low frequency stimuli to activate bone formation [161]. Similar results were obtained in other studies where the duration of the stimuli and its frequency were varied. Long periods of stimulations have no significant difference in driving cell commitment as continuously loaded hMSCs downregulated the expression of both osteogenic and chondrogenic genes [158]. hMSCs are also sensitive to accumulation of

stress as reported by previous studies claiming a stronger chondrogenic commitment associated to high frequency stimuli and prolonged stimulation (54 or 120 min versus 12 min) [159]. Despite the high amount of studies claiming chondrogenic commitment as a result of scaffold compression, short bursts of compressive load were found to activate the same response as dexamethasone elicits on matrix mineralization by hMSCs cultured in polyurethane scaffolds [162]. This suggests the possibility to induce osteogenic differentiation by compression forces within polymeric scaffolds.

2.3.5 Electromagnetic field bioreactors and differentiation

Electromagnetic field (EMF) and pulsed EMF (PEMF) in vivo arise from the piezoelectric effect induced by bone deformation as a consequence of muscular action [163]. EMF stimuli arise in vivo in two ways: (1) as a consequence of postural or walking activities causing displacement in bone and resulting in EMF frequencies ranging between 5 and 30 Hz, and (2) when bone fracture occurs giving rise to a negative potential due to accumulation of negative charges at the injured site [164].

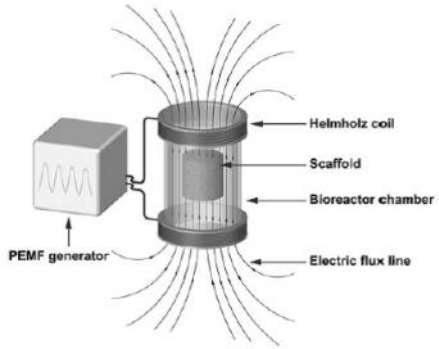

Fig. 2.16: Common design for PEMF bioreactors. Taken from [113]

In the recovery process, EMF and PEMF had a beneficial effect on patients affected by osteoporosis or non-union fractures, decreasing the bone resorption action performed by osteoblasts or accelerating the bone forming process by osteoblasts [165], [166]. In order to observe the effect of EMF and PEMF on cellular conformational changes, proliferation and differentiation, EMF-based bioreactors were developed. These systems consist of two Helmholtz coins hosting a chamber for scaffold allocation and connected to an external EMF generator (Fig. 2.16). Applying continuous stimuli of PEMF was found to have no effect on osteoblasts or BMSCSs proliferation, ALP or calcium content up to day 14 where an increase in calcium deposition occurs in BMSCSs at the expense of proliferation [167]. In other studies employing short resting periods between consecutive stimulations (8 h), EMF increased hMSCs proliferation, viability and multi-lineage differentiation [168]. MEF was found to affect bone progenitor cell proliferation rate depending on their bone differentiation stage (BMSCSs versus osteoblasts) and the presence of osteogenic media [169]. BMSCSs had a higher proliferation rate compared to untreated controls in presence of osteogenic media whereas previously differentiated osteoblasts decreased in cell number compared to untreated controls. Increased ALP and BMP2 were observed at early stages culturing BMSCSs in osteogenic media. Following these findings, studies were performed using mainly BMSCSs culture in osteogenic media to maximize the osteogenic performance (osteogenic BMSCSs). Increased osteogenic markers expression and proliferation rate were achieved by applying PEMF over shorter periods at low amplitude. Osteogenic BMSCSs undergoing 0.13 mT quasi-rectangular pulses at 7.5 Hz for 2 h a day showed higher production of ALP at day 7 and enhanced mineralization at day 28 compared to untreated controls [170]. The effect of frequency on BMSCSs osteogenic marker expression was further investigated at 1mT of EMF by varying frequencies at 10, 30, 50 and 70 Hz. Enhanced proliferation was observed in samples stimulated at 10 Hz, as well as expression of ALP and OCN after a week of treatment. Despite this, enhanced cell viability was observed at 50 Hz together with maturation of osteoblasts after 2 weeks of exposure and extensive matrix mineralization [171]. Similar studies were performed supplementing hMSCs

with chondrogenic media and applying 5 mT sinusoidal EMF at 15 Hz, 4 times a day (45 min every 8 h), over 21 days, demonstrating that sinusoidal low frequency EMF stimulates and maintains differentiation toward a lineage when supplemented with specific growth factors [172].

Chapter 3

GENERAL MATERIALS AND PROCEDURES

3.1 Introduction

This chapter presents a collection of reagents and equipment employed in the project. Moreover, methodologies repeated among studies are here presented to avoid repetitions among chapters following the same procedure. Examples are the static seeding mentioned in Chapters 5, 6 and 7, or the reconstruction of samples by microCT mentioned in Chapters 4, 6 and 7. Here, commonly used protocols related to assay kits, such as Presto Blue, DNA assay and ELISA, are also described in detail. More information about how a protocol described here contributed to a particular study is further explained in the "Materials and Methods" section of each chapter.

3.2 Materials, reagents and buffers

1. Human embryonic stem cell-derived mesodermal progenitors (hES-MPs). HES-MPs were obtained by following the procedure cited by Karlsson consisting in perorming consecutive enzymatic passages of human embryonic cells (hES) on gelatin 2D substrates (ref.). the procedure increased homogeneity of the cell culture by reducing the proportion of the non-mesenchymal cell types which are present in the initial high-density cultures of pluripotent undifferentiated hES cells.

2. Scaffold: Commercially available 3D Insert ® PCL (3D PCL) (Sigma Aldrich, UK, cod. Z724513) fabricated by 3D Biotek, USA. It is produced by fuse deposition modelling and, according to manufacturer, is characterized by:
   - Fiber diameter and spacing between fibers: 300 µm,
   - Laydown pattern between overlapping layer of fibers: 0°/90°,
   - Overall Height: 1.5 mm,
   - Overall diameter, 300 um pores fabricated by fuse deposition;

3. Scaffold sterilization: 99.9% pure Ethanol biological degree (Sigma Aldrich, UK, cod. E7023);

4. Microfluidic chamber sterilization: IMBS (Fisher, UK, cod. M/4450/17), Acetone (Fisher, UK, cod. 20065.327);

5. Gel embedded in the 3D PCL structure: Collagen I, Bovine (Gibco, UK, cod.A10644-01);

6. Media for cells culture:

COMPONENTS	CONCENTRATION	REF. COD.
α-MEM culture media		SLS, UK, cod. LZBE12-169F
Fetal Bovine Serum	10%	Labtech, UK, cod. FCS-SA
Penicillin/streptomycin/L-glutamine	1%	SLS, UK, cod. G6784
FGF (for hMSCs in culture only)	2 ng/ml	Gibco, UK, cod. PHG0024

7. Particles for shear stress evaluation in the microfluidic device: Green fluospheres, 10 µm (Gibco, cod.F8836) mimicking cells dimensions;

8. Cell fixative for Sirius Red staining: 10% formalin (Sigma Aldrich, UK, cod. HT5011);

9. Cell fixative for MicroCT: 25% Glutaraldehyde (Sigma Aldrich, UK, cod. G6257), 10 times diluted in distilled water;

10. Lysis buffer used to detach cells from the scaffold aiming to preserve protein content for ELISA assay.

COMPONENTS	CONCENTRATION	REF. COD.
dH_2O	-	-
$MgCl_2$	1 mM	Sigma Aldrich, UK, cod. , M8266
$CaCl_2$	5 mM	Sigma Aldrich, UK, cod. , C1016
Triton X	1%	Sigma Aldrich, UK, cod. , X100
Tris-EDTA	10%	Sigma Aldrich, UK, cod. , T9285

11. Fabrication of microfluidic devices by soft lithography: Polydimethylsiloxane (PDMS) composed of silicon elastomer curing agent and monomer (Sylgard, US, cod. 2699150);

12. Washing solution: PBS (Sigma, UK, cod.D8537);

3.3 Equipment

1. Kern analytical balance ABJ-NM/ABS-N (Kern & Sohn GmbH, Germany) to register mass of scaffolds and reagents;

2. Sub Aqua 12 plus Water bath (Grant, UK) for warming up media, PBS or any reagent to be put in contact with alive cells;

3. Eppendorf Centrifuge 5702 (Fisher, UK) for resuspension of cells in new media before seeding;

4. Eppendorf mini-spin (Fisher, UK) for centrifugation of cells once removed from the scaffold;

5. Class II Cell culture hood (ESCO GB Ltd., UK) to guarantee a sterile environment handling cells;

6. Ultrasonic bath (VWR, UK) for cell removal from scaffolds;

7. Motic Microscope for cell counting (Motic, UK);

8. Tecan Infinite F200 pro plate reader (Labtech, UK) for absorbance and fluorescent reading during biological assays (Presto Blue, DNA, Sirius Red, OCN ELISA);

9. Vacuum pump (Diener, Germany) for bubble removal during PDMS curing;

10. Hoven (Frigidaire, UK) for curing of PDMS into desired mold;

11. Plasma machine (Diener, Germany) for enhanced bonding between PDMS and glass slides as well as scaffolding surface treatment;

12. Aladdin Syringe pump AL-1000 (World Precision Instruments, US) for controlled perfusion of fluid through the microfluidic system;

13. Eclipse fluorescent microscope (Nikon, Japan) equipped with UVP UV lamp for visualization of fluorescent stained cells and auto-fluorescent scaffold;

14. Electroforce Bose Bioreactor 5500 (BOSE Corp., US) for mechanical loading of scaffolds to determine mechanical properties or cellular behaviour;

15. Water purification system (VWR, UK) dispensing distilled water to be used for biological assay after filtration with 0.2 um cellulose sterile filters;

16. Absolute AOS Digimatic calliper (Mitutoyo, UK) for measuring scaffold height;

17. Scanning electronic microscope XL-20 (Philips, US) for visualization of collagen structure;

18. Micro Computed tomography by SkyScan 1172 (Bruker, Belgium) for evaluation of scaffold architecture, and collagen, tissue and mineral distribution.

3.4 General procedures and assay kits

3.4.1 Plasma treatment and sterilization of samples

Samples were put into a plasma machine and treated for 5 min at 1 mBar and 30W by air plasma. Then, samples were removed and placed in 96 well plates to undergo further sterilization by alternating 3 times 200 µl of ethanol 70% and 1X PBS solutions. Then, samples were dried for 20 min and moved to a new 96 well plate before further processing.

3.4.2 Cell thawing and culturing

Cells (MG63 or hES-MPs) were removed from liquid nitrogen and re-suspended in culture media upon dissolution of the ice. Then, cells were centrifuged and seeded in T75 flasks in a density of 15-20*10^3 cells/cm^2. hES-

MPs were cultured in media supplemented with FGF for preventing differentiation, while MG63 were cultured in standard media. At the desired passage (5-6 for hES-MPs or 72-100 for MG63), cells were detached by trypsinization and resuspended in culture media for seeding of scaffolds.

3.4.3 Static seeding

Cells were suspended in a culture media solution and 20 µl of suspension was placed on the top marked surface of sterile samples. After 1.5 hour incubation at 37°C, 5% CO_2 and 99% humidity, 180 µl of culture media were added to samples.

3.4.4 Fluorescent imaging

Calcein AM (Gibco, UK, cod. C34852) and Ethidium bromide homodimer (Sigma Aldrich, UK, cod. E1903) were diluted in PBS in a concentration of respectively 2µM and 4µM. 200 µl of fluorescence stain was added and, then, samples were incubated covering the plate with aluminium foil to prevent exposure to light. After 40 minutes in a dark environment, samples were rinsed 3 times with PBS to remove unreacted stain and avoid signal background. Samples immersed in PBS were imaged by fluorescent microscopy and pictures were elaborated by the Metamorphosis software (Nikon, Japan). The time of exposure was set to:

- Blue light (scaffold autofluorescence): 40 ms
- Red light (dead/apoptotic cells): 40 ms
- Green light (alive/viable cells): 200 ms

and reconstructed by ImageJ.

3.4.5 Viability assay

(Presto Blue™ Cell Viability Reagent, Gibco, cod.A13261)

Samples were fitted in a 96 well plate and washed with PBS. 200 µl of Presto Blue (1:10 v/v in culture media) was added to samples and let react for 1 hour in incubator. Viability was assessed withdrawing 180 µl of fluorescent solution from each well and reading fluorescence by microplate reader at ex/em 540/590 nm.

3.4.6 DNA assay

(Quant-IT DNA kit, Gibco, cod.*Q-33120)*

3.4.6.1 DNA standard curve

A standard curve was determined per each cell line before performing the experiments to associate fluorescent values and number of cells (Fig. 3.1).

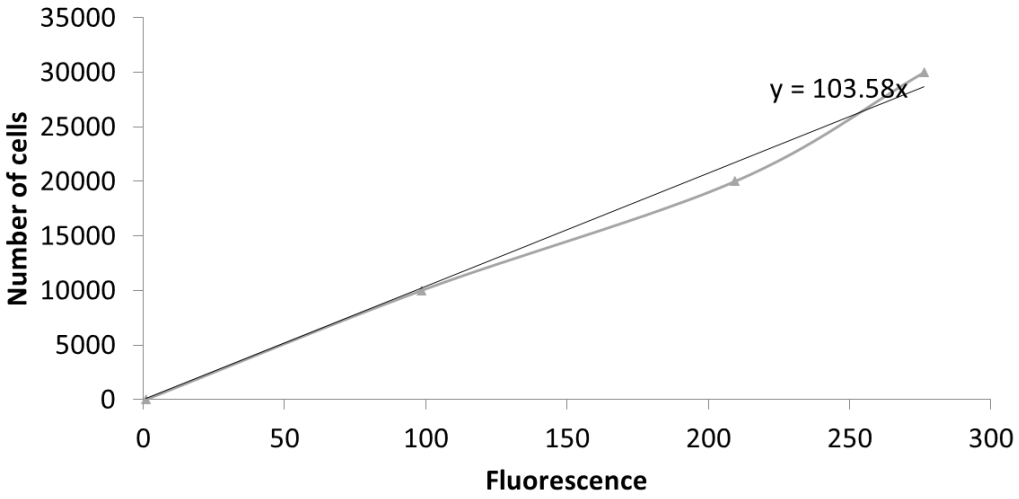

Fig. 3.1: Standard curve to relate fluorescent values to number of cells by DNA assay.

Cells were re-suspended in media and cultured in petri dishes for 24 hours before DNA quantification. Cells were detached from the petri dish by adding 0.5% trypsin for 5 minutes. After 5 s of vortex, 20 µl of cell suspension was used for DNA quantification Fluorescent values were obtained by subtraction of the background obtained from empty wells. The relationship between fluorescence value and cell number matched the linear trendline extrapolated from the data using Microsoft Excel.

3.4.6.2 DNA assay of samples

Samples were collected, washed in PBS and cut in small pieces to facilitate cellular detachment from the inner part of the specimen. 200 µl of 0.5% trypsin was then added following incubation for 5 minutes. Then, 200 µl of culture media was added to samples to block the action of trypsin and prevent damage of the cellular membrane. In order to achieve complete detachment of cells, samples underwent 5 s vortex. Then, 20 µl of suspension were tested for DNA quantification adding 180 µl of working solution made of lysis buffer and PicoGreen fluorescent stain (200:1 v/v). After incubation for 10 minutes in a dark environment, plates were read at ex/em 485/535 nm. Samples were then centrifuged for 3 minutes at 3,000 rpm to allow cell sedimentation. Afterwards, the overlaying medium was removed and the pellet was resuspended in lysis buffer, briefly vortexed and stored at -80°C.

3.4.7 MicroCT

3.4.7.1 Working principle

MicroCT is a well-established technique employing x-rays to characterize complex 3D structures in vivo as well as in vitro. In this study, microCT was used to provide 3D volumes of 3D polymeric scaffolds and to investigate the

distribution of other materials previously embedded in the structure. MicroCT requires the use of an x-ray source and a detector. The first provides an x-ray beam whose intensity approaching the detector is related to the attenuation coefficient of the scanned object. It depends on the atomic number of the material and is therefore, strictly connected to its density. In order to reconstruct 3D volumes, the object needs to be placed between the x-ray source and the detector and progressively rotated around its long axis. At each rotation, a 2D projection is acquired representing per each pixel the linear attenuation coefficient of the material along the x axis of the x-ray beam. As a consequence, dense materials appear as black structures due to their high x-ray absorption capabilities, while the signal becomes progressively brighter decreasing density. 2D projections of the scaffolds are then elaborated, through automatic algorithms implemented by commercially available softwares, and 2D images of the cross-section of the structure are reconstructed. The visualization of low density materials by x-ray can be achieved employing a high-density contrast agent able to chemically bound the substrate and to provide attenuation of the x-ray beam crossing the sample.

3.4.7.2 Osmium staining

Samples were collected and washed in 1X PBS. Samples were then immersed in 180 µl of 2.5% of glutaraldehyde for 2 hours [173]. Eventually, 20 µl of 10% osmium tetroxide were added to the solution [174]. Samples were stained overnight, washed in dH_2O and air dried for 2 days to allow complete evaporation of water from the interior of the sample. MicroCT scanning was performed within 7 days from the staining procedure to avoid degradation of biological material in the sample.

3.4.7.3 Scanning

Samples were stacked one upon another (up to 3 samples) into a straw and separated by small pieces of paper. Then, they were placed on a holder located in the microCT equipment between the x-ray source and the detector. Scaffolds were scanned at 40 kV, 10 W, and 250 mA. Moreover, no filters were applied and the pixel size was set to 17.4 μm. During the scanning, scaffolds were automatically rotated and consecutive projection images were acquired by the detector. Through algorithms implemented in the CTAn reconstruction software (Bruker, Belgium), projections were automatically analysed, and cross-sectional slices showing the density profile of the material were provided. Such 2D slices were obtained by applying ring artefacts and beam hardening corrections of respectively 10% and 15%. From the histogram, grey values (GV) between 0 and 0.2 were selected to improve image contrast. 2D slices were then stacked, and 3D volumes were reconstructed by ScanIP software (Simpleware Ltd., UK).

3.4.7.4 Reconstruction and analysis

A 0.5 μm Gaussian filter was applied to remove the random error from images. Considering cell, collagen, scaffold and background, the overall signal results in the following histogram (Fig. 3.2).

Quantitative analysis was performed considering overall masks or a cylindrical region of interest (ROI) 4 mm in diameter, 0.5 mm in height, and concentric to the scaffold (Fig. 3.3). GV between 8,000 and 13,000 were selected to highlight the 3D PCL structure and to eliminate the background provided by the straw (Fig. 3.2).

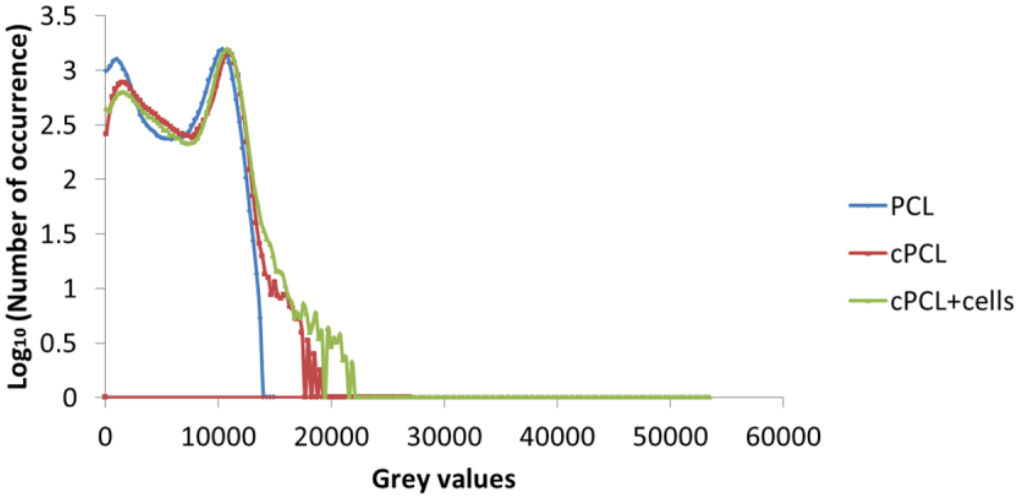

Fig. 3.2: histograms of a reconstructed 3D PCL (PCL, blue), 3D PCL with collagen (cPCL, red) and 3D PCL embedding collagen and cells (cPCL+cells, green). Zero grey values refer to black pixels. The first peak (GV 0-3500) was related to the void regions in the image. GV between 3500 and 7500 were instead representing the signal of collagen and of the structure used as support to stack scaffolds. The second peak (GV 8000-13000) was linked to the 3D PCL while high GV (13000-60000) were correlated to densified collagen and cellular content.

A median filter (1 μm) and a Gaussian smoothing filter (value: 0.5 μ) were eventually applied to further remove random error in the image.

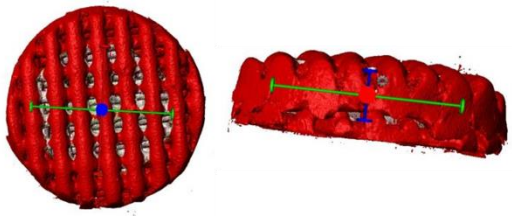

Fig. 3.3: Scaffold volume rendering by Simpleware. Grey volume underneath the surface of the scaffold represents the cylindrical volume selected for porosity evaluation. Red and green lines indicate respectively the radial plane while blue line defines the perpendicular plane.

Two ranges of GV were affected from the presence of collagen at respectively 3500-7500 and 13000-60000 (Fig. 3.2). The identification of different densities of collagen was achieved by segmentation of images, leading to the distinction

of areas occupied respectively by low density (LD) or hard density (HD) collagen by manual selection and merging of masks (Fig. 3.4).

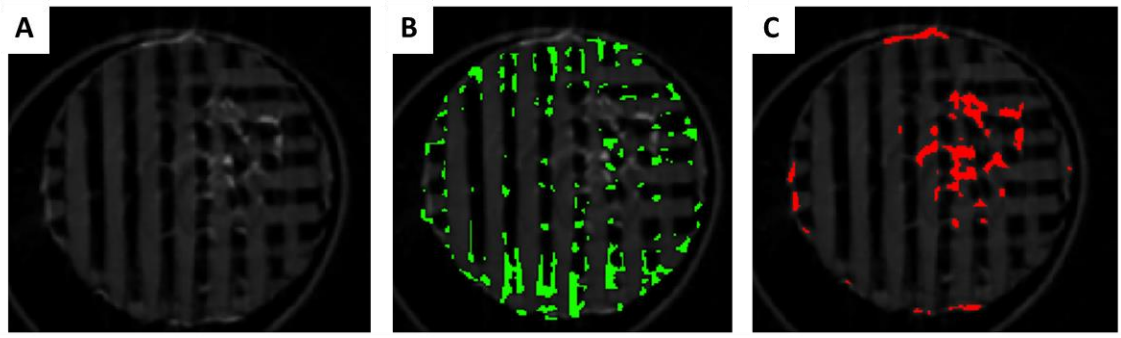

Fig. 3.4: 2D slides obtained from reconstruction of microCT images. (A) 3D PCL embedding collagen gel. (B) LD collagen (green) and (C) HD collagen (red) were manually selected through the structure by the FloodFill feature provided by Simpleware.

A further distinction of the distribution and content of collagen in the interior (IN) and on surface of the scaffold (OUT) was provided by selecting a ROI fitting the interior of the scaffold. 2D slices segmentation was performed by selecting different areas of the slice, and merging multiple selections in an overall mask by employing the Simpleware feature FloodFill. The use of such feature helped increasing accuracy of the segmentation process and eliminated the large amount of background otherwise included applying common automatic masking methods. Gaussian filter (0.7 μm) was applied twice to masks to eliminate random error before quantification. Performing long experiments, the signal in the GV interval 3500-7500, before attributed to LD collagen, was instead associated to tissue formation as it accounted for the production of extracellular matrix (ECM) and the increase in cells number. Furthermore, the signal in the GV interval 10000-60000 (before attributed to HD collagen) was hypothesised to be associated with the growth of mineral crystals. Reconstructions of tissue and mineral content followed the same segmentation procedure employed for collagen.

3.4.8 OCN ELISA assay

(CytoSet™ kit, Life Technologies, cod.CNB0011)

A flat bottom Costar 96 well plate was treated overnight with 100 µl of coating antibody solution (Mouse monoclonal anti-OCN (Life Technologies, cod. 33-5400)) diluted in coating buffer B at room temperature. After 3 washing steps with 200 µl of washing buffer, the plate was blocked with 300 µl of assay buffer for 1 hour at room temperature. 100 µl of standards, samples (Labtech, cod.W4500) and controls were pipetted in duplicates as quickly as possible to avoid variation in the absorption of OCN between wells. Then, 50 µl of working detection antibody (Goat anti-Mouse IgG H+L-HRP (Life Technologies, cod. 62-6520) diluted in assay buffer) was added to each well and the plate was incubated for 2 hours. Eventually, the plate was again washed 3 times with washing buffer and 100 µl of TMB substrate was added to each well to enhance release of OCN in solution. After 30 min incubation in the dark, 100 µl of stop solution were added and absorbance was read at 405 nm.

3.4.9 Statistical analysis

Statistical analysis was performed by SPSS software. Normality and equality of variances were tested respectively by Shapiro [175], [176] and Levene's tests [177] to justify the involvement of parametric tests T-Test and ANOVA for detecting significant differences among series of data. Applying Shapiro and Levene's tests, all series showing =probability values below 0.05 were considered respectively normal distributed and with equal variance. These tests were particularly relevant in the assessment of the variability associated to the response of scaffolds to mechanical compression in Chapter 4.

Chapter 4

MECHANICAL CHARACTERIZATION OF 3D Insert ® PCL SCAFFOLDS

4.1 Introduction

The Tissue Engineering (TE) approach aims to closely mimic the biological environment found in the body to drive progenitor cells toward a defined differentiation pathway and obtain fully functional tissue as replacement for injured sites. Although the behaviour of several cellular lineages seeded on two dimensional (2D) surfaces is nowadays well defined on a wide range of materials [16], it does not enable a physiological replication of the biological environment because of the lack of 3D structure. As a consequence, the first challenge addressed by TE regards the possibility of employing structures closely mimicking the geometry and chemistry of the biological environment found in the target tissue. For bone regeneration purposes, a basic requirement is for the scaffold to be able to bear mechanical stimuli as bone is constantly under mechanical forces by the action of muscles and body movements. Gelatine-like scaffolds made by natural polymers such as collagen, fibrin or chitosan represent a good choice for cellular studies as they naturally mimic the main components of the extracellular matrix. However, soft matrices present inadequate properties to bear mechanical forces, preventing their use for bone regeneration purposes. Synthetic materials made by polymerization of lactic acid, glycolic acid or caprolactone were explored to manufacture composite scaffolds, often embedding natural proteins. This approach led to the fabrication of scaffolds able to bear mechanical forces, providing at the same time an architecture and a matrix similar to the bone tissue niche [79]. Among those, poly caprolactone (PCL) is gaining increasing

interest as it is a thermoplastic polymer presenting low glass transition and low melting temperature [178]. As a consequence, temperature dependent processes can be employed to confer on PCL the desired shape providing control over features at micro scale [179]–[181]. Moreover, PCL showed to be highly biocompatible [182] and it presents slow degradation rates [183] due to its high degree of crystallinity and hydrophobicity. These last mentioned properties make it suitable for studies requiring consistency in the mechanical properties of the material over time. This study aims to define the mechanical properties of 3D Insert® PCL scaffolds (3D PCL) under compression stimuli and to test their suitability in providing a controlled mechanical environment. In the literature, porous 3D biomaterials with similar architecture and chemical composition were mainly characterized under compression stimuli [106], [184], due to the limitation in applying tensile strain related to their structure. A prerequisite for the use of polymeric structures for mechanobiology purposes is the reproducibility of consecutive stimulations by preventing viscoelastic effects to occur. For this purpose, static pre-conditioning was proposed in multiple studies [185]–[187] as a method to prevent viscoelastic response to dynamic compression and to achieve relaxation of scaffolds. Environmental conditions also affect the mechanical response of 3D scaffolds as demonstrated by Dynamic Mechanical Analysis (DMA) analysis in previous literature studies [106], [188], [189]. DMA was used in this study to capture any difference in the mechanical response of scaffolds when surrounded by liquid (water) as cellular experiments require immersion in culture media during the stimulation. The architecture of scaffolds is claimed to elicit a strong impact on the mechanical properties of polymeric scaffolds [75], [106], [188], [189]. The aims of this[75], [106], [188], [189]. The final aims of the chapter consist in 1) characterizing the mechanical response of 3D PCL to compression to prove the reproducibility of the loading protocol, 2) quantifying the error due to geometrical variability, and 3) investigating how the surrounding environment affects the mechanical properties of 3D PCL.

4.2 Materials and Methods

4.2.1 Mechanical characterization of 3D PCL

4.2.1.1 Stress/strain curve

The stress/strain curve of 3D porous polymeric structures fabricated by fuse deposition modelling in general show a different trend compared to that observed for bulk polymers. Indeed, while the latter show an initial linear region with strain increasing proportionally to the stress (Fig. 4.1A) [190], the linearity characterizes just a limited portion of the curve in the former [189] making it difficult to identify. In general, porous materials show three different regions (Fig. 4.1B).

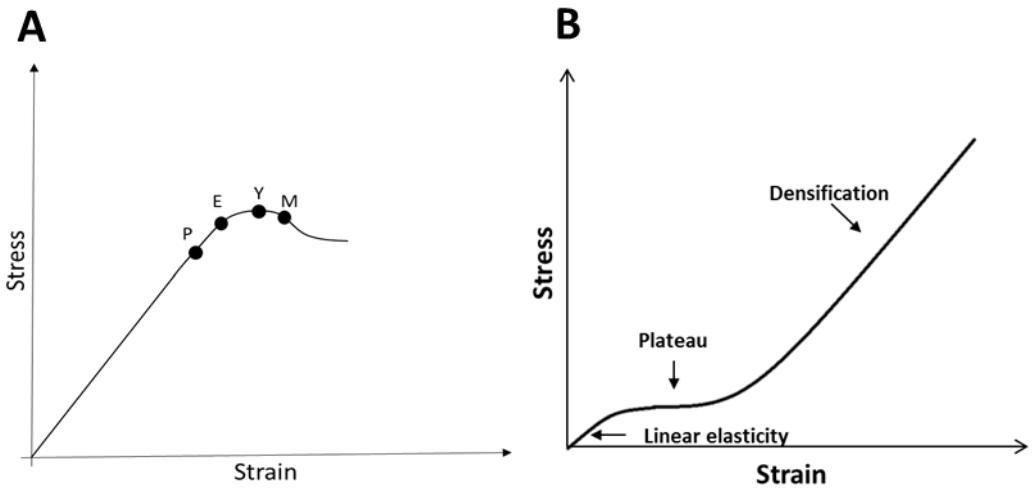

Fig. 4.1: Stress/strain curve of (A) bulk polymeric materials showing the ultimate point of linear behaviour where strain varies linearly with stress (P), the maximum strain achieved prior to plastic deformation (E), the yield point showing constant stress with increasing strain (Y) and the necking point (M).(B) Porous polymeric structures showing a liner elastic behaviour followed by a plateau and a final densification of the material for high strains.

After the initial linear region from which the elastic modulus of the structure can be calculated, the curve is characterized by a plateau of roughly constant stress with increasing strain, and a final region of densification of the material governed by plastic effects, where the stress values increase rapidly with strain [189] due to deformation and relative movements between polymeric fibers.

Stress/strain curves were obtained applying loading ramps of 14% compressive strain at 10 µm/s. This task was performed by the BOSE Biodynamic System 5500 (BOSE Corp., US). This mechanical testing machine was already employed in different studies requiring highly precise mechanical stimulation of polymeric scaffolds for cellular studies [100], [146], [162]. Low strain values were chosen to avoid rupture or significant plastic deformation of the structure occurring when elevated strains were applied. Scaffolds (n=5) were tested at 25°C in air and at 40% of humidity. The zero position was defined by load referring to an initial preload of 0.1 N on the structure as zero stress/strain condition. Such value corresponded to the minimum variation detectable by the load sensor. Load (*F*) and displacement (*d*) data were acquired at 20 Hz using the Wintest 7.0 software (BOSE Corp., US).

The stress σ *(Eq.4.1)* was defined as:

$$\sigma = \frac{F}{A} \qquad \text{Eq. 4.1}$$

where *A* was the area of the scaffolds, considering an average diameter of 5 mm.

Strain ε *(Eq.4.2)* was defined as:

$$\varepsilon = \frac{d}{h} \qquad \text{Eq. 4.2}$$

Where *h* was the height of the scaffold.

4.2.1.2 Secant modulus

Secant modulus is recognised as a standard parameter involved in the definition of the mechanical response of polymeric materials [189], [190] due to difficulties in identifying linear regions in the stress/strain curve when forces are applied. The secant modulus is identified as the slope of the line connecting the origin with any point on the stress/strain curve (Fig. 4.2). As it remains constant in correspondence of linear regions on the stress/strain curve, it helped identifying the range of strain to calculate the apparent elastic modulus.

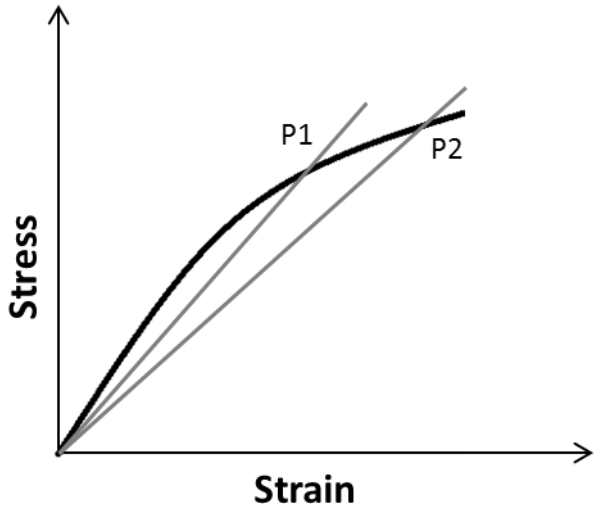

Fig. 4.2: stress strain curve of polymeric materials. The secant moduli are represented as straight lines connecting the origin (O) to random points (P1 or P2) on the curve [190]**.**

4.2.1.3 Apparent elastic modulus

5% strain ramps at 10 μm/s were applied at 25, 30 and 37°C allowing stabilization of the temperature inside the incubator for 30 minutes at each temperature variation. Samples (n=3) were tested with 10 ramps and recovery of the structure was achieved by allowing 10 min recovery between

consecutive ramps (Fig. 4.3). The apparent elastic modulus was calculated as average of stress/strain ratio in the range of linear response of scaffolds, hence where the secant modulus was constant.

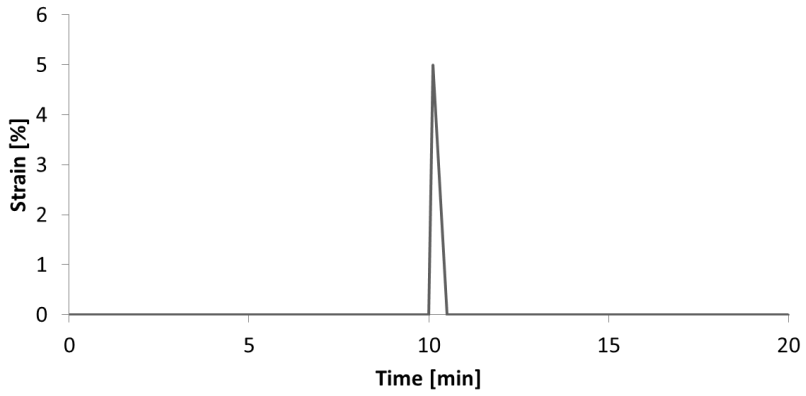

Fig. 4.3: single loading ramps for evaluation of the apparent elastic modulus. The compression is applied 10 times allowing a recovery of 10 minutes between 2 consecutive cycles.

4.2.2 Sample preconditioning and dynamic compression

Scaffold relaxation was obtained by static preconditioning.

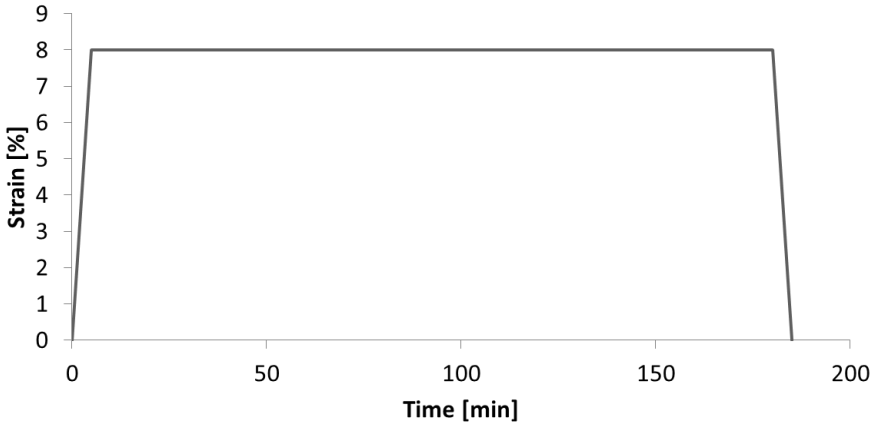

Fig. 4.4: relaxation protocol performed maintaining constant strain for 180 min.

A 8% compressive ramps was applied at 10 μm/s and the resulting displacement was kept constant for 3 hours (Fig. 4.4). To confirm absence of viscoelastic effects as consequence of the application of the static preconditioning protocol, samples (n=3) underwent cyclic compression before and after relaxation at 37°C and 40% humidity. Dynamic forces were applied as 5% strain triangle waves for 10 times at 1 Hz (Fig. 4.5).

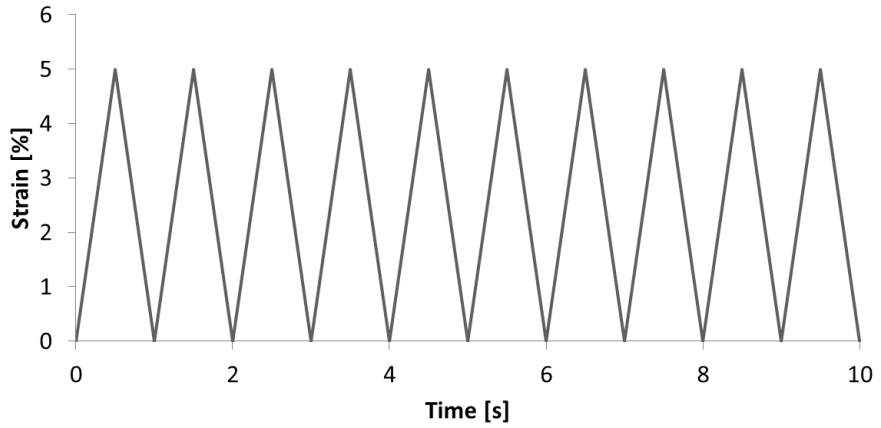

Fig. 4.5: Cyclic compression applied before and after relaxation of 3D PCL to test the viscoelastic response of scaffolds.

4.2.3 Dynamic mechanical analysis (DMA)

Different parameters defining the response to cyclic forces are considered. Among these, the storage modulus (*E'*) gives insight of the elastic response of the structure and of the energy stored by the specimen while the loss modulus (*E''*) takes in account the dissipation effects caused by the viscoelastic component. The two moduli can be combined to obtain the complex elastic modulus (Eq.4.3) and tan δ (Eq.4.4).

$$E^* = E' + E'' \qquad \text{Eq. 4.3}$$

$$\tan \delta = \frac{E''}{E'} \qquad \text{Eq. 4.4}$$

Tan δ is defined as the phase shift occurring between load and displacement signals (Fig. 4.6) and it is more commonly known as loss factor. It is particularly useful in the evaluation of the dynamic mechanical response of composite structures because it allows to account for the energy dissipated regardless of the mechanism involved [191].

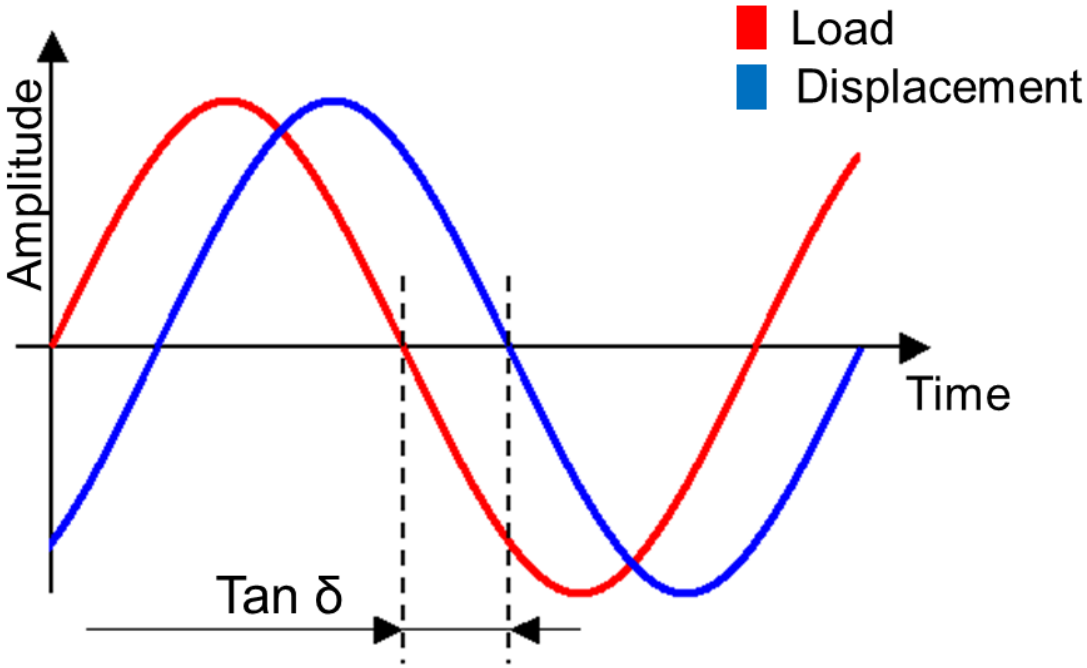

Fig. 4.6: phase shift due to dissipation phenomena in viscoelastic materials undergoing cyclic compression.

DMA was performed in dry or wet conditions keeping samples (n=3) respectively in air or water at 37°C. Samples (

Table 4.1) were preloaded at 0.1 N and a ramp at 5% strain was superimposed to induce a pre-stress on the structures.

Table 4.1: geometrical features of samples used for DMA analysis.

PCL SAMPLE	HEIGHT [mm]	POROSITY [%]
S2	1.37	42
S3	1.52	44
S4	1.54	45

Then, consecutive sinewaves 2% peak to peak (Fig. 4.7) were applied at 0.1, 0.5, 1, 5, 10 Hz by BOSE. DMA analysis was performed by the DMA software (BOSE Corp., USA) and post processing of data was automatically provided by the DMA Analysis software (BOSE Corp., USA).

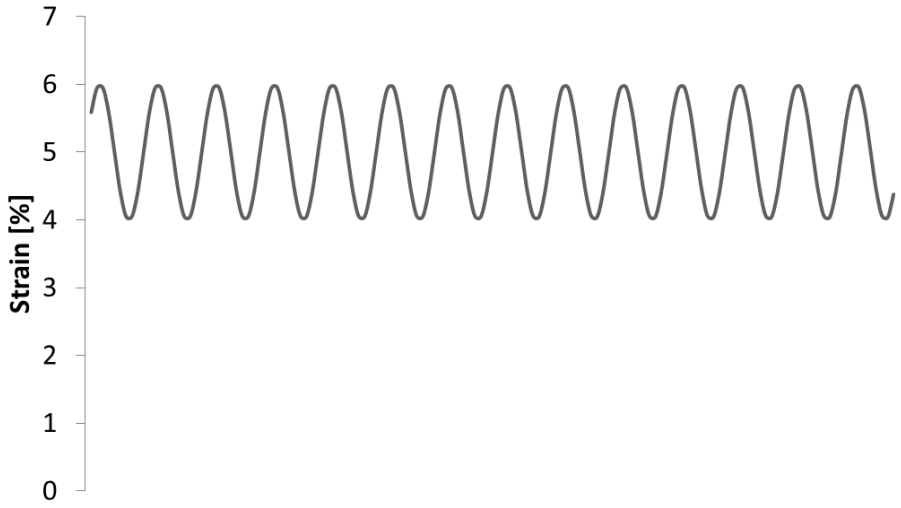

Fig. 4.7: 2% peak to peak sinewave centred at 5% strain and applied at different frequencies to test behaviour of 3D PCL under cyclic compression.

DMA analysis was repeated three times on the same sample to determine *E'*, *E''* and tan δ without varying the orientation of the structure into the machine.

4.2.4 Geometric variability

Analysis on geometrical variability of samples (n=14) was performed by microCT scans (Chapter 3.4.7). According to histograms interpretation (Chapter 3.4.7.4), GV between 8,000 and 13,000 were selected to compute a mask of the scaffold architecture and quantify volume, surface area and porosity. Volume and surface area were calculated automatically by Simpleware on the overall mask while porosity measurements required the selection of an internal volumetric region of interest (ROI). The percentage of material (V_{mat}) occupying the overall selected volume (V_{ROI}) was considered in the estimation of the final porosity (Eq.4.5) and the relative density (Eq.4.6).

$$p = 1 - \left(\frac{V_{mat}}{V_{ROI}}\right)*100 \qquad \text{Eq. 4.5}$$

$$Relative\ density = 100 - p \qquad \text{Eq. 4.6}$$

3D volumes were further elaborated in ImageJ to evaluate the average fiber diameter. Fiber diameter was measured on a cross-section of the scaffold whose cutting plane passes through the centroid of the structure. Then, circular areas were drawn matching the fibers profile. Other parameters taken into account were the height and the mass of scaffolds measured respectively using a calliper and a digital scale.

4.2.5 Boundary effects and mechanical variability

The effect of geometry and porosity on the response to compression was first investigated on a mechanically well-known material such as polydimethylsiloxane (PDMS) in the effort to provide reference measurements, helping the clarification of the source of variability. Indeed, the complicated geometrical texture contributes to the standard deviation just when 3D PCL is considered, while the human and systematic errors affect both materials.

PDMS was prepared mixing curing reagent and monomer at 1:10 (w/w) ratio. Vacuum was applied until complete removal of bubbles was achieved and then PDMS was cured at 75°C for 20 min in a temperature controlled oven. Once solidified, PDMS was cut into a cylindrical shape by punching holes 5 mm in diameter through the structure. Through this procedure, it was possible to obtain PDMS samples whose dimensions match 3D PCL. PDMS and 3D PCL mechanical properties were tested by applying a preload of 0.1 N followed by a 5% strain loading ramp at a fixed velocity. E_a values obtained by performing 10 ramps were averaged to perform statistical analysis and allowing 10 min recovery between consecutive ramps (Fig. 4.3). In this study the effect of three variables on the mechanical response of samples were studied: height, velocity and sample orientation. The first was explored to test the existence of a link between the height of the specimen and its measured mechanical properties.

Table 4.2: 3D PCL samples used in the variability analysis.

PCL SAMPLE	HEIGHT [mm]
A	1.54
B	1.61
C	1.39

For this purpose, PDMS samples (n=3) 2 mm (PDMS2) and 10 mm (PDMS10) tall were tested under the same conditions in terms of strain amplitude and rate. To evaluate the adaptation of the material when displacement was applied at different rates, the velocity of the loading ramp was varied at 1 and 10 μm/s on both PDMS2 and 3D PCL.

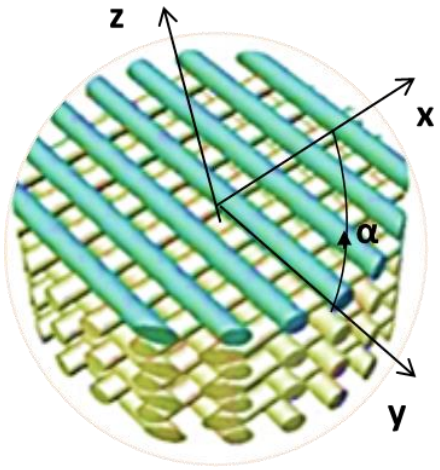

Fig. 4.8: 3D PCL representation with local coordinate system highlighting the rotation α of the sample occurring in the xy plane perpendicular to the z plane.

The 3D PCL samples (n=3) used in the experiments were chosen randomly from the same batch (

Table 4.2). The last variable considered was the orientation α of the sample inside the machine (Fig. 4.8).

Table 4.3: Statistical tests used to evaluate the effect of height and ramp rate on the mechanical response of 3D PCL.

MATERIAL	COSTANTS	VARIABLE	STATISTICAL TEST
PDMS	v = 10 um/s	α h = 2, 10 mm	ANOVA
PDMS2 or PCL	h = 2 mm	α v = 1, 10 μm/s	T TEST

At each velocity, E_a was statistically analysed to evaluate the effect elicited by repositioning the samples on a compact or a 3D porous material. Normality and equality of variances among series of data were tested with common methods (Chapter 3) and statistical analysis was performed (Table 4.3).

4.3 Results

4.3.1 Microcomputed tomography and 3D PCL architecture

Scaffolds architecture is believed to play a central role in the variability of the mechanical response observed when compressing different samples. For this reason before undergoing dynamic compression, scaffolds were scanned by microCT and the geometrical features were scrutinized to identify any significant difference in the architecture among different scaffolds. All the parameters tested (Table 4.4) showed high deviation from the average value with percentage error up to 12%.

Table 4.4: Geometrical parameters involved in the evaluation of 3D PCL geometrical variability.

Sample number	Height [mm]	Surface Area [mm2]	Volume [mm3]	Fiber diameter [µm]	Porosity [%]
1	1.42	137.67	13.04	290	31.6
2	1.36	145.91	13.31	254	46.54
3	1.62	148.59	12.59	305	46.61
4	1.52	145.94	13.31	284	43.74
5	1.55	153.04	15.88	348	34.2
6	1.67	155.68	16.76	393	50.9
7	1.61	201.12	15.95	335	48.25
8	1.61	166.03	13	380	47.73
9	1.59	159.31	17.84	335	42.71
10	1.55	147.22	13.56	315	35.5
11	1.66	161.91	12.51	300	40.3
12	1.53	151.22	12.14	299	36.09
13	1.67	157.17	13.28	296	35.5
14	1.53	122.66	13.28	296	51.2
Average	**1.56**	**153.82**	**14.03**	**316**	**42.2**
Standard deviation	**0.09**	**17.39**	**1.79**	**38**	**6.6**

Average samples height was up to 1.56 mm covering a range between 1.36 to 1.67 mm. As revealed by reconstruction of samples (Fig. 4.9), differences in height were due to the dimension of fibers varying within the sample and also among different specimens. Indeed, not only fibers were not perfecly cylindrical, but they were also not equally spaced and with very variable diameter. In the same sample, the diameter of fibers varied up to 8% while, extending the comparison among different samples, the variability increased up to 12%.

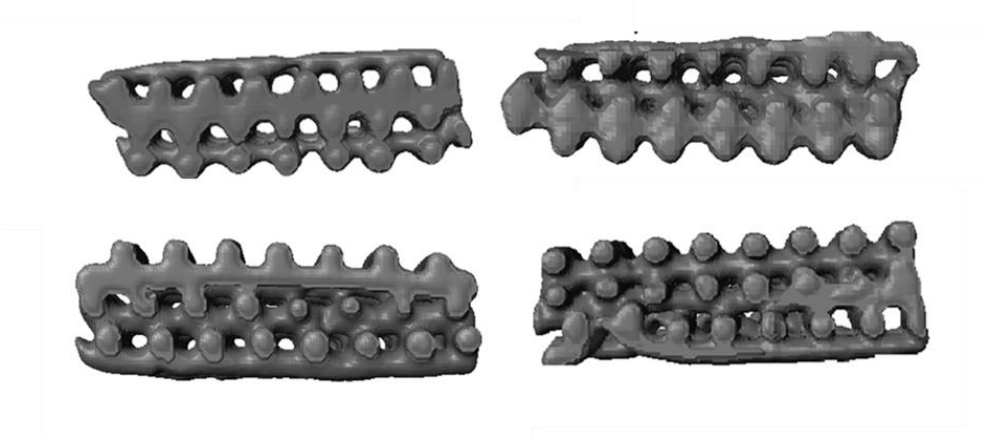

Fig. 4.9: Cross-sections of samples obtained by volume rendering. Misalignment between fibers belonging to different layers, imperfections in the structure and variable pore size characterize all samples.

Beyond scaffold height and fiber diameter, variability above 10% was also noticeable for surface area, volume and porosity amounting respectively to 11.3%, 12.8% and 15.6%.

4.3.2 Stress/strain curve and apparent elastic modulus

Observing the stress/strain curve (Fig. 4.10A), a classic viscoelastic behaviour was identified by the non-linear increase of stress with increasing strain. Moreover, the development of an hysteresis cycle suggests loss of energy associated to the deformation. Indeed, the unloading curve showed 6%

residual strain when a single ramp at 14% strain was applied, suggesting the occurrence of plastic deformation of the structure for strains above 8%.

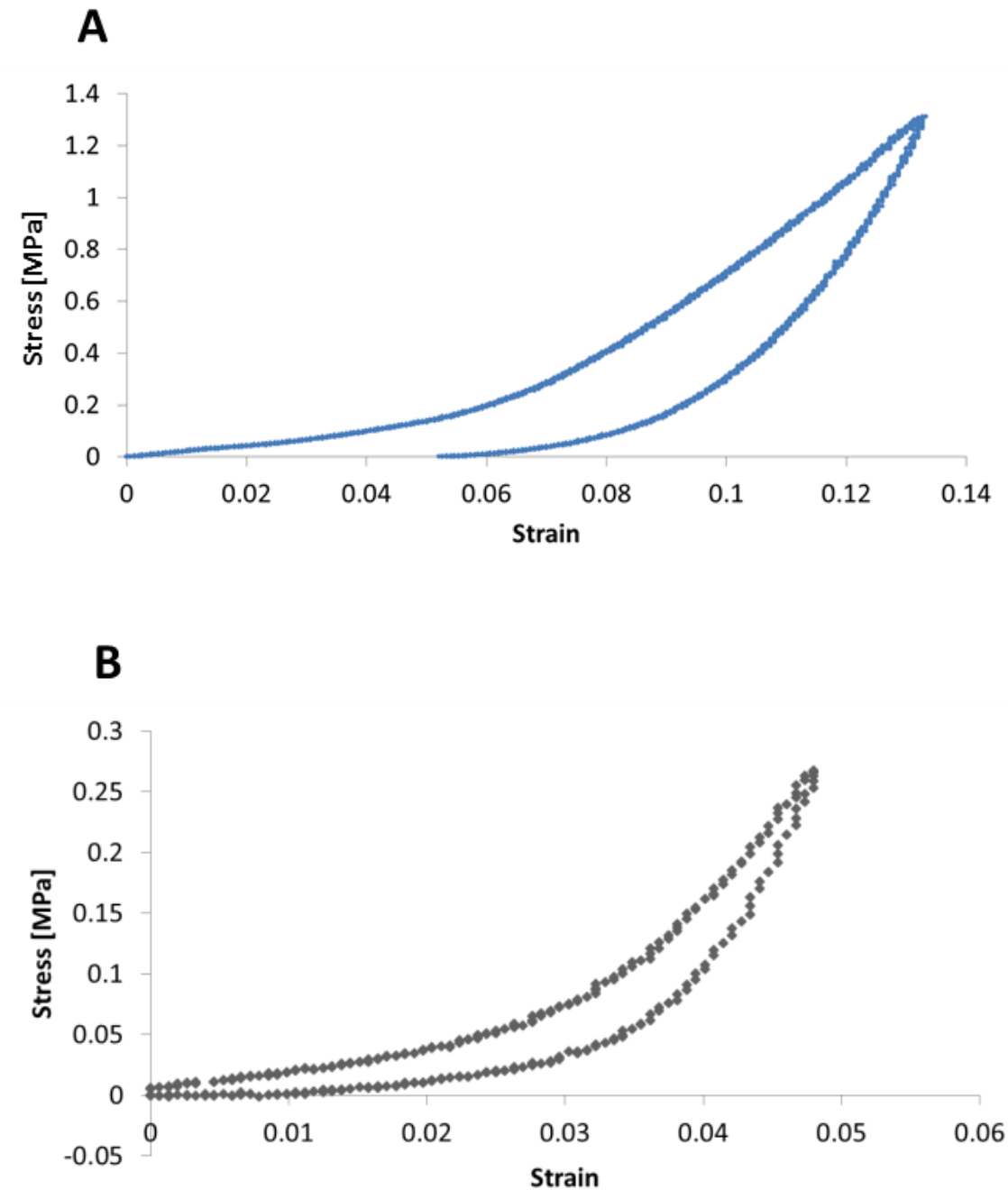

Fig. 4.10: Stress/strain curve applying loading/unloading ramp to evaluate 3D PCL response to mechanical compression for strain up to (A) 14%, (B) 5%.

On the contrary, a single 5% strain ramp (Fig. 4.10B) did not present plastic effects and it showed complete recovery of the structure.

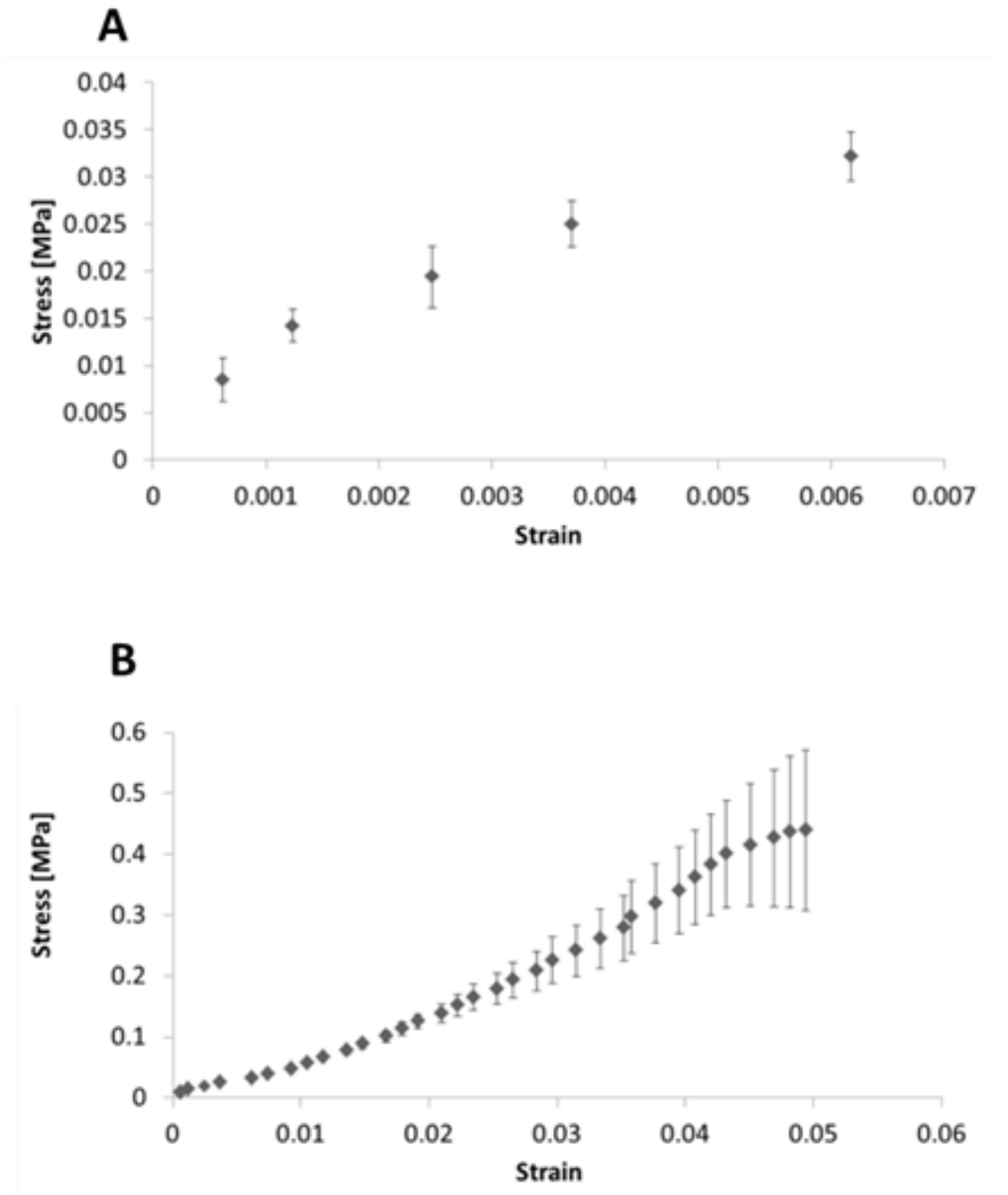

Fig. 4.11: Loading curve resulting of 3D PCL undergoing compression for ranges of strain (A) below 1% and (B) up to 5%. The standard deviation refers to an average of 10 consecutive ramps.

For this reason, low strain values thresholded at 5% were applied in the next experiments involving consecutive loading of samples, while a 8% threshold was used to achieve complete relaxation of scaffolds.response of a single scaffold undergoing cyclic compressive load led to a massive standard deviation for high strains (Fig. 4.11B). However, other two regions were identifiable in the stress/srain curve. Indeed, strain below 1% (Fig. 4.11A) were governed by the non linearity related to an adaptation of the material to compression and local rearrangement of fibers, while a linear region was identifiable above 1% strain and before the densification. At this point, the secant modulus was examined as it remains constant in the range of strain governed by linearity on the stress/strain curve (Fig. 4.12).

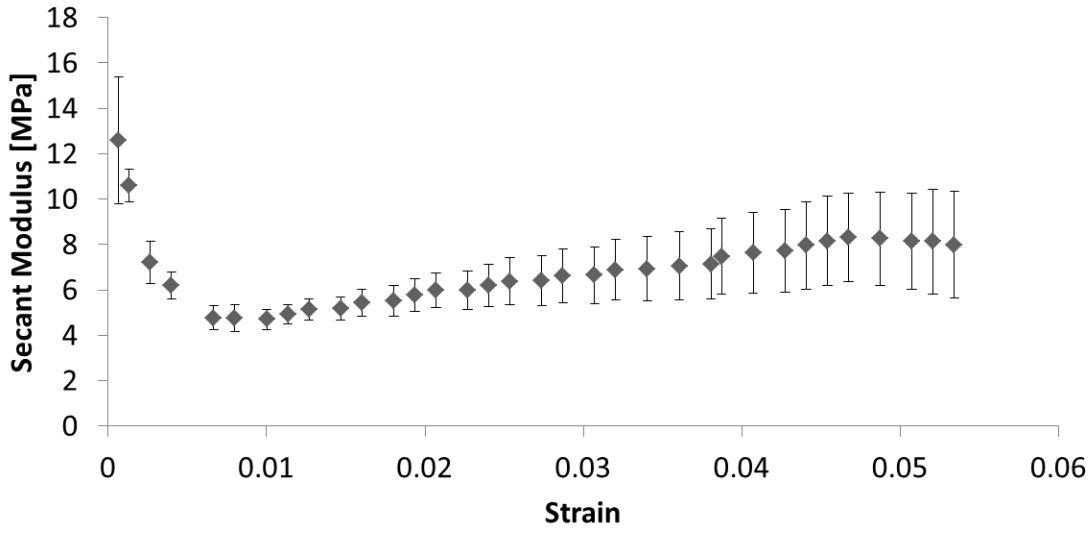

Fig. 4.12: Secant modulus resulting from compression of a 3D PCL sample. The standard deviation refers to an average of 10 consecutive ramps.

Following these findings, a certain strain was considered as belonging to the linear range if the secant modulus underwent a maximum variation of 10% from the value observed at 1%.

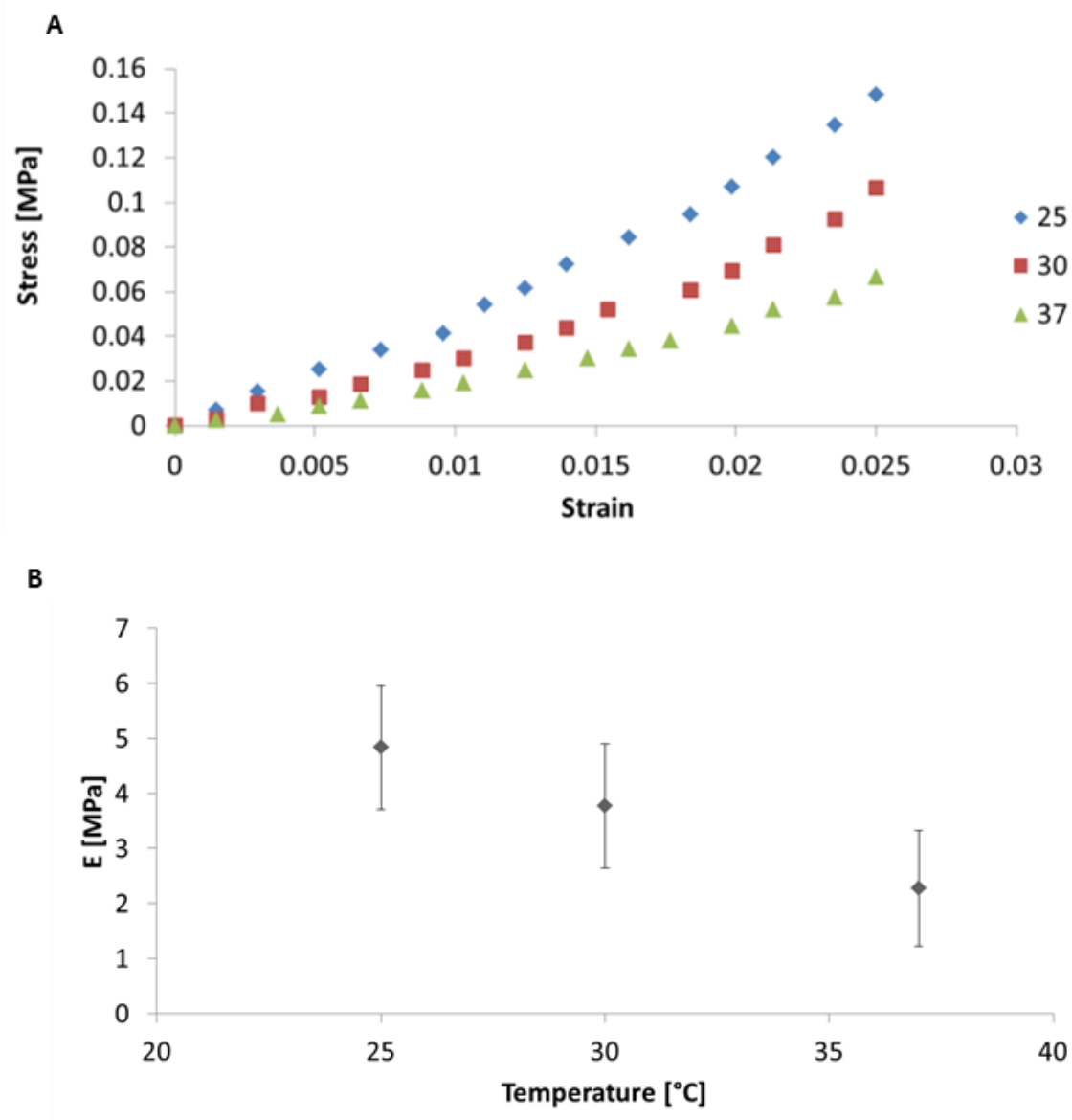

Fig. 4.13: (A) stress\strain curve varying temperature at 25, 30 and 37°C; (B) apparent elastic modulus (n = mean±S.D.) values depending on temperature.

As a result, all secant moduli falling in the range of strain between 1 and 2.5% were averaged and defined as apparent elastic modulus. E_a is a parameter representative of the stiffness of the structure and was involved in the evaluation of the effect of temperature on the mechanical properties of 3D PCL. Indeed, E_a remained constant among stimulations regardless of the previous history of the material if (1) the strains applied previously did not exceed the 8% threeshold for plastic deformation; (2) samples were not repositioned in the machine; and (3) samples were allowed to recover for 10

min between consecutive compression cycles.Respecting these conditions, E_a was found to progressively decrease with raising temperature (Fig. 4.13A). Samples tested at 25, 30 and 37°C showed E_a respectively at 4.8, 3.8 and 2.2 MPa (**Error! Reference source not found.**B). Indeed, not only fibers were not perfectly cylindrical, but they were also not equally space and with very variable diameter. In he same sample, the diameter of fibers varied up to 8% while, extending the comparison among different samples, the variability increased upt o 12%.

4.3.3 Preconditioning and viscoelastic effects

Viscoelastic effects occurred when cyclic loading was applied, enhancing progressive relaxation (Fig. 4.14) as the structure was not allowed to recover between ramps. The highest dissipation of energy was observed during the first cycle and then viscoelastic effects progressively decreased. For strains up to 5%, viscoelastic effects were prevented by static preconditioning applying constant displacement. Samples required an average of 150 min to completely relax under 8% strain compression, reaching a plateau (Fig. 4.15A).

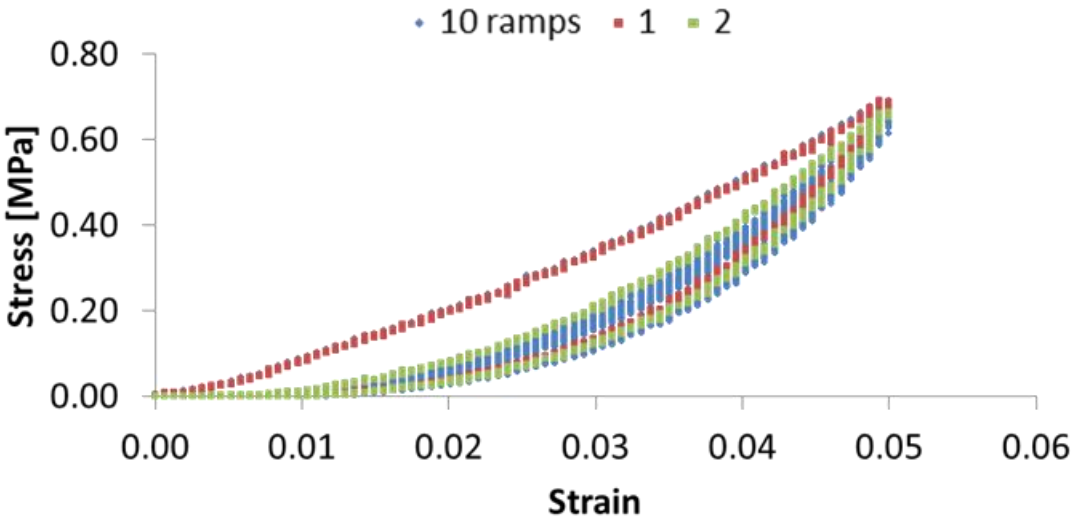

Fig. 4.14: viscoelastic relaxation of scaffolds tested by cyclic loading.

Applying cyclic loading on statically preconditioned specimens, viscoelastic effects were absent with overlapping loading/unloading curves (Fig. 4.15B). Moreover, the absence of plastic deformation was confirmed as no residual strain was observed at the end of the unloading curve.

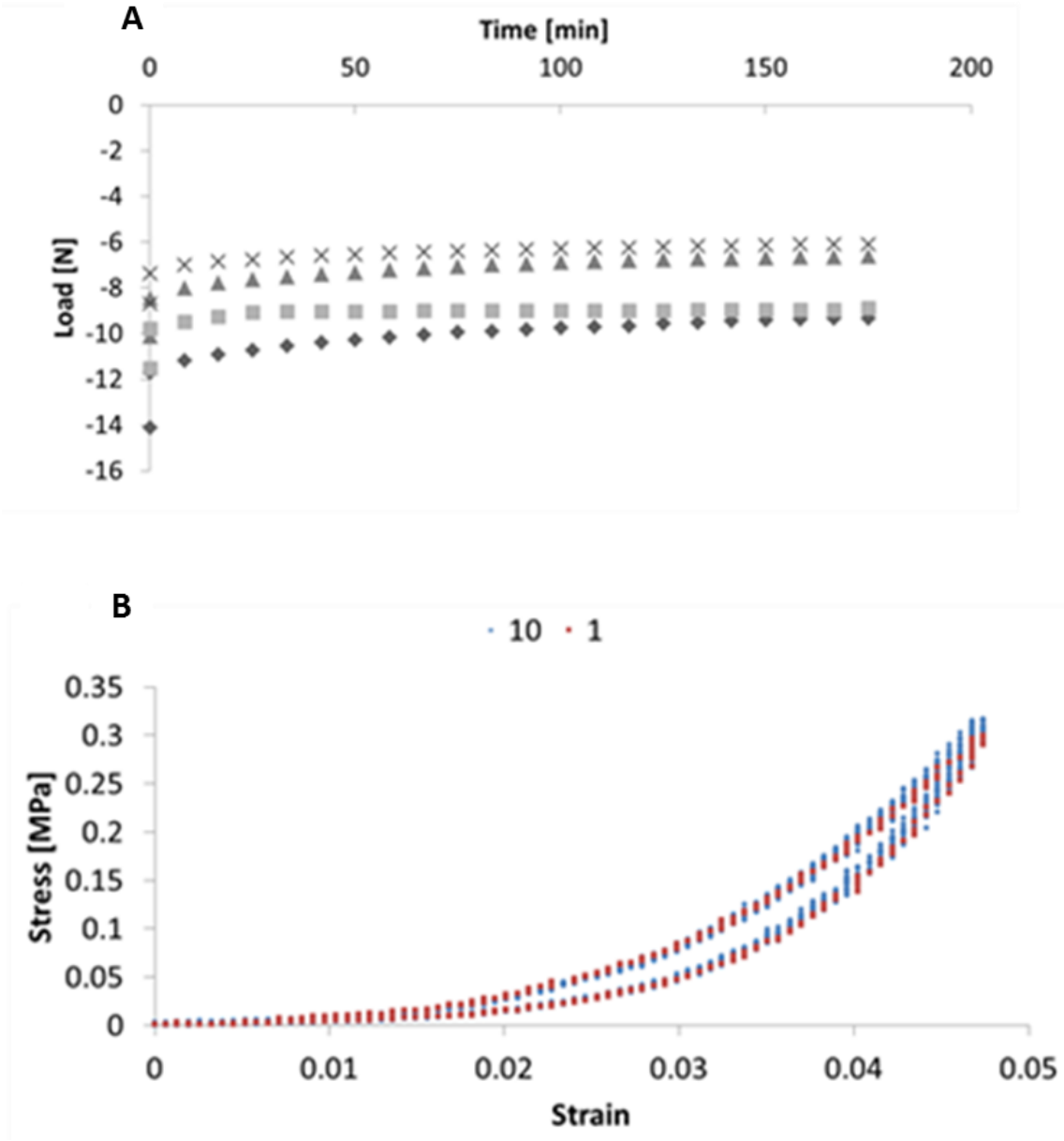

Fig. 4.15: (A) Relaxation pattern of four different samples relaxed under constant displacement over 180 min (B) stress/strain curves showing the behaviour of the material for 10 consecutive compression ramps after undergoing relaxation.

Despite the similarity in the relaxation pattern, the load force registered by the machine varied among samples although the same strain was applied, suggesting geometrical differences play a role in the mechanical response of scaffold to compression.

4.3.4 Mechanical characterization of PDMS

PDMS samples with different height underwent the same compressive protocol as 3D PCL to evaluate the effect of the geometry on the response of the material. At first glance, height seemed to play a fundamental role on the mechanical response, while rate of application of the stimuli did not elicit any strong effect on a compact material such as PDMS (Fig. 4.16).

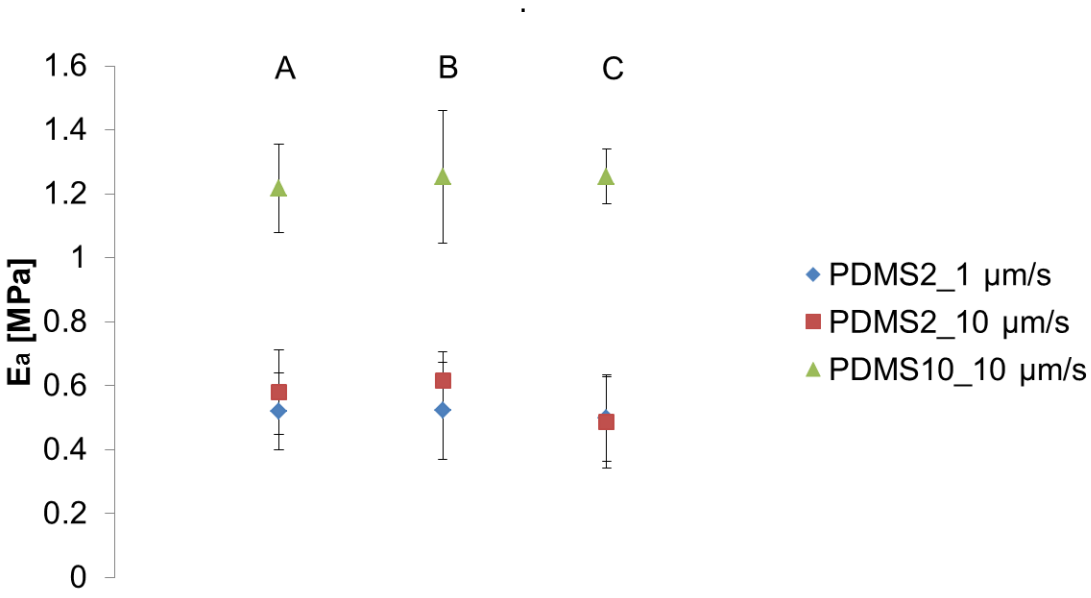

Fig. 4.16: Effect of different heights and compression rates on the response of PDMS samples. The mechanical response of 2 mm height samples compressed at 1 µm/s (blue) and 10 µm/s (red) are compared to that of 10 mm samples compressed at 10 µm/s (green). Each condition was tested on three samples (A, B, C) (n = mean±S.D.).

In order to confirm the truthfulness of this statement, statistical analysis was performed to test data for normality and equality of variances. Data series presented a normal distribution and equal variance as demonstrated respectively by the Shapiro and Levene's test (Table 4.5). These findings together with the hypothesis of independent samples enabled the use of ANOVA and T-Test for comparison among experimental tests. Comparing samples having the same height by ANOVA (Table 4.5) no significant differences were noticed in the mechanical response. This suggests the suitability of PDMS to be used as reference for evaluation of the precision of the methodology and quantification of the human and systematic error. Despite the repeatability in the estimation of the material stiffness for a given height, PDMS10 showed a significantly higher E_a ($p<0.001$) compared to PDMS2 (Table 4.5).

Table 4.5: SPSS statistics of E_a data obtained compressing 10 times PDMS samples. Height was varied at 2 mm (PDMS2) and 10 mm (PDMS10). Series of data obtained by compression of each sample (A, B, C) are tested for normality. Levene's test is performed to confirm equality of variances among different samples presenting same geometry. Afterwards, ANOVA and T-Test are performed to confirm similarity in E_a values by employing respectively different samples with the same height or samples with different height. Eventually T-Test is further adopted to evaluate variability among single samples 2 mm height tested at different velocities.

SAMPLE	TRIPLICATES	SHAPIRO TEST	LEVENE'S TEST	ANOVA	T-TEST	T-TEST VARYING VELOCITY
PDMS2	A	0.263	0.547	0.923	0.000	0.309
	B	0.575				0.113
	C	0.143				0.824
PDMS10	A	0.558	0.597	0.073		-
	B	0.802				
	C	0.599				

This suggests that a shorter height causes an underestimation of the final apparent elastic modulus. T-Test statistics showed no significant differences by comparing series of data referring to a single PDMS2 sample compressed

first at 1 µm/s and then at 10 µm/s although its orientation in the machine was varied (Table 4.5). These findings imply the rate of application of the stimuli and the orientation in the machine to not elicit any effect on the mechanical response of samples when a compact and elastic material such as PDMS is considered. Moreover, variances remained consistent among different samples or varying testing conditions. Indeed, standard deviation values were below ± 0.2 MPa regardless of velocity, height and repositioning of the sample. As consequence, this value was considered representative of the standard deviation caused by the human and systematic error.

4.3.5 3D PCL variability analysis

A different situation was instead observed when compressing 3D PCL scaffolds due to the texture of the architecture and the absence of a compact material.

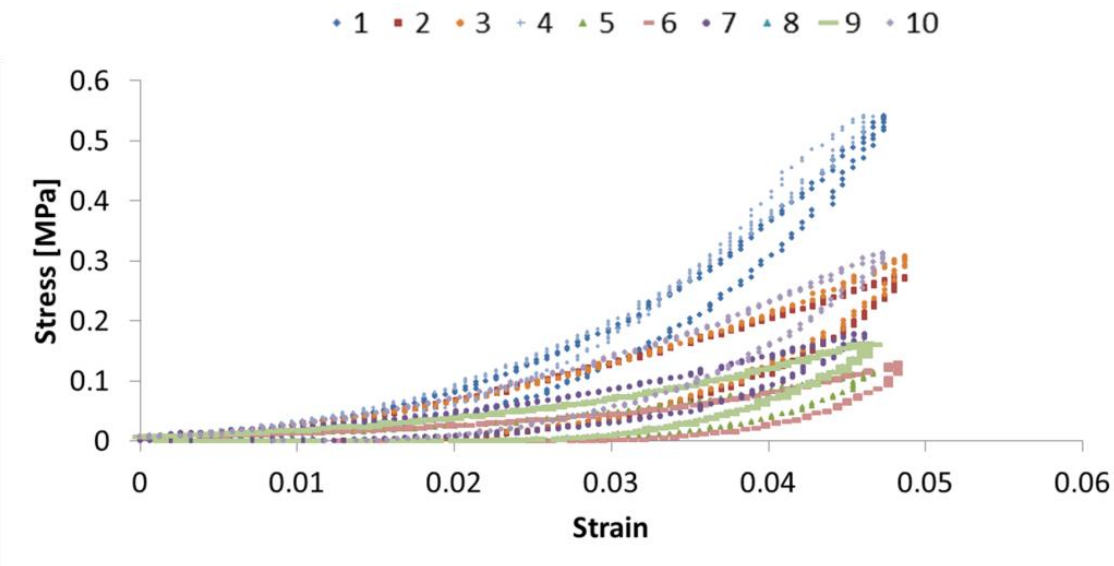

Fig. 4.17: stress/strain curves (1-10) repositioning the same sample among compression ramps applied at 10 µm/s.

Conversely to what was observed testing PDMS in the same conditions, a high variability in the mechanical response was noticed which cannot be clearly associated to any particular feature. Indeed, stress/strain curves did not overlap when a single 3D PCL sample was compressed several times varying its orientation (Fig. 4.17). The average percentage error resulting from the application of a defined compression protocol remained constant among specimens, amounting to 1 MPa.

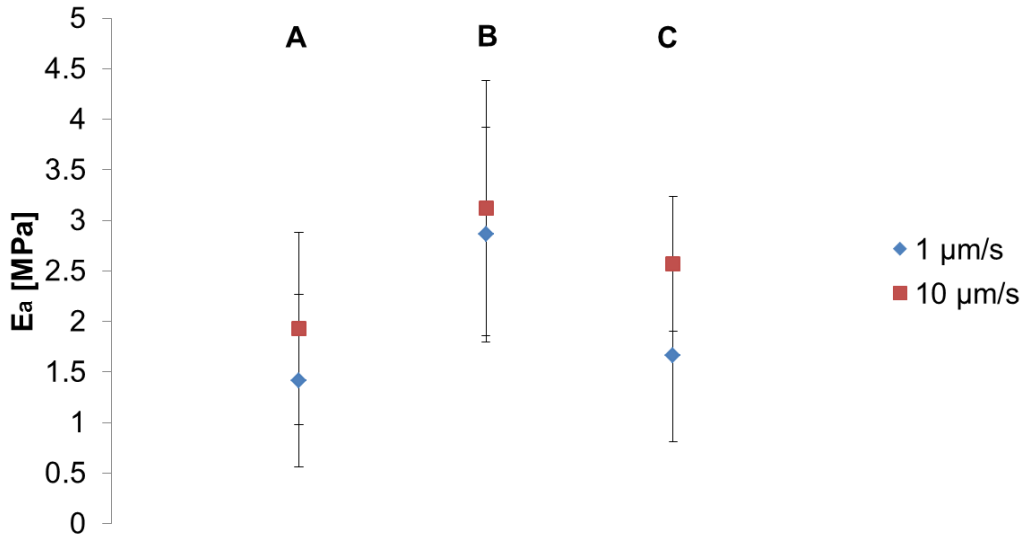

Fig. 4.18: Apparent elastic modulus (n = mean±S.D.) of 3D PCL samples (A, B, C) tested varying the velocity of application of compressive ramps at 1 um/s (blue) and 10 um/s (red).

However, the overall error reached up to 30% of the measure depending on the E_a values associated with the mechanical response of samples to compression. Contrary to PDMS, 3D PCL showed also differences in the overall mechanical response when different samples were tested (Fig. 4.18) as already noticed by testing relaxation (Fig. 4.15A). According to Shapiro test, data series followed a non-normal distribution (Table 4.6) for sample A and B compressed respectively at 1 and 10 µm/s.

Table 4.6: Shapiro tests normality on 3D PCL samples compressed at 1 mm/s and 10 mm/s; Levene and T Test respectively verify equality of variances and identify any significant difference among single samples compressed at different velocity.

PCL SAMPLE	VELOCITY [µm/s]	SHAPIRO TEST	LEVENE TEST	T TEST
A	1	0.003	0.404	0.215
	10	0.069		
B	1	0.473	0.770	0.624
	10	0.034		
C	1	0.093	0.343	0.016
	10	0.199		

However, a further analysis on stem-leaf graphs was performed, revealing symmetry especially at 10 µm/s (Fig. 4.19). Following those outcomes, data series were considered as normally distributed while the presence of outliers was associated to human error occurring during the application of the initial pre-load.

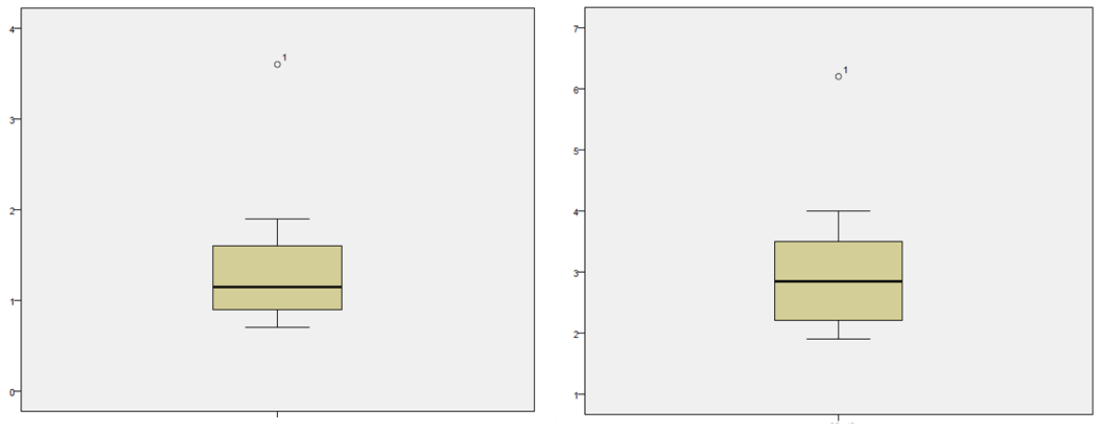

Fig. 4.19: stem-leaf diagrams to evaluate normality on samples with negative Shapiro tests results. From left to right, graphs refer respectively to sample A compressed at 1 µm/s and sample B compressed at 10 µm/s.

Considering normal distribution of data, parametric tests were employed for comparison of means between series, guaranteeing reliability especially at

higher compression rate. Conversely to PDMS, 1 out of 3 samples showed differences in the mechanical response when compressed at different velocity (Table 4.6).

Table 4.7: Tukey post-hoc test showing significant differences among E_a within different samples tested at 1 µm/s and 10 µm/s.

VELOCITY [µm/s]	TUKEY POST-HOC TEST		
	SAMPLES	A	B
1	B	0.010	-
	C	0.792	0.032
10	B	0.072	-
	C	0.221	0.462

Indeed, sample C resulted significantly stiffer ($p<0.05$) when compressed at 10 µm/s, suggesting velocity as a variable in the mechanical response of porous materials.

Table 4.8: Levene's test for equality of variances of samples (A, B, C) compressed at the same velocity.

VELOCITY	SAMPLE	LEVENE'S TEST
1	A	0.752
	B	
	C	
10	A	0.485
	B	
	C	

Given that, Tukey post-hoc test (Table 4.7) showed significant differences ($p<0.05$) between samples A, B and B, C at 1 μm/s. The differences in the mechanical response of samples became less evident at higher velocity as the mean value varied only comparing samples B and C with probability values falling close to the significativity threshold (Table 4.7).These findings highlight once more the importance of height and architecture in the definition of the mechanical response of the material. Despite the difference in the average E_a, the homogeneity of variances between series of data was obtained by Levene's test regardless of the sample architecture (Table 4.8), allowing to define 1 MPa as the maximum standard deviation acceptable.

4.3.6 DMA analysis

Air and water were taken as variables in this study to define the effect of a different surrounding environment on mechanical behaviour of 3D PCL. From the results, no significant differences were found testing the same sample in dry or immersed state. Indeed, storage modulus (Fig. 4.20A), loss modulus (Fig. 4.20B) and tan δ (Fig. 4.20C) remained constant regardless of the environment surrounding the specimen. The pattern followed by samples increasing frequency was the same for all specimens tested. In general, increasing frequency above 5 Hz led to significant increase ($p<0.05$) in storage modulus and a significant decrease ($p<0.05$) in tan δ. Variations in terms of loss modulus were observed just on 1 sample out of 3, showing less dissipation effects with increased frequency.

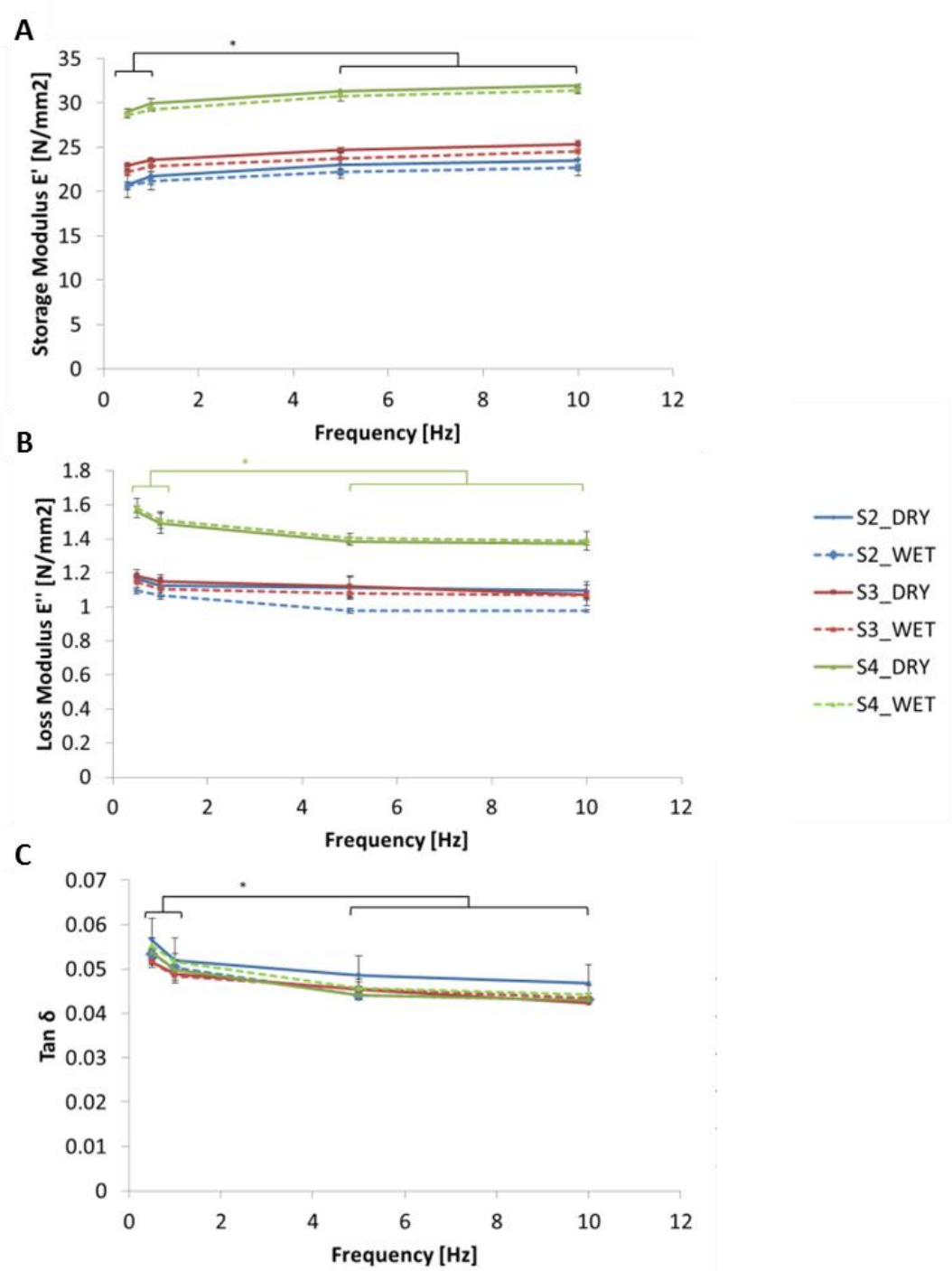

Fig. 4.20: (A) Storage modulus, (B) loss modulus and (C) tan δ (n = mean±S.D.) resulting from DMA analysis on three 3D PCL samples tested in air (continuous line) or water (dot line). Significant differences are marked by * (*p<0.05) referring to all samples (black bracket) or a single sample matching the colour of brackets.

4.4 Discussion

4.4.1 3D PCL apparent elastic modulus

Stress/strain curves showed a viscoelastic behaviour with non-linearity governing through a wide range of strains. E_a calculated as average σ over ε in the range of strain between 1-2.5% amounted to 2.2±1 MPa at 37°C. Such value classifies the 3D PCL as a good substitute for bone recovery as it matches the Young's modulus of fibrous tissue developing during early stage of healing and marrow [192]. However, an underestimation of the real value in terms of stiffness of the material is believed to occur due to the limited height of scaffolds, as demonstrated by applying the same conditions on PDMS samples at different height. Despite this, E_a remained constant among loadings on a single sample whose orientation was not varied. The repeatability of E_a enabled the investigation of the effect of temperature variations on the 3D PCL stiffness. The dependence noticed between mechanical responses to compression over temperature links to the polymeric nature of scaffolds which become softer at higher temperature due to the weaker bonds between adjacent polymeric chains. These thermal properties characteristic of polymeric materials [190] were also reported on PCL scaffolds tested either as a compact [193], [194] or a 3D structure [75], [189]. However, comparison among results is difficult because scaffold architecture affects the mechanical response to a given stimuli. Numerous studies in the literature [106], [184], [189] have shown indeed a strict correlation between porosity, pore size, offset between fibers and mechanical response. Thus, these parameters together with other properties of the sample - such as the geometry, degree of crosslinking and molecular weight – have to be taken into account when comparing results with the literature (Table 4.9). For example, the stiffer E_a values claimed by Hutmacher [189] could be correlated to the different 3D geometry of their scaffolds, or to the molecular weight of the rawmaterial whose value for 3D PCL is 43000-50000 Da. Despite the similar geometry considered in Yeo study [75], a higher modulus than for 3D PCL was

claimed probably due to the different laydown pattern as well as the inclusion of TCP particles in the structure. The stiffness of 3D PCL scaffolds with geometry similar to 3D PCL was tested by Sobral [106] who evaluated the mechanical response of scaffolds with pore size varying between 100 and 750 µm. The pore size of 3D PCL was considered to be 300±48 µm assuming a maximum 15.6% error from the average value provided by the manufacturer. The error was based on the assumption that pore size matched the same variability as the other geometrical features such as height, porosity, fiber diameter, surface area and volume. Given that, the pore size of 3D PCL fits in the range of porosity tested by Sobral allowing a comparison of the results. In their study, Young's modulus of samples ranged between 1.5 and 8 MPa for structures with pore size varying respectively from 750 to 100 µm. Our findings agree with Sobral's as E_a for 3D PCL compressed at 37°C amounts to 2.2 ± 0.1 MPa, therefore falling within the range of stiffness claimed by the literature study. Differences in the surrounding environment can be excluded due to the similar mechanical response obtained testing 3D PCL in air or water at 37°C. In the literature (Table 4.9), the percentage error of the average stiffness reaches 14% when consecutive identical compression cycles are applied on different samples. The deviation from the average value was instead higher in this study because of architectural differences and imperfections which lead to high variability in the 3D PCL mechanical response.

Table 4.9: Comparison among the literature studies evaluating the stiffness of 3D PCL when molecular weight, dimensions, compression protocol, laydown pattern, porosity, Pore size and surrounding environment are varied.

Study	Molecular weight	Dimensions [mm]	Compression protocol	Laydown pattern	Porosity [%]	Pores size [µm]	Surrounding environment	Stiffness [MPa]
Hutmacher	80,000	6.5 x 6.5 x 13.5	0.7% 16.7 µm/s (37°C)	0/60/120°	55	380 x 430 x 590	Air	41.9±3.5
							PBS	29.4±4.0
				0/72/144/36/108°	56	360 x 410 x 620	Air	20.2±1.7
							PBS	21.5±2.9
Yeo	115,000	3 mm height 5 mm diameter	80% strain 16.7 µm/s (27°C)	0/60/120°	70	-	Culture medium	23.1±6.2
Sobral	-	5 x 5 x 5	80% strain 33 µm/s (37°C)	0/90°	31	100	PBS	8±0.5
					81	750		1.5±0.2
					60	100-750-100		3±0.1
					56	750-100-750		3.5±0.5

4.4.2 Mechanical response and geometry

Before testing the dynamic mechanical performance, samples underwent static preconditioning in an effort to remove viscoelastic effects and guarantee reproducibility of the stimuli when several loading cycles are performed. Applying compression strains below 8% prevented the appearance of plastic deformation and enabled a complete relaxation of the structure from pre-stresses. 3D PCL scaffolds with an architecture similar to 3D PCL employed in our study relaxed under constant strain conditions over periods from few hundred of seconds [186] up to 33 minutes [187]. The differences with the literature are believed to correlate to differences in the initial molecular weight and the degree of crystallinity of samples. Despite the consistent response during dynamic compression, the overall stress varied among scaffolds due to differences in the geometry and the architecture. As shown by microCT reconstructions, fibers presented different dimensions and seemed to be fused together, randomly decreasing the spacing between layers in the z-plane. This variability caused significant differences in the porosity distribution and interconnectivity within samples. Moreover, the height of 3D PCL does not meet the requirements for reliable estimation of the elastic modulus, stating the height to be at least twice the diameter [195]. Consequently, boundary effects occurred leading to differences in the mechanical response when the orientation α of the same sample was varied. In addition, scaffolds often present a bullet-like shape due to the fabrication method requiring the cutting of cylindrical shaped scaffolds from large sheets of polymeric fibers produced by fuse deposition modelling. In order to understand the contribution of the geometrical variability of samples loaded in different orientations, PDMS was used as reference material. As a matter of fact, the error resulting from the compression of PDMS was formed by 1) a systematic component associated to the accuracy of displacement and load sensors, and 2) human error lessen by routine and well-established procedures but limited by human eye resolution. Given that, the error with the procedure was demonstrated to be below 10% regardless of the sample orientation. As consequence, the high

variability up to 30% characterizing the 3D PCL response can be reasonably assumed to be related to the geometry and architecture of samples. In order to reduce the geometrical variability, a sub-group of samples presenting the same height and diameter (n=7) was selected to identify a possible relationship between porosity and stiffness.

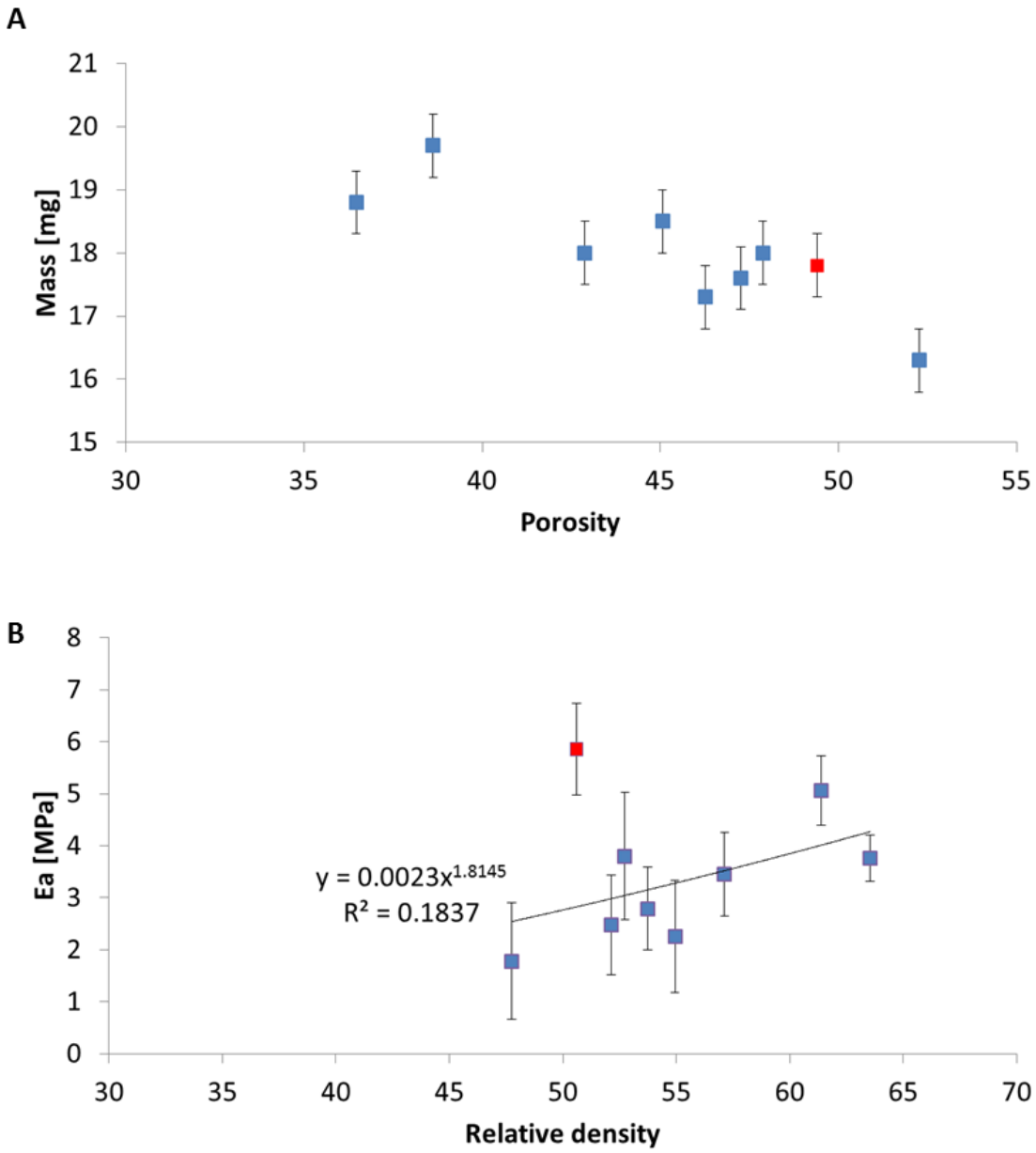

Fig. 4.21: (A) Mass and (B) apparent elastic modulus (n = mean±S.D.) vary with relative density of scaffolds presenting same height and diameter. The red point represents the sample whose behaviour was inconsistent with the general trend followed by the other specimens .

By 3D reconstruction and analysis of samples, a decrease in mass was correlated to an increase of porosity (Fig. 4.21A). Given that, further dependence between E_a and porosity was observed by performing mechanical compression. More porous scaffolds resulted softer than less porous ones matching results found in the literature where the effect of porosity, pore size and offset between fibers was shown to correlate to the stiffness [106], [188]. According to the literature, stiffness of open pores structures made of high molecular weight PCL is expected to increase with increasing material relative density, following a squared power law[196]. Here, a fit line with an exponent of 1.8 was the best representing the variation of stiffness with relative density (Fig. 4.21B), closely approaching the value mentioned in the literature. Indeed, porosity measurements give a good insight of the percentage of voids over material content without taking into account the size of pores and their distribution. In this particular case, the inconsistent mechanical response of the sample represented in red (Fig. 4.21) was further scrutinized by measuring fibers diameter. That step revealed the sample to be characterized by bigger fibers compared to other equally porous specimens, leading to a stiffer structure. Hence, average diameter, relative orientation of fibers or presence of small defects have a strong effect on the mechanical behaviour of scaffolds and must be considered for a more accurate evaluation of 3D PCL response to external forces.

4.4.3 DMA and stress distribution

DMA analysis defined the effect of different frequencies on 3D PCL mechanical response and helped with the evaluation of viscous and elastic properties of the structure. Increasing frequencies led to an increase in the ability of the scaffold to store energy as noticed by the increase in storage modulus and the simultaneous decrease of tan δ affecting all samples. Scaffolds with interconnectivity and geometry very similar to 3D PCL samples but higher height were demonstrated to follow the same pattern in terms of *E'*

and tan δ (Table 4.10). According to Sobral study [106], the differences observed comparing *E'* among samples can be addressed to larger pores characterizing S4. Moreover, *E'* was lower for all conditions tested compared to our findings because of the difference in the amplitude of the sinewave applied. Indeed, the amplitude of the strain at the peak of compression amounted to 6% in our experiment while it was just 1.4% in the literature study. A cylindrical geometry matching 3D PCL scaffolds presented here was investigated by Yilgor [188], although the height of the specimens and the protocol applied to samples during the DMA analysis were not clear. Despite this, storage modulus and tan δ values match the results found in our study when a laydown pattern of 0/90° is considered. Among others, DMA enabled also the investigation of the effect elicited by the external environment on the mechanical response of 3D PCL.

Table 4.10: Comparison of the literature studies testing the mechanical performance of 3D PCL.

Study	Dimensions [mm]	Compression protocol	Laydown pattern	Porosity [%]	Pores size [µm]	Surrounding environment	Storage Modulus [MPa]	Tan δ
Sobral	5 x 5 x 5	1.4% strain	0/90°	31	100	PBS	8 MPa at 0.1 Hz increasing linearly up to 11 MPa at 10 Hz.	Values between 0.10 and 0.16 depending on the porosity and progressively decreasing for frequencies up to 0.5 Hz. It remains constant for higher frequency values.
				81	750		Similar values between 2 and 4 MPa depending on pore size. It remains constant with increasing frequency	
				60	100-750-100			
				56	750-100-750			
Yilgor	10 Layers 5 mm diameter	-	0/90	51	-	Air	18.5±0.2	0.05
			0/90 + offset	66			3.5±0.1	0.07
			0/45/90	65			11.5±0.1	0.05
			0/45/90 + offset	57			9.7±0.1	0.05

No significant differences were observed comparing *E'*, *E"* and tan δ in air or in liquid. These results match findings in the literature related to five-layered pattern structures [189], while slightly different three-layered architectures, tested in the same study, were found to decrease stiffness upon immersion in PBS. The plasticity effect claimed by Hutmacher was also confirmed on different raw polymers in another study [197]. The parameters obtained by DMA analysis were used in the development of a computational model [198] aiming to clarify the distribution of stress into the structure at the peak of compression (Fig. 4.22).

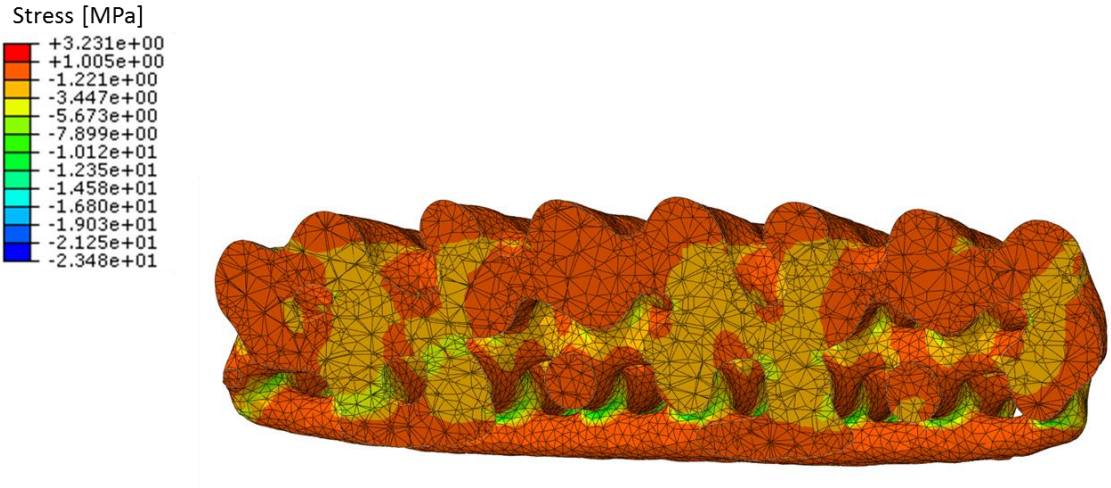

Fig. 4.22: Computational estimation of stress distribution on the surface of a scaffold undergoing 5% strain compression. The cross-section of the sample reveals the development of tensile strains (red) within the structure, while compressive stress (green) are concentrated mainly in the area of contact between fibers occupying consecutive z-planes [198]**. Despite this, the majority of the structure appears not to be affected by compression remaining in its un-deformed state (orange and yellow).**

The computational model revealed non-uniformly distributed stresses within the entire volume of scaffolds. Indeed, some fibers did not deform and compressive stresses were governing mainly at the contact surface between fibers. Moreover, local tensile stress prevailed in certain areas, causing bending of fibers as an effect of compression. Similar outcomes were claimed in literature by applying compression on open-cell nickel foams [199] where

compression led to the development of local strains in the weaker regions of the structure.

4.5 Conclusions

4.5.1 Summary

Despite the high variability encountered with 3D PCL scaffolds, the variation of the stress with the strain can be considered linear between 1% and 2.5%. E_a defined in this range remained constant among stimulations, allowing the investigation of a relationship between temperature and 3D PCL mechanical response. E_a varied consistently when the scaffold was repositioned or compared between different specimens because of boundary effects related to the small height and differences in terms of architecture. In order to define the real stiffness of the scaffold, 10 mm height samples would be required due to the conditions governing mechanical tests in compression and demanding for the height to be at least twice the diameter of the specimen. 3D PCL was manufactured by third parties and so the final dimensions of the construct were not modifiable. Consequently, E_a values obtained here cannot be considered as appropriate to define the mechanical properties of the material. Although the variability is among the main drawback associated to 3D PCL scaffolds, it provides a good representation of the in vivo conditions. As a matter of fact, the mechanical stimuli acting locally on injured bone sites are a combination of stretching and bending forces whose distribution depends on the shape of the fracture, the magnitude of the applied force and the stage of ossification [200]. The same distribution of stress is well mimicked in vitro inside a 3D fibrous specimen where fibers deform, leading to compression and tensile stresses as shown by computational analysis. The findings of this study confirm the suitability of 3D PCL to be used for bone mechanobiology studies

as 3D PCL was demonstrated to provide a reproducible mechanical response and to bear compressive mechanical forces.

4.5.2 Future work

A sample of compact raw material would be the ideal specimen to test to better define the mechanical properties of the 3D PCL. Indeed, the lack of such specimens prevented a full characterization of the single fibrous components not only in terms of response to mechanical forces but also of the chemical properties. Among the principal chemical cues, the molecular weight was indeed found to strongly affect the mechanical response of polymers [201]. However, the effect of pore size and fiber diameter on the mechanical response of 3D PCL cannot be investigated due to the random fibers dimension in the sample. A more reproducible geometry can be achieved by the optimization of parameters playing a role in the dimensional accuracy of fuse deposition modelling (FDM) such as temperature, humidity, wire diameter, layer thickness, road width and speed of deposition [202]. Alternatively, future studies may consider 3D PCL to be substituted with scaffolds made of the same polymer but providing a more regular structure through the use of more precise fabrication techniques such as 3D printing [203] and precision extruding deposition [204].

Chapter 5

MICROFLUIDIC PERFUSION BIOREACTOR

5.1 Introduction

In order to obtain uniform 3D tissue growth, cells must first be homogenously seeded in a scaffolding structure. Perfusion is claimed to be among the best techniques to obtain uniform attachment, although the investigation of various perfusion flow rates was often needed to establish the optimal seeding conditions [116], [122], [205]. Perfusion has also been used in numerous studies to investigate the effect of shear stresses on proliferation and differentiation of cells [124], [126], [129], [206], [207]. Despite the promising results, common perfusion systems require the use of high amount of reagents and to deal with equipment of large dimensions. The demand to decrease costs and facilitate the handling of bioreactors led to the development of microfluidic systems [134]. Microfluidic bioreactors require a low amount of reagents, are easy to develop by common soft lithography techniques, and allow the fabrication of devices easy to handle. Another advantage of microfluidic systems is their versatility which allows to manufacture devices with variable shape and with multiple chambers working in parallel to increase the reproducibility of experiments. Such devices were employed mainly in the study of the effect of fluid flow on cellular masses [208] to maintain the characteristics of the microenvironment otherwise prevented by the embedding of scaffolding structures. This study proposes different configurations of a custom-made microfluidic bioreactor made of Polydimethylsiloxane (PDMS) equipped with multiple chambers to evaluate how the seeding efficiency of 3D Insert ® PCL scaffolds (3D PCL) is affected by fluid flow. Increased flow rates can create large stresses within porous

scaffolds influencing cellular metabolism and shear stress magnitudes which can be detrimental to cell viability exceeding in vivo conditions [116], [205]. Therefore, a compromise has to be met between the mass transfer through porous structures and shear stresses occurring during seeding to prevent cell detachment and death although still supplying the necessary nutrients. According to the literature [120], shear stresses below 2 Pa are optimal in enhancing cell attachment, even though it is strictly dependent on the types of cells, the substrate and the time of exposure [209].

This study aims to 1) develop a custom-made microfluidic bioreactor able to provide a system for perfusion of scaffolds, 2) characterize the flow estimating the shear stresses acting through the structure to validate the suitability of the device for culture studies, and 3) evaluate the effect of different flow rates on cells attachment to establish the best approach for acceptable seeding efficiencies in future studies.

5.2 Material and methods

5.2.1 Fabrication method

The procedure for the development of microfluidic devices followed the same workflow regardless of the design used (Fig. 5.1). First, a mold with the patterns to be printed on the PDMS was created by applying adhesive stickers on top of a petri dish. Then, homodimer and curing reagent were mixed (1:10 w/w) and vacuum was applied for 10 min to remove bubbles from the viscous mixture. PDMS was then poured into the mold and let to cure at 75°C in an oven for 20 min. Once cured, the mold was removed and cut into shape. Holes were punched to hold the scaffold and 3D PCL were placed into the designed spaces. In order to define the path followed by the liquid, the mold and two glass slides underwent air plasma treatment at 100 W, 1 mBar for 30 s.

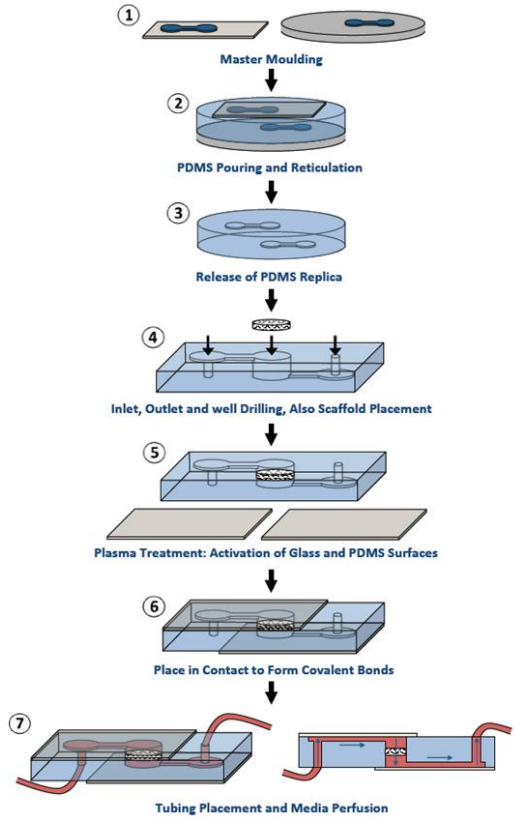

Fig. 5.1: Workflow followed to fabricate the microfluidic device by soft lithography of PDMS.

Immediately after the treatment, PDMS and glass were put in contact to covalently bond the surfaces. Eventually, 0.5 mm diameter tubes were inserted in the inlet and outlet to provide a close system for perfusion of scaffolds.

5.2.2 Fluid flow experiments setup

Microfluidic systems were connected to 1 ml syringes allocated in specific spaces for controlled pumping of fluid back and forward in the system. The liquid was aspirated in the syringes and dispensed by controlling the flow rate with external pumps (Fig. 55.2).

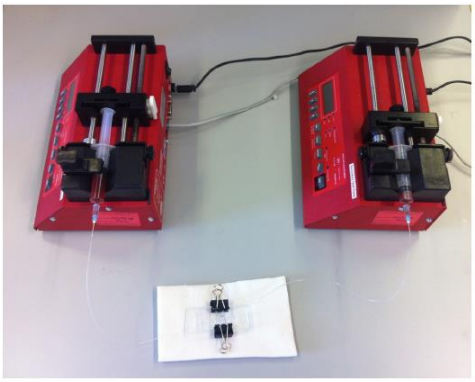

Fig. 5.2: Perfusion system setup composed of two pumps connected to the microfluidic device by syringes.

For cellular seeding experiments, consecutive dispensing and withdrawn of cellular suspension was required to increase the possibility of cell contact with the walls of the scaffold. Given that, the outlet tube was connected to another pump (Fig. 5.2), working in synergy with the first, to guarantee homogenous fluid flow through the system and decrease cell settling phenomena at the outlet.

5.2.3 Particle tracking

Particle tracking was performed by following the movements of fluorescent microspheres injected in a single chamber device. The particle tracking was performed to evaluate how the presence of the scaffold affects the average velocity of the fluid in the seeding chamber. The main hypothesis were formulated on the motion of particles assuming 1) null relative velocity between particles and fluid stream, and 2) the only force acting on particles to be the drag force of the fluid. Following these assumptions, the movement of spheres was reasonable to be considered as a representation of the fluid streams flowing through the device and could then be related to the force sensed by cells suspended in such a media. Particle tracking experiments employed a single chamber device (Fig. 5.3) since air bubbles removal was

easily achieved by manually increasing the pressure applied from the inlet and pumping ethanol into the system.

Fig. 5.3: Single chamber microfluidic system for particles tracking experiments with allocated scaffold and inlet/outlet tubes.

Then, the chamber was flushed with PBS to remove residues of ethanol. Fluorescent particles of 10 µm in diameter were suspended in PBS in a concentration of 10^6 particles/ml, and 8 ml of suspension was perfused varying velocity every 1 ml of volume dispensed. The velocities tested were 0.01, 0.03, 0.05, 0.07, 0.1, 0.3, 0.5, 0.7 mm/s. Images were acquired every 1 second by the Metamorph® software (Molecular Devices, LLC, USA) and analysed by ImageJ. The particle tracking was performed manually selecting the centre of spheres at each time frame. Measurements for each velocity were done on an average of four particles. The experiment was repeated three times in the effort to increase reproducibility when comparing devices fabricated at different time, and to take into account the effect elicited by variation in scaffold geometries.

5.2.4 Shear stress calculation

From the results obtained by the particle tracking, it was possible to calculate the average shear stress τ considering a laminar flow through the specimen by applying the Kozeny-Carman equation. It relates the drop of pressure caused by friction effects to the shear stress acting in the system [210]:

$$\tau = \frac{8\mu v_{in}}{d^2} \qquad \text{(Eq. 5.1)}$$

where μ is the viscosity of the fluid, and d is the diameter of the pores.

The kinematic viscosity μ of PBS was set to 8.9 x 10^{-4} Pa·s [211], while the diameter of pores was 300 µm according to the manufacturer.

5.2.5 Single chamber system validation

In order to show the suitability of the system in enhancing cell attachment within the range of velocities tested, osteosarcoma cells (MG63) were suspended in 10 ml of medium in a concentration of 10^6 cells/ml and 500 µl of cell suspension was perfused through the inlet of the bioreactor at 0.01, 0.1 and 0.5 mm/s. After 2 h of perfusion, specimens were removed from the device and cell viability was qualitatively determined by fluorescence imaging (Chapter 3.4.4). The fluid flow was set in dispense and withdrawal mode to continuously pump cells and increase the probability of scaffold-cell contact.

5.2.6 Multi-chamber system validation

Multi-chamber configurations employed devices fitted with three spaces placed in series or in parallel (Fig. 5.4) for scaffolds allocation. While the in-series configuration provided consecutive perfusion through all the three scaffolds (Fig. 5.4A), the in-parallel configuration divided the main stream in three minor channels each leading to a single scaffold (Fig. 5.4B). In the latter configuration, the fluid coming from each chamber connected again into a main stream and moved toward the opposite pump. Fluid flow was inverted every 500 µl of volume were dispensed.

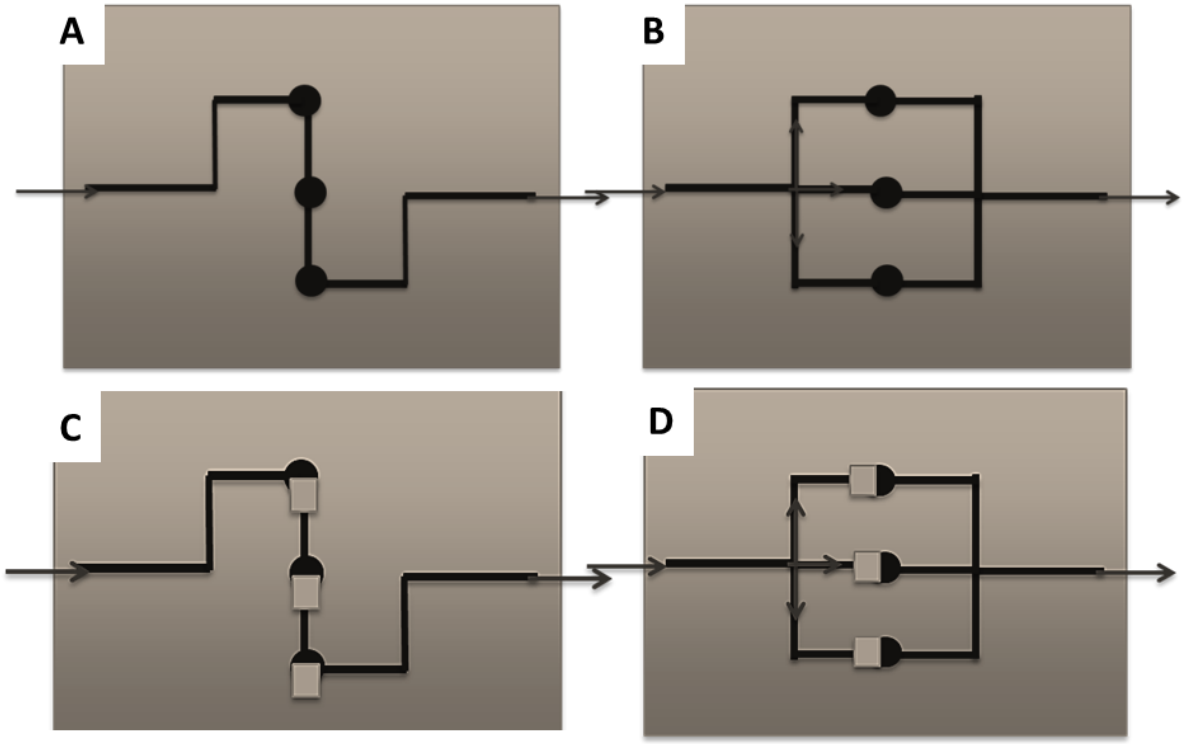

Fig. 5.4: Top view of (A, C) in-series and (B, D) in-parallel design. Both designs are shown (A, B) without or (C, D) with bubble traps.

Following single chamber validation experiments, an inlet flow rate of 0.5 mm/s was set to guarantee optimal seeding conditions. In order to avoid the inconvenience brought by residual air sitting in the middle chamber, both configurations were further provided with bubble traps (Fig. 5.4C&D) by adding two empty specular areas located on the top and bottom of each chamber (Fig. 5.5).

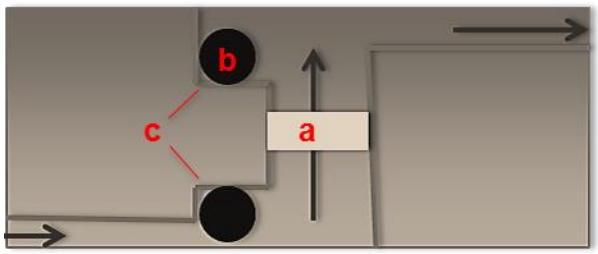

Fig. 5.5: side view of a chamber showing the path followed by fluid flow through (a) the scaffold. (b) Bubbles are trapped in (c) bubble traps areas.

MG63 viability and seeding efficiency was evaluated by fluorescence imaging and quantified by DNA assay (Chapter 3.4.6) at 1,2 and 3 h on three different devices with an in series configuration.

5.2.7 Dynamic seeding

Human embryonic stem cell-derived mesodermal progenitors (hES-MPs) were suspended in 1 ml of media in a concentration of 16 x 10^4 cells/ml and were injected at 0.1 mm/s and 0.5 mm/s into the system, allowing inversion of the fluid stream every 500 µl dispensed.

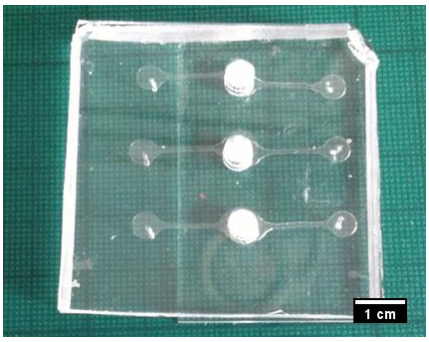

Fig. 5.6: In-parallel configuration fitting three independent scaffolds in the same device.

The bioreactor chosen for the dynamic seeding of cells presented three single chambers placed in parallel on the same device to apply equal conditions on three independent specimens (Fig. 5.6). A total of five scaffolds were accounted for each condition. Chambers developing bubbles within the duration of the experiment were discarded, as their presence led to the failure of the most important hypothesis of our study demanding for uniformity in the fluid flow. After 24 and 48 perfusion cycles from the beginning of the seeding process, the device was sacrificed and specimens were tested for cell number quantification by DNA assay (Chapter 3.4.6).

5.2.8 Static seeding

Scaffolds (n=5) underwent sterilization (Chapter 3.4.1) hES-MPs were then suspended in a concentration of 16 x 10^4 hES-MPs/ml in culture media and statically seeded following common techniques (Chapter 3.4.3). Samples were collected and tested for DNA quantification (Chapter 3.4.6) after 24 h and compared to dynamic seeding results.

5.3 Results

5.3.1 Single chamber devices and fluid flow

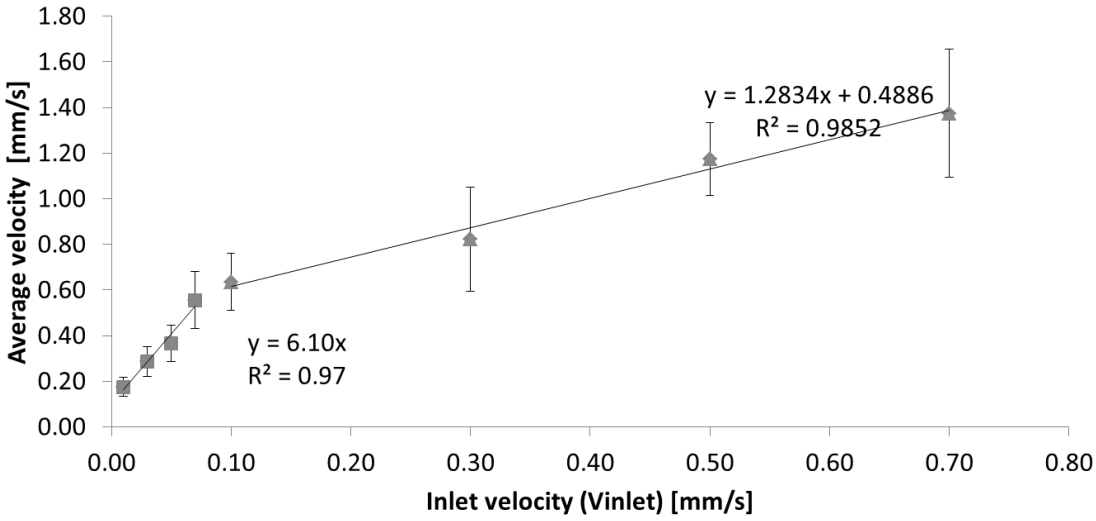

Fig. 5.7: Relationship between internal velocity and inlet velocity obtained by tracking of fluorescent particles.

By particle tracking experiments, it was possible to define a relationship between the inlet flow rate (v_{inlet}) and the average velocity acquired by particles (v) (Fig. 5.7). v increased proportionally to v_{inlet}, leading to a 6-fold increase

when particles were perfused through the scaffold pores with velocities up to 0.1 mm/s. For velocity above 0.1 mm/s, particles varied their kinetic behaviour showing only a 1.33-fold increase in velocity. At higher velocity, a rise of the average error associated to the measure was also observed due to difficulties in precisely tracking the displacement of particles during the manual post processing of images.

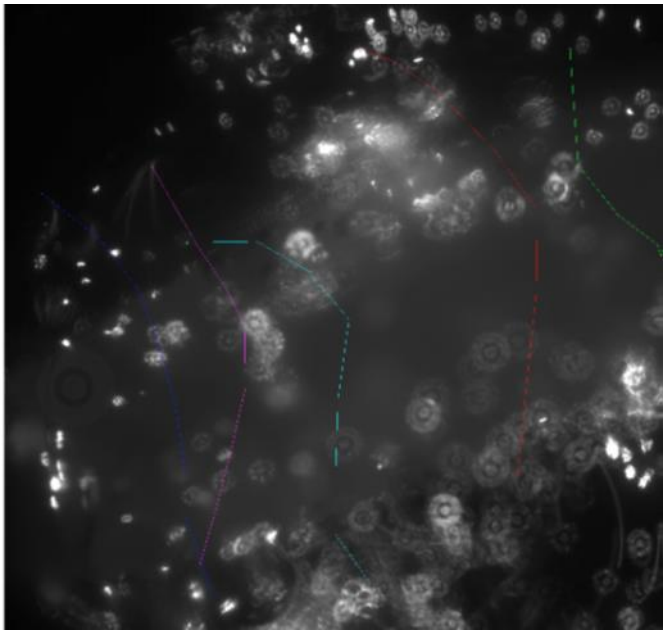

Fig. 5.8: Fluorescent imaging of particles stuck to the PDMS chambers after several perfusion cycles. Coloured lines show the pathway followed by particles through the specimen and are obtained by manual tracking.

Indeed, not only at higher velocities particles were moving faster making difficult manual tracking, but also a higher amount of particles stuck to the PDMS structure causing an increase of the fluorescent background in the images proportional to the duration of the experiments (Fig. 5.8). The values obtained from the tracking experiments were used to calculate the average stress into the system. By applying the Kozeny-Carman relationship, the shear stress never exceeded the recommended values for cell attachment in the range of velocities tested (Fig. 5.9), reaching a maximum value of 0.14 Pa for a velocity of 0.7 mm/s.

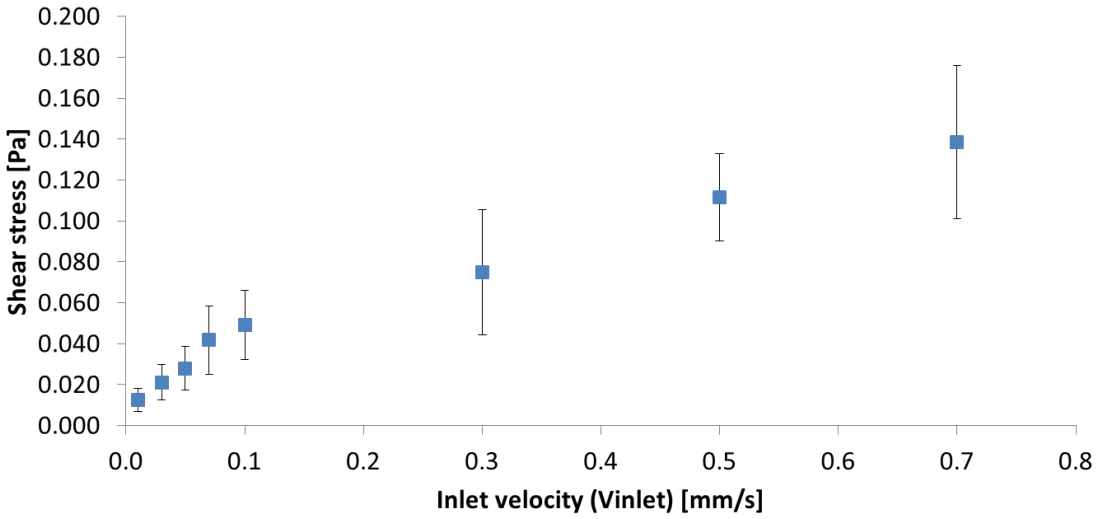

Fig. 5.9: Shear stress calculated using kozeny-Carman equationvarying inlet fluid velocity.

In order to find the velocity giving the highest attachment, three different inlet rates were applied to suspension of MG63 cells cultured in single chamber devices without bubble traps. By qualitative evaluation of cellular viability through fluorescence images, a velocity of 0.01 mm/s was found to prevent cell attachment to the scaffold (Fig. 5.10A) while 0.1 mm/s allowed cell adhesion and enhanced viability (Fig. 5.10B). A velocity of 0.5 mm/s gave the best results with numerous cells occupying the pores of the scaffold (Fig. 5.10C). Indeed, cells seeded at 0.5 mm/s not only were well spread through the pores but also began extending protrusions, suggesting enhanced cellular adhesion. Although perfused cells are expected to uniformly occupy internal areas of the scaffold, not many cells were attached to the surface of fibers and the difference in pore dimensions led to variation in terms of cellular distribution.On the contrary, static seeded 3D PCL showed higher number of cells and uniform cellular distribution on the top of the scaffold. Moreover cells were better spread and presented bridging among neighbour polymeric fibers.

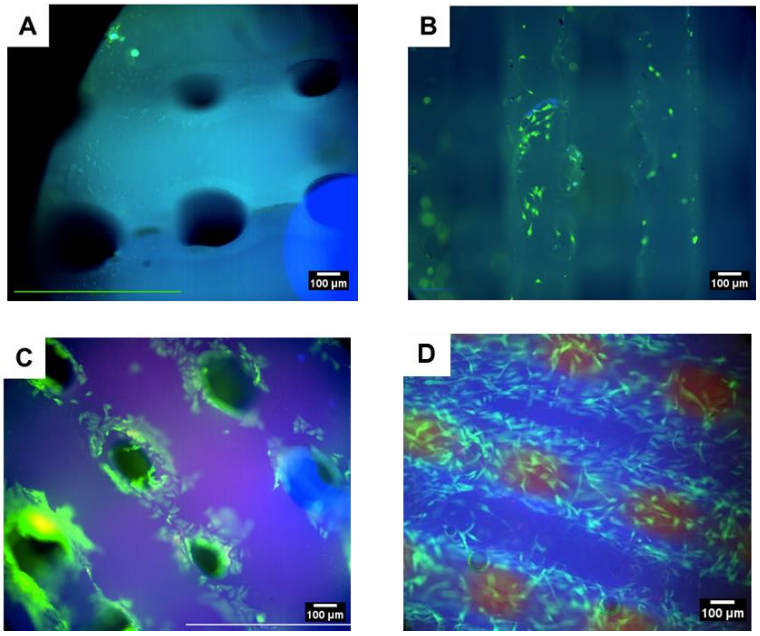

Fig. 5.10: MG63 seeded PCL by perfusion at (A) 0.01, (B) 0.1, (C) 0.5 mm/s, and (D) by static seeding.

5.3.2 Multi chamber configurations

Employing multi-chamber with an in-series configurations led to uniform distribution of cells through a single scaffold (Fig. 5.11). However, considering specimen tested in the same device but located in consecutive chambers, the number of cells attached varied with more cells occupying the first (Fig. 5.11A) and last (Fig. 5.11C) structure compared to the one in the middle. This phenomenon was due to difficulties related to the bubble removal in the central chamber.

For in-parallel setups, the removal of bubbles was difficult, leading most of the time to failure of the glass-PDMS bond achieved by plasma because of the high pressure required at the inlet to push air outside the system. Moreover, as for in series configurations, scaffolds presented significant differences and very low number of cell attached.

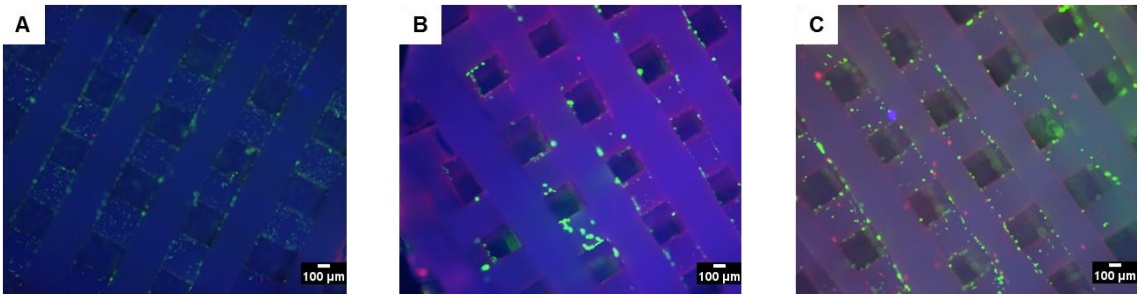

Fig. 5.11: Viability of cells employing a in series configuration considering scaffolds located respectively in the (A) first, (B) middle, (C) last chamber of the device.

The introduction of bubble traps led to very similar results comparing scaffolds belonging to the same device as proved by DNA quantification (Fig. 5.12).

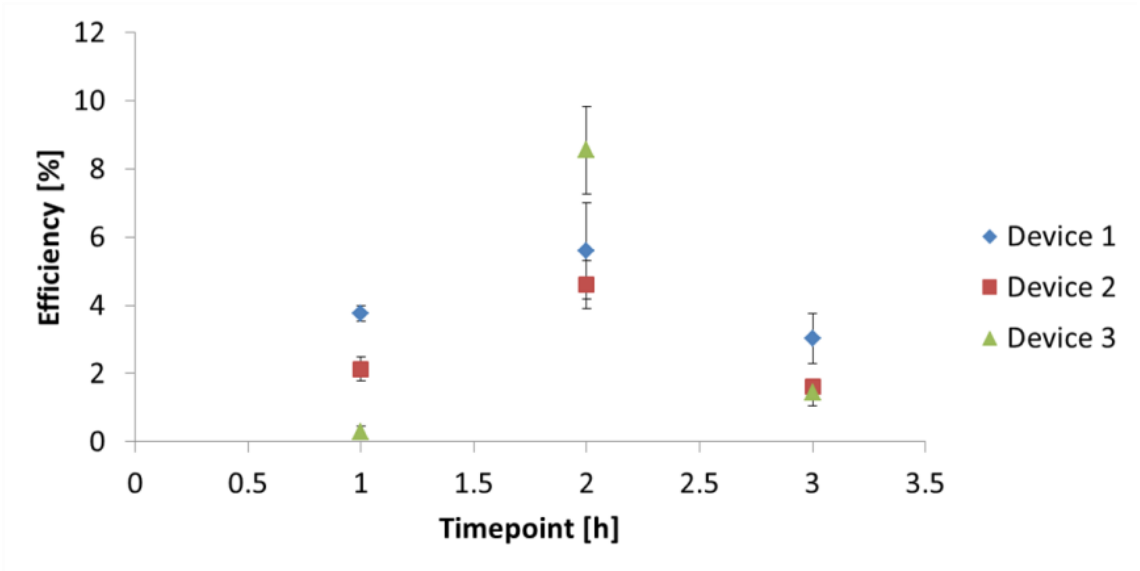

Fig. 5.12: Comparison between seeding efficiencies obtained by perfusion of three different multi-chamber devices within-series configuration.

All systems tested showed the same trend with MG63 attachment reaching a peak after 2 h of seeding and, then, showing a progressive detachment of cells. Despite the similar pattern of attachment in different microfluidic systems, significant differences were detected when comparing the seeding efficiencies among devices. Indeed, although the same initial mold was employed in the

fabrication of the three devices, small imperfections in terms of micro features caused the nucleation of bubbles during the seeding process and produced variations above 20% in the final amount of detected cells.

5.3.3 Static versus dynamic seeding

The dependence between inlet flow rate and cell adhesion capabilities was evaluated by dynamically seeding hES-MPs at different velocities (Fig. 5.13). 0.5 mm/s perfused scaffolds led to lower attachment compared to samples seeded at lower velocity, suggesting hES-MPs to be more sensitive to shear stress than MG63.

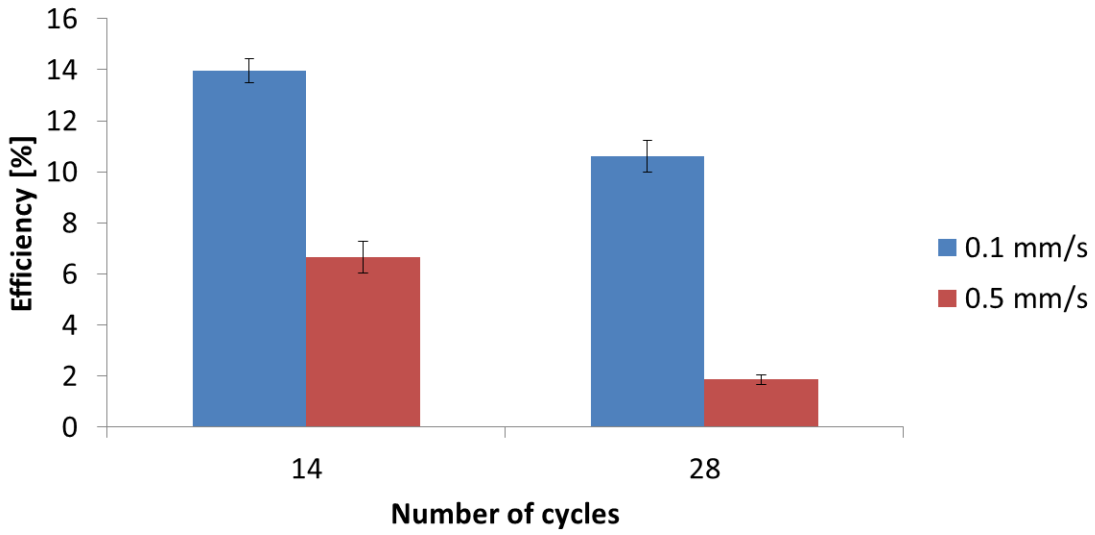

Fig. 5.13: seeding efficiency obtained after perfusing hES-MPs at different velocities and for a variable number of cycles.

Regardless of the velocity applied, shear stress elicited a negative action on cell adhesion, causing progressive detachment in higher amount for higher flow rates. Compared to static seeding results where 40% seeding efficiency was achieved, dynamic seeding induced very low attachment allowing at best only 14% of cells to adhere.

5.4 Discussion

5.4.1 Movement of particles and shear stresses in a single chamber device

As demonstrated by particle tracking experiments, a single chamber configuration provided a uniform and reproducible fluid flow through the system and consistency in the results with errors, in terms of particles velocity, below 10%. Despite this, an increase in the standard deviation was noticeable when particles were moving at velocities higher than 0.1 mm/s due to errors related to post-processing of data. Indeed, particles moving fast were difficult to track and after few minutes from the injection in the systems, fluorescent background was developing preventing precise manual selection of the particles. Moreover, higher velocities may also have caused recirculation phenomena around and within the scaffold, leading to a variation of the common pathway followed by particles and an increase in the variability of the measured velocity [212]. The change in slope observed for velocities above 0.1 mm/s was instead absent in computational simulations [212]. This suggests that the variation was associated to experimental conditions, not considered during simulations, rather than the geometry or architecture of scaffolds. Given that, the variation in slope observed experimentally is believed to be related to a progressive failure of the glass-PDMS bonding when high pressure is acting in the system. Probably, the pressure in the system increases consistently for velocities above 0.1 mm/s causing an enlargement of the microfluidic channels due to the infiltration of liquid between the bonded glass and PDMS. As a consequence, the increase in area accessible by the fluid may cause a decrease in the average particle velocity to maintain the condition of constant inlet flow rate. The range of shear stress resulting from fluid flowing through the scaffold gave acceptable values for cell attachment for all velocities tested. Further comparing with computational results [212], simulations showed lower velocities compared to experiments for a given inlet rate (Fig. 5.14).

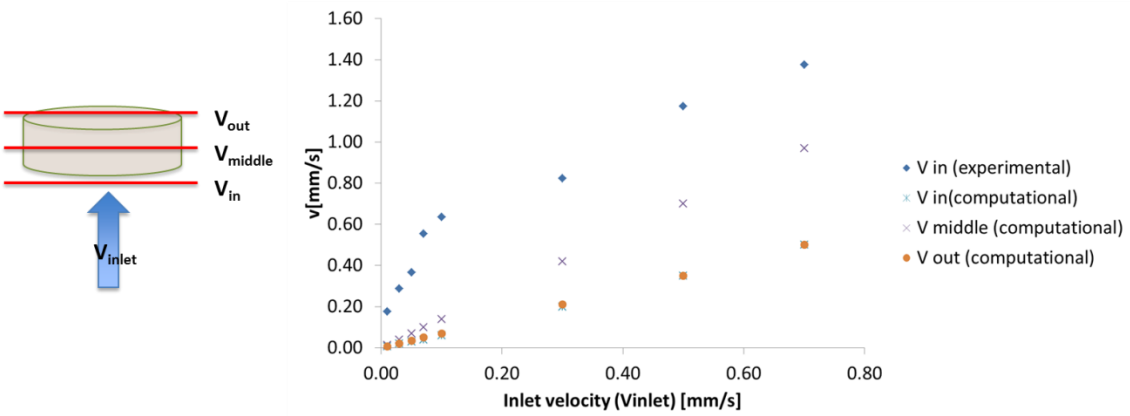

Fig. 5.14: velocity of particles resulting from average among experiments or calculated at different planes by computational simulations.

The discrepancies observed between experiments and computational model can be related to differences in the geometry of the scaffold. As observed analysing scaffolds geometry (Chapter 4.3.1), the architecture of specimens varied significantly in terms of height, pores and interconnectivity, facilitating the passage of particles and decreasing values of resulting shear stress for scaffolds with larger pores, lower interconnectivity and shorter height. Another source of variability was represented by the cross-sectional plane chosen to calculate the velocity.

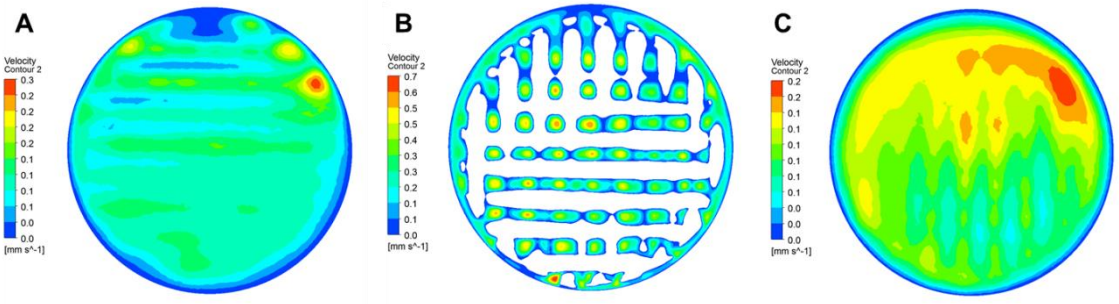

Fig. 5.15: Cross-sectional planes showing the distribution of velocities at the (A) top, (B) middle, (C) bottom of the sample for a 0.1mm/s inlet [212]**.**

Indeed, particles at the entrance (Fig. 5.15A) and at the exit (Fig. 5.15C) of the scaffold moved slower, while higher velocities were detected in the middle plane. Here, pores decreased the area available for the fluid to flow, leading to an increase of the average particles velocity to comply the mass transfer dictated by the inlet flow rate (Fig. 5.15B). Last but not least, the geometry of the chamber used in the simulations was considered to be perfectly cylindrical during the simulations, while scaffolds presented many defects especially at the periphery.

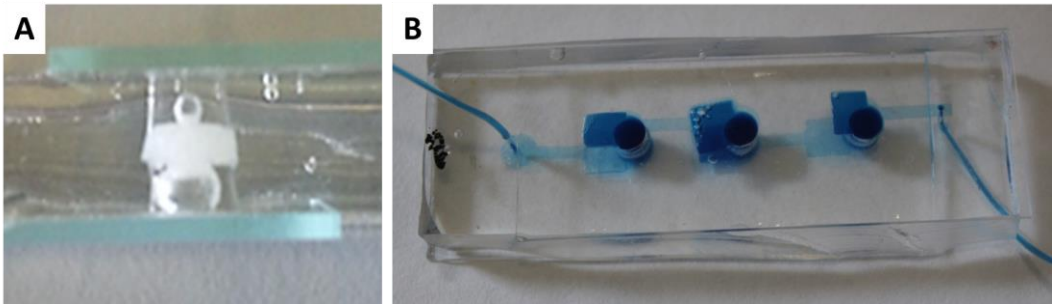

Fig. 5.16: (A) scaffold located in a single chamber microfluidic device. The chamber slightly deform at the bottom of the scaffold, matching the geometry of the structure. Following injection with PBS, bubbles develop (A) the top and bottom of scaffold and (B) bubble traps areas.

For this reason, empty spaces were surrounding specimens during computational simulations where the resistance of the fluid was lessened. As a consequence, particles moved toward those areas rather than through the specimen, causing a decrease in the average velocity of particles crossing the sample. This phenomenon was instead prevented experimentally by the elasticity of PDMS which wrapt the edges of the scaffold, often causing a slight deformation of the internal diameter of the chamber to better adapt to the profile of the structure (**Error! Reference source not found.**A).

5.4.2 Bubble nucleation and variability

The main issue affecting custom-made systems was related to the removal and prevention of air bubbles. When injecting the liquid for the first time, bubbles developed on the top and the bottom of the scaffold requiring further removal by applying manually high pressure from the inlet (**Error! Reference source not found.**A). This procedure worked well with single chamber devices but did not lead to satisfactory results in configurations equipped with multiple chambers. Indeed, the complete removal of bubbles from all the chambers required high pressure from the inlet, often leading to failure of the bonding achieved by plasma treatment between PDMS and glass. Introducing traps at the top and bottom of the scaffolds allowed to confine bubbles in areas where the fluid flowing through the specimen was not affected by their presence, enhancing a more uniform distribution of cells among specimens with comparable results when an in-series configuration was employed (**Error! Reference source not found.**B).

On the contrary, this solution was not equally efficient considering in-parallel configurations due to slight differences in the architecture of channels splitting the fluid in three main streams and leading each to a different sample. Of course, higher pressure acted on chambers characterized by small inlet channels hence facilitating the removal of bubbles while having minimal effect on chamber connected by larger inlet. The negative effect caused by imperfections in the initial mold was also observed in seeding efficiency values obtained comparing bioreactors fabricated at different times.

Indeed, even though bubbles were removed at the beginning of the experiment, new ones were nucleating during the perfusion process. When devices were equipped with traps, bubbles moved away from the main stream but caused a decrease in the area for the passage of the fluid correlated to the amount of accumulated air. Thus, the fluid flow was consistent among specimens placed on the same stream (in-series configuration) but caused differences in the velocity of cells comparing different devices as mass transport varied depending on the amount of accumulated air. Moreover, the

bubble traps were working as storage for air content but also for cells. Indeed, once injected in the chamber cells were free to move following the main stream and remained trapped in large amount in bubbles designated areas (**Error! Reference source not found.**).

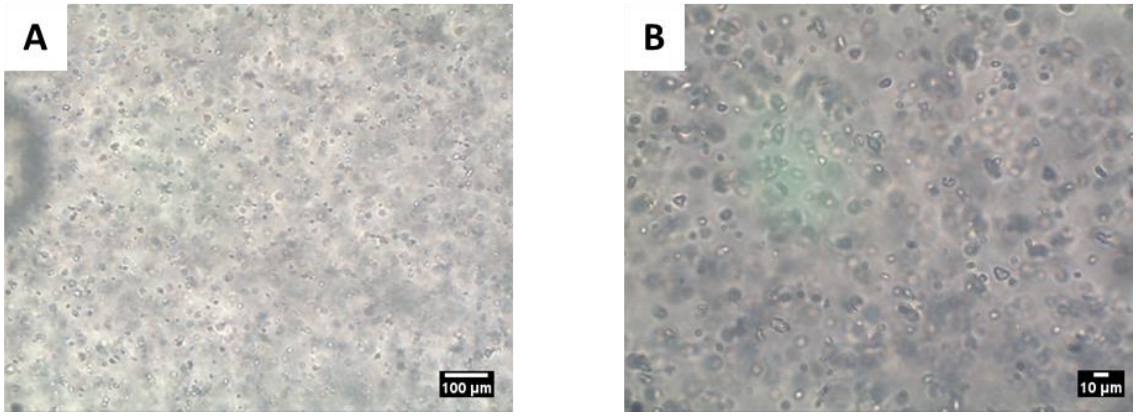

Fig. 5.17: Optical images of cells trapped into bubble trap areas at (A) 4X and (B) 10X magnitude.

5.4.3 Static seeding versus perfusion of hES-MPs

In order to use the microfluidic bioreactor developed in this study in the evaluation of cell attachment over time varying velocity, a compromise between efficiency, repeatability and bubble formation was needed and it was achieved by employing a single chamber system without bubble traps. This configuration guaranteed repeatability of the experiment and minimal dispersion of cells in the system but limited the use of such systems to short time experiments due to the nucleation of bubbles. For this reason, experiments were carried out for a maximum of 3 h, enabling the investigation of the effect of fluid flow on attachment capabilities but not proliferation and differentiation of cells as instead performed in other studies [126], [207]. Indeed, beyond the advantages related to the uniformity of the fluid flow, microfluidic devices are largely affected by the presence of bubbles, causing cellular death and non-homogeneous fluid flow. The selected regimes led to low seeding efficiency values reaching at best 14% at 0.1 mm/s. Similar results

were observed by computational simulations, revealing the preferred pathway followed by cell to match the centre of pores avoiding contact with fibers [212]. By computational simulations, it was also possible to observe the beneficial effect of gravity on seeding efficiency (Fig. 5.18). For all the velocities tested, gravity allowed an increase in the number of cells attached showing respectively 3.1, 1.9 and 1.6 fold increase compared to the case where gravity was not accounted for. Moreover, the increased magnitude of the drag force of the fluid in the perfusion system progressively nullified the action of gravity. This provides a possible explanation to the low attachment observed at low flow rate and confirms the presence of settling phenomena causing cellular sedimentation into the syringe as well as in the interior of the chamber.

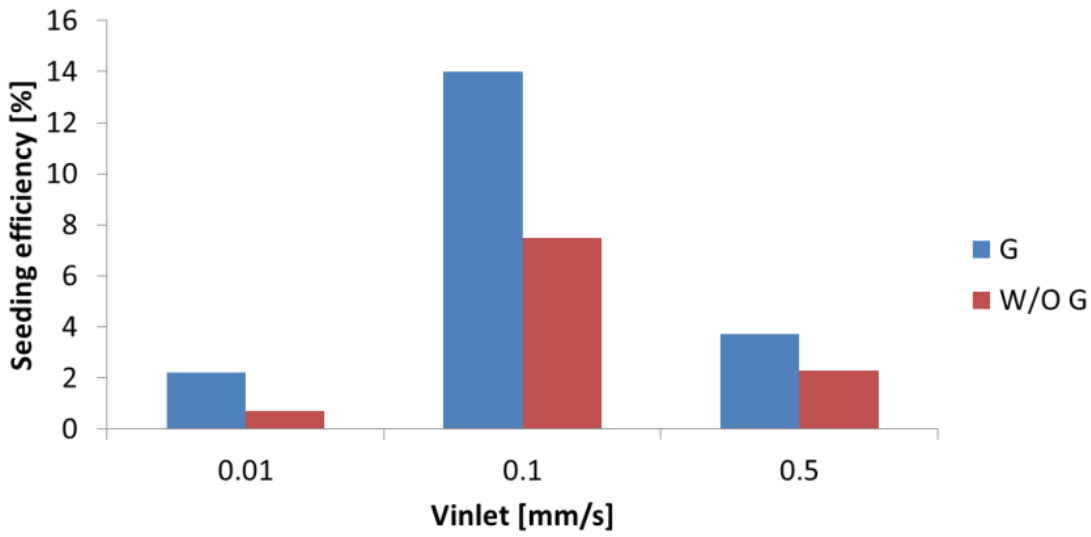

Fig. 5.18: seeding efficiency at 0.01, 0.1 and 0.5 mm/s accounting for gravity (G) or considering gravity less (w/o G) computational simulations [212]**.**

The low attachment can also be related to the unidirectionality of the flow regime. Indeed, the inversion in flow direction was applied covering ranges of minutes, leading to the development of a unidirectional fluid flow. Better attachment could be obtained inverting the fluid flow more frequently. The application of an oscillatory regime is indeed shown to improve cell attachment and induce a more uniform cellular proliferation in 3D perfused scaffolds [205].

Dependence among seeding efficiency and number of cycles as that claimed here was also observed in other studies [116], although they have used a perfusion system of larger dimensions.

5.4.4 Effect of perfusion on cells attachment

Analysis of the distribution of cells in the interior of the scaffold was not performed due to the limited penetration of fluorescence light through the 3D PCL, limiting the qualitative analysis of distribution of cells to the surface of the scaffold and the most external pores. Moreover, the low and variable amount of cells detected by perfusion prevented also the use of x-ray techniques, as the contrast created by cells was too low to give a clear idea of their disposition. The number of cells attached was very variable among samples in multi-chamber devices. A multi-chamber system able to perfuse simultaneously four parallel chambers, each containing three polymeric scaffolds placed in-series was proposed by Zhao et al. [213]. Similarly to what was observed in this study, the number of cells remained constant among scaffolds placed in-series but higher seeding efficiency up to 60% was obtained. Moreover, scaffolds placed in parallel chambers showed consistency in the number of cells attached. This is due to the different perfusion setup and the seeding technique which provided not only a more uniform distribution of stresses through samples belonging to different chambers, but also more uniform distribution of cells by seeding with the depth filtration method. Despite this, observing fluorescent images of MG63 perfused through scaffolds by in-series multi-chamber systems, cells were better distributed within the pores than those injected by static seeding where they looked mainly spread on the surface. Similar results were also found in the literature where oscillatory fluid flow was indeed found to provide more uniformly distributed scaffolds compared to static seeding methods [122].

5.5 Conclusions

5.5.1 Summary

Despite issues related to bubble nucleation and variability of results obtained with multi-chamber configurations, this study clearly defined the flow through a single chamber system determining the shear stresses acting on the scaffold walls and consequently felt by cells immersed in the perfused solution. Low values of seeding efficiency are believed to be related to the lack of contact between cells and scaffold as well as to settling phenomena occurring in the device. As confirmed by computational simulations, the first is correlated to the unidirectional nature of the imposed fluid flow driving cells through the centre of pores rather than close to the fibers, while the second is strongly linked to the dragging action elicited by gravity. Moreover, due to the low attachment, the distribution of cells in the scaffold was difficult to determine, preventing to draw reliable conclusions on the effect of perfusion on cell distribution within the scaffold. Thus, the proposed system allowed to define the flow inside the scaffold when perfused by cell suspension and suggested static seeding methods as the preferred option for increased seeding efficiency of 3D PCL scaffolds rather than continuous perfusion.

5.5.2 Future work

The device developed in this study can be further employed with a single chamber design to investigate the effect of different flow regimes on cellular attachment, while settling phenomena can be overcome by injecting cells directly on the top of the samples already allocated in the perfusion chamber. For example, 30 gauges needles can be used to access the interior of the device exploiting the elastic properties of PDMS. Indeed, a thin needle should be able to penetrate through the side of the microfluidic device and develop a

thin channel disappearing once the needle is removed. This approach based on local injection of cells requires optimization of seeding procedure to guarantee cell survival. Moreover, the volume of cell suspension to inject and the volume of media to perfuse at each cycle need further optimization to guarantee uniform initial distribution of cells among scaffolds embedded in the device and minimal dispersion of cellular content in the perfusion process. Further options to increase the seeding efficiency can involve either the external rotation of the device deviating cells from the main stream and increasing contact occurrences as proposed in previously studies [102], or the physical or chemical functionalization of the scaffolds surface [125], [214]. Last but not least, bubbles formation represent the main constrain of the custom-made device presented in this study limiting the use of such system to short term experiments. The next step toward the use of the microfluidic device developed here for longer differentiation studies concerns the improvement of the initial mold. More precise fabrication techniques, such as 3D printing, could be considered to provide an imperfection-less surface, high accuracy features and high reproducibility of the mold.

.

Chapter 6

A NOVEL COMPOSITE SCAFFOLD: 3D Insert ® PCL AND COLLAGEN GEL

6.1 Introduction

PCL constructs fabricated by rapid prototyping techniques based on the deposition of consecutive layers of fibers are widely employed for studying cells activities [188], [189], [215], [216]. Their architecture overcomes limitations related to lack of structure observed on common 2D substrates. Geometrical features such as pore size, gradients of pores and offset between fibers placed on the same plane as well as on consecutive overlapping fibrous layers play an important role in the interaction between scaffolds and cells [106], [216], [217]. Indeed, the architecture of scaffolds strongly affects the final distribution and activities of cells as well as their proliferative potential [19], [73]. 3D Insert ® PCL (3D PCL) are promising scaffolds to be used in the investigation of cell differentiation. Their ability to support cell activities over long periods of time has already been shown in previous studies investigating endothelial differentiation [218] and nerve regeneration [219]. In order to better mimic the extracellular matrix (ECM), 3D PCL scaffolds were combined with an internal network of collagen to increase cell viability and to increase the 3D dimensionality of the structure[118], [125]. In general hES-MPs seeded in collagenous gel-structures were found to reorganize the surrounding matrix and acquire a spherical shape differentiating mainly toward a chondrogenic pathway [220], depending on the concentration of collagen used and the seeding density [41]. Despite the outcomes highlighting differentiation toward cartilaginous tissue as a consequence of the interaction between cells and the collagen matrix, Mizuno *et al*. [221] found enhanced osteogenic markers

expression when type I collagen was employed with bone marrow stromal cells, suggesting that type I collagen matrix could also offer a suitable environment for the induction of osteoblastic differentiation *in vitro* and osteogenesis. Following these findings, we propose a composite scaffold made of 3D PCL and collagen gel (cPCL) to be used in further studies investigating how mechanical stimuli affect osteogenic potential of human mesenchymal stem cells. Indeed, the soft matrix of gel not only provides a bone tissue-like niche as collagen is the main component of the bone extracellular matrix, but also a support for cell attachment. Furthermore, the collagen gel is responsible for the transfer of externally applied mechanical forces to cells embedded in the structure, overcoming issues related to the limited stress transmitted by PCL alone. Indeed, the deformation of the polymeric structure transmits stresses through the contact surface between cells and fiber, leading to forces distributed on a 2D environment. The collagenous gel instead creates a compact matrix all around cells whose deformation involves forces acting on three dimensions, providing a better reproduction of the real tissue environment.

3D PCL is chemically inert and therefore requires surface activation to guarantee a good interaction at the PCL-gel interphase, facilitating the spreading of collagen through the whole sample and avoiding the formation of clots. Moreover, extraction of cells, ECM and collagen placed in the internal volume is often difficult. Indeed, small pores prevent good exchange of fluids within the internal areas of the scaffold and make it difficult to assess properties related to material placed in the inner volume. For this reason, kinetic assays are not a good tool for the determination of the overall behaviour of cells but can still be used to assess cell viability on the scaffold surface. x-ray techniques have been previously used in the literature to investigate distribution or growth of ECM and mineral within the internal volume of the scaffold [207], [214]. While polymeric scaffolds and mineral do not need further process because of their high density, protein-based materials are commonly stained with contrast agents to provide absorption by x-ray. Osmium is a good candidate for the staining of potein based materials as it is known to react with

sulphydryl and disulphide groups, polyphenols and with the nitrogen groups of tertiary bases such as trytophane and proline [222].

The goal of this study focuses on 1) the selection of the best conditions in terms of surface treatments and collagen concentration enhancing uniform collagen distribution and cell activities and 2) the characterization of distribution and morphology of collagen embedded in a 3D stiff matrix to develop a well-defined environment and a series of protocols to be involved in further studies on cellular differentiation.

6.2 Materials and methods

6.2.1 Collagen gel preparation

A collagen solution was prepared according to protocol mixing collagen bovine 1 (Gibco) 5 mg/ml (V_c), NaOH 1M (V_{NaOH}), PBS 1X (V_{PBS}) and culture media (V_{media}) in ice. Depending on the final concentration of collagen and the final volume of collagen gel needed (V_{tot}) the different solutions were mixed:

$$V_C = 0.5V_{tot} \quad \text{Eq. 6.1}$$

$$V_{NaOH} = 0.025V_C \quad \text{Eq. 6.2}$$

$$V_{PBS} = 0.1V_{tot} \quad \text{Eq. 6.3}$$

$$V_{media} = V_{tot} - (V_C + V_{NaOH} + V_{PBS}) \quad \text{Eq. 6.4}$$

The final concentrations of collagen considered were 0, 1.5, 2 and 2.5 mg/ml. The concentration 0 mg/ml was formed just by culture media without addition of any other chemical.

6.2.2 Collagen injection

Half of the scaffolds underwent plasma treatment (Chapter 3.4.1) while the other half was used without undergoing any further treatment. After 3D PCL sterilization (Chapter 3.4.1), gel was injected by placing a 20 µl drop of collagen solution on the top of the scaffold. Collagen solidification was achieved by incubation at 37°C, 99% humidity, 5% CO_2. After 1.5 h, 180 µl of culture media (α-MEM, 10% fetal bovine serum, 1% pen/strep/glutamine) was added to the samples to preserve collagen integrity, and avoid water evaporation and collagen shrinking.

6.2.3 Scaffold seeding

Human bone marrow progenitor stem cells (hES-MPs) were used at the 5^{th} passage, and were suspended in culture media (0 mg/ml collagen concentration) or in a collagen solution prepared substituting V_{media} with the cellular suspension. The seeding concentration was 20 x 10^3 cells in 20 µl corresponding to about 12,000 cells/cm^2. Scaffolds were seeded following common static seeding methods (Chapter 3.4.3). The role of plasma treatment and collagen concentration on cell distribution, viability and seeding efficiency was evaluated respectively by fluorescence imaging (Chapter 3.4.4), Presto Blue (Chapter 3.4.5) and DNA assay (Chapter 3.4.6). Each condition was tested on three samples and was repeated three times to validate reproducibility between experiments (n=9). Eventually, the cell viability over five days was monitored to select the collagen concentration which gives the best results in terms of cell metabolic activity by Presto blue assay. The

number of samples tested with Presto Blue progressively decreased: day 1 (n=9), day 3 (n=6), day 5 (n=3) because three samples were sacrificed for DNA quantification at each time point. Normality and equality of variance in the data series were tested with common methods (Chapter 3.4.9) and statistical analysis was performed using Student-T test or ANOVA and post-hoc analysis (Table 6.1).

Table 6.1: Statistical tests for assessment of significant differences between cells seeded in treated or non-treated scaffolds using different concentration of collagen and/or at multiple time points.

TIMEPOINT	COLLAGEN CONCENTRATION	PLASMA TREATMENT	ASSAY	STATISTICAL TEST	POST-HOC TEST
FIXED	ACROSS	FIXED	DNA PRESTO BLUE	ANOVA	TURKEY or SCHEFFE
ACROSS	FIXED		PRESTO BLUE	ANOVA REPEATED MEASURES	SCHEFFE
FIXED		ACROSS	DNA	PAIRED T TEST	-

6.2.4 Sirius red staining

Scaffolds (n=3) were washed with PBS and then 200 µl of 10% formalin was added to the samples. After 30 min, samples were again washed in PBS, and 200 µl of 1 mg/ml Sirius red (Direct Red 80, Sigma Aldrich) solution in saturated picric acid was added. After two hours, samples were rinsed five times with deionized water in the effort to completely remove excess of red stain. Then, pictures were taken by fitting a SRL digital camera EOS 750D/T6i (Canon, UK) fitted in an optical microscope. Collagen quantification was performed by cutting samples into pieces with a scalpel and adding a solution of methanol: 0.2M NaOH (1:1 v/v) for 20 min in ultrasound at 37°C to detach and dissolve collagen. Absorbance measurements were taken with a microplate reader at

405 nm to quantify the amount of collagen in the samples through comparison with a standard curve (Fig. 6.1).

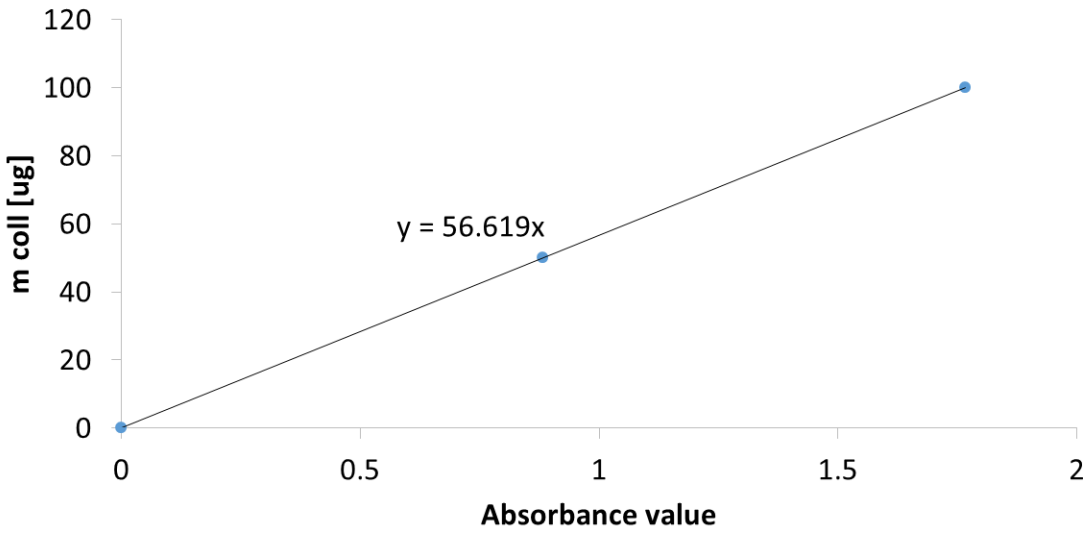

Fig. 6.1: Standard curve for Sirius red quantification relating the absorbance value given by the microplate reader with the amount of collagen in the sample.

6.2.5 MicroCT scanning

Table 6.2: Statistical tests for assessment of significant differences between collagen content considering different collagen density and quantification in ROI.

TIMEPOINT	TEST	POST-HOC
FIXED	PAIRED T TEST	SCHEFFE
ACROSS	ANOVA	TUKEY

Samples were kept in an incubator immersed in culture media and at 1, 3, 7, 14, 21 and 28 days were osmium stained for collagen quantification by microCT (Chapter 3.4.7.2). Within seven days from the osmium staining, samples were scanned by microCT (Chapter 3.4.7.3) and reconstructed by Simpleware using common protocols (Chapter 3.4.7.4) for assessment of collagen distribution and quantification (n=3). Normality and equality of variances among series of data were tested with common methods (Chapter 3.4.9) and statistical analysis was performed (Table 6.2).

6.2.6 Scanning Electron Microscopy (SEM)

Samples were fixed adding 200 µl of 10% formalin for 30 min. After washing three times with PBS, samples were dehydrated by immersion for 1 h in 200 µl of ethanol solution varying concentrations at 70, 80, 90 and 100%. Then, samples were air dried, placed on a holder and gold coated. SEM images were taken at 15kV increasing magnitude to investigate the different organization of collagen at the macro-, micro- and nano-scale.

6.3 Results

6.3.1 Composite scaffolds and cellular interaction

Fluorescence imaging of statically seeded scaffolds showed the benefit of plasma treatment on cell distribution. Considering either scaffolds with collagen or without collagen, the distribution of cells was non-homogeneous in both cases when plasma treatment was not applied (Fig. 6.2). Indeed, cells in 3D PCL tent to attach to the surface they first come in contact with, limiting the presence of cellular content to the top of the scaffold (Fig. 6.2A). Cells injected

with collagen were instead confined to the region where the gel solidified, causing non-uniform cellular distribution through the diameter of the scaffold (Fig. 6.2B). On the contrary, 3D PCL (Fig. 6.2C) and cPCL (Fig. 6.2D) undergoing plasma treatment achieved a good distribution, with cells evenly covering the entire surface area. Plasma treatment did not affect the seeding efficiency (Fig. 6.3) regardless of the collagen concentration in use. No significant differences were identified between treated and non-treated samples, suggesting that plasma treatment did not elicit any modification on the surface topography of scaffolds, leading to the same amount of cells detected by DNA assay regardless of the exposure to plasma.

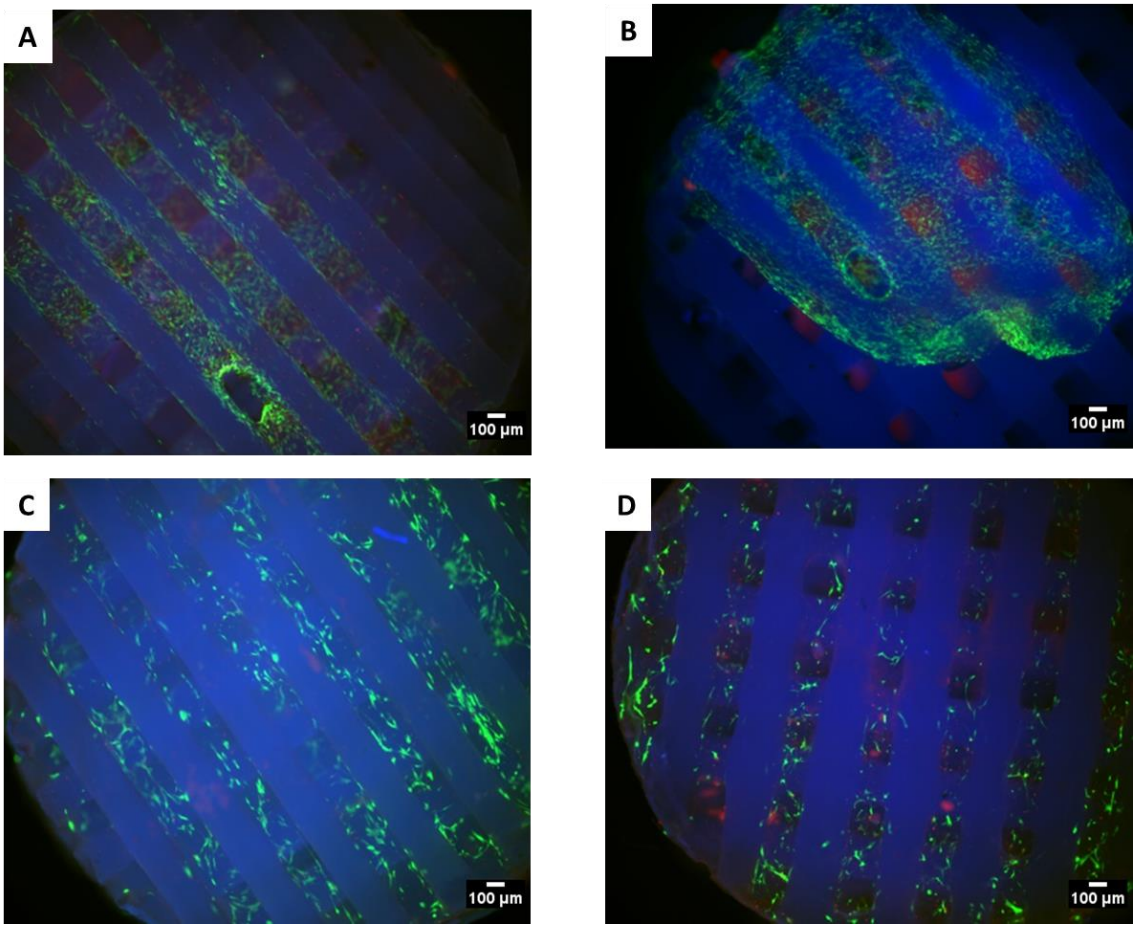

Fig. 6.2: Fluorescence images 24 hours after seeding of hES-MPs seeded on (A) non treated 3D PCL w/o collagen, (B) non treated 3D PCL with collagen, (C) treated 3D PCL w/o collagen and (D) treated 3D PCL with collagen.

On the contrary, the amount of cells attached was significantly higher for scaffolds embedding collagen compared to 3D PCL, showing an increase in efficiency from 40% to 60% for all concentrations (Fig. 6.3). Although the amount of cells in the scaffolds after 24 h from the seeding process was the same for all cPCL scaffolds, the effect of different collagen concentrations on cell behaviour was clarified monitoring the viability of cells (Fig. 6.4).

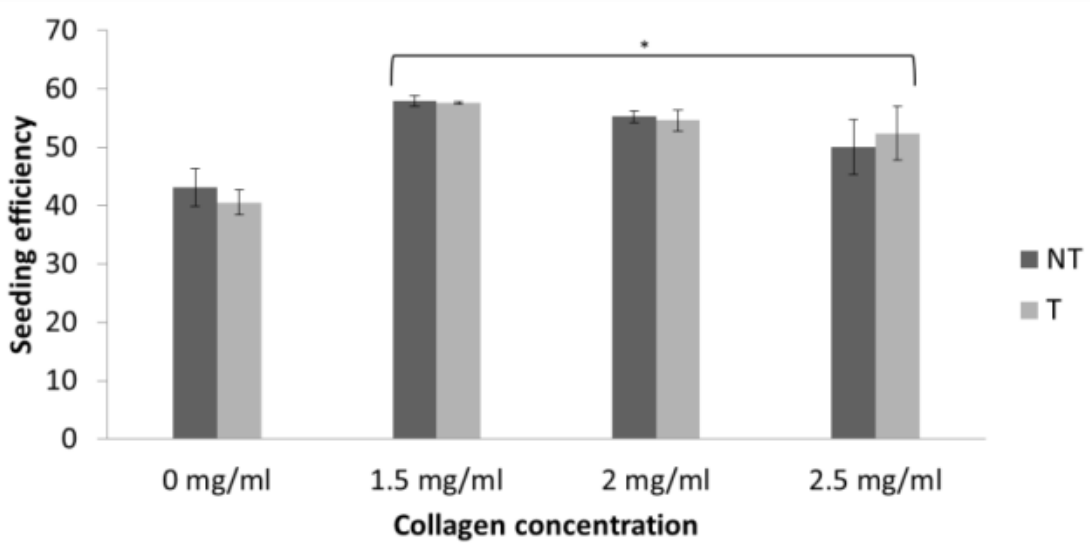

Fig. 6.3: Effect of different collagen concentration on the seeding efficiency for plasma treated (T) and non-treated (NT) samples. (N = mean±S.D.,*p<0.05).

Results from Presto Blue showed increased metabolic activity for cells embedded in 1.5 and 2 mg/ml collagen, whereas for 0 and 2.5 mg/ml, the cellular metabolism was low already at day 1 and over the following 5 days of culture. However, while 3D PCL showed a 2-fold increase in metabolic activity at day 3, cells embedded in collagen maintained constant viability over time. Particularly low values were found in samples embedded in 2.5 mg/ml collagen, featuring a dramatic drop in cell viability at day 5. These outcomes were confirmed by fluorescence imaging of samples at day 5 (Fig. 6.5) where 1.5 and 2.0 mg/ml cPCL presented viable cells on the surface (Fig. 6.5A&B).

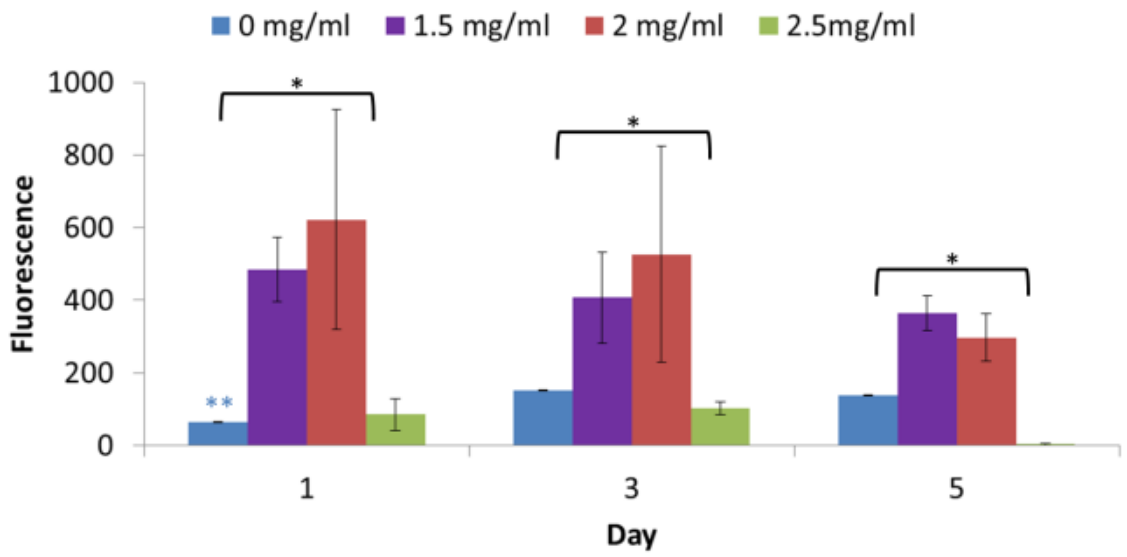

Fig. 6.4: Metabolic activity of hES-MPs at various collagen concentrations over time. (n = mean±S.D.,*p<0.05)

Cells embedded in 2.0 mg/ml collagen showed enhanced viability, leading to a much stronger green signal and a lower amount of red stain. The worst scenario was identified when a concentration of 2.5 mg/ml was considered with enhanced apoptosis characterizing all cells in the scaffold as suggested from the high red signal detected throughout the pores of the sample (Fig. 6.5C).

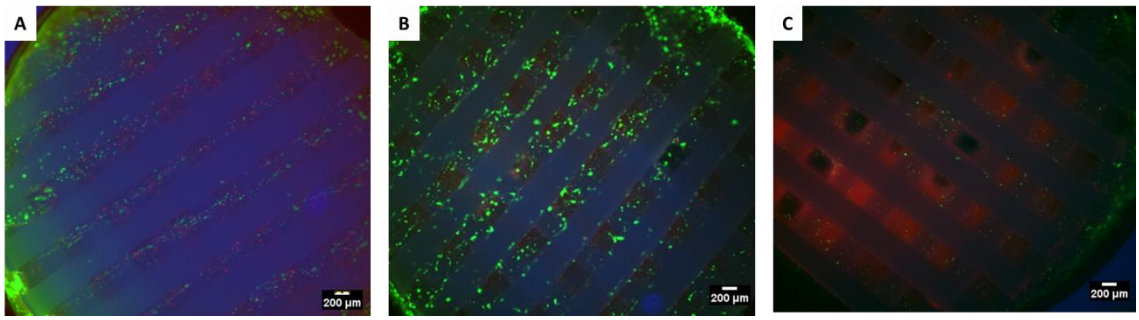

Fig. 6.5: fluorescence images of hES-MPsseeded in cPCL varying collagen concentration at (A) 1.5 mg/ml, (B) 2.0 mg/ml and (C) 2.5 mg/ml.

6.3.2 Collagen characterization

3D volume rendering allowed to observe the distribution of the gel throughout the volume of the scaffold. It also identified the presence of two different collagen densities named as LD (low density collagen) and HD (high density collagen), and referring respectively to grey values (GV) ranging between 3,500-7,500 and 13,000-40,000.

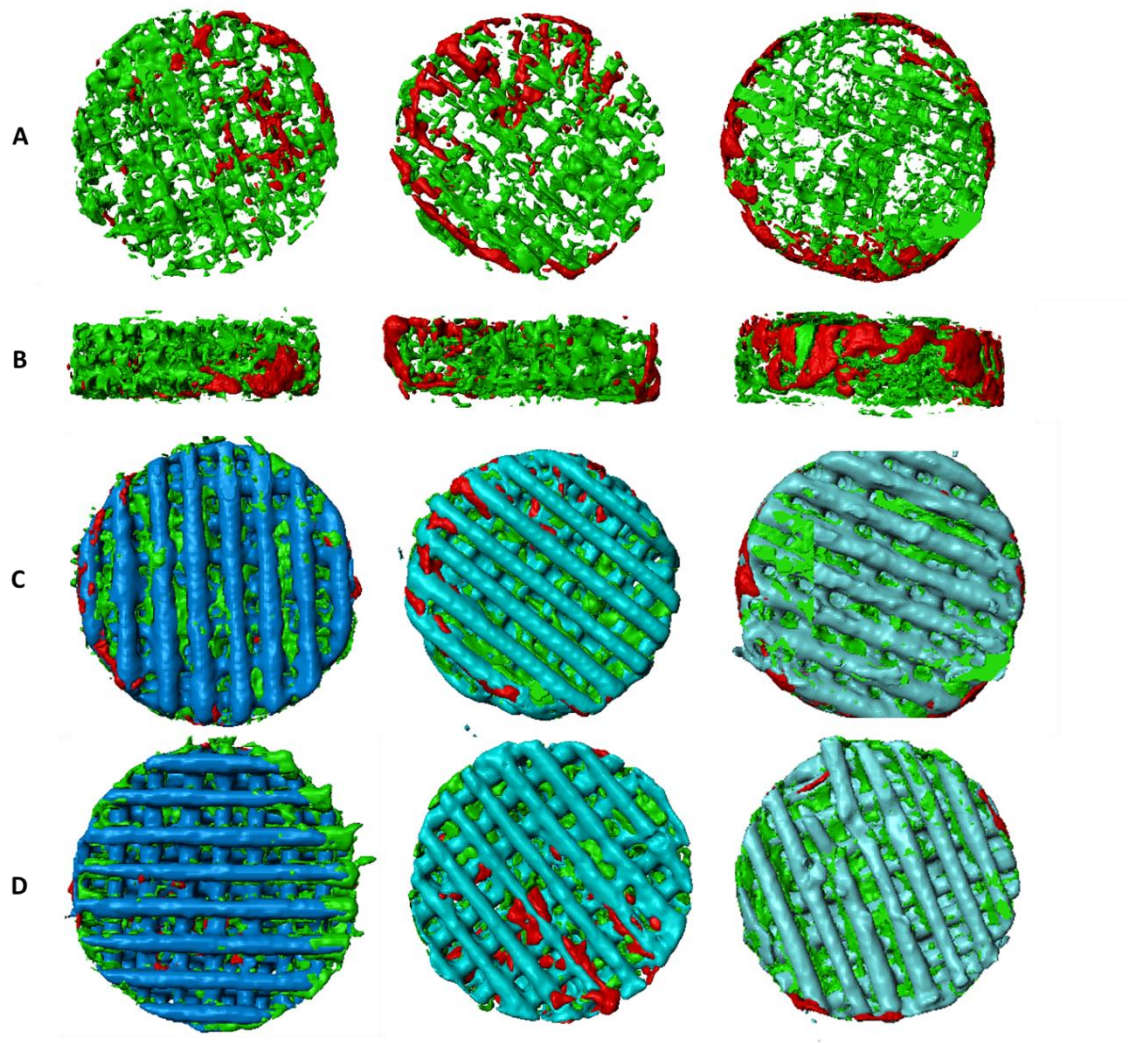

Fig. 6.6: MicroCT reconstruction of (A) top and (B) side view of collagen; (C) top and (D) bottom view of collagen and scaffold. Green and red identify respectively to LD and HD while different tonalities of blue are used to represent three replicates of scaffolds (from left to right).

HD collagen was not uniformly distributed through the scaffold. Increased collagen density was found to occupy central or peripheral areas (Fig. 6.6A) depending on the position where the seeding took place, as well as porosity and pore size of the sample. Indeed, the variable geometry characterizing 3D PCL (Chapter 4) caused collagen to accumulate on the surface at the periphery of the structure rather than in the central volume.

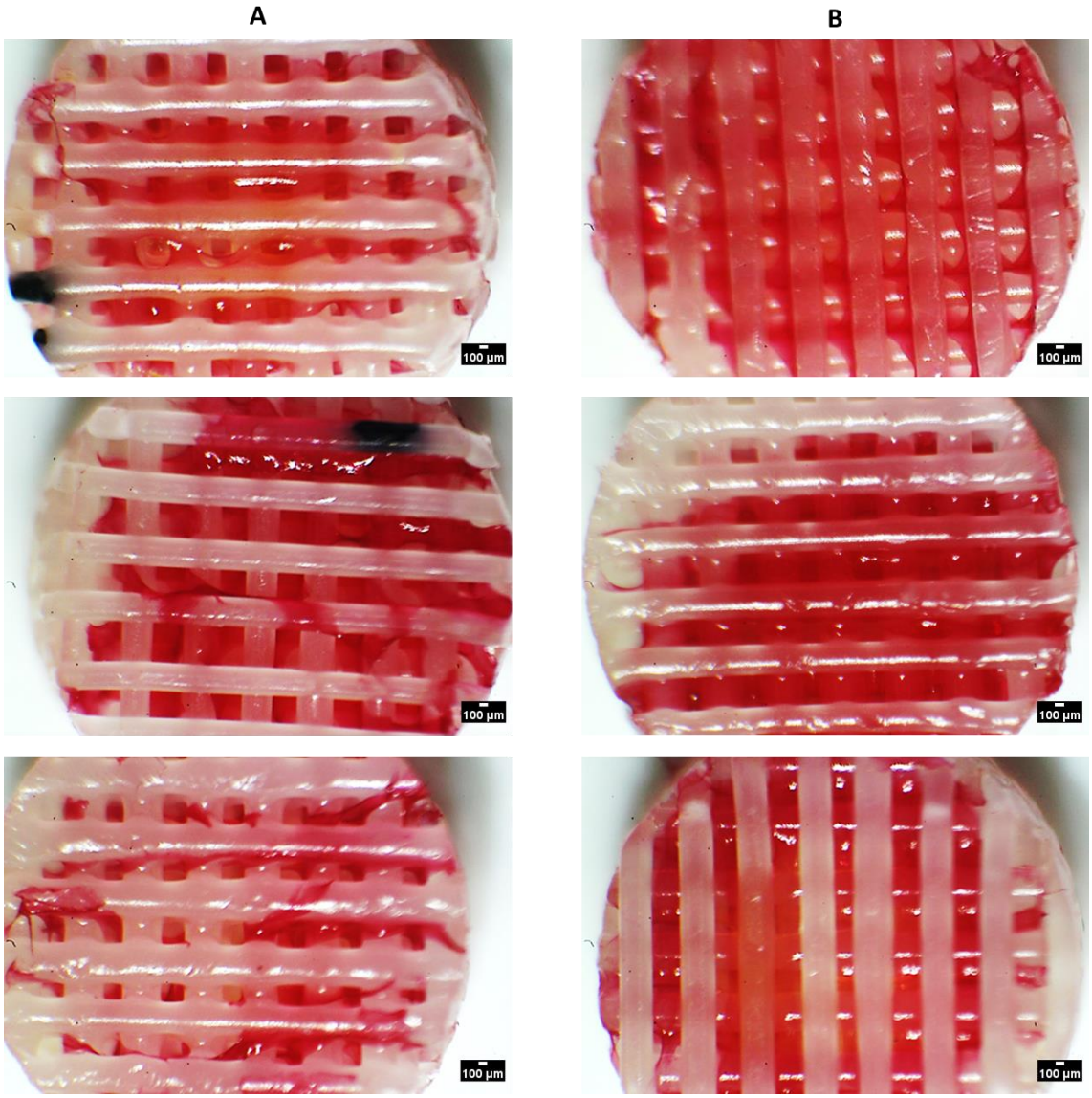

Fig. 6.7: (A) top and (B) bottom distribution of collagen by Sirius red staining of three samples after 24 hours.

However, LD was better distributed through the structure compared to HD, homogeneously filling also pores located in the centre. Indeed, LD penetrated throughout the structure down to the bottom of the scaffold despite the low pore size (Fig. 6.6B).Moreover, an accumulation of collagen occurred at the plate-sample contact surface (Fig. 6.7B) probably due to the effect of gravity.

When the scaffold structure was included into the reconstruction, collagen organization became more evident. Layers of collagen linked adjacent 3D PCL fibers, increasing the connectivity of the construct (Fig. 6.6 C&D). The layer-like organization on the top (Fig. 6.7A) as well as on the bottom (Fig. 6.7B) of cPCL was confirmed by Sirius red staining where the distribution and aggregation of collagen was highlighted by red stain. Quantification by Sirius red of collagen amount after 24 h from the injection led to a total of 24±5 µg embedded in the sample.

The layer distribution observed at the macro scale by microCT reconstruction and Sirius red staining was also investigated by SEM imaging (Fig. 6.8A), showing the morphology and the architecture of collagen at a lower scale. Layers were formed by filaments whose aggregation led to the development of multiple overlapping structures presenting a leaf-like shape (Fig. 6.8B). At higher magnification a tertiary level of organization was observed, where fibers of collagen randomly spread, overlapping one upon each other and creating a well interconnected nano-porous network (Fig. 6.8C).

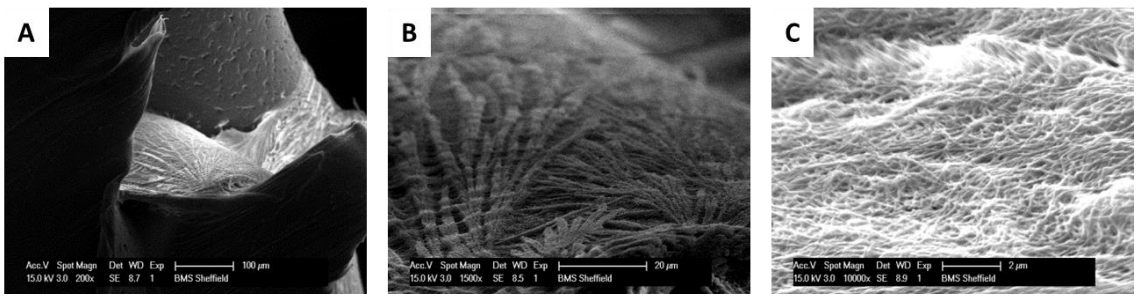

Fig. 6.8: SEM images of collagen organization at (a) macro, (b) micro and (c) nano scale without cells.

6.3.3 Collagen degradation

MicroCT imaging allowed not only observation of the overall distribution of collagen through the scaffold but also monitoring of degradation over time. In order to investigate how different areas were affected by the degradation process, regions of interest (ROI) were selected (Chapter 3.4.7).

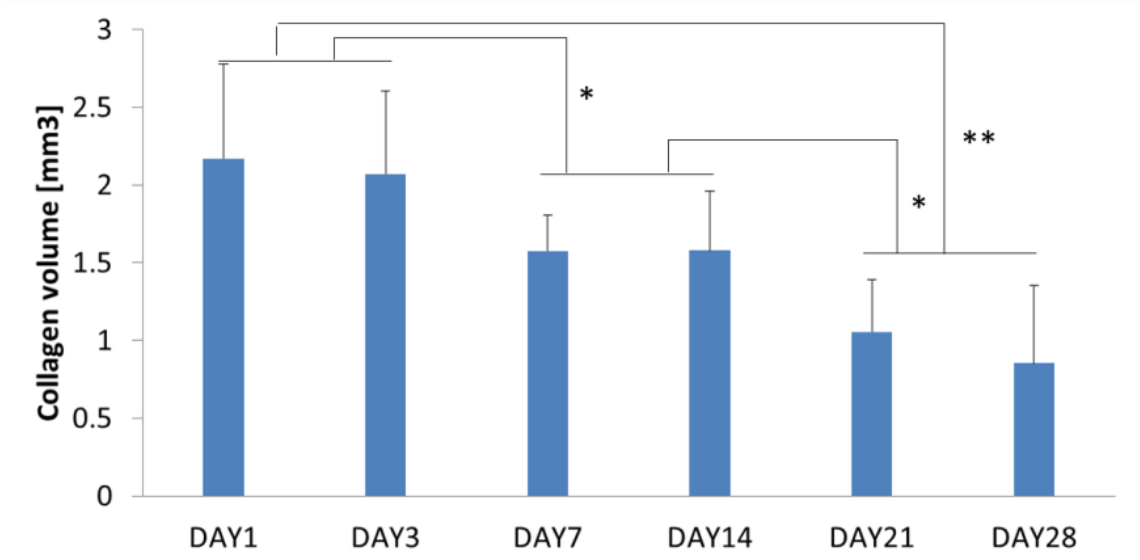

Fig. 6.9: Degradation of the overall collagen content over time (n = mean±S.D.,*p<0.05, **p<0.01).

This procedure allowed the quantification of collagen content in pre-selected volumes within the 3D PCL structure. Considering the overall collagen content, the gel volume was halved over 28 days (Fig. 6.9) with a statistically significant decrease at day 7 ($p<0.05$) and at day 21 ($p<0.01$). Despite the differences in sample geometry the degradation was clearly visible by microCT reconstruction of scaffolds after 1, 7, and 21 days from the injection of collagen especially considering LD due to the higher amount of LD resulting from the solidification. By selecting an internal ROI, it was possible to separate the signal related to collagen occupying internal volumes to the surface of the construct, confirming the aggregation of collagen previously qualitatively observed by the 3D rendering of volumes.

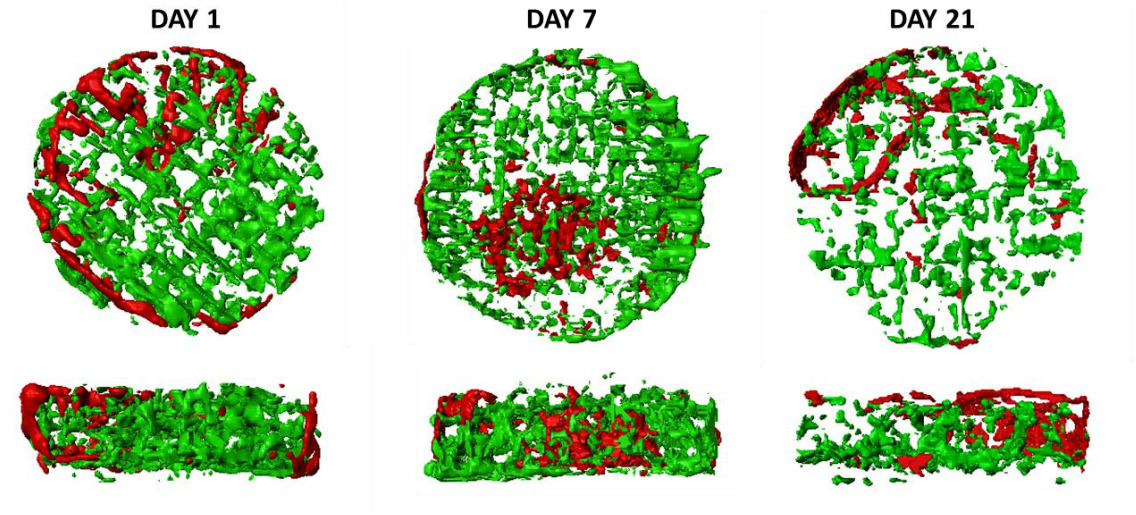

Fig. 6.10: top and side view of samples injected with collagen at three different time points. Green and red represent respectively to LD and HD.

As observed before, collagen tends to accumulate (Fig. 6.11) at the periphery of the sample. A quantification of the gel volume revealed HD and LD to amount respectively to 57±45% and 65±19% on the surface of the scaffold.

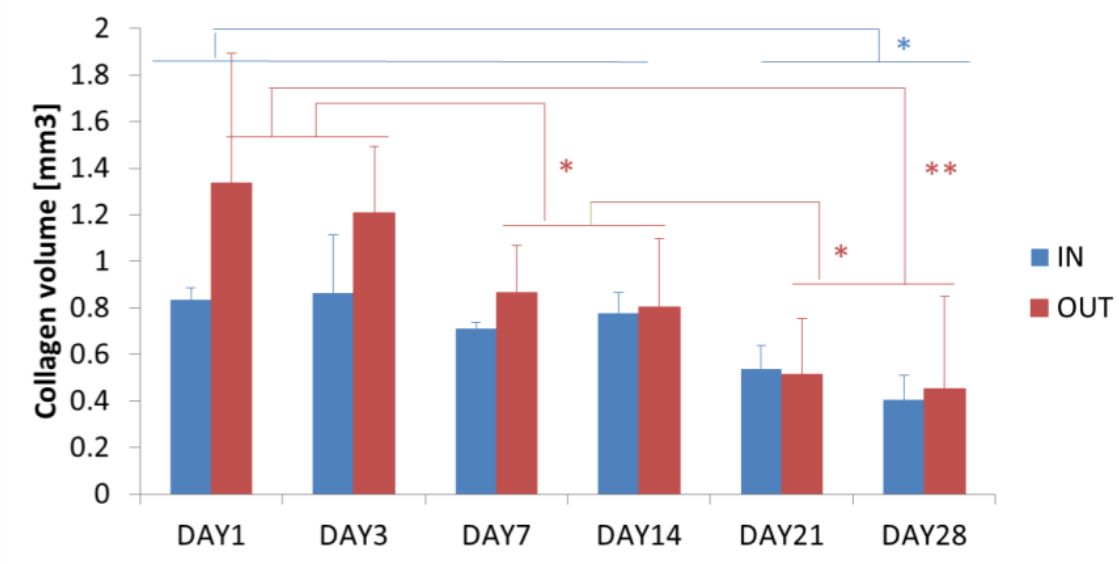

Fig. 6.11: Degradation of the overall collagen content inside the ROI (IN) or on the surface (OUT) over time quantified by microCT reconstruction (n = mean±S.D.).

However, from day 14 comparable amount of collagen was found in the interior and at the surface due to progressive degradation of the gel placed on the superficial layer, becoming significantly lower ($p<0.05$) at day 7. Instead, collagen occupying pores located in the inner of scaffolds decreased significantly ($p<0.05$) only from day 21. The same pattern of degradation was observed looking separately at HD and LD. The degradation process affected both LD and HD progressively decreasing the total volume of collagen over time. HD and LD were equally affected by degradation with matching degradation rates for collagen located on the surface (OUT) and collagen belonging to the ROI (IN).

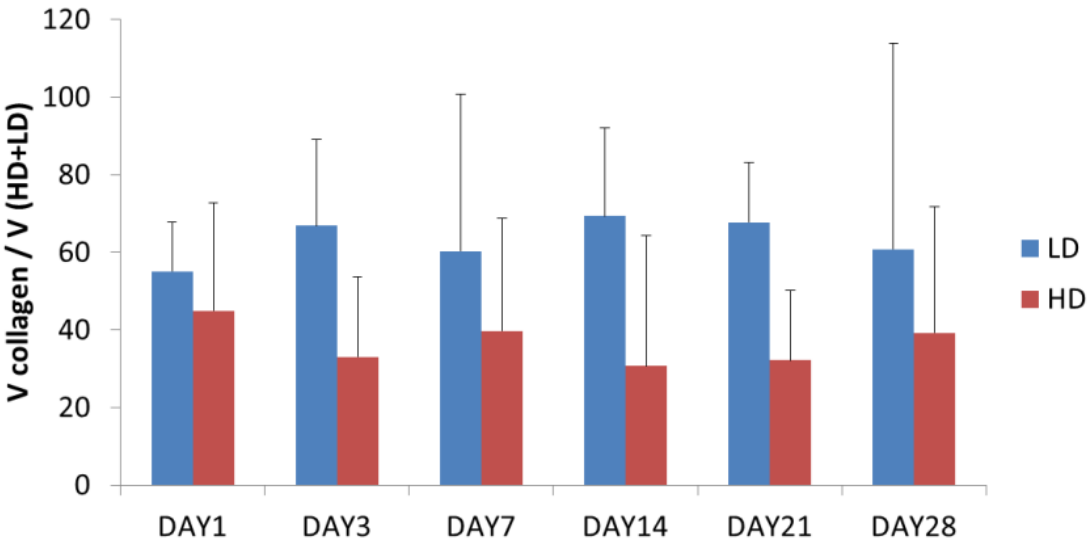

Fig. 6.12: Ratio of HD and LD over the total amount of collagen at each time point (n = mean±S.D.).

Degradation caused a 4-fold decrease in the collagen detectable from day 1 to day 28. Given that HD and LD presented matching degradation rates, ratios between HD or LD volume and the total amount of collagen in the sample at each time points was constant (Fig. 6.12). An average of the percentage of LD and HD collagen over the entire experiment confirmed LD to make up the 63±10% of collagen in the sample against the 37±9% of HD.

6.4 Discussion

6.4.1 Collagen-cells interaction

The composite scaffold developed in this study led to good cellular distribution through the structure with a strong dependence upon plasma treatment and collagen concentration. Treating scaffolds with plasma was sufficient to enhance uniform distribution of collagen and cells without affecting the overall cellular behaviour. Indeed, hES-MPs after 24 h from seeding showed elongated shape and enhanced viability independently from the exposure to plasma. The presence of collagen intensively increased the static seeding efficiency as the gel prevented the wash-off phenomenon responsible for cells to attach at the bottom of the well-plate rather than the wall of the scaffold. Collagen provided a dense matrix which increased the connection between neighbour cells and enhanced bridging among consecutive polymeric fibers. Moreover, it overcomes issues related to the surface topography of samples. Indeed, the polymeric fibers present only few anchorage sites which can be the cause of the low seeding efficiency noticed when collagen was not injected in the scaffold (**Error! Reference source not found.**). cPCL reached seeding efficiencies up to 60%, resulting in an average density of 5,000 cells/cm^2. According to the literature, such a seeding density is in the optimal range to induce stem cells osteogenesis in 2D conditions [223]. The presence of collagen played a central role on the proliferation potential of cells. The absence of proliferation noticed when collagen was embedded in the structure is in accordance with studies in the literature where cells did not proliferate as a consequence of a contraction mechanism dependent on the collagen concentration [62]. While cells cultured on 3D PCL showed enhanced metabolic activity already at day 3, hES-MPs in cPCL varied their behaviours over a relatively short period of 5 days depending on the concentration of collagen used. The decrease in cell viability and extensive cell death observed in 2.5 mg/ml cPCL is believed to be associated to the high compactness of collagen, limiting both cell-cell interaction already prevented by the relatively

low seeding density, and diffusion of nutrients. As shown by SEM, the collagen gel in use was indeed an assembly of randomly distributed fibers, forming nano pores. As the diameter of pores is expected to be inversely proportional to the concentration of fibers [224], a higher amount of fibers led to a more compact structure with smaller pores limiting the diffusion of molecules throughout the structure. Moreover, the presence of cells is likely to affect the distribution of collagen in the samples as cells are known to reorganize the fibers by interaction between integrins and matrix [220]. As result, collagen degradation could be faster or slower depending on the action elicited by cells. A faster degradation of collagen may be associated to the progressive differentiation of cells and, for example, the production of mineral. On the other hand, a slower degradation may be due to a mechanism of protection initiated by cells which produce further further ECM to reinforce the surrounding niche. Unfortunately, the techniques employed in the study did not allowed any assessment of how the collagen degradation was varied by cellular activities due to difficulties in distinguishing pre-injected collagen from the protein matrix produced by hES-MPs.

6.4.2 Distribution and morphology of collagen embedded in 3D PCL

Once the optimal conditions to obtain a uniform seeding distribution and cell survival were selected, distribution of the collagen into the internal volume of the scaffold was studied, since so far the investigation was limited to the surface. For the collagen characterization, a concentration of 2 mg/ml was selected as it enhanced cellular viability and because it was previously employed for differentiation of mesenchymal stem cells [152], [225], [226]. The small pores characterizing 3D PCL samples affected more HD penetration capability than LD. As HD was denser than LD, it experienced higher resistance when passing through the scaffold, leading to an increased amount of LD embedded in the structure. This statement was also confirmed by the percentage of voids filled by collagen amounting to 11±5% for LD and only

5±3% for HD. Similar outcomes claiming non homogenous material distribution As a consequence of static seeding are extensively discussed in the literature [106], [151], [227]. Vacuum was also tested as an option to facilitate the injection of collagen into the structure but elicited a negative effect on cell survival even if applied for short periods of time, provoking 2D cultured cells to shrink and detach (Fig. 6.13). The main hypothesis of the technique was that the signal from the osmium is proportional to the protein concentration. Indeed, HD referred to a brighter x-ray signal and it was associated with an accumulation of material but whether it correlates to accumulation of collagen or osmium stain is still not clear. Sirius red staining confirmed the morphology observed by MicroCT with collagen organizing in layers between 3D PCL fibers.

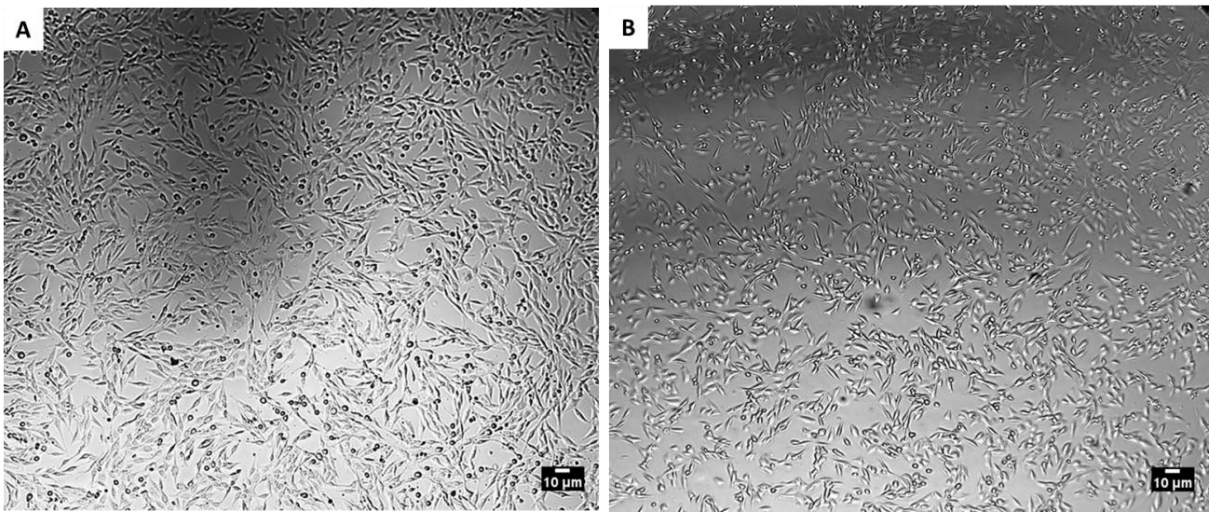

Fig. 6.13: Osteosarcoma cells (MG63) seeded on collagen coated Petri dish (A) before and (B) after application of vacuum for 10 min.

Moreover, Sirius Red stained samples showed higher red staining in some areas which may be related to the accumulation of collagen claimed in the MicroCT reconstructions. An issue affecting the reliability of the method was related to the fact that, during the experiment, collagen was kept in a hydrated condition while images were taken on dry samples. Common sense dictates the drying process would cause reorganization and aggregation of collagen

into the sample as a consequence of the evaporation of water. Another issues affecting the reliability of the method were related to the use of fixative agents which are known to reorganize the collagen. For example, glutaraldehyde is commonly used to chemically crosslink collagen by reaction between the aldehyde group and the amine groups of the protein [64]. For this reason, the intense MicroCT signal as well as the layer-like organization of collagen could be due to the fixation of the samples performed before imaging. Similarly to glutaraldehyde, formaldehyde could have caused the same reorganization when used to fix the samples in the visualization of collagen by Sirius red as it also presents an aldehyde group.

6.4.3 Degradation of collagen in 3D PCL

Observing the degradation behaviour over time, collagen degraded as a consequence of the action elicited from external agents. The degradation affected first the outer layer directly exposed to the culture media. Then, it progressively altered gel placed in the internal volume of the structure As a consequence of the disappearance of most external layer. The study of degradation processes by microCT allowed also confirming the accumulation of collagen into the sample by observing LD and HD rate of degradation. Indeed, the accumulation of osmium in the sample due to the staining procedure is expected to affect all samples in equal measure. This is in contradiction with the consistent decrease of HD content over time observed in this study. Moreover, the matching degradation rates of LD and HD suggest the existence of a link among stain absorption and collagen density although further experiments are necessary to confirm these findings.

6.5 Conclusions

6.5.1 Summary

The composite scaffold proposed in this study enhanced viability and homogeneous distribution of cells for a collagen concentration of 2 mg/ml and when samples were plasma treated. hES-MPs did not proliferate in cPCL although cell viability was maintained constant over 5 days, suggesting the suitability of such structure to be used for further studies over longer periods of time. The cellular behaviour investigated in the first part of this study focused on cells located on the outmost layer covering the surface of the scaffold, due to limitation in withdrawing fluorescent solution trapped in the interior of the structure. Despite this, it helped determining 1) the optimal treatment to apply for the achievement of uniform cellular distribution and 2) the concentration of collagen enhancing cellular activity. Collagen was expected to form a compact matrix inside the PCL structure, while it had a layer organization instead. However, it greatly increased the interconnectivity among pores and its overall organization allows to consider a 3D environment surrounding cells very similar to the ideal model proposed at the beginning of this thesis (Chapter 1.3). Despite the high variability obtained in terms of collagen distribution within different samples, the amount of gel detected at each time point (average of three samples) present acceptable deviation (maximum 10% standard deviation) from the average value. Moreover, this study gives for the first time an insight of how degradation affects collagen embedded in 3D structures. The scaffold developed here can be used to investigate cellular activities in further studies. Indeed, these outcomes will be fundamental to eliminate the background signal due to the collagen presence, hence enabling the quantification of tissue formation and mineralization by the action of cells.

6.5.2 Future work

Plasma treatment was used in an effort to overcome issues related to poor distribution of collagen/cells in 3D structures. Although it decreases the aggregation phenomena throughout the diameter of the superficial area, it was not sufficient to avoid densification of collagen toward the height of the specimen. Multiple seeding points may be considered by injecting the seeding solution at different locations on the surface of the scaffolds to homogenize the collagen content throughout the structure. Also employing perfusion of a collagen-cells suspension through the scaffold for a limited amount of cycles may avoid formation of densification areas. However, the viscosity of the collagen and the small pores size of the material might present a limitation for perfusion processes, leading to high shear stresses and preventing cellular attachment. Moreover, non-uniform distribution could still be an issue due to the variable pore size of the material enhancing the passage of collagen towards volumes providing less resistance to the fluid. Eventually, the seeding efficiency exploiting perfusion is expected to be low due to 1) dispersion of material into the system, requiring optimization of the volume to dispense, and 2) limitation in the number of applicable cycles due to the progressive solidification over time of the collagen gel.

Chapter 7

hES-MPs RESPONSE TO CYCLIC MECHANICAL COMPRESSION OF cPCL

7.1 Introduction

Until recently, cell behaviour under mechanical forces was mainly investigated on 2D substrates [147]–[149], [153] whose geometry does not provide a good representation of the 3D architecture of biological tissues. The increasing demand for a structure matching architecture and chemistry of bone fracture sites led to the development of 3D scaffolds. Among those, hydrogels were extensively proved to enhance cell survival and provide a tissue-like environment for cell growth and differentiation [228]. Moreover, they offer a compact matrix, often made by proteins, which guarantees uniformity of stresses when mechanical forces are applied. However, the forces applicable to such scaffolds are limited by their soft matrix, preventing their use for applications which require to bear high stresses [229] as those acting on bone. As consequence, the focus moved toward the use of 3D polymeric structures able to bear mechanical loading. Scaffolds made by polymerization of lactic, glycolic or polycaprolactone acid were widely investigated because they are easy to shape through high-temperature processes, allowing the fabrication of high reproducible fibrous structures [79]. Despite their remarkable resistance to forces, 3D polymeric scaffolds are characterized by low deformability. Moreover, they are also affected by plastic deformation when high strains are applied as shown, for example, on 3D Insert ® PCL in this study (Chapter 4). This study aims to investigate the possibility of differentiating cells by transmitting externally applied forces through a soft gel, embedded in a 3D polymeric scaffold, whose deformation results as effect of the displacement

applied to the external structure. At present, mechanical differentiation of cells was mainly investigated on hydrogels, 2D substrates or 3D foam-like scaffolds. In general, high amplitude compression strains applied to scaffolds embedding cells mainly induced chondrogenic differentiation [88], [104], [157], [159], while tensile stimuli with frequencies mimicking forces affecting bone in vivo [32] have been shown to induce osteogenic differentiation on 2D substrates [149], [153]. Despite this, compression of scaffolds enhanced osteogenesis on 2D [149] as well as 3D structures [162], if the force was applied for short periods of time. Eventually, including resting periods of 5 days among stimulations in combination with short bursts of compression was previously shown to induce mineral production on differentiated osteoblasts [100]. In order to overcome these limitations and take advantage from the mechanical properties of both hydrogels and polymeric structures, a new composite scaffold made of stiff 3D Insert ® PCL and soft collagen (cPCL) is proposed here as support for mechanically-induced differentiation of cells.

This study aims to investigate how short bursts of compression applied to 3D scaffolds embedding collagen and cells, and the repetition of the stimuli at late stage of culture affect 1) mesenchymal stem cells proliferation; 2) spatial formation of ECM and mineral deposition; and 3) osteogenic protein expression. Here, techniques commonly used to assess cell activities, such as assays quantifying metabolic activity, cell number and protein expression, are put alongside to x-ray scanning to determine distribution of collagen, cells, ECM and mineral through the whole structure. According to the literature, X-ray contrast to protein-based materials can be achieved by staining with osmium tetroxide [222], [230], while the mineral phase is identifiable without the use of any contrast agent, due to the diffraction properties related to its chemical nature [231]. Indeed, micro computed tomography (microCT) was already proved to provide reliable insight of bone mass variations in vivo [232] as well as of the mineral distribution through 3D structures in vitro [215], [233], confirming the possibility of visualizing mineral without the use of any contrast agent.

7.2 Materials and methods

7.2.1 Mechanical characterization of PCL scaffolds

Samples were divided in groups depending on the mechanical protocol to be applied. A total of 48 samples were used in each experiment: 18 were kept in free-floating conditions, 18 were cyclically loaded and 12 were controls without cells. Before seeding, PCL specimens were marked on the top surface with a black marker to allow recognition of the surface where the seeding took place. All samples were then named and scanned by microCT (Chapter 3.4.7). Samples undergoing cyclic loading during the experiment were further mechanically relaxed at 37°C, as previously shown (Chapter 4.2.2), by applying a 8% strain ramp calculated over the height of the sample. Any stress from the structure was removed maintaining a constant displacement for 180 min (Chapter 5). Before seeding, samples were treated by air plasma and sterilized (Chapter 3.4.1) to avoid the outbreak of bacterial infections during the experiment.

7.2.2 Mechanical compression of seeded cPCL

Samples (n=36) were statically seeded with hES-MPs in a concentration of 40,000 cells per scaffold following common techniques (Chapter 3.4.3). A collagen concentration of 2 mg/ml was used, as it was found to be the best enhancing cellular activity among those tested (Chapter 6). After five days in culture to allow the adaptation of cells to the environment, samples were collected and placed into a previously autoclaved biodynamic chamber (Fig. 7.1).

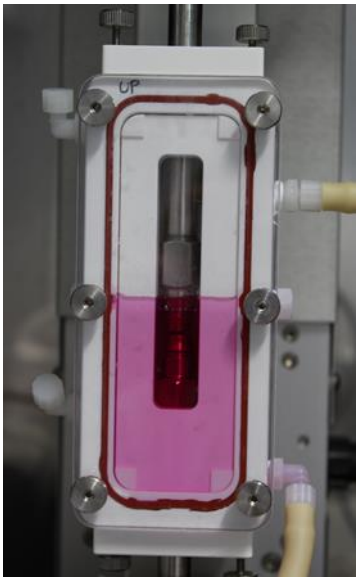

Fig. 7.1: Electroforce biodynamic chamber embedding shafts and filled with culture media (pink) for mechanical compression of samples.

The chamber was then mounted onto the BOSE bioreactor and a preload of 0.1 N was applied to avoid shifting of the specimen. Then, the chamber was filled with media by pumping the fluid with a peristaltic pump and samples underwent cyclic compression (Fig. 7.2):

1) superimposing a 5% strain ramp at 10 μm/s,

2) applying a 2% peak-to-peak sinusoidal waveform at 1 Hz for 15 min,

3) removing the superimposed ramp by unloading the sample at 10 μm/s.

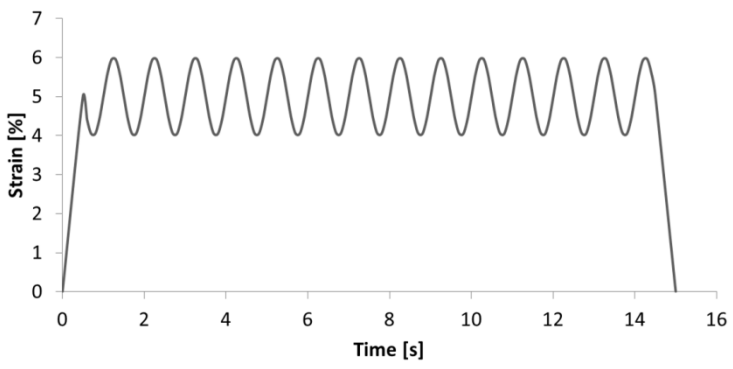

Fig. 7.2: Cyclic compression of samples with superimposed initial ramp at 5% strain.

The chamber was then removed from the bioreactor, placed under a culture cabinet, and samples were moved to 96 well plates in presence of culture media. The latter was changed every day with 200 µl of new culture media. Non-loaded samples (U) were kept in static culture and no compression was applied. The response of cells cultured in non-loaded samples was compared to samples loaded for 15 min per day (Table 7.1), from day 6 to day 10 (L1). Half L1 samples were then compressed again from day 16 to day 20 (L2).

7.2.3 Analysis of hES-MPs response

Time points were set at 1, 3, 7, 14, 21 and 28 days and the initial number of samples varied among conditions.

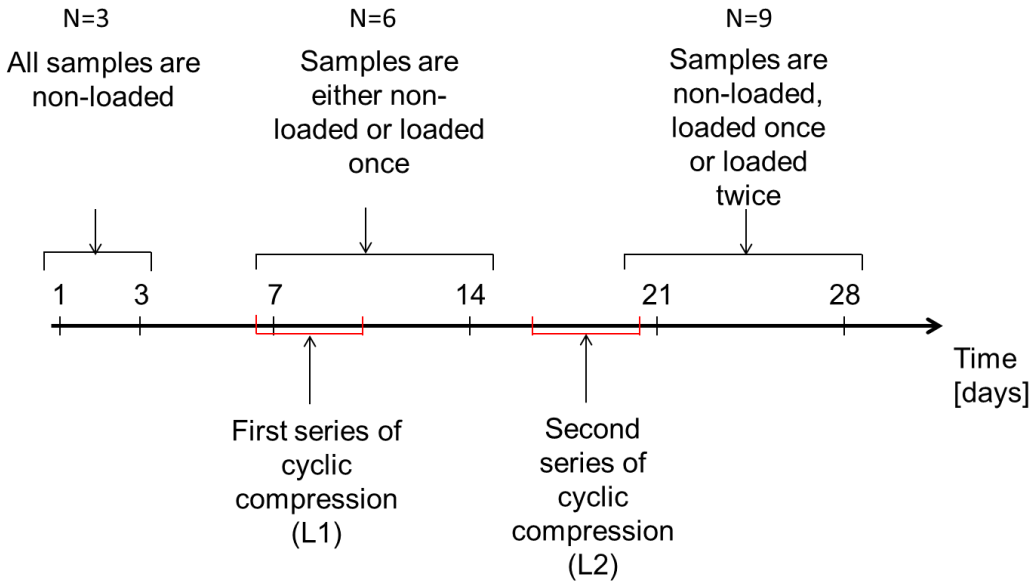

Fig. 7.3: schematic representation of the experiment. Samples were kept in culture for 28 days. Timepoints were set at day 1, 3, 7, 14, 21 and 28. At the time of the first two time points, samples were all non-loaded, so just three samples were tested for DNA and OCN expression, and microCT. The following two time points match the period of the first series of compression. So at day 7 and 14, six samples, three non-loaded and as many loaded, were tested. As the second series of stimuli was applied between day 16 and 20, three more samples were tested at the last two time points to account simultaneously for U,L1 and L2.

At day 1 and day 3, no samples had undergone compression yet (Fig. 7.3), therefore testing three random samples over the entire batch provided a good representation of the behaviour of cells for all samples involved in the experiment. At day 7 and 14, samples were either non-loaded or loaded with a single series of cycles and therefore a total of six samples needed to be tested, three for each condition.

Table 7.1: loading conditions applied to samples and total number of samples involved per each stimulation protocol. It is important to notice that non-loaded (U), loaded once (L1) and twice loaded (L2) samples were monitored respectively since day 1, day 7 and day 21.

CONDITION	ABREVIATION	LOADING PROTOCOL	NUMBER OF SAMPLES
NO LOAD	U	-	18 (3x day 1,3,7,14,21,28)
LOAD 1	L1	From day 6 to day 10	12 (3x day 7,14,21,18)
LOAD 2	L2	From day 6 to day 10 and from day 16 to day 20	6 (3x day 21,28)

The last time points were preceded by a second series of compression cycles, therefore nine samples were tested at day 21 and 28. Thus, at day 0 (Table 7.1):

- 18 samples accounted for U as 3 samples were tested at each time point (3x6=18);
- 12 samples accounted for L1 as 3 samples were tested at day 7, 14, 21 and 28 (3x4=12);
- 6 samples accounted for L2 as 3 samples were tested at day 21 and 28 (3x2=6).

Before performing any further analysis, the condition of equality among samples belonging to different groups (U, L1, L2), but undergoing the same protocol (Fig. 7.3), was tested at each time point by Presto Blue.

For every condition at each time point:

1) All samples were tested with Presto Blue (Chapter 3.4.5) to evaluate cellular viability. Variable number of samples was considered due to the sacrifice of three samples at each time point (Table 7.2). The number of samples tested by Presto Blue differed among conditions up to day 21, as U and L1 were tested for a higher number of time points (Fig. 7.3).

Table 7.2: Summary of the number of samples teste for metabolic activity by Presto Blue assays per each condition at each time point. The number indicates the total of samples tested in 3 different experiments.

TIMEPOINT / CONDITION	DAY 1	DAY 3	DAY 7	DAY 14	DAY 21	DAY 28
NO LOAD	54	45	36	27	18	9
LOAD 1	36	36	36	27	18	9
LOAD 2	18	18	18	18	18	9
CTRL	36	30	24	18	12	6

2) Two samples were sacrificed and tested for DNA quantification (Chapter 3.4.6). Once removed from the structure, cells were centrifuged and stored in lysis buffer at -80°C for osteocalcin (OCN) quantification by ELISA (Chapter 3.4.8).

3) One sample was osmium stained (Chapter 3.4.7.2) for microCT evaluation of cellular proliferation and quantification of mineral content, by following segmentation of microCT slides as previously reported (Chapter 3.4.7.4). As the intensity of the signal resulting from the x-ray is related to the density of the scanned material, signal in the low (3,500-7,500) grey values

(GV) range was associated to volumes occupied by cells and ECM. Higher GV (13,000-60,000) were instead attributed to the mineral phase. The amount of tissue and mineral was further divided, among material developing on the surface or in the internal volume of the scaffold, through selection of a region of interest (ROI), following the procedure previously reported (Chapter 3.4.7).

4) Two controls were collected for removal of the background. One was used as control for DNA assay (Chapter 3.4.6) and, then, was stored in the same conditions as samples for OCN ELISA (Chapter 3.4.8). The other underwent osmium staining (Chapter 3.4.7.2) and x-ray scanning (Chapter 3.4.7.3) to remove the background due to the initial injection of collagen gel.

Table 7.3: Summary of the total number of samples used for DNA, OCN and microCT analysis at each time point. The number of samples refers the total number of samples. So, the number of tested samples 1) at day 1 and 3 were three because all samples were non-loaded, 2) at day 7 and 14 were six to consider any difference caused by L1, and 3) at day 21 and 28 were nine to account for non-loaded (U), loaded once (L1) and twice loaded (L2).

TIMEPOINT / TEST	TIMEPOINT	DAY 1	DAY 3	DAY 7	DAY 14	DAY 21	DAY 28
	CONDITION	U		U and L1		U, L1 and L2	
DNA & OCN	NUMBER OF SAMPLES	6	6	12	12	18	18
	CTRL	3	3	3	3	3	3
MICROCT	NUMBER OF SAMPLES	3	3	6	6	9	9
	CTRL	3	3	3	3	3	3

The entire experiment, from day 1 to day 28, was repeated three times in the effort to investigate reproducibility of the results and account for the variability due to slightly different external conditions and scaffold architecture. The number of samples, involved in Presto Blue (Table 7.2) or other assays (Table 7.3), allowed to perform statistical analysis. Per each condition, a minimum of

three samples were considered, averaging values from the three repeats of the experiment. Data were tested for normality and equality of variances (Chapter 3.4.9), but due to the high variability between series, statistics was run based on Games-Howell non-parametric test.

7.3 Results

7.3.1 hES-MPs viability

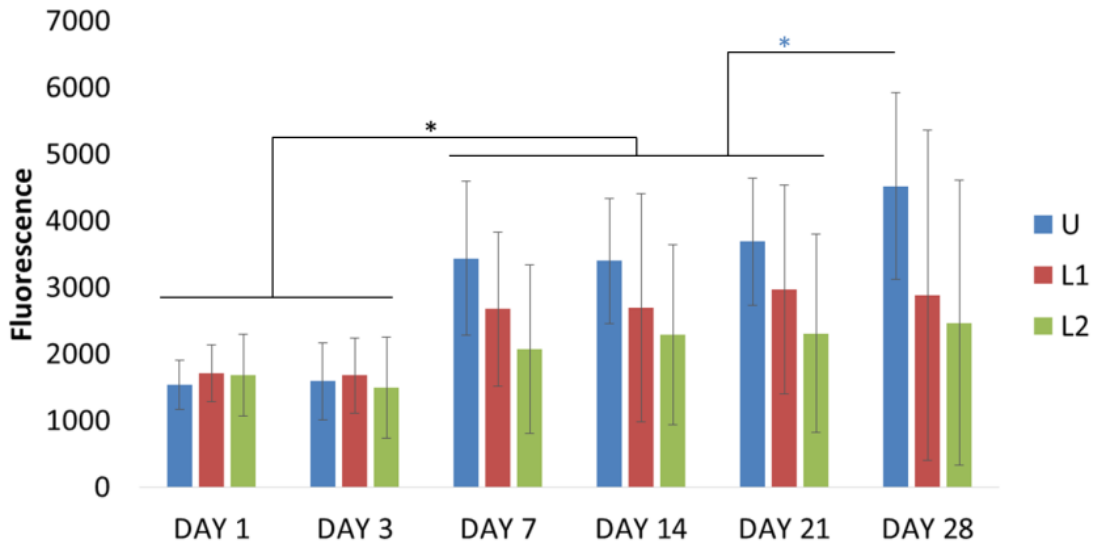

Fig. 7.4: Viability of cells (n = mean±S.D.) by Presto Blue measurement over 28 days considering non-loaded (U), loaded once (L1) and twice loaded (L2) samples as average of three experiments. Stars highlight significant differences with p<0.05 referring to * all the series or * just U samples.

At day 1 and 3 cells showed enhanced viability and samples from different groups had similar fluorescent values, confirming uniformity of the seeding among samples (Fig. 7.4). After one day of stimulation (day 7), the fluorescent signal of loaded samples was weaker compared to free-floating samples, although cells metabolic activity increased for both conditions. Between day 7

and day 21, the metabolic activity remained unvaried among time points as well as comparing loaded and non-loaded samples. Due to the high standard deviation, no significant differences among conditions were identified by statistical analysis at any time point, except at day 28 when non-loaded samples underwent a further increase in cellular metabolism.

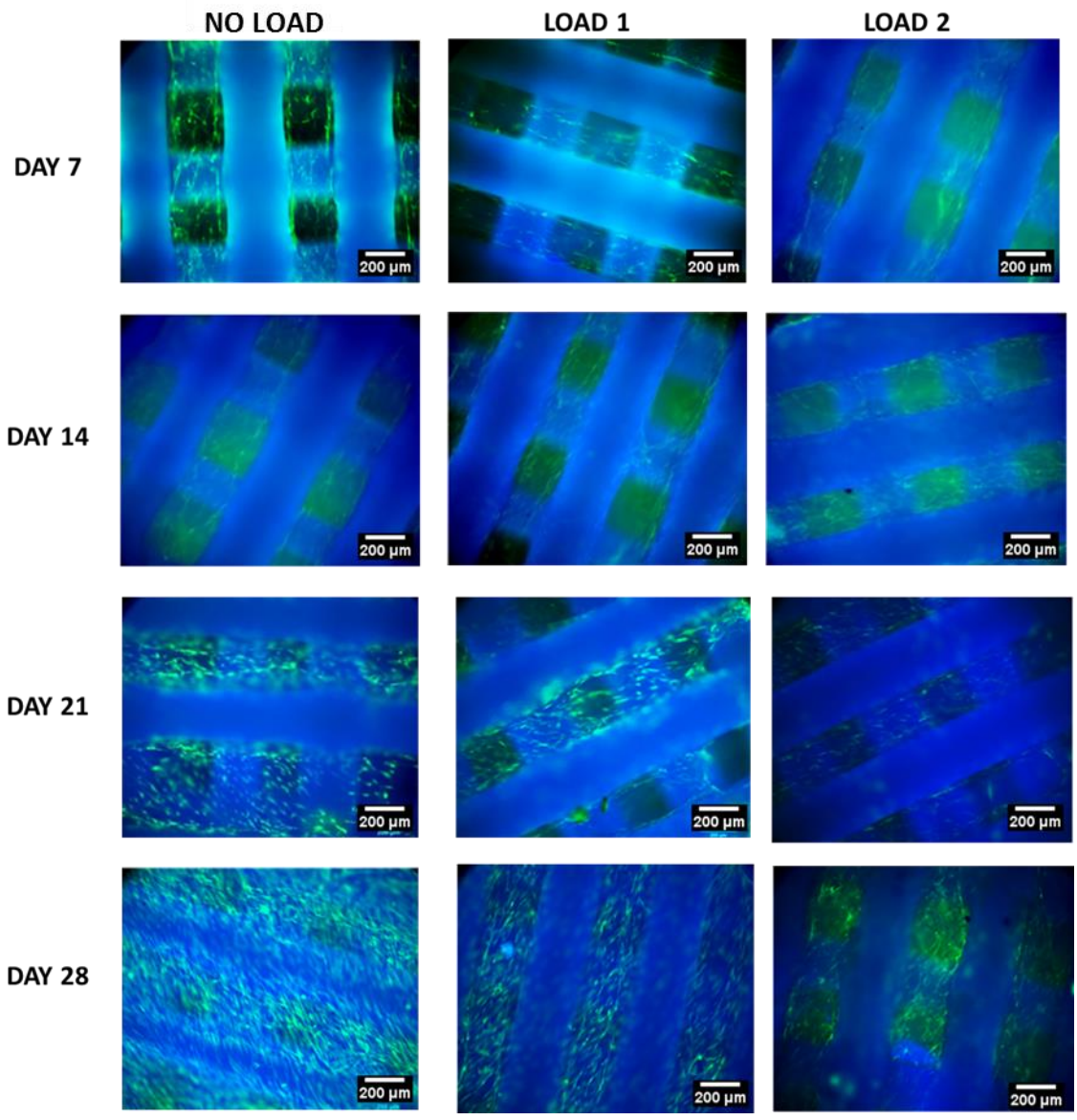

Fig. 7.5: Fluorescent images of samples seeded with hES-MPs at 10X. Viable cells are green, while scaffold fibers are blue due to auto-fluorescent properties of PCL. At day 28 loaded samples show cells randomly oriented with a star-like shape.

Similar results were obtained by fluorescence images taken at each time point (Fig. 7.5). A lower green signal characterized scaffolds undergoing compression at both day 7 and day 28. At the latter time point, cells were well elongated and spread in all cases, but clear sign of proliferation was mainly observed on non-loaded conditions where cells covered the entire surface of the scaffold. Cells oriented in the same direction, developing a highly interconnected cellular network in U and L1. On the contrary, cells embedded in samples undergoing twice the cyclic loading appeared less oriented, with thin protrusions spreading in different directions and conferring a more star-like shape (Fig.7.5).

7.3.2 hES-MPs proliferation and ECM production

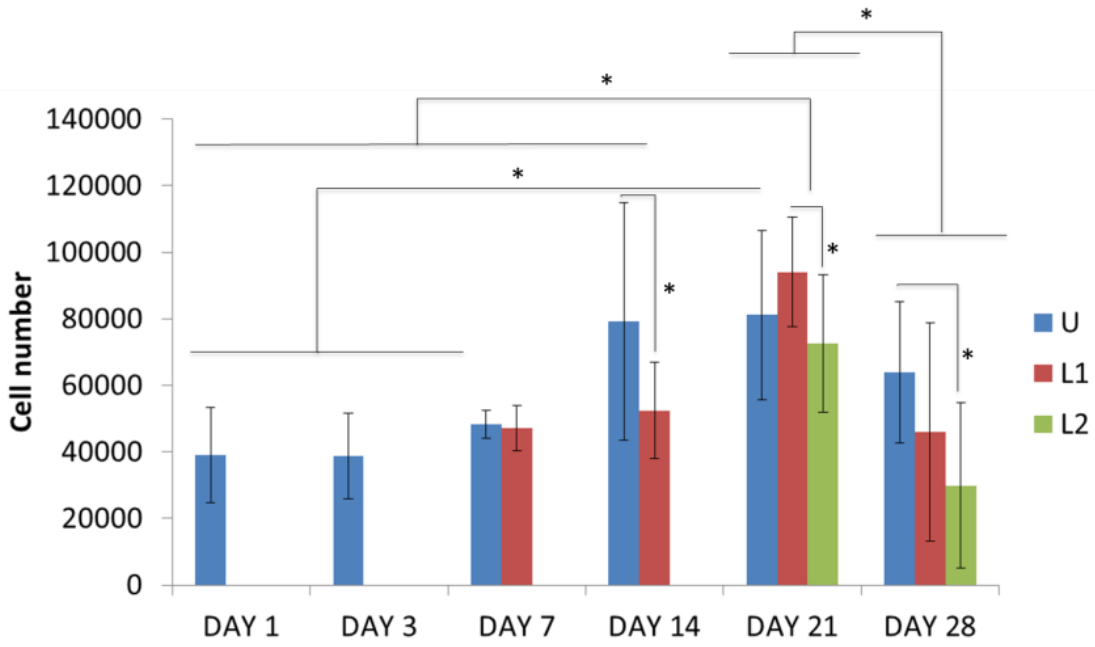

Fig. 7.6: Cell number (n = mean±S.D.) over time for non-loaded (U), loaded once (L1) and twice loaded (L2) over 28 days. Samples from different groups were considered the same as at day 1 and day 3, as no statistical differences were found comparing metabolism of U, L1 and L2 by Presto Blue. Due to the ANOVA results on Presto blue assay, loaded (L1 and L2) samples at day 7 and day 14 were also considered as belonging to the same group. As a consequence, the amount of cells attributed to L1 for those two time points was simultaneously representative for the behaviour of L1 and L2. Significant differences are underlined: *p<0.05.

The proliferation of cells was also quantified by DNA assay. An increase in cell number was observed at day 14 for U ($p<0.05$), and day 21 for L1 ($p<0.05$) and L2. However, L2 showed lower cell content compared to L1 at every time point, suggesting that a second series of cyclic mechanical load prevents proliferation. A decrease in cell number occurred at day 28 for all tested conditions, indicating an extensive cell death. A similar trend was observed by considering the x-ray signal (Fig. 7.7), confirming a relationship between the proliferation of cells and the signal detected by microCT in the range 3,500-7,500 of GV. At day 1, the signal from cells was hidden by the surrounding collagen due to their reduced dimension and the low seeding number. Cellular content started to be detected from day 3 when cells assumed a more elongated shape and produced ECM. Tissue content experienced a decisive increase at day 21 for all conditions, although an earlier increase in cell proliferation for U was already observed at day 7.

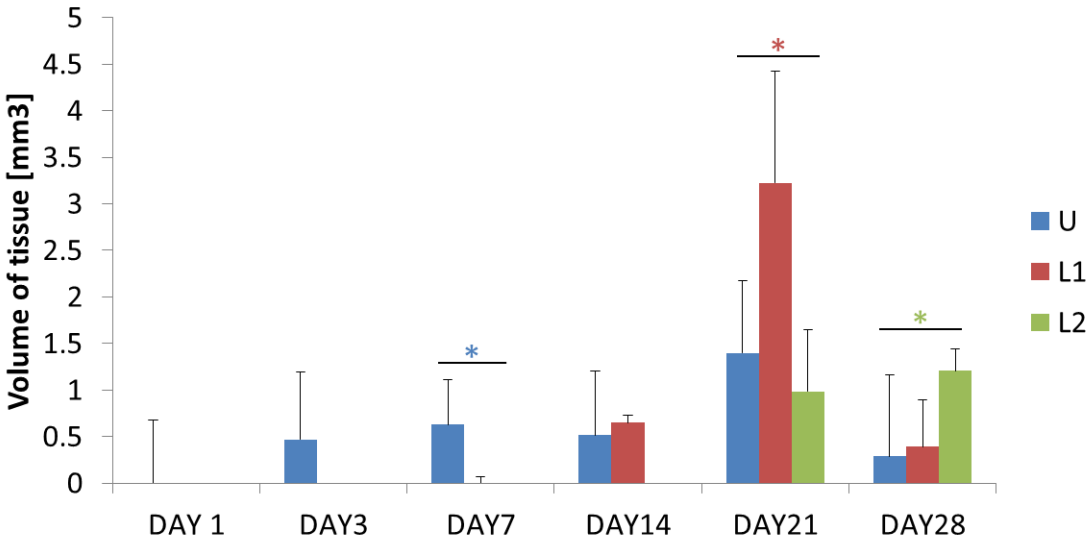

Fig. 7.7: Volume of tissue (n = mean±S.D.) accounting for cells and ECM content considering GV ranging between 3,500 and 7,500 (*$p<0.05$).

The increase in cell content following the end of the first cycle of stimuli was not noticed on samples undergoing a second series of stimulation. This suggests that proliferation began after the 5 days of rest, when L2 samples

had already undergone the second series of compression. For this reason, proliferation was further delayed on L2 samples while cell number increased for L1 samples as they had time to recover from the first proliferation-inhibitory series of compression.

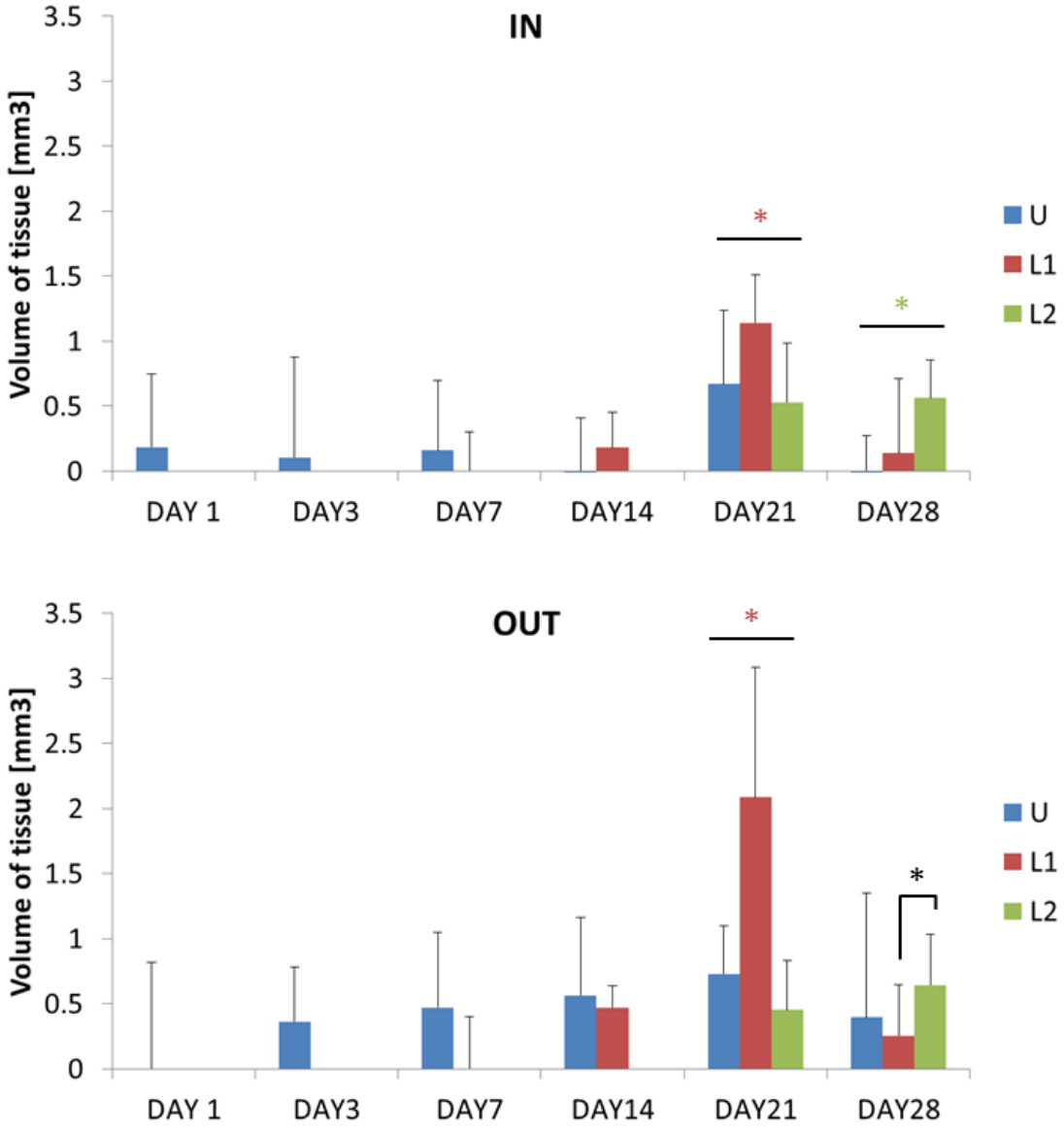

Fig. 7.8: internal (IN) and superficial (OUT) amount of tissue (n = mean±S.D.) quantified by microCT scanning of non-loaded (U), loaded once (L1) and twice loaded (L2) samples over 28 days (*p<0.05).

These findings suggest the role of cyclic loading in delaying the proliferative response of cells. Eventually, the enhanced decrease in cellular content associated to U and L1 at day 28 was not observed for L2, contrasting the DNA results. This discrepancy is probably related to ECM production at day 21 in L2, not detectable by DNA, but contributing to the x-ray signal (Fig. 7.7). The spatial variation of tissue distribution in samples was examined by selecting an internal ROI allowing the assessment of different sites in the sample (Fig. 7.8). The growth of tissue was enhanced on the surface of the scaffold, while the average tissue volume in ROI amounted to 40±12%, 45±7% and 47±8% respectively for U, L1 and L2 samples over the entire duration of the experiment. The increase in tissue content detected for loaded conditions suggests cyclic loading to promote gasses and nutrients exchange with the internal region of the scaffold otherwise prevented by static conditions.

A progressive increase of the tissue on the surface of the scaffold was observed by microCT. Tissue growth involved volumes either inside or outside the ROI at day 21 for L1, suggesting cyclic stimulation as a trigger for increased proliferation when applied at early stage of culture. In this case, it was not clear if the increase in tissue amount was related just to proliferation or ECM production. However, the quick drop of tissue content in L1 at day 28 suggests absence of ECM production as the degradation was expected to occur at lower rate. On the other side, a second burst of cyclic stimulation applied at late stage of culture delayed cellular proliferation but enhanced formation of ECM through all the volume of scaffolds.

7.3.3 Mineralization

Further observation of microCT scans allowed the isolation of the signal from the mineral formed by the action of cells by selecting high intensity GV (Fig. 7.9). U samples mineralized at day 14 and then the mineral content remained constant through the whole duration of the experiment. Differentiating among growth occurring in the interior or the surface of scaffolds (Fig. 7.10), mineral

content was 2 mm^3 on the surface but it was below 0.5 mm^3, close to the detectable threshold, in the internal volume. On the contrary, cells in loaded samples started to produce mineral inside the ROI as well as on the surface from day 7, suggesting an early mineralization process triggered by the cyclic load applied.

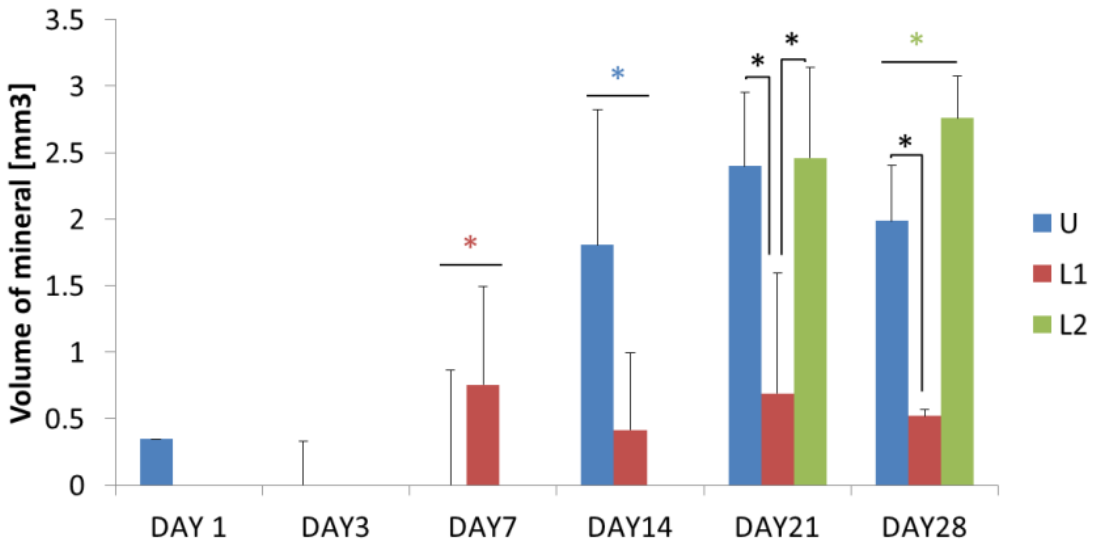

Fig. 7.9: Overall volume of mineral (n = mean±S.D.) detected by microCT for non-loaded (U), loaded once (L1) and twice loaded (L2) samples over 28 days, and referring to GV in a range between 13,000 and 60,000.

Although the early mineralization response triggered in L1 samples was not observed in free-floating conditions, U samples showed a 6-fold higher volume of mineral compared to L1 from day 14 onwards, suggesting that cyclic load prevented mineralization when applied at early culture time. The load elicited a strong effect on mineralization also when applied at advanced culture stage. Indeed, L1 samples did not show any further sign of mineralization after day 7, and the mineral phase at day 28 was only 25% of the amount detected in U. Conversely, a second series of compression cycles enhanced mineralization at day 21, and the mineral content became 30% significantly higher at day 28 compared to U ($p<0.05$). Moreover, the mineralization in ROI for L2 was 3-fold

higher than the other tested conditions from day 21, suggesting late cyclic stimuli to induce mineralization on previously compressed samples.

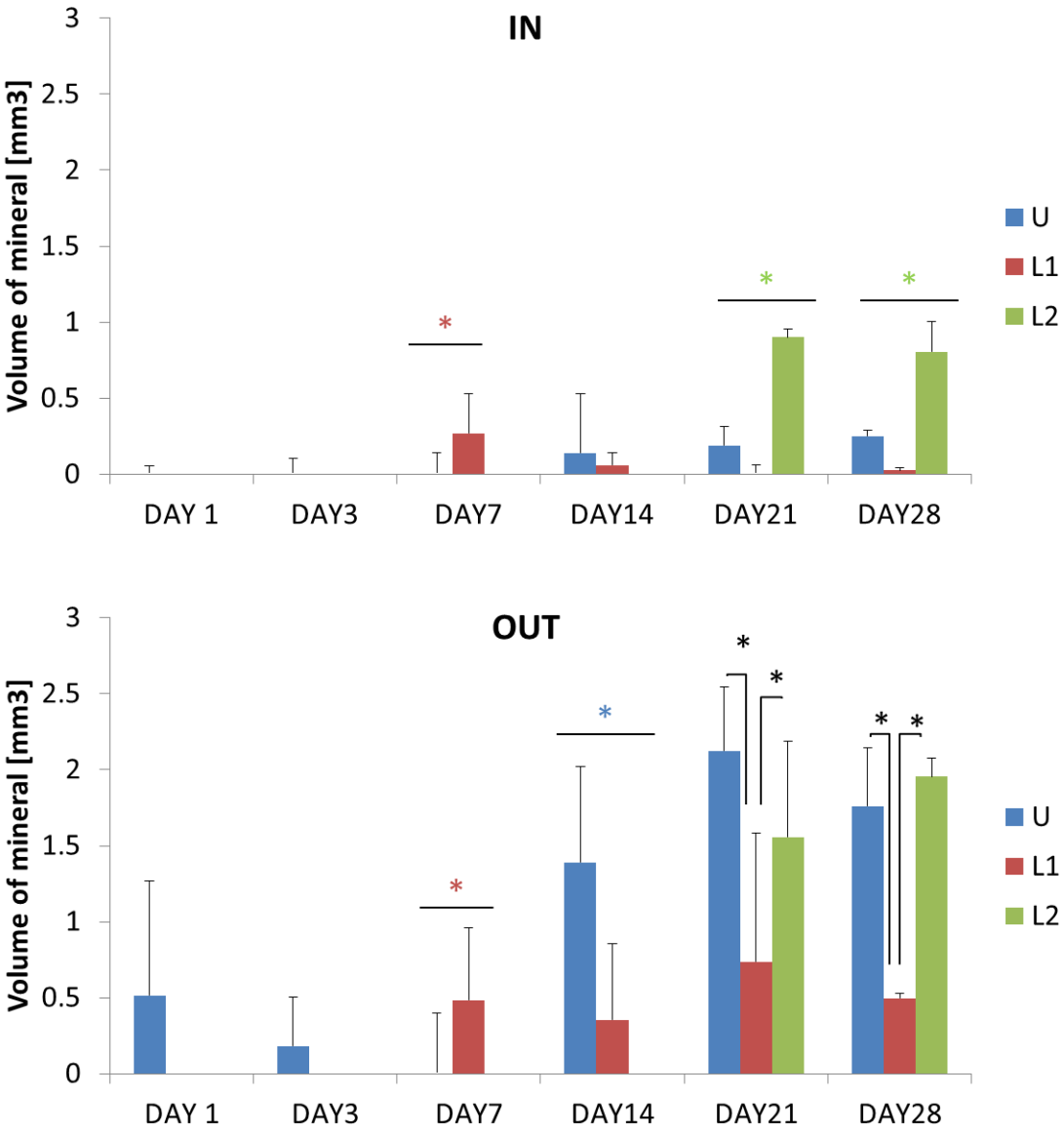

Fig. 7.10: internal (IN) and superficial (OUT) amount of mineral (n = mean±S.D.) quantified by microCT scanning of non-loaded (U), loaded once (L1) and twice loaded (L2) samples over 28 days (*p<0.05).

The pattern of mineralization observed by microCT was confirmed by quantification of OCN by sandwich ELISA (Fig. 7.11). Although not statistically significant, OCN was expressed on L1 samples at day 7, suggesting the

possibility to consider an early cellular response triggered by the mechanical loading.

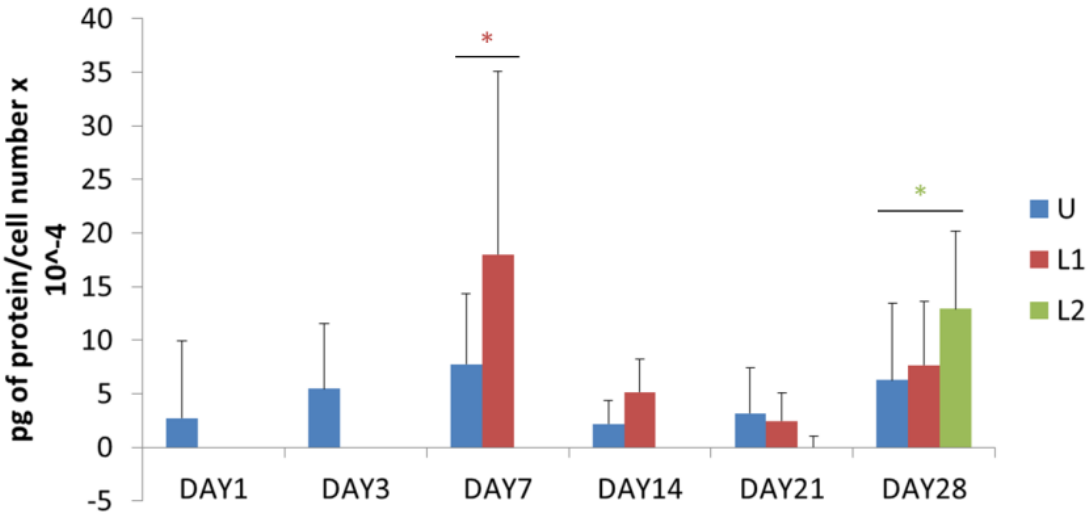

Fig. 7.11: OCN content (n = mean±S.D.) over time normalized over total cell number measured by DNA. The test was performed on six samples per time point, for non-loaded (U), loaded once (L1) and twice loaded (L2). Stars indicate significant differences among conditions at the same time point.

Moreover, the effect of cyclic loading, applied at later stage of culture on mineralization potential of cells was further confirmed at day 28 by the significantly higher (*$p<0.05$) amount of OCN expression detected in L2 samples compared to U and L1. The total amount of osteocalcin for U, L1, and L2 at day 28 was respectively 35.1, 28.3 and 35.9 pg.

7.4 Discussion

7.4.1 Mechanical compression and proliferative response

3D PCL showed to be suitable for studies requiring prolonged culturing of cells and to promote proliferation of hES-MPs in the structure. As a matter of fact, Presto Blue gave a good insight of the behaviour of hES-MPs located only on the surface of the sample due to limitations related to 1) the porosity of samples preventing the washout of the fluorescent solution from the internal volume, and 2) the development of an external layer of cells, blocking the diffusion of molecules in the interior of the structure. Despite this, Presto Blue was used to confirm the equality among samples in terms of initial number of embedded cells and cellular metabolic activity. As a consequence, any difference in the cellular response could be related to the applied mechanical conditions rather than to initial differences among samples. As long as Presto Blue results gave the same fluorescent signal, specimens assigned to different groups but undergoing the same loading conditions were considered as belonging to the same group. Thus, choosing random samples among those following the same protocol provided a reliable insight of the behaviour of cells also in samples which were still kept in culture for later analysis. This assumption refers to outcomes obtained 1) at day 1 and 3 when all samples were non-loaded, and 2) at day 14 and 21 when samples L1 and L2 underwent the same loading protocol. According to statistical analysis on Presto Blue results, the equality among different groups of samples was statistically met here, allowing to halve and reduce to a third the number of respectively L1 and L2 specimens to test in the experiment. A reliable proliferation profile was provided by quantification of DNA content. Conversely to Presto Blue, DNA quantification required the destruction of the sample, enabling the complete extraction of cells and accounting also for the information related to cells located in the internal volumes of samples. Moreover, DNA is a highly sensitive test and, therefore, provides precise measurements with standard deviations below the 30% of the average values except for loaded samples at day 28. The high standard

deviation observed at the end of the experiment can be due to differences among the repeats - in terms of initial seeding density, initial concentration of collagen, scaffolds geometry, slightly different media formulations - which progressively affect the behaviour of cells over time and become more evident at later stage of culture. According to DNA quantification, cyclic compression applied over 5 days caused a delayed proliferation, although significantly increasing the amount of cells at day 21 compared to the other tested conditions. On the contrary, L2 samples did not show any sign of proliferation after 5 days of rest, suggesting that 1) cyclic compression of scaffolds over a 5 day-length period induces proliferation only if the stimulus is applied once; 2) equally long resting periods are not enough to recover from the previous series of compression cycles and enhance proliferation; and 3) a second series of cyclic compression further delays or may block the proliferation, although enhancing ECM and mineral production. Whether a second series of cyclic compression causes delay or blocks the proliferation of cells can be clarified by performing longer experiments, testing samples at day 31, at least, to equalize the time elapsed between loading series. However, comparison with the other loading conditions could be difficult due to the progressive apoptosis already observed at day 28 for U and L1 samples. Improved proliferation after cyclic load was also claimed in the literature, although different scaffolds, compression protocols and cell type were employed. For example, murine embryonic stem cells seeded in collagen type 1 scaffolds and compressed 4 hours a day presented higher viability over time compared to non-loaded samples [101]. Enhanced variability associated with daily compression of 3D samples was also observed in other studies on hES-MPs seeded, bone mineralized scaffolds [111].

7.4.2 ECM deposition and tissue development

A proliferation profile similar to DNA was obtained from the reconstruction of microCT images. A further differentiation between tissue and mineral formation was performed by splitting the signal among different densities. Tissue content

was related to a less dense material associated to growth of cells and ECM deposition. Observing the growth of tissue in the internal volume of samples, the high variability up to 12% in U is likely to reflect the differences in porosity among samples (Chapter 4). Indeed, diffusion of molecules is expected to be facilitated through larger porous samples, enhancing cell survival. A less variable and higher percentage of alive cells was found in the inner volumes of loaded samples, suggesting a possible involvement of cyclic load in the mass transport of nutrients throughout the structure. As a result of cyclic deformation, a gradient of pressure is believed to arise, enhancing convective transport of fluid and cell survival through the whole structure.

At day 21, the absence of proliferation detected in L2 confirmed prolonged cyclic load to prevent proliferation. Last but not least, at day 28 all conditions were affected by cellular apoptosis, which is believed to be associated to lack of nutrients in the interior regions of samples because of the development of the external layer. Apoptosis affected also cells on the surface of L1 samples, suggesting the occurrence of a programmed cell death phenomenon due to the high density achieved [234], [235] at day 21.

Differences in the cell quantification among DNA and microCT may be related to the production of ECM, which signal is accounted for during microCT reconstruction while being excluded in the DNA quantification. The impossibility to split the signal coming from cells and ECM into two separate components was related to the type of contrast agent employed in the study, presenting the same absorbability to cells and ECM. Following this observation, the absence of decrease in tissue volume in L2 between day 21 and day 28, can be reasonably associated with matrix production as well as variations in cell number. Increased production of ECM as a consequence of shorts bursts of compression was also claimed in another study [162] where hES-MPs seeded on a polyurethane scaffolds underwent stimulation at 5% global strain for 2 hours. Similarly to our study, resting periods of 5 days were allowed among series of compression.

7.4.3 Tissue and mineral growth

Cyclic loading affected proliferation, tissue formation, cell survival, as well as mineralization potential of cells. Mineralization went along with the appearance of a more dense material into the scaffold, associated to the deposition of salt crystals.

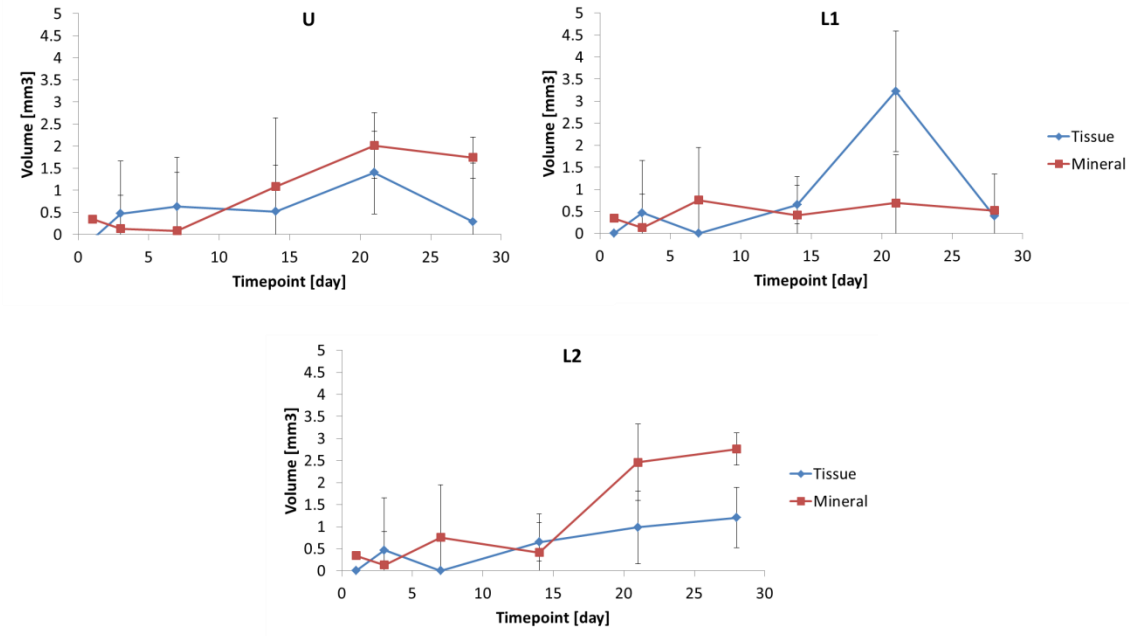

Fig. 7.12: Cellular (blue) and mineral (red) tissue growth over time for non-loaded (U) (left), loaded once (L1) (centre) and twice loaded (L2) (right).

At day 7, an early sign of mineralization was observed in loaded samples and confirmed also by OCN quantification. However, the early presence of mineral content and the mechanism governing such activation needs to be further clarified and it needs to be confirmed due to the high standard deviation associated to both measurements. In general, no degradation of the mineral content was observed over long periods of time (Fig. 7.12). Indeed U increased mineral volume up to 2 mm^3 in the first 14 days, L1 showed a slight sign of mineralization at day 7 and L2 reached the highest mineral content of 3 mm^3 after 21 days, but the amount of mineral remained constant until day 28 for all

conditions. The mineral content increased without ongoing proliferation and this phenomenon leads to hypothesize the existence of a strong link between the two processes whose turnover is largely affected by the mechanical cues provided by the surrounding environment. Applying load at day 6 seemed to enhance mineralization and to temporary decrease the proliferation potential of cells. At the same time, it seems to have triggered a postponed, highly enhanced cellular tissue growth as noticed for L1 at day 21, while further delaying the mineralization which may occur after day 28. Unfortunately, longer studies, not involving compression of samples, are difficult to perform due to the enhanced cellular death observed after 28 days in culture. This phenomenon was probably caused by the barrier to diffusion developing on the surface due to the high proliferation rate of cells in contact with constantly accessible nutrients and gases, as well as the production of ECM reducing the diffusion capability of the matrix. However, similar results claiming the increase in calcium or OCN content as consequence of cyclic compression of scaffolds were previously reported in the literature. For example, expression of OCN was noticed on cells cultured on 2D substrates which underwent continuous strain over 14 days [147]. Enhanced calcium deposition at late stage of culture was also shown to be elicited on 3D scaffolds [100] by using relatively shorts bursts of compression (2 hours).

7.4.4 Mechanical differentiation of hES-MPs in cPCL

The shape of cells at day 28 excluded differentiation toward the chondrogenic pathway, as in all cases cells were well elongated with extended protrusions rather than spherical. Loaded samples exhibited a less compact tissue-like organization on the surface compared to non-loaded samples probably due to the repetitive contact between the sample surface and the bioreactor shafts, causing a slight damage to the most exposed tissue. Moreover, L2 cells appeared star-like shaped, extending multiple, random oriented, thin protrusions. These findings, together with the volume of mineral found by x-ray scanning and the expression of osteocalcin detected for L2 at day 28 may

be sign of osteogenic differentiation. In the literature, studies performed on 2D substrates [147]–[149], [153] showed enhanced osteogenesis when tensile strains were applied, while chondrogenesis was associated mainly with compression applied on hydrogels [88], [104], [156], [159]. On the contrary, mineralization occurred in this study as consequence of compression of scaffolds. This discrepancy comparing to the literature is mainly due to the different type of scaffolds considered. Indeed, 2D substrates transmits stresses to cultured cells just through the attachment surface while hydrogels provide a different distribution of stresses through space compared to that elicited by the cPCL structure due to their soft and compact matrix. Another important fact to highlight regards the distribution of stresses in cPCL. Indeed, diverse stresses act throughout the structure because of irregularities in the geometry of fibers (Chapter 4.2.4) and also the presence of collagen further increases the variability in the mechanical environment surrounding cells. So far, it was shown that local tensile stresses were also developing from the compression of 3D PCL [198] while further clarification of the deformations affecting collagen is required to find a link between the cellular response obtained in this study and the mechanical forces sensed by cells. According to other studies where load was applied to 3D scaffolds by four-point bending devices, compression of scaffolds could elicit a decrease in the chondrogenic potential of cells [155] and enhance osteogenic differentiation [111], [154]. However, the different type of cells and the different loading protocols applied in the experiments do not allow a direct comparison with those studies. As matter of fact, the response to mechanical stimuli, as well as other environmental cues, is strongly linked to the cell lineage, and cells are highly sensitive to the amplitude, frequency, the day the stimulation starts, and the duration of the stimuli, leading to different responses as reported in Chapter 2.3.4.2. For example, polyurethane scaffolds showed enhanced chondrogenesis on hES-MPs for high strain above 10% [157], while more moderate strains below the 10% enhanced matrix production on hES-MPs [100] and mineral deposition on MLO-A5 [162].

7.5 Conclusions

7.5.1 Summary

This study highlights how cyclic compression stimuli of scaffolds embedding cells can modify cell response while maintaining good exchange of fluids with the interior of the scaffold. A peculiar characteristic of this study relates to the accurate methodology and the effort to provide repeatability by performing the experiment three times on a large number of previously relaxed, mechanically characterized and x-rays scanned PCL scaffolds. Cell behaviour was evaluated on the overall amount of material in the sample without distinguishing among local stress variation, geometrical differences or imperfections, increasing the variability of the experiment and enabling a stronger linkage between compressive protocol and overall cellular response. Scaffolds undergoing short daily bursts of compression showed not only variations in terms of proliferation but also the mineralization potential of cells. The mineral content detected by microCT, the expression of osteocalcin observed at day 28, and the overall shape acquired by cells permit to exclude the formation of cartilaginous tissue, and support bone development as pathway likely to be triggered by the applied cyclic loading conditions.

7.5.2 Future work

In order to clarify the influence of cyclic load on cell response as well as to further assess osteogenic differentiation, the expression of osteogenic marker such as RunX2, ALP, OPN and OCN by RT-qPCR can be the next step, giving a deeper insight of the commitment of hES-MPs. Investigation of genes expression could also clarify the early mineralization process observed by microCT and OCN quantification to distinguish among genes associated to proliferation rather than mineralization. In order to identify the effect of

mechanical stimuli on cell survival, a gradient of pressure enhancing mass transport in the internal volumes of specimens could be proven by a combination of experimental and computational results. This approach would also better define the stresses felt by cells giving an insight of the stimuli transmitted from the scaffold to collagen and from collagen to cells. A further step forward regards the distinction between signal coming from cell and ECM content. An accurate quantification of ECM content would clarify differences rising from the comparison of DNA and tissue quantification, and would help to fully understand the process governing tissue formation into scaffolds. With this purpose, possible candidates are Hexabrix and Lipiodol, ionic contrast agents already used in clinical practice for visualization of the internal structure of the body by CT scanning [236] as well as for assessing tissue formation in vivo [237] and in vitro [238], [239]. Hexabrix was already used in the quantification of the ECM by nano-CT demonstrating higher diffusion compared to phosphotungstenic acid (PTA) [239] due to its low molecular weight. The low specificity of Hexabrix allowed the visualization of the ECM components whose detection was prevented from the use of PTA due to its high affinity for collagen-fibrin rich components [238]. Hexabrix allows automated image analysis as the signal is independent from exposure time and matrix quantity [239]. Eventually, in an effort to distinguish among x-ray signals of ECM and cells, iron oxide nanoparticles can be used for cell labelling and assessment of their distribution into the scaffold, as previously proposed by Albertini et al. [240]. Considering alternative techniques to microCT, nanoparticle were also recently used for labelling cells and track their activity by Magnetic Resonance Imaging (MRI) in vivo [241], [242] as well as in vitro [243], [244].

Chapter 8

GENERAL DISCUSSION

8.1 PCL geometrical and mechanical characterization

The first part of this thesis aims to verify the geometrical repeatability of 3D Insert ® PCL (3D PCL) scaffolds and investigate its mechanical response to compression (Chapter 4). The main challenge at this stage consisted in defining an apparent elastic modulus (E_a) able to provide a good representation of the linear response to compression due to the variable architecture of scaffolds. At first, viscoelastic effects were prevented by static preconditioning. In the literature, constant strain is often used to obtain relaxation of samples [185]–[187]. In this study, equilibrium was reached by imposing constant displacement on samples for 180 minutes. The reason for the large amount of time required to achieve complete relaxation is believed to be related to the high degree of crystallinity of 3D PCL. This assumption is further confirmed evaluating the degradation potential and water uptake of 3D PCL. Indeed, slow degradation and low water uptake are correlated in the literature to a crystalline state of the material rather than an amorphous one [245]. In this study, the crystalline state of 3D PCL is suggested by the similar values in term of dynamic modulus found testing the same scaffold in air or water. The static strain applied during the relaxation prevented any plastic behaviour to occur for strain amplitude below 8%. This limited to 8% the maximum strain applicable in experiments to guarantee reproducibility of the mechanical stress among stimulations and to avoid the presence of plastic deformation. Once relaxed, a range of strains eliciting an elastic response was identified for further analysis of the mechanical behaviour of 3D PCL varying temperature, or under cyclic load. As expected from a polymeric material, the mechanical response was dependent to temperature. Apparent stiffness

values found here are in accordance with other studies presenting comparable order of magnitude [75], [106], [189]. The main drawback in the evaluation of the stiffness of the structure was related to the high variability in the measurement. Indeed, considering a different orientation on the xy plane, the same scaffold led to E_a varying up to 30% from the average value. This variation was much higher than the percentage error found applying the same protocol to standard PDMS samples with identical geometry but compact architecture. This difference between the two materials suggests a link between the architecture of PCL and the variability of the measure. As extensively claimed in the literature [106], [188], [189], the mechanical properties of scaffolds vary greatly depending on the diameter of the fibers, their relative orientation or the presence of defects. As observed by microCT, 3D PCL is characterized by many structural irregularities which cause a highly randomized distribution of stresses. Furthermore, the sample height is 3-fold lower than the diameter, causing an underestimation of the overall stiffness of the structure as demonstrated compressing PDMS samples with different height. DMA analysis provided the required parameters to implement computational models [198] that can simulate the scaffold mechanical response to compression and better clarify the local distribution of stress within the structure. The variability observed in the mechanical response of PCL can be also considered advantageous in an effort to simulate the in vivo environment. Indeed, the bone fracture site is characterized by a combination of tensile, compressive and bending forces strictly connected to the synergic action of muscles, tendons, blood flow and external factors, rather than a single and uniform compressive component. In fracture sites, stresses felt by cells vary consistently with the shape and the dimensions of the defect [200]. According to a computational models developed by Claes and Heigele, intramembranous ossification occurs for strains below 5% while endochondral ossification was predicted applying hydrostatic pressures greater than 0.15 MPa and local strains below 15% [246]. Moreover, the callus tissue forming in bone fracture sites has variable stiffness ranging from 0.6 to 1010 MPa as measured by nanoindentation [247]. These findings confirm the suitability of using PCL for in vitro experiments aiming to reproduce the same global

mechanical environment present in bone fracture as well as the ability of the stiff PCL structure to bear mechanical compression. Further analysis of the local distribution of strains and stresses within 3D PCL is necessary to better define the mechanical environment sensed at the cellular level and correlate the differentiation toward a certain lineage with the mechanical cues developing in the structure. The use of 3D PCL for in vivo applications requiring the replacement of bone in large fracture sites is limited to its height. In spite of this, the mechanical properties and the low degradation rate shown by 3D PCL allow to consider structures of the same material and with a similar architecture but higher height for in vivo studies as it would provide the support to the mechanical forces affecting bone as well as a good tolerability from the host body.

8.2 PCL seeding techniques

The second part of this thesis aims to establish a well-defined methodology to be used for further studies requiring minimum differences in seeding efficiencies and consequently high reproducibility of the initial seeding conditions. Once the mechanical properties were defined, cellular attachment on PCL was investigated by comparing perfusion and static approaches (Chapter 5). In order to apply perfusion of cells, a custom made bioreactor was designed and manufactured by common soft lithography techniques. After having been defined by experiments and confirmed by computational simulations [212] the shear stress acting on the wall of the scaffold in a single chamber device, other multi-chambered configurations were tested. The main challenge encountered at this stage regarded the development of identical systems. Indeed, marginal differences in the design and the presence of imperfections in the initial mold caused respectively differences in the inlet flow rate approaching the scaffold and the nucleation of bubbles into the system. The necessity to overcome these issues required a compromise between the number of samples included in the microfluidic system and the time of culture. A single chamber device was used in the comparison between perfusion and

static seeding performances as the fluid flow in such a simple system was already well-characterized experimentally and computationally [212]. The simplest configuration proposed in this study, indeed, proved to support a good perfusion of scaffolds with shear stress values in a beneficial range for attachment. Seeding efficiencies obtained by static and perfusion were compared considering two different velocities. Using different devices and different scaffolds led to a slight variation in the amount of cells attached, confirming the ability of a single chambered design to provide a repeatable shear stress stimuli for a given inlet rate. However, due to the architecture and topography of the scaffolds as well as the regime of constant perfusion, static seeding methods provided a higher number of cells attached compared to perfusion. These outcomes are in contradiction with the literature where either unidirectional [114] or oscillatory perfusion [116], [122], [213] were generally found to increase seeding efficiency and provide a better cellular distribution within the constructs. The reason for such low values of seeding efficiency were clarified by computational simulations [212] carried out on a model replicating the real geometry of scaffolds. It was shown that cells pass through the centre of pores rather than contacting with PCL walls. Furthermore, discrepancies in the literature can also be justified by differences in the number and type of cells involved in the seeding process, velocities applied, and architecture and topography of scaffolds. Due to the increased seeding efficiency, common static techniques were preferred for the seeding of specimens in the next part of the study. The spatial distribution assumed by collagen injected in the structure (Chapter 6) is likely to reproduce the pathway followed by the cellular suspension when static seeding was performed regardless the use of collagen. So after static seeding, cells are expected to occupy the full thickness of the scaffold. This phenomenon can be related to the short height of 3D PCL. Indeed, the limited thickness of 3D PCL requires cells to migrate over a short distance resulting in a good distribution also in the interior of the structure. This phenomenon instead prevented employing taller scaffolds where cells probably move toward the centre as noticed in our case, but the thickness of the structure is too high preventing them to reach internal volumes just through diffusion (Chapter 2.3). In such cases, perfusion is

indeed preferred because it allows cells to reach internal areas of the construct, whereas in this study the reduced thickness promotes a uniform distribution of cells by common static seeding methods.

8.3 Collagen characterization and cellular interactions

While the stiff PCL structure is able to bear the mechanical force and sustain tissue growth, its deformability is limited, preventing the transmission of mechanical stress to seeded cells. Hence, a collagen gel was included in the structure (cPCL) to provide a soft matrix mimicking the bone-tissue niche and to transmit external mechanical stimuli to the cultured cells (Chapter 6). When injected in PCL, collagen must be evenly distributed to guarantee equal conditions within the whole volume of the scaffold. Distribution, architecture and degradation of collagen over time were investigated to verify this requirement. The task was conducted by microCT and Sirius red stain. The former enabled the observation of the internal volume of scaffolds while the second excluded drying steps to cause modifications in the overall distribution and organization of collagen. The micro and nano organization of collagen was further assessed by SEM imaging to give an insight of the type of pores and collagenous matrix provided by the gel. A very similar architecture composed by overlapping, randomly oriented fibers was also imaged in another study aiming to investigate the micro and nano structure of collagen hydrogel [174]. By x-ray imaging collagen was found to be organized in a layered structure bridging neighbour 3D PCL fibers, leading to a well interconnected matrix. However, differences in the architecture of scaffolds were responsible for a non-homogeneous densification of collagen observed when comparing samples. Indeed, less interconnected portions of the scaffold provided less resistance, facilitating the infiltration of molecules through larger pores. Collagen placed on the surface of scaffolds degraded first due to continuous exposure to culture media while collagen located in internal volumes was affected later. Embedding cells into the structure confirmed the ability of collagen in promoting cell survival and proliferation at early stage of culture.

Plasma treatment and various gel concentrations were applied to samples to investigate how different conditions affect the behaviour of cells. Seeding efficiency and distribution of cells were compared among conditions to define the best enhancing cell survival. Static seeding of cells led to higher attachment when collagen was embedded in PCL. This was due to the higher viscosity of the solution used to seed cells in cPCL, contrasting the action of gravity and providing layers to connect neighbour polymeric fibers. A uniform spreading of the overall cellular content through the structure was instead guaranteed by plasma treatment of samples before embedding cells. According to the literature, plasma not only contribute to the sterilization process [248] but also improves the surface reactivity [249] increasing interaction with collagen [250] and cells [251]. Here, plasma treatment was proved [251]. Here, plasma treatment was shown to improve the distribution of cells and collagen on the surface of the scaffolds. Collagen concentration was also found to play an important role in cell survival. Cell viability was enhanced for low concentration while extensive cellular apoptosis and necrosis was noticed for high concentration of collagen. The extensive apoptosis observed for high concentration of collagen was probably due to the reduced porosity for increased collagen content, preventing diffusion of vital nutrients and gasses through the structure. Moreover, an even mixture of cells within the collagenous solution at time of injection guarantees the distribution of collagen to be a good representation of the spreading of cells in the sample. According to the results, this study identifies plasma treatment of scaffolds and a collagen concentration of 2 mg/ml as the best condition to apply to obtain optimal seeding efficiency and uniform collagen and cellular distribution. These findings, together with the consistency of the seeding efficiency among different samples, confirm the suitability of cPCL in providing a proper environment for prolonged cellular studies.

8.4 Collagen, tissue and mineral quantification by microCT

Among the main challenges, the necessity to identify a staining technique able to give contrast for microCT imaging without affecting the collagen structure was overcome by exploiting osmium tetroxide as contrast agent. A strict correlation between density of the material and intensity of the x-ray signal resulting from osmium stain is not provided by the state of the art. In our study, a higher intensity signal may therefore be correlated to accumulation of osmium rather than associated to an increase of collagen density. Despite this, hypothesizing a link between intensity of the signal and density of the collagen is reasonable since the staining procedure was kept identical through the whole experiments. Thus, variations in the x-ray signal due to the differences in the staining procedure performed at different time points were minimized. Accumulation of collagen was also confirmed by Sirius Red. As Sirius Red absorption is linearly proportional to the concentration of collagen in the sample [252], a more intensely stained volume indicated collagenous densification (HD). MicroCT was also used in the visualization of collagen, cells, ECM and mineral distribution, and it was correlated with DNA and protein expression assays to validate the results. Following staining with osmium tetroxide, a clear visual distinction between initially injected bovine collagen, cellular content and ECM was not possible due to matching intensity of their signals. Indeed, bone-like ECM, as well as cells themselves, presents a structure very similar to the bovine collagen employed here [253]. As a consequence, they contribute to the x-ray signal in the same range of GV as collagen and they are also equally affected by osmium staining due to their proteinaceous nature. This phenomenon prevented distinction among newly deposited ECM, increase in cellular content and initially injected collagen. The latter was instead removed from the quantitative analysis by providing cell-less controls and accounting for the progressive degradation of collagen at each time point. Therefore, the growth of tissues quantified in this thesis (Chapter 7) accounts at the same time for increase in cell number and in matrix production. An example of this was observed at day 21 for single loaded

samples where the enhanced signal detected by microCT was attributed to proliferation but it could also have been further influenced by matrix production. The same issue affected the visualization of mineral content as it matched the same range of GV as collagen undergoing accumulation. Despite this, it is still unclear how the osmium staining affects the signal from the mineral component although there is no significant evidence of interaction between osmium and salts. Thus, the higher intensity of the signal attribute to the mineral phase could be due to a higher absorption of osmium on the crystal surface compared to the ECM or, most likely, to the direct attenuation of x-ray by salt crystals [254]. However, quantification of mineral content was possible by employing controls to subtract the signal of the collagen initially injected. The signal in the GV initially attributed to aggregation of collagen injected in the sample increased its volume over time when cells were embedded, suggesting the production of a material denser than ECM which is believed to represent the mineral phase. The growth of mineral was further confirmed by the enhanced osteocalcin production.

8.5 Effect of compression of cPCL on ECM and mineral production

The last part of the study (Chapter 7) aims to evaluate the effectiveness of cyclic mechanical compression applied for short amount of time on seeded scaffolds and the application of resting periods between stimulations on the proliferative response and commitment of progenitor cells. Compression of cPCL was shown to delay proliferation if applied once (L1) at early stages of culture but to enhance mineralization and matrix production if a second cyclic stimulus (L2) was added at later stage of culture. Indeed, L2 samples showed enhanced mineral content as a result of the applied compression, further confirmed by expression of OCN and the shape of cells noticed by fluorescence imaging. Compression of scaffolds in the literature was mainly found to drive chondrogenesis of cells when culture in hydrogels [88], [104],

[156], [159] while tension was preferred to induce an osteogenic differentiation on 2D substrates [147]–[149], [153]. However, contradictory results claiming inhibition of chondrogenic as well as osteogenesis [152], [158], or enhanced bone marker expression [111], [154], [255] as consequence of compression were found. Discrepancies are attributed to differences not only in the surrounding matrix providing support for cells growth and transmission of stress, but also in the protocol adopted. Indeed, the duration of application of the stimuli [156] as well as amplitude [154], frequency [157] and start point of the stimulation [156] were shown to affect cell activities and differentiation. The effectiveness of the compression protocol adopted here in modifying the metabolic and proliferative response of cells is in accordance with previous studies [146], [256], confirming similar behaviour. Although compression was applied here for a short period of time, it demonstrated to be effective in varying mineralization potential of hES-MPs. These findings match results in the literature [100] where applying the same stimuli several times elicited a negative effect on proliferation. The osteogenic potential claimed in this study may be related to the translation of the external compression into tension forces acting on fibers as proven by computational analysis simulating the distribution of stresses into compressed samples [198].

8.6 Stress sensed by cells and collagen deformation

cPCL proved to fulfil the requirements for a reproducible mechanical response and for a niche enhancing cellular activities. As mentioned before, the collagen embedded in cPCL was expected to transmit external forces to cells through the deformation of its soft structure. While the mechanical properties and the deformation of PCL under compression forces were extensively determined by static and dynamic tests, the mechanics of collagen is currently still unclear. This is due to the unfeasibility of performing experiments to directly measure how the collagen was affected by a force applied externally to cPCL. Computational models [257] are currently under development to clarify the amplitude and distribution of stresses for embedded collagen. The mechanical

properties of collagen were tested by experiments performed on samples at different concentration [257] to provide parameters for modelling the material properties. cPCL samples reconstructed by microCT and described here (Chapter 6) are used as models to provide a realistic representation of the collagen distribution. Although the stresses sensed by cells are still unknown, the effectiveness of the cPCL in transmitting forces to cells was shown in the last part of the study where different loading protocols induced different responses of cells. As mentioned earlier, collagen is assumed to transfer the forces to cells, leading to the possibility of the real strain felt by cells to be very different than the one applied externally. However, whether the stresses here transferred by the deformation of collagen or of the polymeric 3D PCL structure was not clear and a comparison with experiments performed on cells cultured only in the 3D PCL structure without collagen can help to elucidate this point. Beyond the distribution of stresses in the collagen, another variable not considered in this study is the effect of fluid flow generated indirectly from the application of compression in the interior of the scaffold. The outcomes of this study identified a link among cyclic compression of cPCL, hES-MPs proliferation and mineralization potential with consistent response among specimens despite the variable geometry of the scaffold. These findings are very valuable due to the high number of tested scaffolds and the repeats of the experiment. The same experiment was indeed performed three different times to account for uncontrolled variables related to external environmental conditions, initial sample preparation, small differences in cell number, expanding conditions and culture media formulation among experiments.

Chapter 9

CONCLUSIONS

9.1 Summary

In this study, a novel composite scaffold was developed, merging in the same construct the force-bearing properties of polymers with the deformability of the 3D matrix characterizing collagen gels. This study, due to the large number of tested samples and repeats, accounts for the contribute given to the variability by the geometrical irregularities among samples as well as by the random external variables such as medium composition, environmental temperature, and collagen concentration, distribution and densification.

The main contributions of this thesis concern:

- The development of a 3D hybrid scaffold with a solid external structure able to bear cyclic mechanical load and an internal collagenous matrix reproducing the in vivo bone environment. Although the collagen did not form a compact matrix within the scaffold, it was very well interconnected through the structure, increasing the three-dimensionality of the construct. Moreover, the in vivo variability of the mechanical environment was well reproduced by the local geometrical irregularities and the different stresses elicited by the deformation of fibers as well as collagen.
- The evaluation of the overall contribution given by geometrical features to the variability in the mechanical response of 3D PCL. 3D PCL was indeed able to provide repeatability in the stress with a range of variability up to 30% due mostly to the architecture and the small dimensions of samples. This range can be improved considering taller scaffolds as proved by testing polydimethylsiloxane under compression.
- The investigation of the effect of constant fluid flow regimes on attachment of stem cells and the development of an in-house microfluidic device to provide perfusion of PCL. Static seeding was proved as suitable to achieve

uniform distribution of cells through 3D structures as long as specimens are plasma treated before the seeding procedure and they are sufficiently short to guarantee diffusion through the whole height of the construct.

- The assessment of the distribution and the degradation profile over time of collagen embedded in 3D porous scaffolds. Collagen was found to organize in layer-like structures increasing the interconnectivity in the sample. Collagen progressively degraded over time becoming significantly lower on the surface of scaffold from day 7 and in the internal volumes from day 21. Moreover, osmium tetroxide was proved to be efficient as stain to image proteins in vitro by x-ray techniques. The investigation of the collagen distribution when it was embedded in 3D Insert® PCL (3D PCL) defined controls to be used in further experiments requiring the embedding of cells.
- The evaluation of the best experimental conditions promoting cell survival and tissue development. Air plasma treated scaffolds embedding 2 mg/ml collagen were found to greatly enhance cellular viability and enhance cell proliferation from day 7 onwards on free-floating scaffolds.
- The effectiveness of cyclic mechanical stimuli in modifying the response of mesenchymal stem cells (hES-MPs). Proliferation and mineralization potential of hES-MPs were indeed proved to be affected by the external mechanical cues even if applied for short periods of time. Indeed, not only a 15 min stimulation delayed proliferation and differentiation of cells, as noticed applying a 5 days long series of cycles, but repeating the same stimuli a second time increased the production of mineral phase. Particularly worth to mention is the growth of tissue and mineral occurring in the interior of the scaffold only when mechanical stimuli were applied.

These outcomes open the frontiers for a new approach where mechanobiology and 3D composite structures can be used as a tool for the development of engineered bone tissue applicable in the large fracture repair practice. Due to the high variability encountered in the mechanical response of 3D PCL and to satisfy the increasing demand for more repeatable measures, taller scaffolds with the same porosity and structure, and presenting a more regular geometry will be most likely considered for future studies. This would allow a more

uniform distribution not only of compressive stress, but also in terms of fluid shear stress when a liquid is perfused though the structure. DMA analysis used alongside with computational simulation and microCT provides the necessary tools to achieve the next goal aiming to 1) define local stresses distribution in the scaffold, 2) include collagen layers into the 3D structure and quantify the stresses transmitted by the gel to cells, and 3) link the formation of tissue in a certain sub volume of the scaffold to a well-defined range of forces acting locally. A combination of ionic, non-toxic contrast agents and metallic nanoparticles provide a promising approach for a reliable representation of the tissue growth process within 3D fibrous polymeric scaffolds. Alternatively, magnetic resonance imaging could be considered to follow the growth of tissue in a single scaffold in the effort to better link mechanical stresses and cells differentiation. Eventually, the effect of compression on cPCL seeded with hES-MPs can be further explored considering the same protocol presented here but adding a further loading condition which consider compression of samples just at late culture stage.

9.2 Future work

This work can be further developed to better clarify the mechanobiology of hES-MPs. Future studies include:

- PCR: which could be employed to investigate expression of ostegenic genes such as RunX2, ALP, ostepontin and osteocalcin. Other differentiation pathways could be considered expanding the study to the expression of markers for chondrogenesis or adipogenesis. As the commitment toward such lineages are the most likely alternative pathways to occur due to the process undergone in the differentiation of hES-MPs from hESCs [20]. That would allow the clarification of how mechanical stimuli induce differentiation toward a certain tissue and, testing other protocols could enable the determination of a strong link

between cell commitment and mechanical environment which is fundamental for the development of implantable engineered tissue prepared in vitro.

- Histology: which would clarify the spatial tissue formation and better define the differentiation pathway followed by cells through staining of proteins such as alcian blue and alizarin red. In order to apply this methodology, PCL requires embedding in resin as it would to enable the cutting of thin slices, avoiding the destruction of the structure otherwise occurring due to the brittleness of the polymer.

- Other loading conditions consist in applying the same protocols described here to 3D PCL samples without collagen. Those experiments allow the determination of whether the stiff PCL scaffolds contributes to the transmission of the stress resulting from the compression of samples or if PCL just has a role in bearing the force preventing the cellular culture to collapse.

- DMA on samples with similar height to provide mechanical parameters such as elastic and dynamic modulus to be imported in computational models to elucidate the local stresses developing in the structure either with or without collagen. This would also allow clarification of the fluid shear stresses arising in the structure as results of cyclic loading and define their role in the differentiation of hES-MPs.

- As mentioned in Chapter 6, the use of alternative non-destructive techniques for staining of protein tissue would avoid the drawbacks encountered here with the use of fixatives and drying procedures, giving a better insight of the distribution and organization of collagen, tissue and cells into the scaffold.

REFERENCES

[1] J. Rubin, C. Rubin, and C. R. Jacobs, “Molecular pathways mediating mechanical signaling in bone.,” *Gene*, vol. 367, pp. 1–16, Feb. 2006.

[2] R. M. Delaine-Smith and G. C. Reilly, “Mesenchymal stem cell responses to mechanical stimuli.,” *Muscles. Ligaments Tendons J.*, vol. 2, no. 3, pp. 169–80, 2012.

[3] G. M. Cooper, M. P. Mooney, A. K. Gosain, P. G. Campbell, J. E. Losee, and J. Huard, “Testing the critical size in calvarial bone defects: revisiting the concept of a critical-size defect.,” *Plast. Reconstr. Surg.*, vol. 125, no. 6, pp. 1685–92, Jun. 2010.

[4] D. J. Knight, L. a Rymaszewski, a a Amis, and J. H. Miller, “Primary replacement of the fractured radial head with a metal prosthesis.,” *J. Bone Joint Surg. Br.*, vol. 75, no. 4, pp. 572–576, 1993.

[5] G. Mahendra, H. Pandit, K. Kliskey, D. Murray, H. S. Gill, and N. Athanasou, “Necrotic and inflammatory changes in metal-on-metal resurfacing hip arthroplasties.,” *Acta Orthop.*, vol. 80, no. 6, pp. 653–659, 2009.

[6] K. Abul-Kasim and A. Ohlin, “Evaluation of implant loosening following segmental pedicle screw fixation in adolescent idiopathic scoliosis: a 2 year follow-up with low-dose CT.,” *Scoliosis*, vol. 9, no. 1, p. 13, 2014.

[7] M. Geetha, A. K. Singh, R. Asokamani, and A. K. Gogia, “Ti based biomaterials, the ultimate choice for orthopaedic implants – A review,” *Prog. Mater. Sci.*, vol. 54, no. 3, pp. 397–425, 2009.

[8] C. Piconi and G. Maccauro, “Zirconia as a ceramic biomaterial,” *Biomaterials*, vol. 20, no. 1, pp. 1–25, 1999.

[9] F. W. Cooke, “Ceramics in orthopedic surgery,” *Clin. Orthop. Relat. Res.*, vol. 276, pp. 135–46, 1992.

[10] C. G. Finkemeier, “Bone-Grafting and Bone-Graft Substitutes,” *J. Bone Jt. Surg.*, vol. 84A, no. 3, pp. 454–63, 2002.

[11] I. Pountos, T. Georgouli, G. Kontakis, and P. V Giannoudis, “Efficacy of minimally invasive techniques for enhancement of fracture healing : evidence today,” *Int. Orthop.*, vol. 34, pp. 3–12, 2010.

[12] R. J. Beaver, M. Mahomed, D. Backstein, A. Davis, D. J. Zukor, and A. E. Gross, “Fresh Osteochondral Allografts for Post-traumatic Defects in the Knee,” *J. bone Jt. Surg.*, vol. 74, no. 1, pp. 105–10, 1992.

[13] R. Langer, “Tissue engineering: perspectives, challenges, and future directions.,” *Tissue Eng.*, vol. 13, no. 1, pp. 1–2, Jan. 2007.

[14] S. J. Hollister and W. L. Murphy, “Scaffold Translation: Barriers Between Concept and Clinic,” *Tissue Eng. Part B*, vol. 17, no. 6, pp. 459–74, Dec. 2011.

[15] P. M. Govey, A. E. Loiselle, and H. J. Donahue, “Biophysical regulation of stem cell differentiation.,” *Curr. Osteoporos. Rep.*, vol. 11, no. 2, pp. 83–91, Jun. 2013.

[16] A. J. Engler, S. Sen, H. L. Sweeney, and D. E. Discher, “Matrix Elasticity Directs Stem Cell Lineage Specification,” *Cell*, vol. 126, no. 4, pp. 677–89, 2006.

[17] H. F. Hildebrand, N. Blanchemain, G. Mayer, F. Chai, M. Lefebvre, and F. Boschin, “Surface coatings for biological activation and functionalization of medical devices,” *Surf. Coatings Technol.*, vol. 200, no. 22–23, pp. 6318–6324, Jun. 2006.

[18] D. Lee, M. M. Knight, J. J. Campbell, and D. L. Bader, “Stem cell mechanobiology.,” *J. Cell. Biochem.*, vol. 112, no. 1, pp. 1–9, Jan. 2011.

[19] V. Karageorgiou and D. Kaplan, “Porosity of 3D biomaterial scaffolds and osteogenesis,” *Biomaterials*, vol. 26, no. 27, pp. 5474–91, 2005.

[20] C. Karlsson, K. Emanuelsson, F. Wessberg, K. Kajic, M. Z. Axell, P. S. Eriksson, A. Lindahl, J. Hyllner, and R. Strehl, “Human embryonic stem cell-derived mesenchymal progenitors-Potential in regenerative medicine,” *Stem Cell Res.*, vol. 3, no. 1, pp. 39–50, 2009.

[21] G. M. de Peppo, M. Sladkova, P. Sjövall, A. Palmquist, K. Oudina, J. Hyllner, P. Thomsen, H. Petite, and C. Karlsson, “Human Embryonic Stem Cell-Derived Mesodermal Progenitors Display Substantially Increased Tissue Formation Compared to Human Mesenchymal Stem Cells Under Dynamic Culture Conditions in a Packed Bed/Column Bioreactor,” *Tissue Eng. Part A*, vol. 19, no. 1–2, pp. 175–187, 2013.

[22] B. Clarke, “Normal bone anatomy and physiology.,” *Clin. J. Am. Soc. Nephrol.*, vol. 3, pp. 131–39, Nov. 2008.

[23] A. J. Salgado, O. P. Coutinho, and R. L. Reis, “Bone Tissue Engineering: state of the art and future trends,” *Macromol. Biosci.*, vol. 4, pp. 743–65, 2004.

[24] J. Sodek and M. D. McKee, “Molecular and cellular biology of alveolar bone,” *Periodontol 2000*, vol. 24, pp. 99–126, 2000.

[25] D. W. Sommerfeldt and C. T. Rubin, “Biology of bone and how it orchestrates the form and function of the skeleton,” *Eur. Spine J.*, vol. 10, pp. S86–S95, 2001.

[26] I. H. Kalfas, “Principles of bone healing,” *Neurosurg. Focus*, vol. 10, no. 4, pp. 1–4, 2001.

[27] J. E. Aaron and T. M. Skerry, “Intramembranous trabecular generation in normal bone,” *Bone Miner.*, vol. 25, no. 3, pp. 211–30, 1994.

[28] B. R. Olsen, A. M. Reginato, and W. Wenfang, “Bone development,” *Annu. Rev. Cell Dev. Biol.*, vol. 16, pp. 191–220, 2000.

[29] M. C. H. Van der Meulen and R. Huiskes, “Why mechanobiology? A survey article.,” *J. Biomech.*, vol. 35, no. 4, pp. 401–14, Apr. 2002.

[30] J. Klein-Nulend, R. G. Bacabac, and M. G. Mullender, “Mechanobiology of bone tissue.,” *Pathol. Biol. (Paris).*, vol. 53, no. 10, pp. 576–80, Dec. 2005.

[31] A. Ruggiu and R. Cancedda, “Bone mechanobiology, gravity and tissue engineering: effects and insights,” *J. Tissue Eng. Regen. Med.*, vol. 2, pp. 1–13, Jul. 2014.

[32] C. T. Rubin, K. J. McLeod, and S. D. Bain, “Functional strains and cortical bone adaptation: Epigenetic assurance of skeletal integrity,” *J. Biomech.*, vol. 23, no. SUPPL. 1, pp. 43–54, 1990.

[33] D. B. Burr, C. Milgrom, D. Fyhrie, M. Forwood, M. Nyska, A. Finestone, S. Hoshaw, E. Saiag, and A. Simkin, “In vivo measurement of human tibial strains during vigorous activity,” *Bone*, vol. 18, no. 5, pp. 405–410, 1996.

[34] J.-H. Chen, C. Liu, L. You, and C. a Simmons, “Boning up on Wolff’s Law: mechanical regulation of the cells that make and maintain bone.,” *J. Biomech.*, vol. 43, no. 1, pp. 108–18, Jan. 2010.

[35] R. J. O’Keefe and J. Mao, “Bone tissue engineering and regeneration: from discovery to the clinic: an overview.,” *Tissue Eng. Part B*, vol. 17, no. 6, pp. 389–92, Dec. 2011.

[36] D. W. Hutmacher, “Scaffolds in tissue engineering bone and cartilage,” *Biomaterials*, vol. 21, pp. 2529–43, 2000.

[37] A. Salerno, D. Guarnieri, M. Iannone, S. Zeppetelli, and P. Netti, “Effect of micro- and macroporosity of bone tissue three-dimensional-poly(epsilon-caprolactone) scaffold on human mesenchymal stem cells invasion, proliferation, and differentiation in vitro.,” *Tissue Eng. Part A*, vol. 16, no. 8, pp. 2661–73, 2010.

[38] N. Gomez, Y. Lu, S. Chen, and C. E. Schmidt, “Immobilized nerve growth factor and microtopography have distinct effects on polarization versus axon elongation in hippocampal cells in culture,” *Biomaterials*, vol. 28, pp. 271–84, 2007.

[39] T. Weiß, R. Schade, T. Laube, A. Berg, G. Hildebrand, R. Wyrwa, M. Schnabelrauch, and K. Liefeith, “Two-photon polymerization of biocompatible photopolymers for microstructured 3D biointerfaces,” *Adv. Eng. Mater.*, vol. 13, no. 9, pp. 264–73, 2011.

[40] G. Silva, O. P. Coutinho, P. Ducheyne, I. M. Shapiro, and R. L. Reis, “The effect of starch and starch-bioactive glass composite microparticles on the adhesion and expression of the osteoblastic phenotype of a bone cell line,” *Biomaterials*, vol. 28, no. 2, pp. 326–34, 2007.

[41] T. Y. Hui, K. M. C. Cheung, W. L. Cheung, D. Chan, and B. P. Chan, “In vitro chondrogenic differentiation of human mesenchymal stem cells in collagen microspheres: Influence of cell seeding density and collagen concentration,” *Biomaterials*, vol. 29, pp. 3201–12, 2008.

[42] G. Chen, T. Ushida, and T. Tateishi, “A hybrid network of synthetic

polymer mesh and collagen sponge," *Chem. Commun.*, vol. 60, no. 16, pp. 1505–1506, 2000.

[43] Z. Ruszczak, "Effect of Coll matr on dermal," *Adv. Drug Deliv. Rev.*, vol. 55, no. 12, pp. 1595–1611, 2003.

[44] Y. Tabata and Y. Ikada, "Protein release from gelatin matrices," *Adv. Drug Deliv. Rev.*, vol. 31, pp. 287–301, 1998.

[45] R. Zehbe, J. Goebbels, Y. Ibold, U. Gross, and H. Schubert, "Three-dimensional visualization of in vitro cultivated chondrocytes inside porous gelatine scaffolds: A tomographic approach.," *Acta Biomater.*, vol. 6, no. 6, pp. 2097–107, Jun. 2010.

[46] C. Correia, S. Bhumiratana, L.-P. Yan, A. L. Oliveira, J. M. Gimble, D. Rockwood, D. L. Kaplan, R. a Sousa, R. L. Reis, and G. Vunjak-Novakovic, "Development of silk-based scaffolds for tissue engineering of bone from human adipose-derived stem cells.," *Acta Biomater.*, vol. 8, no. 7, pp. 2483–92, Jul. 2012.

[47] M. R. Neidert, E. S. Lee, T. R. Oegema, and R. T. Tranquillo, "Enhanced fibrin remodeling in vitro with TGF-??1, insulin and plasmin for improved tissue-equivalents," *Biomaterials*, vol. 23, no. 17, pp. 3717–3731, 2002.

[48] J. J. Delgado, C. Evora, E. Sánchez, M. Baro, and A. Delgado, "Validation of a method for non-invasive in vivo measurement of growth factor release from a local delivery system in bone," *J. Control. Release*, vol. 114, no. 2, pp. 223–229, 2006.

[49] X. L. Xu, J. Lou, T. Tang, K. W. Ng, J. Zhang, C. Yu, and K. Dai, "Evaluation of different scaffolds for BMP-2 genetic orthopedic tissue engineering," *J. Biomed. Mater. Res. - Part B Appl. Biomater.*, vol. 75, no. 2, pp. 289–303, 2005.

[50] T. Guo, J. Zhao, J. Chang, Z. Ding, H. Hong, J. Chen, and J. Zhang, "Porous chitosan-gelatin scaffold containing plasmid DNA encoding transforming growth factor-??1 for chondrocytes proliferation," *Biomaterials*, vol. 27, no. 7, pp. 1095–1103, 2006.

[51] C. Alemdaroğlu, Z. Değim, N. Çelebi, F. Zor, S. Öztürk, and D. Erdoğan, "An investigation on burn wound healing in rats with chitosan gel formulation containing epidermal growth factor," *Burns*, vol. 32, no. 3, pp. 319–327, 2006.

[52] M. Fujita, M. Ishihara, Y. Morimoto, M. Simizu, Y. Saito, H. Yura, T. Matsui, B. Takase, H. Hattori, Y. Kanatani, M. Kikuchi, and T. Maehara, "Efficacy of photocrosslinkable chitosan hydrogel containing fibroblast growth factor-2 in a rabbit model of chronic myocardial infarction," *J. Surg. Res.*, vol. 126, no. 1, pp. 27–33, 2005.

[53] H. Keshaw, A. Forbes, and R. M. Day, "Release of angiogenic growth factors from cells encapsulated in alginate beads with bioactive glass," *Biomaterials*, vol. 26, no. 19, pp. 4171–4179, 2005.

[54] C. Kaps, C. Bramlage, H. Smolian, A. Haisch, U. Ungethüm, G. R.

Burmester, M. Sittinger, G. Gross, and T. Häupl, “Bone morphogenetic proteins promote cartilage differentiation and protect engineered artificial cartilage from fibroblast invasion and destruction,” *Arthritis Rheum.*, vol. 46, no. 1, pp. 149–162, 2002.

[55] Y. Park, M. Sugimoto, a. Watrin, M. Chiquet, and E. B. Hunziker, “BMP-2 induces the expression of chondrocyte-specific genes in bovine synovium-derived progenitor cells cultured in three-dimensional alginate hydrogel,” *Osteoarthr. Cartil.*, vol. 13, no. 6, pp. 527–536, 2005.

[56] K. Y. Lee, M. C. Peters, and D. J. Mooney, “Comparison of vascular endothelial growth factor and basic fibroblast growth factor on angiogenesis in SCID mice,” *J. Control. Release*, vol. 87, no. 1–3, pp. 49–56, 2003.

[57] C. K. Kim and E. J. Lee, “The controlled release of blue dextran from alginate beads,” *Int. J. Pharm.*, vol. 79, no. 1, pp. 11–19, 1992.

[58] Y. H. Yun, D. J. Goetz, P. Yellen, and W. Chen, “Hyaluronan microspheres for sustained gene delivery and site-specific targeting,” *Biomaterials*, vol. 25, no. 1, pp. 147–157, 2004.

[59] E. Pianigiani, a. Andreassi, P. Taddeucci, C. Alessandrini, M. Fimiani, and L. Andreassi, “A new model for studying differentiation and growth of epidermal cultures on hyaluronan-based carrier,” *Biomaterials*, vol. 20, no. 18, pp. 1689–1694, 1999.

[60] R. Parenteau-Bareil, R. Gauvin, and F. Berthod, “Collagen-based biomaterials for tissue engineering applications,” *Materials (Basel).*, vol. 3, pp. 1863–87, 2010.

[61] J. Keefe, L. Wauk, S. Chu, and F. DeLustro, “Clinical use of injectable bovine collagen: A decade of experience,” *Clin. Mater.*, vol. 9, no. 3, pp. 155–62, 1992.

[62] B. Chevallay and D. Herbage, “Collagen-based biomaterials as 3D scaffold for cell cultures: applications for tissue engineering and gene therapy.,” *Med. Biol. Eng. Comput.*, vol. 38, pp. 211–18, 2000.

[63] D. G. Wallace and J. Rosenblatt, “Collagen gel systems for sustained delivery and tissue engineering,” *Adv Drug Deliv. Rev.*, vol. 55, pp. 1631–49, 2003.

[64] L. H. Damink, P. J. Dijkstra, M. J. Van Luyn, P. B. Van Wachem, P. Nieuwenhuis, and J. Feijen, “Glutaraldehyde as a crosslinking agent for collagen-based biomaterials,” *J. Mater. Sci.*, vol. 6, pp. 460–72, 1995.

[65] T. Barrows, “Degradable implant materials: A review of synthetic absorbable polymers and their applications,” *Clin. Mater.*, vol. 1, no. 4, pp. 233–257, 1986.

[66] P. B. Malafaya, A. Silva, and R. L. Reis, “Natural – origin polymers as carriers and scaffolds for biomolecules and cell delivery in tissue engineering applications,” *Adv. Drug Deliv. Rev.*, vol. 59, pp. 207–33, 2007.

[67] M. E. R. Coimbra, C. N. Elias, and P. G. Coelho, “In vitro degradation of poly-L-D-lactic acid (PLDLA) pellets and powder used as synthetic alloplasts for bone grafting,” *J. Mater. Sci. Mater. Med.*, vol. 19, no. 10, pp. 3227–3234, 2008.

[68] O. Böstman, E. Hirvensalo, J. Mäkinen, and P. Rokkanen, “Foreign-body reactions to fracture fixation implants of biodegradable synthetic polymers.,” *J. Bone Joint Surg. Br.*, vol. 72, no. 4, pp. 592–596, 1990.

[69] N. Tamai, A. Myoui, M. Hirao, T. Kaito, T. Ochi, J. Tanaka, K. Takaoka, and H. Yoshikawa, “A new biotechnology for articular cartilage repair: Subchondral implantation of a composite of interconnected porous hydroxyapatite, synthetic polymer (PLA-PEG), and bone morphogenetic protein-2 (rhBMP-2),” *Osteoarthr. Cartil.*, vol. 13, no. 5, pp. 405–417, 2005.

[70] D. J. Mooney, D. F. Baldwin, N. P. Suh, L. P. Vacanti, and R. Langer, “Novel approach to fabricate porous sponges of poly(D,L-lactic-co-glycolic acid) without the use of organic solvents,” *Biomaterials*, vol. 17, no. 14, pp. 1417–22, 1996.

[71] N. S. Dunkelman, M. P. Zimber, R. G. Lebaron, R. Pavelec, M. Kwan, and a F. Purchio, “Cartilage production by rabbit articular chondrocytes on polyglycolic acid scaffolds in a closed bioreactor system.,” *Biotechnol. Bioeng.*, vol. 46, no. 4, pp. 299–305, 1995.

[72] M. I. Santos, S. Fuchs, M. E. Gomes, R. E. Unger, R. L. Reis, and C. J. Kirkpatrick, “Response of micro- and macrovascular endothelial cells to starch-based fiber meshes for bone tissue engineering,” *Biomaterials*, vol. 28, no. 2, pp. 240–248, 2007.

[73] H. Declercq, T. Desmet, E. E. Berneel, P. Dubruel, and M. J. Cornelissen, “Synergistic effect of surface modification and scaffold design of bioplotted 3-D poly-ε-caprolactone scaffolds in osteogenic tissue engineering.,” *Acta Biomater.*, vol. 9, no. 8, pp. 7699–708, Aug. 2013.

[74] K.-Y. Chang, L.-H. Hung, I.-M. Chu, C.-S. Ko, and Y.-D. Lee, “The application of type II collagen and chondroitin sulfate grafted PCL porous scaffold in cartilage tissue engineering.,” *J. Biomed. Mater. Res. A*, vol. 92, no. 2, pp. 712–23, Feb. 2010.

[75] A. Yeo, B. Rai, E. Sju, J. J. Cheong, and S. H. Teoh, “The degradation profile of novel , bioresorbable PCL – TCP scaffolds : An in vitro and in vivo study,” *J. Biomed. Mater. Res. Part A*, vol. 84, no. 1, pp. 208–18, 2007.

[76] R. Kronenthal, *Biodegradable polymers in medicine and surgery*. Boston, MA: Springer US, 1975.

[77] X. Liu and P. Ma, “Polymeric scaffolds for bone tissue engineering,” *Ann. Biomed. Eng.*, vol. 32, no. 3, pp. 477–86, 2004.

[78] C. J. Liao, C. F. Chen, J. H. Chen, S. F. Chiang, Y. J. Lin, and K. Y. Chang, “Fabrication of porous biodegradable polymer scaffolds using a

solvent merging/particulate leaching method," *J. Biomed. Mater. Res.*, vol. 59, no. 4, pp. 676–81, 2002.

[79] G. Chen, T. Ushida, and T. Tateishi, "Scaffold Design for Tissue Engineering," *Macromol. Biosci.*, vol. 2, no. 2, pp. 67–77, 2002.

[80] L. D. Harris, B. S. Kim, and D. J. Mooney, "Open pore biodegradable matrices formed with gas foaming," *J. Biomed. Mater. Reseach*, vol. 42, no. 3, pp. 396–402, 1998.

[81] S. R. Bhattarai, N. Bhattarai, H. K. Yi, P. H. Hwang, D. I. Cha, and H. Y. Kim, "Novel biodegradable electrospun membrane: scaffold for tissue engineering," *Biomaterials*, vol. 25, no. 13, pp. 2595–602, Jun. 2004.

[82] T. Billiet, M. Vandenhaute, J. Schelfhout, S. Van Vlierberghe, and P. Dubruel, "A review of trends and limitations in hydrogel-rapid prototyping for tissue engineering.," *Biomaterials*, vol. 33, no. 26, pp. 6020–41, Sep. 2012.

[83] S. Rajaraman, H. S. Noh, P. J. Hesketh, and D. S. Gottfried, "Rapid, low cost microfabrication technologies toward realization of devices for dielectrophoretic manipulation of particles and nanowires," *Sensors Actuators, B Chem.*, vol. 114, no. 1, pp. 392–401, 2006.

[84] L. Liu, Z. Xiong, R. Zhang, L. Jin, and Yongnian Yan, "A Novel Osteochondral Scaffold Fabricated via Multi-nozzle Low-temperature Deposition Manufacturing," *J. Bioact. Compat. Polym.*, vol. 24, no. 1 Suppl, pp. 18–30, 2009.

[85] V. Liu Tsang and S. N. Bhatia, "Three-dimensional tissue fabrication," *Adv. Drug Deliv. Rev.*, vol. 56, no. 11, pp. 1635–1647, 2004.

[86] A. Pfister, R. Landers, A. Laib, U. Hübner, R. Schmelzeisen, and R. Mülhaupt, "Biofunctional Rapid Prototyping for Tissue-Engineering Applications: 3D Bioplotting versus 3D Printing," *J. Polym. Sci. Part A Polym. Chem.*, vol. 42, pp. 624–638, 2004.

[87] A. I. Caplan, "Adult Mesenchymal Stem Cells for Tissue Engineering Versus Regenerative Medicine," *J. Cell. Physiol.*, vol. 213, pp. 341–47, 2007.

[88] V. Terraciano, N. Hwang, L. Moroni, H. B. Park, Z. Zhang, J. Mizrahi, D. Seliktar, and J. Elisseeff, "Differential response of adult and embryonic mesenchymal progenitor cells to mechanical compression in hydrogels.," *Stem Cells*, vol. 25, pp. 2730–38, 2007.

[89] M. T. Mitjavila-Garcia, C. Simonin, and M. Peschanski, "Embryonic stem cells: meeting the needs for cell therapy.," *Adv. Drug Deliv. Rev.*, vol. 57, no. 13, pp. 1935–43, Dec. 2005.

[90] R. Quarto, M. Mastrogiacomo, and C. Ranieri, "Repair of Large Bone Defects with the Use of Autologous Bone Marrow Stromal Cells," *N. Engl. J. Med.*, vol. 344, no. 5, pp. 385–86, 2001.

[91] B. Levi and M. T. Longaker, "Concise Review : Adipose-Derived Stromal Cells for Skeletal," *Stem Cells*, vol. 29, pp. 576–82, 2011.

[92] G. M. de Peppo, S. Svensson, M. Lennerås, J. Synnergren, J. Stenberg, R. Strehl, J. Hyllner, P. Thomsen, C. Karlsson, G. de Peppo, and S. Svensson, “Human embryonic mesodermal progenitors highly resemble human mesenchymal stem cells and display high potential for tissue engineering applications.,” *… Eng. Part A*, vol. 16, no. 7, pp. 2161–2182, 2010.

[93] B. D. Hoffman, C. Grashoff, and M. A. Schwartz, “Dynamic molecular processes mediate cellular mechanotransduction,” *Nature*, vol. 475, no. 7356, pp. 316–23, 2011.

[94] C. J. Wilson, R. E. Clegg, D. I. Leavesley, and M. J. Pearcy, “Mediation of Biomaterial – Cell Interactions by Adsorbed Proteins : A Review,” *Tissue Eng.*, vol. 11, no. 1, pp. 1–18, 2005.

[95] P. J. Ehrlich and L. E. Lanyon, “Mechanical Strain and Bone Cell Function : A Review,” *Osteoporos. Int.*, vol. 13, pp. 688–700, 2002.

[96] D. J. Kelly and C. R. Jacobs, “The Role of Mechanical Signals in Regulating Chondrogenesis and Osteogenesis of Mesenchymal Stem Cells,” *Birth Defects Res. Part C*, vol. 85, no. Part C, pp. 75–85, Mar. 2010.

[97] J. Klein-Nulend, R. Bacabac, and A. Bakker, “Mechanical loading and how it affects bone cells: the role of the osteocyte cytoskeleton in maintaining our skeleton,” *Eur. Cells Mater.*, vol. 24, pp. 278–291, 2012.

[98] P. S. Vezeridis, C. M. Semeins, Q. Chen, and J. Klein-Nulend, “Osteocytes subjected to pulsating fluid flow regulate osteoblast proliferation and differentiation.,” *Biochem. Biophys. Res. Commun.*, vol. 348, no. 3, pp. 1082–8, Sep. 2006.

[99] J. Klein-Nulend, C. M. Semeins, N. E. Ajubi, P. J. Nijweide, and E. H. Burger, “Pulsating fluid flow increases nitric oxide (NO) synthesis by osteocytes but not periosteal fibroblasts - correlaation with prostaglandin regulation,” *Biochem. Biophys. Res. Commun.*, vol. 217, no. 2, pp. 640–48, 1995.

[100] A. Sittichockechaiwut, A. M. Scutt, A. J. Ryan, L. F. Bonewald, and G. C. Reilly, “Use of rapidly mineralising osteoblasts and short periods of mechanical loading to accelerate matrix maturation in 3D scaffolds.,” *Bone*, vol. 44, no. 5, pp. 822–9, May 2009.

[101] S. Damaraju, J. R. Matyas, D. E. Rancourt, and N. A. Duncan, “The Effect of Mechanical Stimulation on Mineralization in Differentiating Osteoblasts in Collagen-I Scaffolds.,” *Tissue Eng. Part A*, pp. 1–12, Jul. 2014.

[102] Z. Zhang, S. Teoh, E. Y. Teo, M. S. Khoon Chong, C. W. Shin, F. T. Tien, M. Choolani, and J. K. Y. Chan, “A comparison of bioreactors for culture of fetal mesenchymal stem cells for bone tissue engineering,” *Biomaterials*, vol. 31, no. 33, pp. 8684–95, Nov. 2010.

[103] S. M. Tanaka, “A new mechanical stimulator for cultured bone cells using piezoelectric actuator,” *J. Biomech.*, vol. 32, no. 4, pp. 427–30, 1999.

[104] S. D. Thorpe, T. Nagel, S. F. Carroll, and D. J. Kelly, “Modulating gradients in regulatory signals within mesenchymal stem cell seeded hydrogels: a novel strategy to engineer zonal articular cartilage.,” *PLoS One*, vol. 8, no. 4, pp. 60764–77, Jan. 2013.

[105] A. Ratcliffe and L. E. Niklason, “Bioreactors and bioprocessing for tissue engineering,” *Ann. New York Acad. Sci.*, vol. 961, pp. 210–15, 2002.

[106] J. M. Sobral, S. G. Caridade, R. Sousa, J. F. Mano, and R. L. Reis, “Three-dimensional plotted scaffolds with controlled pore size gradients: Effect of scaffold geometry on mechanical performance and cell seeding efficiency.,” *Acta Biomater.*, vol. 7, no. 3, pp. 1009–18, Mar. 2011.

[107] R. Mauck, “The role of cell seeding density and nutrient supply for articular cartilage tissue engineering with deformational loading,” *Osteoarthr. Cartil.*, vol. 11, no. 12, pp. 879–90, Dec. 2003.

[108] C. T. Lim, A. Bershadsky, and M. P. Sheetz, “Mechanobiology,” *J. R. Soc. Interface*, vol. 7, pp. 291–3, 2010.

[109] R. McBeath, D. M. Pirone, C. M. Nelson, K. Bhadriraju, and C. S. Chen, “Cell Shape, Cytoskeletal Tension, and RhoA Regulate Stem Cell Lineage Commitment,” *Dev. Cell*, vol. 6, no. 4, pp. 483–95, 2004.

[110] G. T. Salazar and O. Ohneda, “Review of biophysical factors affecting osteogenic differentiation of human adult adipose-derived stem cells,” *Biophys. Rev.*, vol. 5, no. 1, pp. 11–28, May 2012.

[111] J. R. Mauney, S. Sjostorm, J. Blumberg, R. Horan, J. P. O’Leary, G. Vunjak-Novakovic, V. Volloch, and D. L. Kaplan, “Mechanical Stimulation Promotes Osteogenic Differentiation of Human Bone Marrow Stromal Cells on 3-D Partially Demineralized Bone Scaffolds In Vitro,” *Calcif. Tissue Int.*, vol. 74, no. 5, pp. 458–68, May 2004.

[112] L. Meinel, S. Hofmann, V. Karageorgiou, C. Kirker-Head, J. McCool, G. Gronowicz, L. Zichner, R. Langer, G. Vunjak-Novakovic, and D. L. Kaplan, “The inflammatory responses to silk films in vitro and in vivo.,” *Biomaterials*, vol. 26, no. 2, pp. 147–55, Jan. 2005.

[113] J. Rauh, F. Milan, K. Günther, and M. Stiehler, “Bioreactor systems for bone tissue engineering,” *Tissue Eng. Part B*, vol. 17, no. 4, pp. 263–80, Aug. 2011.

[114] A. B. Yeatts and J. P. Fisher, “Bone tissue engineering bioreactors: dynamic culture and the influence of shear stress,” *Bone*, vol. 48, no. 2, pp. 171–81, Feb. 2011.

[115] H. Kausar and R. N. Kishore, “Bone tissue engineering,” *Int. J. Pharm. Pharm. Sci.*, vol. 5, no. 1, pp. 30–32, 2013.

[116] M. A. Koch, E. J. Vrij, E. Engel, J. A. Planell, and D. Lacroix, “Perfusion cell seeding on large porous PLA/calcium phosphate composite scaffolds in a perfusion bioreactor system under varying perfusion parameters.,” *J. Biomed. Mater. Res. Part A*, vol. 95, no. 4, pp. 1011–18, Dec. 2010.

[117] F. P. Melchels, B. Tonnarelli, A. L. Olivares, I. Martin, D. Lacroix, J. Feijen, D. J. Wendt, and D. W. Grijpma, “The influence of the scaffold design on the distribution of adhering cells after perfusion cell seeding.,” *Biomaterials*, vol. 32, no. 11, pp. 2878–84, Apr. 2011.

[118] B. Porter, R. Zauel, H. Stockman, R. Guldberg, and D. Fyhrie, “3-D computational modeling of media flow through scaffolds in a perfusion bioreactor.,” *J. Biomech.*, vol. 38, no. 3, pp. 543–9, Mar. 2005.

[119] Y. Chen, V. Bloemen, S. J. Impens, M. Moesen, F. P. Luyten, and J. J. Schrooten, “Characterization and Optimization of Cell Seeding in Scaffolds by Factorial Design: Quality by Design Approach for Skeletal Tissue Engineering,” *Tissue Eng. Part C*, vol. 17, no. 12, pp. 1211–21, Dec. 2011.

[120] R. S. Cherry, “Animal cells in turbulent fluids: details of the physiscal stimulus and the biological response,” *Biotechnol. Adv.*, vol. 11, pp. 279–99, 1993.

[121] G. Vunjak-Novakovic, I. Martin, B. Obradovic, S. Treppo, J. Grodzinsky, R. Langer, and L. E. Freed, “Bioreactor cultivation conditions modulate the composition and mechanical properties of tissue-engineered cartilage,” *J. Orthop. Res.*, vol. 17, no. 1, pp. 130–8, 1999.

[122] D. Wendt, A. Marsano, M. Jakob, M. Heberer, and I. Martin, “Oscillating perfusion of cell suspensions through three-dimensional scaffolds enhances cell seeding efficiency and uniformity,” *Biotechnol. Bioeng.*, vol. 84, no. 2, pp. 205–14, Oct. 2003.

[123] S. Scaglione, A. Braccini, D. Wendt, C. Jaquiery, F. Beltrame, R. Quarto, and I. Martin, “Engineering of osteoinductive grafts by isolation and expansion of ovine bone marrow stromal cells directly on 3D ceramic scaffolds.,” *Biotechnol. Bioeng.*, vol. 93, no. 1, pp. 181–7, Jan. 2006.

[124] L. Bjerre, C. Bünger, A. Baatrup, M. Kassem, and T. Mygind, “Flow perfusion culture of human mesenchymal stem cells on coralline hydroxyapatite scaffolds with various pore sizes.,” *J. Biomed. Mater. Res. Part A*, vol. 97, no. 3, pp. 251–63, Jun. 2011.

[125] A. Papadimitropoulos, S. A. Riboldi, B. Tonnarelli, E. Piccinini, and M. A. Woodruff, “A collagen network phase improves cell seeding of open-pore structure scaffolds under perfusion,” *J. Tissue Eng. Regen. Med.*, vol. 7, pp. 183–91, 2013.

[126] V. I. Sikavitsas, G. N. Bancroft, J. J. Lemoine, M. Liebschner, M. Dauner, and A. G. Mikos, “Flow perfusion enhances the calcified matrix deposition of marrow stromal cells in biodegradable nonwoven fiber mesh scaffolds,” *Ann. Biomed. Eng.*, vol. 33, no. 1, pp. 63–70, 2005.

[127] Y. J. Li, N. N. Batra, L. You, S. C. Meier, I. A. Coe, C. E. Yellowley, and C. R. Jacobs, “Oscillatory fluid flow affects human marrow stromal cell proliferation and differentiation,” *J. Orthop. Sci.*, vol. 22, pp. 1283–89, 2004.

[128] C. R. Jacobs, C. E. Yellowley, B. R. Davis, Z. Zhou, J. M. Cimbala, and

H. J. Donahue, “Differential effect of steady versus oscillating flow on bone cells,” vol. 31, pp. 969–976, 1998.

[129] G. N. Bancroft, V. I. Sikavitsas, J. Dolder, L. Tiffany, C. G. Ambrose, J. A. Jansen, and A. G. Mikos, “Fluid flow increases mineralized matrix deposition in 3D perfusion culture of marrow stromal osteoblasts on a dose-depend manner,” *Natl. Acad. Sci.*, vol. 99, no. 20, pp. 12600–05, 2002.

[130] S. D. Tan, a D. Bakker, C. M. Semeins, A. M. Kuijpers-Jagtman, and J. Klein-Nulend, “Inhibition of osteocyte apoptosis by fluid flow is mediated by nitric oxide.,” *Biochem. Biophys. Res. Commun.*, vol. 369, no. 4, pp. 1150–4, May 2008.

[131] S. D. Tan, T. J. de Vries, A. M. Kuijpers-Jagtman, C. M. Semeins, V. Everts, and J. Klein-Nulend, “Osteocytes subjected to fluid flow inhibit osteoclast formation and bone resorption.,” *Bone*, vol. 41, no. 5, pp. 745–51, Nov. 2007.

[132] D. J. Beebe, G. A. Mensing, and G. M. Walker, “Physics and applications of microfluidics in biology,” *Annu. Rev. Biomed. Eng.*, vol. 4, pp. 261–86, Jan. 2002.

[133] O. F. Khan, M. D. Chamberlain, and M. V Sefton, “Toward an in vitro vasculature: differentiation of mesenchymal stromal cells within an endothelial cell-seeded modular construct in a microfluidic flow chamber.,” *Tissue Eng. Part A*, pp. 744–56, Apr. 2012.

[134] L. Kim, Y. Toh, and J. Voldman, “A practical guide to microfluidic perfusion culture of adherent mammalian cells,” *Lab Chip*, vol. 7, no. 6, pp. 681–94, Jun. 2007.

[135] A. Plecis and Y. Chen, “Fabrication of microfluidic devices based on glass–PDMS–glass technology,” *Microelectron. Eng.*, vol. 84, pp. 1265–9, May 2007.

[136] S. Bhattacharya, A. Datta, J. M. Berg, and S. Gangopadhyay, “Studies on Surface Wettability of Poly (Dimethyl) Siloxane (PDMS) and Glass Under Oxygen-Plasma Treatment and Correlation With Bond Strength,” *J. Microelectromechanical Syst.*, vol. 14, no. 3, pp. 590–97, 2005.

[137] B. Millare, M. Thomas, A. Ferreira, H. Xu, M. Holesinger, and V. I. Vullev, “Dependence of the Quality of Adhesion between Poly (dimethylsiloxane) and Glass Surfaces on the Conditions of Treatment with Oxygen Plasma,” *Langmuir*, vol. 24, pp. 13218–24, 2008.

[138] A. Tourovskaia, X. Figueroa-Masot, and A. Folch, “Differentiation-on-a-chip: a microfluidic platform for long-term cell culture studies.,” *Lab Chip*, vol. 5, no. 1, pp. 14–19, 2005.

[139] L. Kim, M. D. Vahey, H. Lee, and J. Voldman, “Microfluidic arrays for logarithmically perfused embryonic stem cell culture.,” *Lab Chip*, vol. 6, no. 3, pp. 394–406, Mar. 2006.

[140] B. J. Kane, M. J. Zinner, M. L. Yarmush, and M. Toner, “Liver-specific

functional studies in a microfluidic array of primary mammalian hepatocytes," *Anal. Chem.*, vol. 78, no. 13, pp. 4291–98, 2006.

[141] Y. Toh, C. Zhang, J. Zhang, Y. M. Khong, S. Chang, V. D. Samper, D. van Noort, D. W. Hutmacher, and H. Yu, "A novel 3D mammalian cell perfusion-culture system in microfluidic channels.," *Lab Chip*, vol. 7, no. 3, pp. 302–9, 2007.

[142] S. Park, W. Y. Sim, B. Min, S. S. Yang, A. Khademhosseini, and D. L. Kaplan, "Chip-based comparison of the osteogenesis of human bone marrow- and adipose tissue-derived mesenchymal stem cells under mechanical stimulation.," *PLoS One*, vol. 7, no. 9, pp. 46689–700, Jan. 2012.

[143] N. L. Jeon, S. K. W. Dertinger, D. T. Chiu, I. S. Choi, A. D. Stroock, and G. M. Whitesides, "Generation of Solution and Surface Gradients Using Microfluidic Systems," *Langmuir*, no. 16, pp. 8311–16, 2000.

[144] L. MacQueen, O. Chebotarev, M. Chen, J. Usprech, Y. Sun, and C. A. Simmons, "Three-Dimensional mechanical compression of biomaterials in a microfabricated bioreactor with on-chip strain sensors," in *16th Intern Conf Miniaturized Systems for Chemistry and Life Science*, 2012, pp. 1141–43.

[145] C. K. Abrahamsson, F. Yang, H. Park, J. M. Brunger, P. K. Valonen, R. Langer, J. F. Welter, A. I. Caplan, F. Guilak, and L. E. Freed, "Chondrogenesis and mineralization during in vitro culture of human mesenchymal stem cells on three-dimensional woven scaffolds.," *Tissue Eng. Part A*, vol. 16, no. 12, pp. 3709–18, Dec. 2010.

[146] Z. Kong, J. Li, Q. Zhao, Z. Zhou, X. Yuan, D. Yang, and X. Chen, "Dynamic compression promotes proliferation and neovascular networks of endothelial progenitor cells in demineralized bone matrix scaffold seed.," *J. Appl. Physiol.*, vol. 113, no. 4, pp. 619–26, Aug. 2012.

[147] E. M. Kearney, E. Farrell, P. J. Prendergast, and V. A. Campbell, "Tensile strain as a regulator of mesenchymal stem cell osteogenesis," *Ann. Biomed. Eng.*, vol. 38, no. 5, pp. 1767–79, May 2010.

[148] Y. F. Rui, P. P. Y. Lui, M. Ni, L. S. Chan, Y. W. Lee, and K. M. Chan, "Mechanical loading increased BMP-2 expression which promoted osteogenic differentiation of tendon-derived stem cells.," *J Orthop Res*, vol. 29, no. 3, pp. 390–6, Mar. 2011.

[149] G. Friedl, H. Schmidt, I. Rehak, G. Kostner, K. Schauenstein, and R. Windhager, "Undifferentiated human mesenchymal stem cells (hMSCs) are highly sensitive to mechanical strain: transcriptionally controlled early osteo-chondrogenic response in vitro.," *Osteoarthr. Cartil.*, vol. 15, no. 11, pp. 1293–300, Nov. 2007.

[150] A. K. Haudenschild, A. H. Hsieh, S. Kapila, and J. C. Lotz, "Pressure and distortion regulate human mesenchymal stem cell gene expression.," *Ann. Biomed. Eng.*, vol. 37, no. 3, pp. 492–502, Mar. 2009.

[151] P. Thevenot, A. Nair, J. Dey, J. Yang, and L. Tang, "Method to analyze

three-dimensional cell distribution and infiltration in degradable scaffolds.," *Tissue Eng. Part C*, vol. 14, no. 4, pp. 319–31, Dec. 2008.

[152] K. L. Au-Yeung, K. Y. Sze, M. H. Sham, and B. P. Chan, "Development of a micromanipulator-based loading device for mechanoregulation study of human mesenchymal stem cells in three-dimensional collagen constructs.," *Tissue Eng. Part C*, vol. 16, no. 1, pp. 93–107, 2010.

[153] M. Jagodzinski, M. Drescher, J. Zeichen, S. Hankemeier, C. Krettek, U. Bosch, and M. van Griensven, "Effects of cyclic longitudinal mechanical strain and dexamethasone on osteogenic differentiation of human bone marrow stromal cells.," *Eur. Cells Mater.*, vol. 7, pp. 35–41, 2004.

[154] S. M. Tanaka, J. Li, R. L. Duncan, H. Yokota, D. B. Burr, and C. H. Turner, "Effects of broad frequency vibration on cultured osteoblasts.," *J. Biomech.*, vol. 36, no. 1, pp. 73–80, 2003.

[155] S. D. Thorpe, C. T. Buckley, T. Vinardell, F. J. O'Brien, V. A. Campbell, and D. J. Kelly, "Dynamic compression can inhibit chondrogenesis of mesenchymal stem cells," *Biochem. Biophys. Res. Commun.*, vol. 377, no. 2, pp. 458–62, 2008.

[156] S. D. Thorpe, C. T. Buckley, T. Vinardell, F. J. O'Brien, V. Campbell, and D. J. Kelly, "The response of bone marrow-derived mesenchymal stem cells to dynamic compression following TGF-beta3 induced chondrogenic differentiation.," *Ann. Biomed. Eng.*, vol. 38, no. 9, pp. 2896–909, Sep. 2010.

[157] Z. Li, S. Yao, M. Alini, and M. J. Stoddart, "Chondrogenesis of human bone marrow mesenchymal stem cells in fibrin-polyurethane composites is modulated by frequency and amplitude of dynamic compression and shear stress.," *Tissue Eng.*, vol. 16, no. 2, pp. 575–84, 2010.

[158] N. J. Steinmetz and S. J. Bryant, "The effects of intermittent dynamic loading on chondrogenic and osteogenic differentiation of human marrow stromal cells encapsulated in RGD-modified poly(ethylene glycol) hydrogels.," *Acta Biomater.*, vol. 7, no. 11, pp. 3829–40, Nov. 2011.

[159] S. H. Elder, S. A. Goldstein, J. H. Kimura, L. J. Soslowsky, and D. M. Spengler, "Chondrocyte differentiation is modulated by frequency and duration of cyclic compressive loading," *Ann. Biomed. Eng.*, vol. 29, no. 6, pp. 476–82, 2001.

[160] P. J. Mack, M. R. Kaazempur-Mofrad, H. Karcher, R. T. Lee, and R. D. Kamm, "Force-induced focal adhesion translocation: effects of force amplitude and frequency.," *Am. J. Physiol.*, vol. 287, no. 4, pp. 954–62, 2004.

[161] E. Ozcivici, Y. K. Luu, C. T. Rubin, and S. Judex, "Low-Level Vibrations Retain Bone Marrow ' s Osteogenic Potential and Augment Recovery of Trabecular Bone during Reambulation," *PLoS One*, vol. 5, no. 6, pp. 11178–88, 2010.

[162] A. Sittichokechaiwut, J. H. Edwards, A. M. Scutt, and G. C. Reilly, "Short

bouts of mechanical loading are as effective as dexamethasone at inducing matrix production by human bone marrow mesenchymal stem cells," *Eur. Cells Mater.*, vol. 20, pp. 45–57, 2010.

[163] A. V Kramarenko and U. Tan, "Effects of High-Frequency Electromagnetic Fields on Human EEG : a Brain Mapping Study," *Intern. J. Neurosci.*, vol. 113, pp. 1007–19, 2003.

[164] E. K. Antonsson and R. W. Mann, "The frequency content of gait," *J. Biomech.*, vol. 18, no. 1, pp. 39–47, 1985.

[165] C. A. L. Bassett, A. Pilla, and R. Pawluk, "A Non-Operative Salvage of Surgically-Resistant Pseudarthroses and Non-Unions by Pulsing Electromagnetic Fields: A Preliminary Report," *Clin. Orthop. Relat. Res.*, vol. 124, pp. 128–143, 1977.

[166] R. K. Aaron, D. Ciombor, and B. J. Simon, "Treatment of Non-unions with Electric and Electromagnetic Fields," *Clin. Orthop. Relat. Res.*, vol. 419, pp. 21–29, 2004.

[167] J. H. Jansen, O. P. Van der Jagt, B. J. Punt, J. Verhaar, J. P. Van Leeuwen, H. Weinans, and H. Jahr, "Stimulation of osteogenic differentiation in human osteoprogenitor cells by pulsed electromagnetic fields: an in vitro study.," *BMC Musculoskelet. Disord.*, vol. 11, pp. 188–99, 2010.

[168] L. Sun, D. Hsieh, T. Yu, H. Chiu, S. Lu, G. Luo, T. K. Kuo, O. K. Lee, and T.-W. Chiou, "Effect of pulsed electromagnetic field on the proliferation and differentiation potential of human bone marrow mesenchymal stem cells.," *Bioelectromagnetics*, vol. 30, no. 4, pp. 251–60, 2009.

[169] L. Sun, D. Hsieh, P. Lin, H. Chiu, and T. Chiou, "Pulsed electromagnetic fields accelerate proliferation and osteogenic gene expression in human bone marrow mesenchymal stem cells during osteogenic differentiation.," *Bioelectromagnetics*, vol. 31, no. 3, pp. 209–19, 2010.

[170] M. Tsai, W. Li, R. S. Tuan, and W. H. Chang, "Modulation of osteogenesis in human mesenchymal stem cells by specific pulsed electromagnetic field stimulation.," *J. Orthop. Res.*, vol. 27, no. 9, pp. 1169–74, 2009.

[171] C. Liu, J. Yu, Y. Yang, X. Tang, D. Zhao, W. Zhao, and H. Wu, "Effect of 1 mT sinusoidal electromagnetic fields on proliferation and osteogenic differentiation of rat bone marrow mesenchymal stromal cells.," *Bioelectromagnetics*, vol. 34, no. 6, pp. 453–64, 2013.

[172] S. Mayer-Wagner, A. Passberger, B. Sievers, J. Aigner, B. Summer, T. S. Schiergens, V. Jansson, and P. E. Müller, "Effects of low frequency electromagnetic fields on the chondrogenic differentiation of human mesenchymal stem cells," *Bioelectromagnetics*, vol. 32, no. 4, pp. 283–90, 2011.

[173] L. Cui, B. Liu, G. Liu, W. Zhang, L. Cen, J. Sun, S. Yin, W. Liu, and Y. Cao, "Repair of cranial bone defects with adipose derived stem cells and

coral scaffold in a canine model.," *Biomaterials*, vol. 28, no. 36, pp. 5477–86, Dec. 2007.

[174] C. B. Raub, V. Suresh, T. Krasieva, J. Lyubovitsky, J. D. Mih, A. J. Putnam, B. J. Tromberg, and S. C. George, "Non invasive assessment of collagen gel microstructure and mechanics using multiphoton microscopy.," *Biophys. J.*, vol. 92, no. 6, pp. 2212–22, Mar. 2007.

[175] S. S. Shapiro and M. B. Wilk, "An Analysis of Variance Test for Normality (Complete Samples)," *Biometrika*, vol. 52, no. 3/4, pp. 591–611, 1965.

[176] S. Shapiro and R. . Francia, "An Approximate of Variance Test Analysis for Normality," *J. Am. Stat. Assoc.*, vol. 67, no. 337, pp. 215–216, 1972.

[177] B. B. Schultz, "Levene's test for relative variation," *Syst. Zool.*, vol. 34, no. 4, pp. 449–456, 1985.

[178] M. E. Hoque, D. W. Hutmacher, W. Feng, S. Li, M.-H. Huang, M. Vert, and Y. S. Wong, "Fabrication using a rapid prototyping system and in vitro characterization of PEG-PCL-PLA scaffolds for tissue engineering," *J. Biomater. Sci. Polym. Ed.*, vol. 16, no. 12, pp. 1595–1610, 2005.

[179] D. Rohner, D. W. Hutmacher, T. K. Cheng, M. Oberholzer, and B. Hammer, "In vivo efficacy of bone-marrow-coated polycaprolactone scaffolds for the reconstruction of orbital defects in the pig.," *J. Biomed. Mater. Res. Part B*, vol. 66, pp. 574–80, 2003.

[180] J. M. Williams, A. Adewunmi, R. M. Schek, C. L. Flanagan, P. H. Krebsbach, S. E. Feinberg, S. J. Hollister, and S. Das, "Bone tissue engineering using polycaprolactone scaffolds fabricated via selective laser sintering," *Biomaterials*, vol. 26, no. 23, pp. 4817–827, 2005.

[181] S. J. Hollister, "Porous scaffold design for tissue engineering.," *Nat. Mater.*, vol. 4, no. 7, pp. 518–24, 2005.

[182] G. G. Pitt, M. M. Gratzl, G. L. Kimmel, J. Surles, and a Sohindler, "Aliphatic polyesters II. The degradation of poly (DL-lactide), poly (ε-caprolactone), and their copolymers< i> in vivo</i>," *Biomaterials*, vol. 2, no. 4, pp. 215–220, 1981.

[183] M. Chasin and R. Langer, *Biodegradable Polymers as Drug Delivery Systems*. New York: M. Dekker, Inc., 1990.

[184] S. Ghosh, V. Gutierrez, C. Fernández, M. Rodriguez-Perez, J. C. Viana, R. L. Reis, and J. F. Mano, "Dynamic mechanical behavior of starch-based scaffolds in dry and physiologically simulated conditions: Effect of porosity and pore size," *Acta Biomater.*, vol. 4, no. 4, pp. 950–59, 2008.

[185] J. M. Cloyd, N. R. Malhotra, L. Weng, W. Chen, R. L. Mauck, and D. M. Elliott, "Material properties in unconfined compression of human nucleus pulposus, injectable hyaluronic acid-based hydrogels and tissue engineering scaffolds," *Eur. Spine J.*, vol. 16, no. 11, pp. 1892–98, 2007.

[186] J. Xie, M. Ihara, Y. Jung, I. K. Kwon, S. H. Kim, Y. H. Kim, and T. Matsuda, "Mechano-Active Scaffold Design Based on Microporous Poly (L-lactide-co-ε-caprolactone) for Articular Cartilage Tissue Engineering:

Dependence of Porosity on Compression Force-Applied Mechanical Behaviors," *Tissue Eng.*, vol. 12, no. 3, pp. 449–59, 2006.

[187] P. K. Valonen, F. T. Moutos, A. Kusanagi, M. G. Moretti, B. O. Diekman, J. F. Welter, A. I. Caplan, F. Guilak, and L. E. Freed, "In vitro generation of mechanically functional cartilage grafts based on adult human stem cells and 3D-woven poly(ε-caprolactone) scaffolds," *Biomaterials*, vol. 31, no. 8, pp. 2193–200, 2010.

[188] P. Yilgor, R. Sousa, R. L. Reis, N. Hasirci, and V. Hasirci, "3D plotted PCL scaffolds for stem cell based bone tissue engineering," *Macromol. Symp.*, vol. 269, no. 1, pp. 92–99, 2008.

[189] D. W. Hutmacher, T. Schantz, I. Zein, K. W. Ng, S. H. Teoh, and K. C. Tan, "Mechanical properties and cell cultural response of polycaprolactone scaffolds designed and fabricated via fused deposition modeling.," *J. Biomed. Mater. Res.*, vol. 55, no. 2, pp. 203–16, May 2001.

[190] I. M. Ward and J. Sweene, *Mechanical Properties of Solid Polymers*. John Wiley & Sons, Ltd, 2012.

[191] M. Carfagni, E. Lenzi, and M. Pierini, "The loss factor as a measure of mechanical damping," *SPIE Proc. Ser.*, pp. 580–84, 1998.

[192] D. Lacroix, P. J. Prendergast, G. Li, and D. Marsh, "Biomechanical model to simulate tissue differentiation and bone regeneration: Application to fracture healing," *Med. Biol. Eng. Comput.*, vol. 40, no. 1, pp. 14–21, Jan. 2002.

[193] F. Yoshii, D. Darwis, H. Mitomo, and K. Makuuchi, "Crosslinking of poly(epsilon-caprolactone) by radiation technique and its biodegradability," *Radiat. Phys. Chem.*, vol. 57, no. 3–6, pp. 417–20, 2000.

[194] L. Averous, L. Moro, P. Dole, and C. Fringant, "Properties of thermoplastic blends: Starch-polycaprolactone," *Polymer (Guildf).*, vol. 41, no. 11, pp. 4157–4167, 2000.

[195] B. Gama, S. L. Lopatnikov, and J. W. Gillespie, "Hopkinson bar experimental technique: A critical review," *Appl. Mech. Rev.*, vol. 57, no. 4, pp. 223–51, 2004.

[196] I. Zein, D. W. Hutmacher, K. C. Tan, and S. H. Teoh, "Fused deposition modeling of novel scaffold architectures for tissue engineering applications," *Biomaterials*, vol. 23, no. 4, pp. 1169–1185, 2002.

[197] J. F. Mano and R. L. Reis, "Viscoelastic monitoring of starch-based biomaterials in simulated physiological conditions," *Mater. Sci. Eng. Part A*, vol. 370, no. 1–2, pp. 321–25, 2004.

[198] A. Castro and D. Lacroix, "Response of PCL scaffolds to mechanical compression: a computational model," *not Publ.*, 2015.

[199] T. Dillard, F. N'guyen, E. Maire, L. Salvo, S. Forest *, Y. Bienvenu, J.-D. Bartout, M. Croset, R. Dendievel, and P. Cloetens, "3D quantitative

image analysis of open-cell nickel foams under tension and compression loading using X-ray microtomography," *Philos. Mag.*, vol. 85, no. 19, pp. 2147–2175, 2005.

[200] D. Lacroix and P. J. Prendergast, "A mechano-regulation model for tissue differentiation during fracture healing: analysis of gap size and loading," *J. Biomech.*, vol. 35, no. 9, pp. 1163–71, 2002.

[201] R. F. Landel and L. E. Nielsen, *Mechanical properties of polymers and composites*. CRC Press, 1993.

[202] R. Anitha, S. Arunachalam, and P. Radhakrishnan, "Critical parameters influencing the quality of prototypes in fused deposition modelling," *J. Mater. Process. Technol.*, vol. 118, no. 1–3, pp. 385–88, 2001.

[203] M. Castilho, I. Pires, B. Gouveia, and J. Rodrigues, "Structural evaluation of scaffolds prototypes produced by three-dimensional printing," *Int. J. Adv. Manuf. Technol.*, vol. 56, no. 5–8, pp. 561–69, Feb. 2011.

[204] F. Wang, L. Shor, a. Darling, S. Khalil, W. Sun, S. Güçeri, and a. Lau, "Precision extruding deposition and characterization of cellular poly--caprolactone tissue scaffolds," *Rapid Prototyp. J.*, vol. 10, no. 1, pp. 42–49, 2004.

[205] D. Du, K. S. Furukawa, and T. Ushida, "3D culture of osteoblast-like cells by unidirectional or oscillatory flow for bone tissue engineering.," *Biotechnol. Bioeng.*, vol. 102, no. 6, pp. 1670–8, 2009.

[206] A. S. Goldstein, T. M. Juarez, C. D. Helmke, M. C. Gustin, and A. G. Mikos, "Effect of convection on osteoblastic cell growth and function in biodegradable polymer foam scaffolds," *Biomaterials*, vol. 22, no. 11, pp. 1279–88, 2001.

[207] G. H. Van Lenthe, H. Hagenmüller, M. Bohner, S. J. Hollister, L. Meinel, and R. Müller, "Nondestructive micro-computed tomography for biological imaging and quantification of scaffold-bone interaction in vivo.," *Biomaterials*, vol. 28, no. 15, pp. 2479–90, May 2007.

[208] M. J. Powers, D. M. Janigian, K. E. Wack, C. S. Baker, D. B. Stolz, and L. G. Griffith, "Functional Behavior of Primary Rat Liver Cells in a," *Tissue Eng.*, vol. 8, no. 3, pp. 499–513, 2002.

[209] D. D. Deligianni, N. D. Katsala, P. G. Koutsoukos, and Y. F. Missirlis, "Effect of surface roughness of hydroxyapatite on human bone marrow cell adhesion , proliferation , differentiation and detachment strength," *Biomaterials*, vol. 22, pp. 87–96, 2001.

[210] R. G. Holdich, "Fluid flow in porous media," *Fundam. Part. Technol.*, vol. 23, pp. 21–28, 2002.

[211] J. Kestin, M. Sokolov, and W. A. Wakeham, "Viscosity of liquid water in the range -8oC to 150oC," *Journal of Physical Chemistry Reference Data*, vol. 7, no. 3. pp. 941–48, 1978.

[212] A. Campos and D. Lacroix, "Ph.D thesis," *not published*. 2015.

[213] F. Zhao and T. Ma, “Perfusion bioreactor system for human mesenchymal stem cell tissue engineering: Dynamic cell seeding and construct development,” *Biotechnol. Bioeng.*, vol. 91, no. 4, pp. 482–493, 2005.

[214] B. D. Porter, A. S. P. Lin, A. Peister, D. Hutmacher, and R. E. Guldberg, “Noninvasive image analysis of 3D construct mineralization in a perfusion bioreactor.,” *Biomaterials*, vol. 28, no. 15, pp. 2525–33, May 2007.

[215] A. C. Jones, C. H. Arns, A. P. Sheppard, D. W. Hutmacher, B. K. Milthorpe, and M. a Knackstedt, “Assessment of bone ingrowth into porous biomaterials using MICRO-CT.,” *Biomaterials*, vol. 28, no. 15, pp. 2491–504, May 2007.

[216] J. M. Kemppainen and S. J. Hollister, “Tailoring the mechanical properties of 3D-designed poly(glycerol sebacate) scaffolds for cartilage applications.,” *J. Biomed. Mater. Res. Part A*, vol. 94, no. 1, pp. 9–18, Jul. 2010.

[217] M. Stoppato, E. Carletti, D. Maniglio, C. Migliaresi, and A. Motta, “Functional role of scaffold geometries as a template for physiological ECM formation : evaluation of collagen 3D assembly,” *J. Tissue Eng. Regen. Med.*, 2011.

[218] G. Marino, F. Rosso, P. Ferdinando, A. Grimaldi, G. De Biasio, G. Cafiero, M. Barbarisi, and A. Barbarisi, “Growth and endothelial differentiation of adipose stem cells on polycaprolactone,” *J. Biomed. Mater. Res. Part A*, vol. 100 A, no. 3, pp. 543–48, 2012.

[219] M. Barbarisi, G. Marino, E. Armenia, V. Quagliarello, F. Rosso, P. M., and A. Barbarisi, “Use of polycaprolactone (PCL) as scaffolds for the regeneration of nerve tissue,” *Soc. Biomater.*, pp. 1–6, 2014.

[220] C. Chang, M. Lee, P. Kuo, Y. Wang, Y. Tu, and S. Hung, “Three-dimensional collagen fiber remodeling by mesenchymal stem cells requires the integrin – matrix interaction,” *J. Biomed. Mater. Res. Part A*, vol. 80, no. 2, pp. 466–74, 2006.

[221] M. Mizuno, M. Shindo, D. Kobayashi, E. Tsuruga, a. Amemiya, and Y. Kuboki, “Osteogenesis by bone marrow stromal cells maintained on type I collagen matrix gels in vivo,” *Bone*, vol. 20, no. 2, pp. 101–107, 1997.

[222] V. B. Wigglesworth, “The Use of Osmium in the Fixation and Staining of Tissues,” *Proc. R. Soc. London*, vol. 147, no. 927, pp. 185–99, 1957.

[223] S. H. McBride and M. L. Knothe Tate, “Modulation of stem cell shape and fate A: the role of density and seeding protocol on nucleus shape and gene expression.,” *Tissue Eng. Part A*, vol. 14, no. 9, pp. 1561–72, 2008.

[224] M. Mendoza-Miron, J. Seemann, and F. Grinnell, “The Differential Regulation of Cell Motile Activity Through Matrix Stiffness and Porosity In Three Dimensional Collagen Matrices,” *Biomaterials*, vol. 31, no. 25, pp. 6425–35, 2010.

[225] H. Cheng, K. Luk, K. Cheung, and B. P. Chan, “In vitro generation of an osteochondral interface from mesenchymal stem cell–collagen microspheres,” *Biomaterials*, vol. 32, no. 6, pp. 1526–35, 2011.

[226] W. Saadi, S. W. Rhee, F. Lin, B. Vahidi, B. G. Chung, and N. L. Jeon, “Generation of stable concentration gradients in 2D and 3D environments using a microfluidic ladder chamber,” *Biomed. Microdevices*, vol. 9, no. 5, pp. 627–35, Oct. 2007.

[227] Y. Li, T. Ma, D. a. Kniss, L. C. Lasky, and S. T. Yang, “Effects of filtration seeding on cell density, spatial distribution, and proliferation in nonwoven fibrous matrices,” *Biotechnol. Prog.*, vol. 17, no. 5, pp. 935–944, 2001.

[228] H. Shin, S. Jo, and A. G. Mikos, “Biomimetic materials for tissue engineering,” *Biomaterials*, vol. 24, no. 24, pp. 4353–64, Nov. 2003.

[229] K. S. Anseth, C. N. Bowman, and L. Brannon-Peppas, “Mechanical properties of hydrogels and their experimental determination,” *Biomaterials*, vol. 17, no. 17, pp. 1647–57, 1996.

[230] V. B. Wigglesworth, “The union of protein and nucleic acid in the living cell and its demonstration by osmium staining,” *Q. J. Microsc. Sci.*, vol. 3, no. 69, pp. 113–122, 1964.

[231] B. E. Warren, *X-ray diffraction*. Addison-Wesley Publishing Company Inc., 1969.

[232] M. Guan, W. Yao, R. Liu, K. S. Lam, J. Nolta, J. Jia, B. Panganiban, L. Meng, P. Zhou, M. Shahnazari, R. O. Ritchie, and N. E. Lane, “Directing mesenchymal stem cells to bone to augment bone formation and increase bone mass.,” *Nat. Med.*, vol. 18, no. 3, pp. 456–62, Mar. 2012.

[233] S. Cartmell, K. Huynh, A. Lin, S. Nagaraja, and R. Guldberg, “Quantitative microcomputed tomography analysis of mineralization within three-dimensional scaffolds in vitro.,” *J. Biomed. Mater. Res. Part A*, vol. 69, no. 1, pp. 97–104, 2004.

[234] M. C. Raff, “Social controls on cell survival and cell death,” *Nature*, pp. 397–400, 1992.

[235] M. Guo and B. Hay, “Cell proliferation and apoptosis,” *Curr. Opin. Cell Biol.*, vol. 11, no. 6, pp. 745–752, 1999.

[236] L. Nimeskern, E. Feldmann, W. Kuo, S. Schwarz, E. Goldberg-Bockhorn, S. Dürr, R. Müller, N. Rotter, and K. S. Stok, “Magnetic Resonance Imaging of the Ear for Patient-Specific Reconstructive Surgery,” *PLoS One*, vol. 9, no. 8, pp. 1–7, 2014.

[237] Y. Chen, G. Lin, Y. Chen, A. Fok, and J. Slack, “Micro-Computed Tomography for Visualizing Limb Skeletal Regeneration in Young Xenopus Frogs,” *Anat. Rec. Adv. Integr. Anat. Evol. Biol.*, vol. 295, no. 10, pp. 1562–65, 2012.

[238] M. Sonnaert, I. Papantoniou, L. Geris, and F. P. Luyten, “Contrast enhanced nanoCT for 3D quantitative and spatial analysis of in vitro

manufactured extracellular matrix in metallic tissue engineering scaffolds," *Abstr. B. Micro-Ct User Meet. Bruker microCT*, pp. 36–41, 2013.

[239] M. Sonnaert, G. Kerckhofs, I. Papantoniou, and F. P. Luyten, "Contrast enhanced nanoCT parameter optimisation for volumetric analyses of in vitro manufactured tissue-engineered bone constructs," *Micro-CT User Meet.*, vol. 320, no. 1, pp. 1–6, 2014.

[240] G. Albertini, A. Giuliani, V. Komlev, F. Moroncini, A. Pugnaloni, G. Pennesi, M. Belicchi, C. Rubini, F. Rustichelli, R. Tasso, and Y. Torrente, "Organization of Extracellular Matrix Fibers Within Micro Computed Tomography," *Tissue Eng. Part C*, vol. 15, no. 3, pp. 403–11, 2009.

[241] E. M. Shapiro, K. Sharer, S. Skrtic, and A. P. Koretsky, "In vivo detection of single cells by MRI.," *Magn. Reson. Med.*, vol. 55, no. 2, pp. 242–9, Feb. 2006.

[242] C. K. Sung, K. A. Hong, S. Lin, Y. Lee, J. Cha, J.-K. Lee, C. P. Hong, B. S. Han, S. Il Jung, S. H. Kim, and K. S. Yoon, "Dual-modal nanoprobes for imaging of mesenchymal stem cell transplant by MRI and fluorescence imaging.," *Korean J. Radiol.*, vol. 10, no. 6, pp. 613–22, 2009.

[243] N. Ganesh, A. Ashokan, R. Rajeshkannan, K. P. Chennazhi, M. Koyakutty, and S. Nair, "MR Functional Nano-Hydroxyapatite Incorporated PCL Composite Scaffolds for In situ Monitoring of Bone Tissue Regeneration by MRI.," *Tissue Eng. Part A*, vol. 20, pp. 1–47, 2014.

[244] C. Lalande, S. Miraux, S. M. Derkaoui, S. Mornet, R. Bareille, J. C. Fricain, J. M. Franconi, C. Le Visage, D. Letourneur, J. Amédée, and a K. Bouzier-Sore, "Magnetic resonance imaging tracking of human adipose derived stromal cells within three-dimensional scaffolds for bone tissue engineering.," *Eur. Cell. Mater.*, vol. 21, pp. 341–354, 2011.

[245] K. L. Harrison and M. J. Jenkins, "The effect of crystallinity and water absorption on the dynamic mechanical relaxation behaviour of polycaprolactone," *Polym. Int.*, vol. 53, no. 9, pp. 1298–304, 2004.

[246] L. E. Claes and C. A. Heigele, "Magnitudes of local stress and strain along bony surfaces predict the course and type of fracture healing," *J. Biomech.*, vol. 32, no. 3, pp. 255–266, 1999.

[247] P. L. Leong and E. F. Morgan, "Measurement of fracture callus material properties via nanoindentation," *Acta Biomater.*, vol. 4, no. 5, pp. 1569–1575, 2008.

[248] M. Moisan, J. Barbeau, M. Crevier, J. Pelletier, N. Philip, and B. Saoudi, "Plasma sterilization. Methods and mechanisms," *Pure Appl. Chem.*, vol. 74, no. 3, pp. 349–58, Jan. 2002.

[249] A. Martins, E. D. Pinho, S. Faria, I. Pashkuleva, A. P. Marques, R. L. Reis, and N. M. Neves, "Surface modification of electrospun polycaprolactone nanofiber meshes by plasma treatment to enhance

biological performance," *Small*, vol. 5, no. 10, pp. 1195–206, 2009.

[250] J. Yang, J. Bei, and S. Wang, "Enhanced cell affinity of poly (D,L-lactide) by combining plasma treatment with collagen anchorage.," *Biomaterials*, vol. 23, no. 12, pp. 2607–2614, 2002.

[251] M. Domingos, F. Intranuovo, A. Gloria, R. Gristina, L. Ambrosio, P. J. Bártolo, and P. Favia, "Improved osteoblast cell affinity on plasma-modified 3-D extruded PCL scaffolds.," *Acta Biomater.*, vol. 9, no. 4, pp. 5997–6005, Apr. 2013.

[252] H. Tullberg-Reinert and G. Jundt, "In situ measurement of collagen synthesis by human bone cells with a sirius red-based colorimetric microassay: effects of transforming growth factor beta2 and ascorbic acid 2-phosphate.," *Histochem. Cell Biol.*, vol. 112, no. 4, pp. 271–76, 1999.

[253] C. Maniatopoulos, C. Maniatopoulos, J. Sodek, J. Sodek, a H. Melcher, and a H. Melcher, "Bone formation in vitro by stromal cells obtained from bone marrow of young adult rats.," *Cell Tissue Res.*, vol. 254, no. 2, pp. 317–30, 1988.

[254] L. Uebersax, H. Hagenmüller, S. Hofmann, E. Gruenblatt, R. Müller, G. Vunjak-Novakovic, D. L. Kaplan, H. P. Merkle, and L. Meinel, "Effect of scaffold design on bone morphology in vitro.," *Tissue Eng.*, vol. 12, no. 12, pp. 3417–3429, 2006.

[255] B. Rath, J. Nam, T. J. Knobloch, J. Lannutti, and S. Agarwal, "Compressive forces induce osteogenic gene expression in calvarial osteoblasts.," *J. Biomech.*, vol. 41, no. 5, pp. 1095–103, Jan. 2008.

[256] H. Kang, E. Peng, and G. Bao, "The Effects of Short Period Mechanical Loading on Type I Collagen and Aggrecan mRNA Expression of Goat TMJ Disc Fibrochondrocytes," *2012 Int. Conf. Biomed. Eng. Biotechnol.*, pp. 1113–16, May 2012.

[257] D. Lacroix, "Computational Modelling of Soft Collagen Gel Substrates," in *Multiscale Mechanobiology in Tissue Engineering*, Springer Science & Business Media, 2015.